

N71-28158  
NASACR-119796

ADVANCED INJECTOR CONCEPTS INVESTIGATION

Contract NAS 8-21052

Final Report to

GEORGE C. MARSHALL SPACE FLIGHT CENTER  
National Aeronautics and Space Administration

Report 21052-3F

30 April 1971



CASE FILE  
COPY

**AEROJET LIQUID ROCKET COMPANY**

A DIVISION OF AEROJET-GENERAL ©

SACRAMENTO, CALIFORNIA

Final Report 21052-3F

ADVANCED INJECTOR CONCEPTS INVESTIGATION

Prepared Under

Contract NAS 8-21052  
Plus Modifications 7 through 10

for

George C. Marshall Space Flight Center  
National Aeronautics and Space Administration  
Huntsville, Alabama



**AEROJET LIQUID ROCKET COMPANY**

SACRAMENTO, CALIFORNIA • A DIVISION OF AEROJET-GENERAL ©

FOREWORD

This report summarizes the work accomplished under Contract NAS 8-21052, "Advanced Injector Concepts Investigation." The program technical effort extended over a 18-month period and was completed on 31 December 1970.

The work was conducted under the cognizance of the Engine Components Department, Aerojet Liquid Rocket Company, Sacramento, California. Key Aerojet program personnel included Dr. N. E. Van Huff, program manager; Mr. J. F. Addoms, project manager; Mr. R. L. Boyce, project engineer; and Dr. R. J. LaBotz, technical specialist. Overall program direction was provided by the NASA technical manager, Mr. R. J. Richmond.

TABLE OF CONTENTS

	<u>Page</u>
I. Introduction	1
II. Summary	2
III. Conclusions	
A. Tapoff Cycle	4
B. Annular Injector Design	4
C. Fabrication	5
D. Operating Characteristics	5
IV. Recommendations	6
V. Tapoff Cycle Analysis	
A. Introduction	7
B. Discussion	8
C. Operating Requirements and Conditions	10
D. Injector Model	10
E. Combustion Gas Conditioning Requirements for Turbopump	12
F. Results	15
VI. Annular Injector Design	19
VII. Heat Exchanger Samples Design	23
VIII. Water-Cooled Chamber Design	25
A. Hydraulic Analysis	26
B. Thermal Analysis	27
C. Noncoated Chamber	28
D. Coated Chamber	29
IX. Fabrication	
A. Injector Assembly	31
B. Water-Cooled Chamber	36
C. Nozzle Extension	39
D. Heat Exchanger Samples	39
X. Test Results	
A. Heat Exchanger Evaluation	40
B. Mass Distribution	44
C. Hot Firing	46

APPENDICES

	<u>Appendix</u>
Computer Listing and Discussion of SINDA Logic and Subroutines for Heat Transfer Calculations	A
Computer Listing and Sample Output for Turbopump Flow Requirements	B
Advanced Injector Computer Program	C
Distribution List	D

TABLE LIST

	<u>Table</u>
GH <sub>2</sub> /GO <sub>2</sub> Test Summary	I
Phase III Nickel Injector Test Summary - LO <sub>2</sub> /GH <sub>2</sub>	II

FIGURE LIST

	<u>Figure</u>
Annular Segment Injector	1
Annular Combustor Assembly Components	2
Annular Combustor Assembly	3
Simple Tapoff Schematic	4
Thermal Node Network for Tapoff Cycle Injector	5
Turbopump Operating System	6
Turbine Flow Requirements for LO <sub>2</sub> /LH <sub>2</sub> at MR = 5.0 for [100 ≤ P <sub>c</sub> (psia) ≤ 2500] Throttling Conditions	7
Hot Gas Outlet Temperature	8
Injector Face Structure Temperature	9
Temperatures of Key Locations	10
Temperature Comparison Between Copper and Nickel at Injector Face Nodes and Hot Gas Outlet	11
Injector Platelet Assembly Sequence	12
Nickel Injector Orifice Details	13
Design Configurations for Sample Heat Exchanger Evaluation	14
Water-Cooled Combustion Chamber Details	15
Assembly Details - Water-Cooled Chamber	16

FIGURE LIST (cont.)

	<u>Figure</u>
Assembled Water-Cooled Chamber	17
Flow Rate vs Overall Pressure Drop	18
Coolant Flow vs Pressure Drop - Contour Side	19
Coolant Flow vs Pressure Drop - Flat Side	20
Coolant Flow Rate vs Chamber Pressure - No Coating	21
$R_{BO}$ vs Coolant Flow Rate - Uncoated Copper Chamber Throat Section	22
Gas-Side Wall Temperature vs $R_{BO}$ - Noncoated Wall	23
Gas-Side Wall Temperature vs Chamber Pressure - No Coating	24
Coolant Flow Rate vs Chamber Pressure - 0.002 in. Hafnia Coating	25
Throat Section $R_{BO}$ vs Coolant Flow Rate - 0.002 in. Hafnia Coating	26
Gas-Side and Wall/Coating Interface Temperature vs $R_{BO}$ - 0.002 in. Hafnia Coating	27
Gas-Side and Wall/Coating Interface Temperature vs Chamber Pressure	28
Injector Repair Procedure	29
Annular Segment Injector Flat Face Configuration	30
Nickel Platelet with Nickel Plating over Copper Flash	31
Injector Sample Stack No. 2 Bond Quality	32
Nozzle Extension	33
Heat Exchanger Samples	34
Heat Exchanger Evaluation Test Fixture	35
Phase II Injector Heat Exchanger Evaluation Test Setup	36
Heat Exchanger Evaluation Test Results	37
Heat Exchanger Sample Test Setup	38
Heat Exchanger Samples - Test Results Comparison	39
Mass Distribution Test Fixture	40
Coarse Pattern Fuel Flow Distribution	41
Coarse Pattern Oxidizer Flow Distribution	42
Relative Mass Flux Type I	43
Relative Mass Flux Type II	44

FIGURE LIST (cont.)

	<u>Figure</u>
Relative Mass Flux Type III	45
Relative Mass Flux Type IV	46
Relative Mass Flux Type V	47
Energy Release Efficiency vs Mixture Ratio	48
Energy Release Efficiency vs Velocity Ratio	49
Energy Release Efficiency vs Fuel Density x Velocity	50
Test Bay Seven - Physics Lab	51
Hardware Setup for Testing	52
Energy Release Efficiency vs Chamber Pressure	53
Energy Release Efficiency vs Mixture Ratio	54
Energy Release Efficiency vs Mixture Ratio for Phase III and Phase II Gas/Gas Injectors	55
Energy Release Efficiency Corrected for Mixture Ratio Variations vs Chamber Pressure	56
Energy Release Efficiency vs Chamber Pressure for Gas/Gas Engines with Different Chamber Lengths	57

I. INTRODUCTION

The purpose of this program was to continue exploration of a throttling injector concept that is applicable to an advanced cryogenic engine. This program is Phase III of Contract NAS 8-21052, initiated by Marshall Space Flight Center.

Phase I of the program included evaluation of injectors suitable for staged combustion systems incorporating primary and secondary injectors as well as an annular-shaped combustor in which hydrogen is preheated in a regeneratively cooled jacket. These engine systems had in common the requirement for successful operation while throttling over a wide thrust range. The concept utilized in each of the injector designs is designated HIPERTHIN\*. The four subscale HIPERTHIN injector systems investigated during Phase I were: (1) an annular heat exchanger/injector combustor segment designed for liquid oxygen and gaseous hydrogen--this injector segment simulates the conditions anticipated in a hydrogen regeneratively cooled annular combustor; (2) a primary combustor injector which produces hydrogen-rich hot gas required in a staged-combustion system; (3) a secondary combustor injector which operates with liquid oxygen and hot hydrogen-rich primary combustor gas; and (4) an alternative secondary combustor injector design for use in staged-combustion cycles that employ both fuel- and oxidizer-rich primary combustors. Phase I was reported in Report 21052-1F, dated 31 July 1968.

During Phase II, the areas of performance, injector  $\Delta P/P_c$  behavior, face cooling, throttling range, and combustion stability characteristics of the HIPERTHIN annular heat exchanger/injector combustor segment were examined in more detail. Additionally, certain fabrication problems met during Phase I were resolved. The annular heat exchanger/injector segment development was continued, as this injector appeared to be the best for use in conjunction with an advanced cryogenic rocket engine. This segment was designed for liquid oxygen and gaseous hydrogen, simulating the conditions anticipated in a hydrogen regeneratively cooled annular combustor. Phase II was reported in Report 21052-2F, dated January 1970.

---

\*A concept developed and owned by Aerojet-General Corporation on which AGC holds Patent No. 3,413,704 and other patents pending.

II. SUMMARY

Phase III of Contract NAS 8-21052 was initiated 1 July 1969 and was divided into two tasks:

Task I was an analytical investigation of the feasibility of tapping turbine drive gases from the chamber and passing them through the HIPERTHIN injector. This effort consisted of analysis and preliminary design only; no hardware was fabricated for experimentation.

In operation, gases tapped from the combustion chamber are passed back through the injector counter to the flow of incoming propellants. The problem was to determine if--by proper sizing of the hot gas channels and the propellant injection channels--an optimum heat transfer area could be provided to enable the hot gases to yield sufficient energy to gasify the incoming propellants, and yet retain sufficient energy to drive the turbopump after leaving the injector/heat exchanger.

It was concluded that the hot gas tapoff cycle injector concept is feasible and can operate successfully over the full throttling range specified (33:1), using nickel as the injector material. Certain practical considerations such as the extremely short length of the injector (0.3 in.) may tend to diminish the desirability of employing this concept. Copper was also briefly considered for the tapoff injector material and, from an analytical standpoint, is superior to nickel for this application.

Task II was devoted to further exploration of the annular segment injector, Figure 1, primarily to gain additional data regarding combustion stability, injector face cooling, and steady-state performance at chamber pressures up to 2500 psia. The longer firing durations required to ensure steady-state data and the higher chamber pressures required the use of nickel injector platelet material for improved injector face cooling and water cooling of the chamber.

II, Summary (cont.)

The objectives of the annular segment injector work for Phase III were to demonstrate that the HIPERTHIN is adequate for mechanical strength operation at high chamber pressures, to determine the maximum pressure (up to 2500 psia) at which the thruster could be operated without burning the injector face, and to demonstrate that the desired throttling range could be realized at short L' with high performance.

Most of these objectives were met. The mechanical strength of HIPERTHIN was demonstrated by ten tests of one injector at chamber pressures varying from 100 to 1300 psia. The same injector was also subjected to numerous cold flow cycles and is still structurally sound. No face burning was evident up to the highest chamber pressure level tested (1300 psia) and combustion was stable. Performance ranged from an energy release efficiency of 98% at the 100 psia  $P_c$  level to 94% at the higher chamber pressure.

The chamber used for test firings was a copper-lined water-cooled thrust chamber with a two-dimensional rectangular converging section and throat. The basic chamber length was 2.5 in. (7.3 in. L\*), but attachments for nozzles were provided so that nozzle extensions could be added for operation. The test hardware is shown in Figures 2 and 3.

Use of the Nickel 200 platelet material, required because of face overheating experienced with the stainless steel injectors of Phase II, presented some fabrication problems. Many of the platelets were inadequately plated with the electroless nickel braze material. As a result, both platelet stacks leaked at the edges, but both were successfully repaired and one injector was later tested at 1300 psia with no leakage problems. A procedure has been devised to preclude recurrence of this problem. Two nickel injectors were fabricated for Phase III, although only one was required to conduct the test series.

III. CONCLUSIONS

A. TAPOFF CYCLE

1. The basic tapoff cycle is analytically sizeable up to chamber pressures of 2500 psia with nickel platelet injectors.
2. Above 2500 psia, the permissible tolerances on operating conditions are too small for a practical tapoff cycle with nickel injectors.
3. Copper should be considered as a substitute for nickel in the tapoff system at pressures of 2500 psia and above.

B. ANNULAR INJECTOR DESIGN

1. The integral heat exchanger/injector design concept for extended throttling was demonstrated to be feasible over a throttling range of 13:1 (chamber pressures of 100 to 1300 psia).
2. The design modifications to the heat exchanger section were effective in vaporizing the oxygen and providing uniform, nonpulsing injection.
3. The basic analytical tools employed in injector hydraulic design are suitable for conventional platelet passages. Some modification to the model is required to account for the hydraulic affect of the turbulators added to the LO<sub>2</sub> heat exchanger section.
4. The injector is structurally adequate at chamber pressures of at least 1300 psia and differential manifold pressures of at least 1600 psi.
5. The nickel platelet material was effective in extending the face cooling capacity to at least 1300 psia chamber pressure.
6. The 2.50-in. chamber length may be too short for maximum efficiency.

III, Conclusions (cont.)

C. FABRICATION

1. Full-scale injectors can be fabricated from Nickel 200 platelets as readily as from stainless steel platelets.

2. The technique of copper flashing the nickel platelets prior to depositing the electroless nickel braze alloy is an effective quality control technique for assuring complete braze alloy coverage.

D. OPERATING CHARACTERISTICS

1. A 2.50-in. L' chamber is adequate for HIPERTHIN injectors to provide combustion efficiency in excess of 97% at chamber pressures in the 100 to 500 psia range using  $O_2/H_2$  propellants at O/F of between 5.73 and 6.45.

2. The combustion efficiency measured was lower at higher chamber pressures and/or higher mixture ratios.

3. The observed reduction in ERE with increasing  $P_c$  and decreasing O/F is due mainly to increasing  $P_c$ .

4. The short 2.50-in. length chamber may denote performance characteristics such as reaction isolation zones, which tend to inhibit mixing, that would normally not be seen in longer length chambers.

5. Results cast doubt that a combustion system can be made to throttle over a wide range while maintaining a constant, high ERE.

IV. RECOMMENDATIONS

1. Determine quantitatively the efficiency and heat transfer capabilities of the injector heat exchanger section.
2. Determine the minimum injector  $\Delta P$  and/or  $\Delta P/P_c$  required for stable operation.
3. Expand the platelet technology to include copper platelets for application to the tapoff cycle.
4. Modify the heat exchanger computer model to improve hydraulic predictions.
5. Determine the parameters causing the observed combustion efficiency reduction at higher chamber pressures.
6. Determine the interrelationship between operating mixture ratio and operating chamber pressure on combustion efficiency.

V. TAPOFF CYCLE ANALYSIS

A. INTRODUCTION

This section documents a study to investigate the feasibility of employing a platelet injector that will simultaneously provide the functions of heat exchanger and propellant injector. Under this concept, cryogenic hydrogen and oxygen are gasified by hot combustion gas, which is "tapped-off" from the combustion chamber and directed in a counterflow manner through the injector and subsequently used to drive the turbines in the propellant feed system.

The tapoff cycle concept is shown schematically in its simplest form in Figure 4. Hot gas is bled from the combustion chamber through a heat exchanger, where it gives up heat, vaporizing the incoming propellants. From the heat exchanger, the bleed gas enters the engine turbines which drive the pumps. Vaporizing the incoming propellants gives the injector a gaseous flow characteristic for throttling purposes and may also help in obtaining high combustion efficiencies in short lengths. The quantity of bleed gas required is determined by an overall engine system balance, as the bleed gas flow must contain sufficient energy to completely vaporize the incoming propellants and drive the engine turbomachinery.

The tapoff cycle is particularly well adapted to the platelet injector concept, since the heat exchanger can be built directly into the injector body. This feature permits construction of a very compact system, eliminating the necessity of constructing additional cooled ducts for bringing the bleed gas from the chamber to the heat exchanger. However, it must be recognized that even with the platelet injector introduction of combustion chamber gases directly into the injector poses a very difficult injector face cooling problem.

## V, Tapoff Cycle Analysis (cont.)

## B. DISCUSSION

The initial step in the analysis was the establishment of operating conditions and limits. The thrust chamber operating conditions established in the contract are:

Chamber pressure, psia	2500 maximum
Propellants	O <sub>2</sub> /H <sub>2</sub>
Mixture ratio	5 to 6
Propellant temperature, °R	36 to 200
Throttling range	33:1

The turbopump operating conditions and limits were selected to cover a range representative of advanced oxygen/hydrogen engines. The parameters selected were:

	<u>Min</u>	<u>Max</u>
Gas inlet to turbine	1600°R	2400°R
Turbopump efficiency	50%	70%
Pump outlet pressure	1.5 P <sub>c</sub>	
Pump flow rate	1.05 $\dot{w}_t$	thrust chamber

The injector/heat exchanger design limitations were chosen on the basis of previous HIPERTHIN injector experience. A minimum separator thickness of 0.010 in. a maximum unsupported span of 0.100 in., and a minimum land thickness of 0.015 in. were chosen as limits. Nickel was assumed as the injector material for the bulk of the analysis because this is the material being used in Task 2 and because Aerojet had previously demonstrated a capability for fabricating HIPERTHIN injectors from nickel. A single computer run was performed assuming the injector was fabricated from copper for comparative purposes.

The second step in the analysis was establishment of a mathematical model to describe the thermal behavior of the integral heat exchanger/injector. The model devised is basically an electrical analog representation of the platelets. The network is relaxed by means of a thermal analyzer computer program using a UNIVAC 1108

## V, B, Discussion (cont.)

computer. Several subprograms were coupled with the main program to provide values for parameters such as pressure drops, boundary conditions, turbopump requirements, and thermodynamic and physical properties of the fluids and structure as a function of temperature and pressure.

The results of the analysis indicate that full thrust operation imposes the most severe conditions on the hardware. At full thrust, when nickel is used as the injector material, operation of the tapoff cycle system appears marginal. The limiting parameters are injector face temperature and gas temperature delivered to the turbine. No difficulties are analytically apparent in vaporizing the propellants or in operation at throttled conditions. The problem area is in the percentage of gas tapped from the thrust chamber. Anything in excess of about 6% results in excessive injector face temperature, and anything less than 6% is insufficient to supply the required turbine enthalpy. This results in an extremely narrow allowable tapoff range and allows no margin for system nonuniformity. Several actions are possible to improve the situation. These are (1) increase the turbopump efficiency, (2) reduce the assumed system pressure drop, (3) lower the chamber pressure at maximum thrust, and (4) fabricate the injector from copper rather than nickel.

An analysis comparing injectors fabricated from copper with injectors made from nickel showed that the copper injector is analytically superior to nickel. Comparing the two critical parameters, using copper and nickel injectors, shows:

	<u>Nickel</u>	<u>Copper</u>
Maximum injector face temperature, °R	2550	1440
Maximum gas temperature to turbine, °R	2780	2160

Although no platelet injectors have as yet been fabricated from copper, no problems are apparent which would prevent its use. The tapoff cycle using a platelet injector fabricated from copper is feasible within the limitations assumed for the analysis.

## V, Tapoff Cycle Analysis (cont.)

## G. OPERATING REQUIREMENTS AND CONDITIONS

The primary requirements for successful operation of the tapoff cycle injector concept are maintaining structural temperature limits and properly conditioning the combustion gas necessary to drive the turbopumps. Secondary considerations are pressure drop and propellant outlet temperature. The resulting envelope size and configuration of the injector must also be considered.

The operating conditions considered were:

Chamber pressure	75 - 2500 psia
Throttling range	33:1
Thrust	5000 lb nominal at 2500 P <sub>c</sub>
Hydrogen inlet temperature range	36 to 200°R
Mixture ratio	5 to 6

## D. INJECTOR MODEL

In order to perform the parametric studies required to evaluate concept feasibility, it was necessary to establish a mathematical model describing the thermal behavior of the injector/heat exchanger. Schematically, this model is shown in Figure 5. It is basically an electrical analog representation of a portion of the platelets transporting the fluids, selected to yield known boundary conditions. A finite differencing scheme was used to relax the network by means of the SINDA<sup>(1)</sup> Thermal Analyzer computer program used on a UNIVAC 1108 computer. The model was programmed for maximum flexibility in input quantities and parameter values. Several subprograms were coupled with the main program to provide such quantities as pressure drop calculation, boundary conditions, thermodynamic and physical properties of the fluids and structure as a function of temperature and pressure and turbopump requirements.

(1) J. D. Gaski, "Chrysler Improved Numerical Differencing Analyzer for Third Generation Computers," TN-SP-67-287, Chrysler Corp. Space Division, New Orleans, La., October 1967.

## V, D, Injector Model (cont.)

The model provided for two-dimensional temperature profiles to be established through the three fluids and the injector structure. A listing of the SINDA program input, as well as the subroutines used, are presented and discussed in Appendix A. (A listing of the rather extensive thermodynamic properties program for oxygen and hydrogen is not included. However, their contents and use made of them are discussed.)

One difficulty associated with throttling is that the heat exchanger injector is required to operate at both supercritical and subcritical pressures. For this injector, maximum chamber pressure ( $P_c$ ) is 2500 psia. Since the system must be throttlable over a thrust range of 33:1, the lower limit on  $P_c$  is about 75 psia. The critical state points for the respective propellants are as follows:

	<u>Oxygen</u>	<u>Hydrogen</u>
Critical temperature	278.6°R	59.4°R
Critical pressure	734.8 psia	187.6 psia

It can be seen that, for maximum thrust operation, both propellants are in a supercritical state during their injector residence time. For throttling to chamber pressures below 734.8 psia for oxygen and 187.6 psia for hydrogen, each propellant undergoes phase changes from supercritical, to two-phase, to gas.

Predicting heat transfer and pressure drop for two-phase flow is difficult at best. In these studies, the beginning of the two-phase flow regime was determined for each propellant and saturated vapor properties at the pressure encountered at this point were used to establish the heat transfer coefficient and Reynolds number. It was recognized that the heat transfer coefficient derived in this manner will be somewhat less than might be expected, hence resulting in a longer channel requirement to transfer heat and a conservative design. Other methods were considered\* but their complexity were deemed not justified for this conceptual design study.

\*P. J. Giarratano and R. V. Smith, "Comparative Study of Forced Convection Boiling Heat Transfer Correlations for Cryogenic Fluids," Paper No. H-1 (Cryogenic Engineering Conf., Houston, Texas, 23-25 August 1965).

## V, Tapoff Cycle Analysis (cont.)

## E. COMBUSTION GAS CONDITIONING REQUIREMENTS FOR TURBOPUMP

Combustion gas requirements necessary for successful turbopump operation were obtained by assuming a nominal combustion gas mixture ratio of 5.0 and using standard turbine expressions to derive gas weight flow and temperature ranges. The system configuration is shown schematically in Figure 6. Expressions used are listed below. The subscripts used refer to the conditions at that specific station as shown in Figure 6.

1. Fuel Pump Weight Flow Requirement, lb/sec

$$\dot{w}_f = \frac{\dot{w}_{\text{total}}}{1 + \text{MR}} \times 1.05^* \quad \text{where } \dot{w}_{\text{total}} = \text{total engine flow rate, lb/sec}$$

2. Oxidizer Pump Weight Flow Requirement, lb/sec

$$\dot{w}_o = \frac{\text{MR} \times \dot{w}_{\text{total}}}{1 + \text{MR}} \times 1.05^* \quad \text{where } \dot{w}_{\text{total}} = \frac{P_c}{P_c(\text{full thrust})} \times \dot{w}_{\text{TF}} \text{ and}$$

$\dot{w}_{\text{TF}}$  is the combined oxygen and hydrogen flow rate for the full thrust condition.

3. Turbine Outlet Temperature,  $T_4$ , °R

$$T_4 = T_3 \left[ \frac{P_3}{P_4} \right]^{\frac{1-\gamma}{\gamma}}$$

$T_3$  = Turbine inlet temperature, °R  
 $P_3$  = Total turbine inlet pressure, psia  
 $P_4$  = Static turbine exit pressure, psia

4. Pump Head Requirement,  $\Delta H$ , ft

$$\Delta H = \frac{144 (P_2 - P_1)}{\rho_1} \quad \text{where } \rho = \text{lb/ft}^3 \text{ (fluid density)}$$

\*Factor to account for pump recirculation, tank pressurant, and other miscellaneous flows.

V, E, Combustion Gas Conditioning Requirements for Turbopump (cont.)

5. Shaft Horsepower Requirement, SHP, hp

$$SHP = \frac{\Delta H * \dot{w}}{550 * \eta_p} \quad \text{where } \eta_p \text{ is the pump efficiency}$$

6. Turbine flow rate requirement,  $\dot{w}_{turb}$ , lb/sec

$$\dot{w}_{turb} = \frac{SHP * 550}{\bar{C}_{p,3-4} (T_3 - T_4) * 778 * \eta_T} \quad \text{where } \bar{C}_{p,3-4} \text{ is the average specific heat of the combustion gas from the turbine inlet to exit, and } \eta_T \text{ is the turbine efficiency.}$$

7. Percent of Total Weight Flow Required for the Fuel Turbopump,  $P_{\dot{w}_F}$ , %

$$P_{\dot{w}_F} = \frac{\dot{w}_{turbine}}{\dot{w}_{total}} * 100$$

Percentage of total weight flow required to drive both the oxygen and hydrogen turbines were determined from the above relationships over a wide range of typical operating conditions. The turbopump operating parameters were selected to cover a range associated with advanced oxygen/hydrogen engines. Input quantities were as follows:

	<u>Level 1</u>	<u>Level 2</u>	<u>Level 3</u>
$T_3$ (°R)	1600, 2000, 2400	1600, 2000, 2400	1600, 2000, 2400
$\eta_p$	0.790	0.740	0.680
$\eta_T$	0.888	0.811	0.735
$\eta_p \eta_T$	0.70	0.60	0.50

Calculations were performed for each level at each of the following chamber pressures:

$$P_c = 100, 200, 500, 1000, 1500, 2000, 2500 \text{ psia}$$

## V, E, Combustion Gas Conditioning Requirements for Turbopump (cont.)

The pump outlet pressure was assumed to be 50% greater than the chamber pressure, and the turbine inlet to outlet pressure ratio was assumed to be twenty to one. These values are representative of systems operating at conditions similar to those being considered. Fluid densities were determined from a computerized table as a function of temperature and pressure. Specific heat ratio and average specific heat for the combustion gas across the turbine were assumed as follows:

$$\begin{aligned} \text{MR} &= 5.0 \\ \gamma &= 1.3 \\ \bar{C}_{p,3-4} &= 0.815 \end{aligned}$$

Liquid temperatures at Station 1 were maintained just below saturation conditions, i.e.,

$$\begin{aligned} \text{Oxygen:} & \quad \text{for } P_1 > 50 \text{ psia, } T_1 = 176^\circ\text{R} \\ & \quad \quad \quad P_1 \leq 50 \text{ psia, } T_1 = 140^\circ\text{R} \\ \text{Hydrogen:} & \quad \text{for } P_1 > 50 \text{ psia, } T_1 = 40^\circ\text{R} \\ & \quad \quad \quad P_1 \leq 50 \text{ psia, } T_1 = 30^\circ\text{R} \end{aligned}$$

A listing of the computer program used to obtain the turbopump flow requirements together with the output from which Figure 7 was derived is given in Appendix B. Required cryogenic properties were obtained from the OXP and HYDP sub-routines discussed in the next section.

Figure 7 is a summary of the combined oxygen and hydrogen turbine flow requirements as a percentage of the total propellant flow over the desired throttling range. Several trends can be observed with respect to the percentage of propellant flow required for oxygen and hydrogen turbine operation:

- (1) The percentage increases as the turbine inlet temperature is reduced; decreasing the temperature from 2400°R to 1600°R increases the percentage by about 50%.

V, E, Combustion Gas Conditioning Requirements for Turbopump (cont.)

(2) The percentage increases as the pump-turbine efficiency product decreases; decreasing the pump-turbine efficiency from 0.7 to 0.5 increases the percentage by about 40%.

(3) The percentage decreases as the propellant flow is throttled; over the  $P_c$  range of 25:1, the turbine flow requirement decreases to about 3% of the full thrust value.

Figure 7 establishes an operating band for the throttling conditions, and point selections were made from within this band to obtain the weight flow requirements of the hot gas channels. Operating points will primarily be a function of turbopump size and material selection; 6% of the total flow rate was selected as a design point for further analysis.

## F. RESULTS

### 1. Nickel Injector

Figures 8, 9, and 10 summarize the results of the tapoff cycle heat transfer analysis. Full thrust operating conditions were investigated first because (1) they represented the "worst case"--highest propellant flow rates and heat transfer requirements--and (2) computer program modifications were required to handle the two-phase flow calculations necessary for representing the throttling conditions.

Figure 8 is a plot of hot combustion gas outlet (turbine inlet) temperature as a function of chamber pressure and throttling ratio for two injector (channel) lengths and 6% hot bleed gas flow rate. The primary consideration here is that the hot bleed gas has sufficient energy--after giving up heat to the cryogenic propellant--to operate the turbopumps. The results show that the hot gas exit temperature is strongly affected by heat exchanger channel length and hot gas flow rate.

## V, F, Results (cont.)

The minimum acceptable channel length appears to be on the order of 0.3 in. without exceeding structural limitations. The percentage of hot gas tapped from the combustion chamber was assumed to remain constant during throttling because the heat exchanger channel geometry was fixed. At the lower throttling conditions, the hot gas exit temperature drops. This, however, is not a problem because the hot bleed gas volume (percentage of combustion gas flow rate) is considerably higher than theoretically required (Figure 7), thus the total volume supplied to the turbine at throttled conditions is more than adequate.

Figure 9 is a plot showing the effect of throttling on injector face temperature at its hottest point. This location is at node 66 of Figure 5, which is the oxidizer side of the hot gas channel at the injector face. The trends are similar to those of the hot gas outlet temperature. Injector face temperature decreases with throttling--on the order of  $700^{\circ}\text{R}$  over the entire range. It is weak function of injector length, decreasing about  $200^{\circ}\text{R}$  for a 50% reduction in length. It is a strong function of hot gas flow rate; reducing the hot gas flow rate from 10 to 6% reduces the face temperature by about  $1000^{\circ}\text{R}$ . This is within  $100^{\circ}\text{R}$  of the assumed maximum of  $2460^{\circ}\text{R}$ . (The melting point of nickel is about  $3110^{\circ}\text{R}$ .)

Figure 9 indicates that the maximum injector face temperature will vary between  $2590^{\circ}\text{R}$  and  $1780^{\circ}\text{R}$  as the chamber is throttled, assuming a 6% hot gas flow rate and heat exchanger channel length of 0.3 in. Considering the maximum heat flux, the lowest face temperature occurs at node 22 of Figure 5, immediately adjacent to the fuel channel where the temperature is  $413^{\circ}\text{R}$ . The heat transfer coefficient at the injector face was calculated to be  $0.00140 \text{ Btu/in.}^2\text{-sec-}^{\circ}\text{R}$ . Using a recovery temperature of  $5487^{\circ}\text{R}$ , the maximum heat flux is approximately  $7.1 \text{ Btu/in.}^2\text{-sec}$ .

Figure 10 shows the effect of number of channels on wall and fluid temperatures at key locations. Results presented are for a 6% hot gas flow rate, 0.3-in. heat exchanger channel length, and full thrust conditions. This channel length selection results from noting trends on Figures 8 and 9. Figure 8 indicates that, the longer the channel length, the hotter the injector face temperature becomes, which is slightly above the maximum allowable at 0.3 in. With respect to hot gas

## V, F, Results (cont.)

flow rate, both the injector face temperature and the turbine inlet temperature increase with increasing hot gas flow. Hence, the minimum acceptable hot gas flow rate of 6% was selected, which, after looking at Figure 7, is sufficient to supply the required enthalpy at the full thrust condition with no margin of safety.

Figure 10 indicates that the minimum number of channels is approximately 2900, corresponding to an injector face area of 26.2 in.<sup>2</sup>. Since the key temperatures decrease significantly with an increase in the number of channels, providing more than 2900 channels would result in a greater margin of safety with respect to operating temperatures. It can be noted that the propellant outlet temperatures increase only slightly with number of channels. Throttling to lower chamber pressures results in lower temperatures, as shown on Figures 8 and 9; hence, Figure 10 represents the most severe conditions.

Pressure drop ( $\Delta P$ ) calculations were made only to assure that channel geometries selected would provide reasonable  $\Delta P$ 's. No attempt was made to optimize with respect to  $\Delta P$ . Entrance losses were assumed; momentum and frictional  $\Delta P$ 's were calculated for each case by the subroutine provided. For the full thrust, 6% hot gas flow case,  $\Delta P$ 's were as follows:

$\Delta P$ fuel channel	=	276 psi
$\Delta P$ oxidizer channel	=	1013 psi
$\Delta P$ hot gas channel	=	0.03 psi

(Fuel and oxidizer internal channel size is 0.005 x 0.050 in.; hot gas channel size is 0.050 x 0.050 in.)

It is concluded that the hot gas tapoff cycle injector concept is feasible and can operate successfully over the full throttling range specified. However, certain practical considerations, such as the extremely short channel length (0.3 in.), may tend to diminish the desirability of employing this concept.

V, F, Results (cont.)

2. Copper Injector

A single computer run was made in which copper was substituted for nickel as the raw material. Considering the two most critical parameters, maximum injector face temperature and maximum bleed gas temperature at the turbine inlet, the comparison shows:

<u>Parameter</u>	<u>Nickel</u>	<u>Copper</u>
Maximum injector face temperature, °R	2550	1440
Maximum gas temperature at turbine, °R	2780	2160

Thus, from an analytical standpoint, copper is significantly superior to nickel for this application.

Figure 11 shows the temperatures calculated at each of the various injector face nodes for both nickel and copper. While no platelet injectors have been fabricated from copper, there is nothing immediately apparent that would prevent its use. Certainly, the tapoff cycle, using a copper platelet injector, is feasible within the limitations of this analysis.

VI. ANNULAR INJECTOR DESIGN

The fundamental approach to the design of a throttlable annular injector for Phase III was the same as that employed during Phase I and Phase II; that is, to design the injector to vaporize the oxidizer prior to injection into the chamber. Warm hydrogen and liquid oxygen are supplied to the injector. As the propellants flow through the injector, there is sufficient interpropellant heat transfer to completely vaporize the liquid oxygen. This gives the oxygen circuit a flow-pressure drop relationship completely different from that of a conventional liquid system. With a conventional liquid system, the pressure drop is proportional to the square of the flow rate so that the feed system hardness--as indicated by the ratio  $\Delta P_{inj}/P_c$ --decreases as the flow rate is throttled down. However, by vaporizing the oxygen, this circuit takes on gaseous feed system behavior, which maintains the  $\Delta P_{inj}/P_c$  ratio nearly constant over a wide throttling range. This is important in the design of a throttling injector since it indicates adequate feed system stiffness can be maintained at low thrust without the necessity of using excessive injector pressure drops at full thrust.

The Phase III nickel injector design was originally to incorporate results of the Phase II injectors' cold flow heat exchanger testing and gaseous testing and would have been completed early in the program. However, after the heat exchanger results pointed out the injector heat exchanger section to be less effective than originally calculated, the Phase III injector design was suspended while five concept variation heat exchangers were fabricated, tested, and the results evaluated. After completion of the sample heat exchanger testing, design work on the injector was again initiated, incorporating the best heat exchanger design into the Phase III nickel injector. The computer program to estimate heat transfer and pressure drop was modified to include the heat exchanger results and is presented in Appendix C.

Injector modifications between the Phase II and Phase III designs were held to a minimum, consistent with available data from the cold flow work. The face dimensions and baffling technique were unchanged. The method of manifolding was

VI, Annular Injector Design (cont.)

changed to improve the observed unevenness of the heat exchange. In the Phase II design, the platelets were stacked in the direction of the minimum height (1.77 in.) of the injector face to achieve a minimum platelet stack height. However, this resulted in a wider platelet and, consequently, more unevenness in the heat exchange because the fuel has a longer distance to go from the manifolds on each side to the center of the platelet. For the Phase III design, the platelets were stacked in the opposite direction, which resulted in a higher stack height (3.46 in.) but a much narrower platelet. This allowed the platelets to be fed alternately from the fuel manifolds located on each side of the platelets and resulted in a more uniform heat exchange. The heat exchanger design changed substantially as dictated by the data from the cold flow tests reported in Section X,A. Injection velocities were based on the gaseous test series as reported in Section X,C. A major change was made to improve face cooling capability. This change was the substitution of Nickel 200 for stainless steel for injector fabrication. This improved face cooling characteristics because of the superior thermal conductivity of nickel.

The heat exchanger design selected consisted of several large channels with numerous turbulator buttons extending from one side of the channel to the other. This modification was necessary to force the liquid droplets into contact with the hot wall. In the previous Phase II design, a vapor barrier was formed which prevented the continuation of boiling at the exchanger wall, thereby greatly reducing the heat transfer coefficient prior to complete vaporization of the liquid. The turbulators effectively destroyed this vapor boundary and, in addition, increased the available heat transfer area.

The nickel injector platelet stack consisted of four types of Nickel 200 platelets (fuel separator, oxidizer separator, fuel metering, and oxidizer metering) which are stacked as shown in Figure 12.

VI, Annular Injector Design (cont.)

The fuel platelet was 0.008 in. thick and contained 0.004 in. depth-etched plenums, heat exchanger and injection sections. The fuel and oxidizer manifolds and metering passage of the fuel platelet are through-etched. Two fuel manifolds are provided: one at the right and one at the left of the platelets. These alternately direct fuel from the right to the left and from the left to the right through the triangular-shaped plenum sections of the manifold. This alternating pattern minimizes differential heat transfer to the oxidizer. The fuel platelet heat exchanger section and injection sections are both 0.050 in. wide. The pressure drop portion of the fuel platelet is 0.040 in. wide.

The fuel separator platelet is 0.020 in. thick and is depth-etched 0.012 in. in the plenum section, heat exchanger section, and injection section to match the fuel metering platelet. This results in a groove depth of 0.016 in. in these sections.

Liquid oxidizer enters the oxidizer metering platelet and oxidizer separator platelet from the manifold at the top and passes straight downward through the heat exchanger section where the oxidizer is gasified. From the heat exchanger section, the oxidizer passes into the pressure drop section, then the injection section, and then is injected axially.

The oxidizer metering platelet was 0.006 in. thick and had through-etched fuel manifolds, oxidizer manifolds, and metering passages. The heat exchanger section and injection section are depth-etched 0.004 in. Groove width in the heat exchanger section was 0.284 in. with an alternating four-row button pattern in the channel. Groove width in the metering passages and injection section was a constant 0.042 in.

The oxidizer separator platelet was 0.020 in. thick and was depth-etched 0.012 in. in the heat exchanger section and injection section. Groove widths and the button pattern match the oxidizer metering platelet. Total groove depth was 0.016 in. in the heat exchanger and injection sections. The injector face orifice details are shown in Figure 13.

VI, Annular Injector Design (cont.)

The platelets are assembled as shown in Figure 12 with the following design details resulting:

	<u>Oxidizer</u>	<u>Fuel</u>
No. of platelets	62	63
Depth of plenum, in.	--	0.016
Depth of heat exchanger passage, in.	0.016	0.016
Width of heat exchanger passage, in.	0.284	0.050
Depth of pressure drop passage, in.	0.006	0.008
Width of pressure drop passage, in.	0.042	0.040
Depth of injection passage, in.	0.016	0.016
Width of injection passage, in.	0.042	0.050
No. of orifices	1240	1386
Pattern index (distance between fuel and oxidizer orifices), in.	0.011 avg	

VII. HEAT EXCHANGER SAMPLES DESIGN

The results of the heat exchanger evaluation with the Phase II injectors, discussed in Section X,A,1, showed that the liquid oxygen was not being completely vaporized and work was therefore initiated to examine alternate heat exchanger designs. The heat exchanger designs were evaluated in the same manner as the Phase II injectors--by flowing gaseous hydrogen in its own circuit and then substituting liquid nitrogen for the liquid oxygen in its circuit. In this manner, the most efficient heat exchanger configuration was determined by visual observation. There were five different designs, four new configurations and one configuration similar to the Phase II injectors and preliminary injector design for Phase III. Figure 14 shows the design configurations.

Each sample consisted of twenty-four 20-mil-thick platelets (12 fuel and 12 oxidizer), thus making a stack approximately 0.50 in. thick. The platelet contained only the heat exchanger portion of a regular injector platelet to minimize the size and cost of the samples. Each platelet contained 20 channels, which was similar to the preliminary Phase III design. All platelets, except Type II of Figure 14, were depth-etched halfway through to form the flow passage. Type II was depth-etched 5 mil on each side, which butted together to form the 10-mil-deep passage. Type I of Figure 14 shows the design configuration similar to the Phase II injectors. This configuration had straight through channels and was used as a standard for comparison purposes. The four remaining configurations were designed to generate mixing of the core of liquid and break up the vapor film along the heated wall while still maintaining a low level of pressure drop. This was done by putting obstructions (buttons) in the oxidizer channel only. Four designs were deemed necessary to fully investigate tradeoffs between minimum pressure drop, minimum heat exchanger length, and maximum mixing.

Type II of Figure 14 had 2.5-mil bars approximately 0.30-in. apart and alternately on one side of the channel and then the opposite side. To fabricate this design, it was necessary to depth-etch each platelet on both sides.

VII, Heat Exchanger Samples Design (cont.)

Type III and IV of Figure 14 were very similar in design. The only difference was in the height of the button in the channels. Type III had 10-mil full height (across the channel) buttons which Type IV had buttons that were half as high--5 mil. The buttons were spaced such that the fluid did not have a straight path down the channel but instead had to move back and forth on its route from the manifold to the face.

The last configuration, Type V, had seven large channels instead of 20 smaller channels. In place of where the land between the channels would normally be, buttons were substituted to increase the heat transfer area. Again, the buttons were spaced such that the fluid had to move back and forth on its route to the injector face.

The manifold feed system for each configuration was the same in all cases. Liquid oxidizer (simulated by liquid nitrogen) entered the heat exchanger portion of the platelet from one manifold at the top. Fuel (gaseous hydrogen) entered from two separate manifolds located on the right and left sides of the platelet. These alternately direct fuel from the right to the left and from the left to the right through the triangular-shaped manifolds. This alternating pattern minimized differential heat transfer to the oxidizer.

Stainless steel was used for platelet fabrication rather than the nickel proposed for the actual Phase III injector. This substitution was made because nickel sheet stock was in short supply. The substitution had an insignificant influence on test results for two reasons. First, the metal thermal resistance was not a major resistance in the heat exchanger; and second, the test data were evaluated primarily by comparison of the new patterns with each other and against the Phase II control pattern.

VIII. WATER-COOLED CHAMBER DESIGN

To overcome duration deficiencies discovered in the original chamber design during Phase II testing, it was determined that the Phase II chamber should be water cooled, have a single contour, and be capable of operating at pressures up to 2500 psia. The water cooling permitted long duration firings necessary to gather more reliable performance data. The simplified chamber contour improved the reliability of the performance data over the Phase II testing data.

The chamber was designed to be capable of operating at a mixture ratio of 5:1 over a range of chamber pressures from 75 to 2500 psia. Cooling was achieved by water making a single pass (from injector to nozzle exit) through small coolant channels of 0.055 in. height and 0.050 in. width, spaced 0.050 in. from each other (see Figure 15). The wall thickness from the hot gas side to the coolant side was nominally 0.030 in. The chamber material was oxygen-free copper. Two chamber gas-side configurations were investigated: a noncoated gas-side surface and a 0.002-in.-thick hafnia gas-side surface coating. At the maximum intended chamber pressure of 2500 psia, the predicted heat flux in the throat region was  $97 \text{ Btu/in.}^2\text{-sec}$  for the noncoated configuration and only  $30 \text{ Btu/in.}^2\text{-sec}$  for the 0.002-in. hafnia-coated chamber.

The combustion chamber was a two-dimensional copper/stainless steel assembly. The chamber had a contraction ratio of 4.8:1 and a 2:1 expansion ratio nozzle. The unit was capable of operation up to 2500 psia chamber pressure as confirmed by a stress analysis of the design. The basic coolant channel configuration consisted of seventeen channels on each of the two chamber contour walls and thirty-six channels on each side of the two chamber flat walls.

The housing was machined from stainless steel and incorporates four inlet and four outlet manifolds, distribution manifolds, and provides the sealing surface for the O-rings on the copper liner. It also incorporated injector-chamber interface and seal surface on the forward end and attachment interface for the nozzle extension on the aft end. Figures 16 and 17 show the assembly details.

## VIII, Water-Cooled Chamber Design (cont.)

An uncooled copper insert of the same configuration as the cooled chamber configuration was designed to fit the Phase II housing. This chamber was used for the checkout tests with the Phase III nickel injector. It permitted valve sequencing and manifold fill time checkout testing without risking the more expensive cooled chamber. The uncooled chamber was also used for the  $\text{GH}_2/\text{GO}_2$  hot firing testing.

## A. HYDRAULIC ANALYSIS

The various thermal and hydrodynamic characteristics of the water-cooled copper chamber were obtained from the "HEAT"<sup>(1)</sup> computer program. This program is used for the analysis of regenerative cooling. The temperature and pressure, as well as transport properties, Mach number, etc., of the coolant are determined at each station along the contour by a "marching" calculation that proceeds in the direction of the coolant flow. A variety of coolant passage geometries may be treated. The heat flux and wall temperature are also calculated at each station; two-dimensional enhancement of heat conduction in channel walls is accounted for by means of a fin-type equation. There are a number of analytic options for calculation of the coolant boiling and nonboiling heat transfer coefficients, as well as the gas-side heat transfer coefficients. These options, especially those for the coolant, allow the best choice to be made for the actual fluids under consideration.

A hydraulic analysis of the water-cooled copper chamber was also performed to obtain estimates of the entrance and exit losses due to turns, entrance effects, and sudden expansions. This was necessary since the "HEAT" program can only treat the pressure losses occurring within the coolant channel. Figures 18 through 28 are a summary of the hydraulic results.

Figure 18 shows the predicted overall pressure drop from coolant source to coolant discharge, as a function of the coolant flow rate through a single chamber side wall. Differentiation is made between the contour sides with 17 coolant channels each, and the flat sides with 36 coolant channels each. An average roughness of 39 ( $39 \times 10^{-6}$  in.) was used in the channel friction pressure drop equations, since this was the average of some measurements taken from channels in a test chamber wall.

---

(1) Hester, J. N., Chan, J., Thermocal - Phase I, Aerojet-General Corp., Report No. 9600:M014, September 1969.

## VIII, A, Hydraulic Analysis (cont.)

A total of three measurements were taken per chamber side wall, in three different channels, and at three different axial locations. These measurements were taken at the channel bottom only. There was a factor of 4 variation in measured roughness from channel to channel.

Figure 19 relates the coolant flow rate as a function of pressure drop for a contour side, from the coolant supply to three different locations. These locations are in the coolant channel at the injector end, at the throat section, and at the coolant discharge tube downstream of the chamber and its exit manifold. Figure 20 relates the same parameters as does Figure 19, but for the flat side. These curves are used when it is desired to obtain a specific coolant pressure within the channels at a certain location. An example of this would be the determination of the supply pressure required to obtain a coolant pressure at the throat section equal to that of the contained free-stream gas pressure. The following is a table of throat section free-stream pressures as a function of chamber pressure:

<u>P<sub>c</sub> (psia)</u>	<u>P<sub>throat</sub> (psia)</u>
2500	1411
2000	1229
1500	846
1000	565
500	282
200	113
100	56.5

## B. THERMAL ANALYSIS

The governing assumptions of the thermal analysis were:

1. Use of 100% c\* combustion efficiency for determining recovery temperatures.
2. Use of a factor of two times the nominally calculated gas-side heat transfer coefficient at the injector end and linearly varying with axial length to a factor of one at the throat section, and remaining at one throughout the expansion region.

## VIII, B, Thermal Analysis (cont.)

3. Hines correlation used in "HEAT" program for nonboiling coolant heat transfer coefficient.

$$4. \quad h_{l,boiling} = h_l \left( \frac{T_{wall}}{T_{sat}} \right)^{1.3}$$

where  $h_l$  = nonboiling heat transfer coefficient, Btu/in.<sup>2</sup>-sec-°F  
 $T_{wall}$  = coolant side wall temperature, °R  
 $T_{sat}$  = local coolant saturation temperature, °R

5. Coolant pressure schedule chosen such that the coolant pressure equals the gas pressure at the throat section.

$$6. \quad \phi_{BO} = 5.1 + 0.86 \frac{V_L \Delta T}{1000} \quad (1)$$

where  $\phi_{BO}$  = the burnout heat flux  
 $V_L$  = the local velocity, ft/sec  
 $\Delta T = T_{wall} - T_{sat}$

7. The thermal conductivity used for the hafnia coating was  $1.85 \times 10^{-5}$  Btu/in.-sec-°F.

## C. NONCOATED CHAMBER

Figure 21 is a summary of the coolant flow requirements as a function of chamber pressure and families of throat section  $R_{BO}$ .  $R_{BO}$  is defined as the ratio of predicted operating heat flux to the predicted burnout heat flux. The maximum recommended operational  $R_{BO}$  value was 0.75.

(1) "Heat Transfer Characteristics of 98% H<sub>2</sub>O<sub>2</sub> at High Pressure and High Velocity," Technical Report AFRPL-TR-66-263, AGC Report 10785-SR-1, August 1966, D. C. Rousar and N. E. Van Huff.

## VIII, C, Noncoated Chamber (cont.)

Figure 22 shows the throat section  $R_{BO}$  as a function of coolant flow rate and families of chamber pressures. The coolant flow rates shown on both Figures 21 and 22 are for a single chamber side wall. The total chamber coolant flow requirement would then be twice the sum of the indicated flow for a flat and a contour chamber wall.

Figure 23 shows the throat section gas-side wall temperature as a function of  $R_{BO}$  and families of chamber pressure. The abrupt change in the temperature profile for all chamber pressures in the  $R_{BO}$  range of 0.6 to 0.7 is indicative of the change from nonboiling to nucleate boiling at the coolant wall surface.

Figure 24 shows the throat section gas-side wall temperatures as a function of chamber pressure and families of  $R_{BO}$ .

## D. COATED CHAMBER

Figure 25 is a summary of the coolant flow requirements as a function of chamber pressure and families of throat section  $R_{BO}$ . The slight saddle in the curves from a chamber pressure of 1500 to 2500 psia is a function of the coolant properties corresponding to a coolant pressure of 850 to 1400 psia. If a comparison of required coolant flow is made between the coated and noncoated cases (Figures 21 and 25) for a  $R_{BO}$  level of 0.6 at a  $P_c$  of 2500 psia, the noncoated chamber requires 3-1/3 times the coolant flow of the chamber with a 0.002-in. hafnia coating.

Figure 26 shows the throat section  $R_{BO}$  as a function of coolant flow rate and families of chamber pressures. Again, the coolant flow rates given on Figures 25 and 26 are for a single wall section. Figures 25 and 26 also show that, for a given operation  $R_{BO}$  level in the range of chamber pressures from 1000 psia to 2500 psia, the coolant flow rate is virtually constant for the coated chambers.

VIII, D, Coated Chamber (cont.)

Figure 27 shows both the throat section coating gas-side wall temperatures and the coating/copper wall interface temperatures as a function of  $R_{BO}$ .

Figure 28 is a restatement of the information shown in Figure 26, giving the throat section coating, gas-side wall temperatures, and the coating/copper wall interface temperatures as a function of chamber pressure and families of  $R_{BO}$ .

IX. FABRICATION

A. INJECTOR ASSEMBLY

Two injectors made out of Nickel 200 material were fabricated during this phase of the program. The following is a discussion of the fabrication procedure used on each injector.

An order for the Nickel 200 sheet stock material for the platelet was placed early in Phase III of the program. The thicknesses were based on the preliminary design. The need for placing the order early was due to an International Nickel plant strike which had been on for three months and which resulted in limiting the available thicknesses to then current stockpiles, which were being reduced rapidly. The heat exchanger design investigation which followed placing the order was, at the time, not thought to greatly affect the platelet thickness. However, the heat exchanger investigation did modify the design and made the design of the injector platelets somewhat more complicated in the form of depth-etched separators and metering platelets to get the proper orifice size.

1. Sample Assembly Stack No. 1

Prior to committing the SN 1 injector to its first braze cycle, a sample assembly stack was made. The purpose of the sample platelet assembly was to verify the validity and suitability of the selected plating, assembly, and bonding procedures. The first task in fabricating the sample stack was the plating of braze alloy on alternate platelets. The plating technique used was the Kanigen process for electroless nickel plating. This is a process whereby the part to be plated is submerged in the plating solution for a specific period of time which is dependent on the plating thickness desired. Plating of the metering platelets proved unsuccessful in that the platelets were too flimsy to withstand the plating procedures without damage. The separator platelets were therefore plated in sufficient quantity to complete a sample assembly stack and one complete injector plus spares to permit destructive testing for determination of the plating thickness and uniformity.

IX, A, Injector Assembly (cont.)

The platelets were assembled by alternatively stacking separator and metering platelets on nickel guide pins which assure proper alignment. Twenty-five platelets were used in the sample stack. The assembly was then bonded in a dry hydrogen atmosphere. Thermocouples were placed at various locations on the sample and limits on the furnace cycle were established such that a maximum temperature variation of 50°F between the high and low reading thermocouple was permitted.

The sample stack was tested for leakage using gaseous nitrogen. No leakage was detected. The sample was then sectioned at several locations so that any channel plugging from deformation or excess braze alloy could be observed. No deformation or plugging could be detected. The procedure and braze alloy thicknesses were therefore considered acceptable and the assembly of the SN 1 injector was initiated.

2. Injector Assembly SN 1

The first injector platelet assembly was accomplished using the same procedures used for the sample stack using the identical furnace cycle and loading. The complete injector contains 264 platelets. Pressure testing of the platelet stack subassembly following brazing revealed external leakage, primarily in the oxidizer manifold area, which appeared to be caused by slight separations between platelets which, for some reason, never contacted each other. In areas where the platelets had been in contact, the bond appeared excellent. The nature of leaks was such that they could be effectively sealed on a subsequent braze. Assembly of the unit was therefore continued.

The platelet assembly was machined flat using the technique developed in Phase II of this program and a second braze cycle was conducted to attach the end plates. The end plates also contain the fuel and oxidizer manifolding which permits a more quantitative leak test. During the second braze, the external leak

IX, A, Injector Assembly (cont.)

areas were covered with braze alloy. Leak testing of the assembly following the second braze cycle revealed almost total success in sealing the external leakage. Only one minor external leak still existed. A slight intermanifold leak was observed when the gaseous nitrogen pressure was increased to 120 psi. This leak was not detectable at 30 psi. It was concluded that the injector assembly should continue since the intermanifold leak was slight.

The injector subassembly was machined to accept the flange and a third braze cycle was conducted to attach the flange to the subassembly. The minor external leak area was coated with braze alloy prior to the third cycle.

Pressure testing following the third braze cycle indicated that the external leakage had been completely corrected; however, the intermanifold leak had become more severe. Work was suspended on the injector at this point until the SN 2 injector was successfully fabricated. The procedure used in repairing the intermanifold leakage on SN 2 was the removal of the oxidizer manifold section so the intermanifold leak could be repaired and then brazing a new manifold cover in place as shown in Figure 29. The SN 1 injector was therefore completed in this method. Figure 30 shows the injector.

3. Injector Sample Stack No. 2

One of the major problems encountered in the assembly of the first injector was in assessing the quality of the electroless nickel braze alloy. The primary difficulty lay in the fact that the braze alloy (nickel plated on nickel) cannot be detected visually. The question arises: is the platelet actually plated? And is it plated over the entire surface? On some of the platelets used in the injector assembly, a variation in surface reflectivity from one area to the other was observed which could be an indication that a portion of that platelet had not accepted the plating. If this were the case, it could account for the leakage experienced on the first injector. The method for overcoming this difficulty was to

IX, A, Injector Assembly (cont.)

flash a thin coating of copper on the platelets prior to nickel plating. This permitted ready qualitative inspection of the platelets after nickel plating since, anywhere copper shows, the platelet has clearly not been nickel plated.

A sample assembly using this technique was fabricated to verify that there were no unanticipated metallurgical peculiarities that would influence the bond. The separator platelets were flashed with a maximum of 0.00001-in.-thick copper and delivered to the plater for nickel plating. The platelets were visually inspected following nickel plating. The quality appeared better than those plated using the virgin nickel platelets. Figure 31 is a metallurgical photograph showing the uniform thickness of the plating and the copper flash. The sample, consisting of 11 platelets stacked in an identical sequence to that used in the injector, was then sectioned to check for braze alloy plugging. No plugging was observed. Samples were then prepared for metallurgical examination of the bond quality. Figure 32 shows the excellent bond quality between the platelets. This plating technique was therefore selected for use in fabricating injector SN 2.

4. Injector Assembly SN 2

A thermal analysis of the furnace cycle used to bond the SN 1 platelet assembly was performed prior to attempting the SN 2 platelet assembly braze. It was postulated that perhaps the furnace heat cycle (3.5 to 4 hr from room temperature to braze) was too rapid, thus resulting in large thermal gradients or inadequate center temperatures causing poor brazing quality.

A simplified analysis was run on the braze assembly. The following assumptions were used:

- (1) Thermal radiation was neglected.
- (2) Free convection from the H<sub>2</sub> is the only mode of heat transfer to the part.

IX, A, Injector Assembly (cont.)

- (3) The boundary temperature (i.e., the hydrogen temperature) is constant.
- (4) Thermal properties of the part are constant.
- (5) The part is homogeneous (i.e., voids due to etching were neglected).

The results of this analysis indicated maximum thermal gradients of approximately 18°F/in., which does not appear excessive. However, the void spaces due to etching will lower the effective thermal conductivity and uneven heating due to part configuration could cause substantially higher thermal gradients within the part. The furnace heating cycle was therefore extended to eight hours. In addition, the furnace was cooled prior to placing over the retort to eliminate high initial temperature gradients.

Pressure testing of the platelet assembly after bonding revealed leakage substantially identical to that previously observed in SN 1 injector. The leakage was both external and intermanifold and was concentrated in the top (oxidizer manifold) area. It appeared that the platelets had not contacted in spots. It was conjectured that the dead weight loading used was not sufficient to force the platelets into complete contact. Two hundred fifty pounds of weight was used, which was the maximum available. This amounts to 8 psi loading because of the large platelet size. This loading is somewhat less than is ordinarily used for bonding platelet injectors.

The platelet assembly was recycled through the ALRC diffusion bonding furnace. This furnace is capable of applying a much higher load. The furnace employs an externally loaded ram in lieu of the dead weight system. Twenty-four hundred eighty pounds of load was applied to the part during this recycle. Subsequent pressure testing indicated no change in the leakage characteristics

IX, A, Injector Assembly (cont.)

The platelet assembly was then machined as shown in Figure 29 to remove the oxidizer manifold section and permit access to the platelets for repair of the intermanifold leak. Pressurizing the fuel manifold with the oxidizer platelet passages exposed revealed a small leak which was repaired by a subsequent braze cycle. A new monolithic oxidizer manifold was constructed from nickel and bonded in place as shown in Figure 29. Pressure checking following these repair procedures revealed a leak-free unit. Fabrication of the assembly was then completed by machining the injector face into the transverse baffle configuration selected from Phase II testing.

B. WATER-COOLED CHAMBER

Three water-cooled copper inserts and two stainless steel housings were fabricated. Two complete chambers (copper insert and stainless steel housing) were originally to be fabricated. However, with the advent of an OFHC material problem, a third insert was fabricated as a backup. All three copper inserts were used during the test program.

Sample experiments were conducted prior to the first brazing cycle of the water-cooled chamber. The experiments were to verify the acceptable braze filler metal thicknesses for a satisfactory bond at the interface of the chamber liner gas-side cover plate and chamber liner passage plate without flooding of the water passage with braze alloy. Based on the sample experiment, it was determined that a braze filler metal thickness ranging from 0.001 to 0.003 in. would provide good bonding without flooding the passages.

Upon completion of the SN 1 water-cooled chamber and subsequent hydrotesting, numerous small leaks were discovered in the copper material at the injector-to-chamber interface; the leaks were attributed to hydrogen embrittlement of the copper material. The chamber material purchased was certified to be OFHC

IX, B, Water-Cooled Chamber (cont.)

copper, which is not subject to hydrogen embrittlement. A subsequent investigation by Aerojet and American Brass and Copper Company (who supplied the material) established that a large portion of the copper material was extra tough pitch copper and not oxygen free. This would have resulted in the hydrogen embrittlement experienced with the first chamber and its subsequent leaking through the copper material.

To preclude using contaminated or commercial copper again, a procedure was developed to check the OFHC copper. First, a skim cut (0.050 to 0.060 in.) was made on all surfaces of the copper stock. This skim cut removed any contaminants (oxides) present on the surface which could contaminate the copper further by penetrating the material during the hydrogen braze cycle. Second, the material was measured and then put through a hydrogen braze cycle. If any material growth or surface blistering had been evident, the material would be discarded. Subsequent material showed no evidence of blistering or growth, as a small sample from each piece of material stock was cut off, etched, and then microscopically examined for voids. The latter is the method used by the mills to determine the quality of the copper. This procedure ensured the quality of the OFHC copper for the SN 3 chamber.

Additional flow testing of the first chamber revealed the pressure drop to be substantially higher than that predicted by the design calculations. At the time of discovery of the out-of-specification copper, the SN 2 water-cooled chamber was 60% complete. When the high pressure drops were uncovered, a decision was made to complete the SN 2 chamber to a stage where flow testing could be conducted to investigate the pressure drop of the chamber. A vacuum braze cycle looked promising to circumvent the hydrogen embrittlement problem, but additional investigation with copper brazing experts at Stanford Research Center and experiments showed that a vacuum braze cycle with contaminated copper would result in a worse part than if a hydrogen braze cycle was used. Thus, the SN 2 chamber was brazed in hydrogen similarly to the first chamber.

IX, B, Water-Cooled Chamber (cont.)

Flow testing results with the SN 2 chamber were essentially the same as for the SN 1 chamber--substantially higher than the design predicted. The injector end of the one flat side of the chamber was then machined off so the channel could be visually observed, and the channels were found to be partially plugged with Stop-Off. Stop-Off is a material designed for furnace use and acts as a barrier to molten brazing filler metals by preventing capillary action. Stop-Off was used in the channels during the first braze cycle to preclude any braze alloy plugging the channels. Normally, a 10 to 15% hydrochloric acid solution will completely remove the Stop-Off with no effect on the copper; however, in this case, nothing was found which would remove the Stop-Off. The manufacturers of the Stop-Off (Wall Colmonoy Corp.) had not experienced this problem before and could not suggest any removal procedure other than ones already tried.

To salvage the SN 2 chamber, 0.200 in. of the injector end of the chamber was machined off and the Stop-Off removed by rodding out the channels. A copper piece was later brazed in place to form the injector end closure.

The rework of the SN 1 chamber involved machining off 0.200 in. from both the injector and nozzle end of the chamber to allow access to the coolant channels. This chamber was originally brazed with 0.003 in. foil and the primary cause of pluggage was discovered to be brazing alloy and not Stop-Off as was the case in the SN 2 water-cooled chamber. With both ends off the chamber, all channels could be opened up. A copper piece was then brazed in place on each end to form the end closures for the channels. Flow testing showed the chamber to have a slightly higher pressure drop than calculated due to some remaining alloy in the channels but leaktight otherwise.

The SN 3 chamber, made with copper verified to be OFHC, was successfully completed with no rework required. It was brazed with 0.002 in. foil and using a different type Stop-Off which was easily removed from the channels. Flow testing showed the chamber to be leaktight and the pressure drop to be close to the predicted pressure drop as shown in Figure 18.

IX, B, Water-Cooled Chamber (cont.)

In addition to the water-cooled chambers, one uncooled chamber was fabricated. The uncooled chamber consisted of a copper insert with the same internal configuration as the cooled chamber and was designed to use the Phase II stainless steel housing.

C. NOZZLE EXTENSION

For testing above the 500 psia  $P_c$  level, a nozzle extension was designed. The extension provided a sharp edge to prevent attachment of gases to the back of the water-cooled chamber at the higher pressure tests. The extension increased the exit ratio from 2.07:1 to 3.70:1. It consisted of an outside steel housing with phenolic inserts which were replaceable. Figure 33 shows the nozzle extension.

D. HEAT EXCHANGER SAMPLES

Each sample consisted of twelve oxidizer platelets and twelve fuel platelets assembled alternately on top of one another. One end plate had fittings for flowing the  $LN_2$  and  $GH_2$ . The other end plate was a blank. The platelet stack and end plates were brazed at the same time. All units were leak tight. Five samples were fabricated and machined to the configuration as shown in Figure 34.

X. TEST RESULTS

A. HEAT EXCHANGER EVALUATION

1. Phase II Injector Heat Exchanger

An investigation of the Phase II injector heat exchanger performance was conducted by flowing liquid nitrogen through the liquid oxidizer circuit and then flowing gaseous hydrogen through the fuel circuit in increasing quantities until the liquid nitrogen was demonstrated to be completely vaporized by visual and photographic observation. The purpose of this investigation was to determine whether improvements in the heat exchanger design were needed.

A thermal analysis was conducted in order to determine conditions for the liquid nitrogen/gaseous hydrogen flow tests of the Phase II injector heat exchanger. Since local channel temperature measurements were difficult to make, it was determined that the method of verification of the heat exchanger performance should be visual confirmation by photographing the exit quality of the nitrogen after it passed through the injector. By maintaining a fixed liquid nitrogen flow through the injector and varying the amount of gaseous hydrogen at the injector inlet, it was possible to qualitatively determine the nitrogen quality as a function of mixture ratio and to note the uniformity of quality across the injector face.

The objective of the analytical effort was to determine inlet flow rates, temperatures, and pressures which yield the desired nitrogen qualities. The observations made were subjective, since it was difficult to estimate quality levels in the two-phase region. The model used to make the nitrogen quality prediction was essentially the same as that used to predict injector conditions in the Phase II work.

X, A, Heat Exchanger Evaluation (cont.)

Two equivalent thrust levels were selected for evaluation for both the fine- and coarse-pattern injectors. One thrust level selected was 12% of rated thrust ( $P_c = 200$  psia) and the other thrust level selected was 3% of rated thrust ( $P_c = 50$  psia). The lower thrust levels were picked because it was necessary to stay well below the critical pressure of nitrogen (492 psia) or the nitrogen quality becomes meaningless.

The equivalent  $N_2$  weight flow for pressure drop simulation was calculated by multiplying the oxygen flow rate at the thrust level tested by the ratio of the square roots of the specific gravity of liquid nitrogen at 150°R and liquid oxygen at 200°R.

Orifice sizing required to maintain chamber pressure simulation was determined by calculating the mean temperature of the nitrogen-hydrogen mixture flowing out of the injector and then using this, together with the desired flow rate, pressure, and chamber diameter, a flow Mach number was calculated. The Mach number was used to calculate the required throat area.

Two difficulties became apparent during the initial checkout tests of the setup. First, the view was obstructed by the formation of frost on the outer surface of the transparent acrylic chamber. Second, the acrylic chamber tube contracted when  $LN_2$  was introduced, resulting in a leak between the transparent chamber and the injector. This leakage also obscured visual observation and prevented attaining the desired chamber pressures. Partial correction was achieved by spring loading the studs affecting the chamber seal. The hardware was further modified to improve the sealing surfaces, and another concentric transparent jacket was added around the original transparent chamber. This formed an annulus which was purged with  $GN_2$  during testing to prevent accumulation of frost. Figure 35 illustrates the modified fixture with the baffled fine-pattern Phase II injector in place and Figure 36 shows the coarse-pattern Phase II injector set up on the stand with the fixture in place ready for testing.

X, A, Heat Exchanger Evaluation (cont.)

The cold flow tests were run at a maximum equivalent thrust of 12% of the rated thrust, limited by the lower critical pressure of nitrogen and by the strength of the acrylic tube chamber material. Liquid nitrogen at approximately 160°R and gaseous hydrogen at approximately 550°R were injected using both the double baffled fine-pattern injector and the flat-face coarse-pattern injector.

Initially, high speed motion pictures were taken, but these were generally unsatisfactory due to inadequate lighting. All movies were taken using the double-baffle fine-pattern injector. At the time when the flat-face coarse-pattern injector was being set up for flow testing, a change was made to permit still type photographic coverage.

The test procedure ultimately developed was to run the liquid nitrogen for approximately 30 sec in order to cool down the hardware (to minimize heat transfer due to injector stored heat), then admit ambient temperature hydrogen to the injector and run for approximately 15 sec until a steady quality level was observed on the TV monitor, at which time a Polaroid still photograph was taken. Upon verification of the desired condition being achieved by looking at the Polaroid photograph, a permanent negative film would then be inserted into the camera and a duplicate test run made and photographed.

Visual observation of the tests indicated two situations which are believed to be the major cause of the performance loss experienced in Phase II. The first was that the heat exchange was not uniform. This is attributed to nonuniform heat exchange surface in the injector manifold area. The second was that the heat exchanger has insufficient surface area. This is attributed to a poor assumption of the heat transfer coefficient in the boiling portion of the heat exchanger. The performance loss resulting from the heat exchange inadequacy arises because of the large mass and mixture ratio maldistribution possible.

X, A, Heat Exchanger Evaluation (cont.)

Figure 37 shows the test results with the flat-face coarse-pattern injector going from liquid (A) to very few drops (D). The level at which the computer program predicted complete vaporization was condition (B) of the figure. The unevenness of the heat exchange can easily be seen in condition (B) of the figure. Note the core of drops in the center of the injector, indicating the maldistribution.

Complete vaporization of the oxidizer in the heat exchanger is actually not vital to the concept operation in itself. A small amount of oxidizer injected as a liquid will have an insignificant effect on performance and a substantially constant  $\Delta P_o/P_c$  relationship over the throttling range can still be maintained. The importance lies in maintaining uniform flow distribution. Slight imbalances in heat exchange which might be caused by slight irregularities in flow or heat exchanger surface can be amplified into major imbalances. This comes about in the following manner: assume a given channel receives slightly more heat; the oxidizer is then more completely vaporized in that channel, which increases the pressure drop, thus causing less oxidizer to flow in that channel and more in a channel receiving less heat. The cycle is repetitive until a state of balance is achieved.

Based on these results, four improved heat exchanger designs were tested in this same apparatus and the best one was selected for incorporation into the Phase III injector.

## 2. Sample Heat Exchangers

The purpose of these tests was to establish the best heat exchanger out of four new designs. Five heat exchanger samples were actually flow tested with one sample being similar to the Phase II design and used for a baseline comparison. The samples were flowed with liquid nitrogen and gaseous hydrogen in the same manner as the Phase II injectors. Figure 38 shows a sample setup for testing. A set rate

## X, A, Heat Exchanger Evaluation (cont.)

of liquid nitrogen would be flowing through the sample and then gaseous hydrogen in increasing quantities would be flowed until the quality desired was observed visually.

Photographs were taken at selected points so a comparison could be made between the various designs. Figure 39 shows the comparison of the samples at a  $\dot{w}_H = 0.025$  lb/sec and  $\dot{w}_N = 0.33$  lb/sec. Three of the four new heat exchanger designs (III, IV and V of Figure 14) proved to be better than the Phase II injector design (I of Figure 14). The remaining design (II of Figure 14) was similar in heat exchanger performance to the Phase II design. Of the three configurations that were better than the Phase II design configuration, one proved significantly better than the other two and had considerably less pressure drop. On this basis, it was selected for use in the Phase III nickel injector.

## B. MASS DISTRIBUTION

1. Phase II Injectors

These tests were directed toward obtaining additional mass distribution data in an effort to explain the unexpected low performance obtained when these injectors were tested at low chamber pressures and nominal mixture ratio. The tests consisted of flowing water through the injector and systematically collecting the fluid for volumetric measurement. Figure 40 shows the mass distribution test fixture. The data were then plotted to map the injector mass and mixture ratio distribution. Each circuit was tested individually at 4 lb/sec  $H_2O$  flow. This provided a reasonable indicator of flow distribution for these tests.

The tests were conducted on both the baffled fine-pattern and flat-face coarse-pattern injectors used during the Phase II program. Data on the baffled fine-pattern injector were inconclusive because the water adhered to the baffle wall, thus causing an apparent low mass distribution in that vicinity and an unusually high mass distribution at the baffle tip. This phenomenon is known as the Coanda effect and has been observed on previous HIPERTHIN injectors.

X, B, Mass Distribution (cont.)

The results of the flow distribution for the Phase II flat-face coarse-pattern injectors are shown in Figures 41 and 42 for the fuel and oxidizer systems, respectively. Since the flow tests are conducted without interelement heat transfer, the oxidizer system must be evaluated cautiously. Referring first to the fuel (Figure 41), the water flow is depicted over the entire face of the injector. The flow outboard of the injector face square is indicative of peripheral spray gathered by the collector. The five rows are presented as overlays to define the two-dimensional flow profile. The fuel system exhibits excellent flow characteristics except for row A and station 1 of row B. The flow in row A is indicative of the front edge of the injector overlapping row A in part with the first full row in row B. The one low point of row B at station 1 is indicative of partial plugging or misdirected orifice elements. With the collector located 2 in. from the injector face, any misdirection of flow will form a coalescence which will tend to distort the flow profile in the absence of combustion. Generally speaking, this flow profile is considered good and insufficient to produce significant mixture ratio maldistribution performance losses or uneven heating of the oxidizer.

The oxidizer circuit (Figure 42), on the other hand, denotes an undulating flow profile, particularly in rows B and E. Row D denotes excellent flow distribution. Reviewing row A first, the effect of injector placement partially through the row is noted. The fuel system exhibited a similar effect. Row E denotes a very likely sign of plugging at station 5. This condition would be aggravated when heat transfer is imposed, causing a mixture ratio maldistribution. Row C flow characteristics indicate higher flow at station 1 with a gradual reduction to station 7. Possible plugging of station 7 of row C is denoted by the high flow of station 8 and the low of station 7. The variations of flow in row B most likely results due to angled orifice sprays rather than several points of plugging. Looking back across the rows, the flow appears fairly uniform with no major row-to-row variations.

X, B, Mass Distribution (cont.)

In summary, it is concluded that flow distribution of the coarse-pattern injector is considered uniform from a maldistribution performance loss point of view. The localized plugging denoted in the oxidizer flow can produce a performance loss but is of insufficient mass percentage to greatly affect performance. The fuel distribution is excellent and should produce even heating of the oxidizer and even injection of the fuel.

2. Sample Heat Exchangers

Flowing of the five sample heat exchangers on the mass distribution flow device was conducted to check for manifold maldistribution. A change had been made to the manifolding of the five samples in an effort to improve the evenness of the heat exchange in the manifold area. The change consisted of alternately feeding the fuel from the left side and then the right side instead of feeding from both sides to the center. The results of the flow distribution for the five samples are shown in Figures 43, 44, 45, 46, and 47 for the fuel and oxidizer of each.

No significant differences were noted in flow distribution between the Phase II injector and the sample heat exchangers. The manifolding changes made to the sample heat exchangers were to improve the heat exchange and therefore would not be noticeable in a water flow test.

C. HOT FIRING

1. GH<sub>2</sub>/GO<sub>2</sub> Hot Firing of Phase II Injectors

A total of 47 tests were conducted using gaseous hydrogen and gaseous oxygen as propellants with the double baffle fine-pattern Phase II injector. Three tests utilized the Phase II chamber hardware and the remaining tests utilized the Phase III two-dimensional uncooled chamber hardware. The tests covered the following wide range of operating conditions:

X, C, Hot Firing (cont.)

Chamber pressure	30, 50, 100, 200 and 500 psia
Thrust ( $\epsilon = 40:1$ )	60 to 1575 lbF
Mixture ratio (O/F)	1.4 to 10.2
Vacuum specific impulse efficiency	87.4 to 95.9%

All tests were analyzed using the ICRPG Standard Performance Evaluation Procedure to define the magnitude of the various specific impulse losses so that the energy release loss of the injector could be determined.

The resulting performance data are tabulated in Table I, giving the test number, its operating point, the fuel and oxidizer injection velocities, vacuum specific impulse, and the energy release efficiency. These data have been primarily analyzed in terms of energy release efficiency in an attempt to correlate the data with that presented in the Phase II program final report.

At the completion of the Phase II program, three characteristics were defined which tended to explain the resulting performance data. Highest performance was obtained at low mixture ratios, high chamber pressure, and high velocity ratio. It was therefore the intent of the gas/gas fine-pattern injector test program to evaluate the performance influence of these three parameters in the absence of the heat exchanger vaporization process of the oxidizer.

With this reference established, the results of the  $\text{LN}_2/\text{GH}_2$  heat exchanger tests previously discussed should be noted. In these tests, sufficient flow maldistribution was evidenced to indicate a possible overriding mixture ratio maldistribution loss (MRD) effect on the previously obtained data. Therefore, correlation of the gas/gas tests with the Phase II data is highly questionable.

X, C, Hot Firing (cont.)

The tabulated data are presented as a function of mixture ratio and appear in Figure 48. Symbol coding denotes chamber pressure, injector flow condition and chamber geometry. This presentation of the data indicates a wide data scatter with two apparent data trends. Increases in energy release efficiency are experienced with increased mixture ratio and decreased chamber pressure. These trends are directly opposite to that observed with the Phase II data and offer sufficient data scatter to require a more dependent variable for correlation purposes.

A more desirable correlation is obtained by the data of Figure 49 (energy release efficiency vs velocity ratio). These data are considered indicative of injector performance without the effects of incomplete oxidizer vaporization and heat exchanger induced mixture ratio maldistribution. It must be stated, however, that a flow maldistribution may still be present, the exact magnitude of which has not been determined. Figure 49 also indicates the exact opposite characteristics of the Phase II data previously reported. Higher performance is obtained at lower velocity ratio. Since velocity ratio is primarily changed by variations in mixture ratio, the higher performing low velocity ratio tests occur with high mixture ratios. To separate the effect of mixture ratio alone, the injector was run with reversed circuits which causes the oxidizer velocity to be doubled and the fuel velocity to be halved at the same mixture ratio. Symbol coding denotes chamber pressure and injector flow conditions on the figure. Also noted are data using the Phase II chamber which has a larger throat area; however, both chambers are 2.5 in. in length. The majority of the tests was conducted using a two-dimensional chamber with the narrow dimensions parallel from the face to the nozzle exit.

As can be seen in Figure 49, energy release efficiency drops off with increasing velocity ratio with a wide dispersion in data for the different chamber pressure conditions. These trends denote the dependence of another variable which overrides normally expected velocity ratio effects on mixing induced performance. Increased velocity ratios ( $V_{H_2}/V_{O_2}$ ) should enhance turbulent mixing, thereby

X, C, Hot Firing (cont.)

reducing this performance loss. Apparently, an overriding factor is caused by the increased fuel velocities which reduce effective chamber residence times and, consequently, may result in incomplete combustion within the chamber.

In an attempt to understand the chamber pressure influence, the curve of Figure 50 was constructed. Here, the energy release efficiency is presented as a function of the fuel density - velocity product ( $\rho V$ ). Since tests with the same injection velocity differ in injection density due to chamber pressure changes, the density - velocity product becomes of interest. The data on this curve tend to indicate that high fuel velocities with short chambers and high chamber pressures (high injection gas density) produce increasing losses in the 100 to 500 psia chamber pressure range.

In conclusion, three effects are noted resulting from the fine-pattern injector gaseous propellant test data. First, high performance can be obtained with a 2.5-in. chamber using a HIPERTHIN injector over a wide range of chamber pressure. Second, high fuel velocities or fuel velocity - density products tend to induce significant performance losses in a short 2.5-in. chamber. Third, design variables such as absolute injection velocities affect combustion performance, overriding the effect of operating mixture ratio, which was a primary variable for the Phase II injector with liquid propellant injection.

## 2. Phase III HIPERTHIN Injector

### a. Test Setup and Procedure

All testing was conducted at Test Bay 7 of the Physics Lab (shown in Figure 51). Thrust measurements for performance were made with strain gage load cells. Oxidizer propellant flow rates were measured with turbine type flow meters. Sonic flow venturi were used in the fuel circuit. Sizes were adjusted

X, C, Hot Firing (cont.)

to meet design flow rates. Propellant was supplied to the test stand from a 50-gal  $\text{LO}_2$  tank and a 30-ft<sup>3</sup>  $\text{GH}_2$  cascade system. The  $\text{LO}_2$  vessel was pressurized with  $\text{GN}_2$ . These systems were used for all tests. Injector and chamber pressures were measured with Tabor transducers. For stability measurement, a Photocon transducer was mounted in the fuel manifold of the injector. Temperatures were also recorded at all injector and line pressure measuring points. Ignition was accomplished by a Halex 1196A squib wired into the throat. The squib was therefore replaced for each test. Figure 52 shows the hardware mounted on the test stand ready for testing. The water-cooled chamber was fed through a 3/4 moon-shaped manifold and then exited straight down so to not affect thrust measurements.

b. Test and Performance Summary

A total of ten tests were conducted during the Phase III test program using a single baffled nickel injector which incorporated an integral oxidizer heat exchanger. All tests utilized a 2.5-in. combustion length, two-dimensional water-cooled chamber having an area ratio of 2.07:1. An optional nozzle extension is available, which brings the area ratio to 3.7:1 for use on tests at chamber pressures above 500 psia. Six of the tests provided data which were adequate for detailed thruster performance analysis, with no two tests conducted at either the same chamber pressure or mixture ratio. Chamber pressure variations were intentional in order to define the thruster stability and durability over a throttle range from 100 to 1300 psia chamber pressure. Mixture ratio variations, however, were a result of oxidizer system pressure drop variations associated with each chamber pressure operating point inducing an oxidizer flow variation. As a result, a total of six data points define the thrusters' operating characteristics, each having a different combination of chamber pressure and mixture ratio. With these variations, detailed performance trends are difficult to establish and the performance analysis must rely heavily on additional supporting data to establish nominalized criteria so that separation of these variables can be obtained.

X, G, Hot Firing (cont.)

To accomplish this separation, the performance evaluation of each test involved computation of the specific impulse decrement attributable to the injector/chamber design. These losses were computed using the JANNAF Standardized Performance Evaluation procedure<sup>(1)</sup>, which allows computation of the various real engine specific impulse losses so that the combined energy release and mixture ratio distribution loss of the injector can be deduced. Since no means were available to determine the mixture ratio distribution across the injector face for the various chamber pressure/mixture ratio combinations, a separate loss was not computed. Therefore, the impulse loss remaining after real engine loss identification has been assigned to energy release loss and may include indeterminable mixture ratio distribution losses.

The program test and performance data are summarized in Table II, indicating the test number, date, operating point, duration, and energy release efficiency.

As mentioned earlier, six tests were analyzed for performance. The four remaining tests (101, 102, 106, and 110) were not considered in the performance evaluations for various reasons. Test 101 was a short duration system checkout firing and not suitable for steady-state performance data. Instrumentation malfunctions prohibited evaluation of Test 102. Test 106 ran at a high mixture ratio of 25:1 and was considered out of the range of applicable data. On Test 110, an oxidizer circuit system malfunction induced chamber damage, invalidating performance data.

Previous gas/gas testing with the Phase II injector indicated two primary performance correlation trends. Increasing chamber pressure resulted in energy release efficiency reductions, while mixture ratio increases improved injector energy release. The combined trend was interpreted in terms of increased fuel

---

(1) Performance Evaluation Methods for Liquid Propellant Rocket Thrust Chambers, ICRPG Working Group on Performance Standardization, CPIA Publication No. 132, November 1966.

X, C, Hot Firing (cont.)

density - velocity product. For given injector and chamber configurations, an increasing chamber pressure results in proportional increases in propellant density and flow rate while the velocities remain constant. This condition results since the throat area was held constant over the chamber pressure range. These correlations were possible since both propellants entered at the same temperature, allowing computation of the densities at injection. The Phase III data, on the other hand, employed liquid oxygen with heat exchange, prohibiting the computation of the injectant's density. Therefore, the performance trends evaluated with the Phase III data were only those known operating variables of chamber pressure and mixture ratio.

Performance data with the Phase III injector has been computed from the six valid performance tests and is presented in terms of energy release efficiency versus chamber pressure and mixture ratio in Figures 53 and 54. As mentioned earlier, for the purpose of this discussion, the energy release efficiency computed may include mixture ratio distribution losses which were not calculated separately. Also, the two trends plotted are not considered ideal since no two tests were conducted at either the same mixture ratio or chamber pressure, which means that the trends shown are not necessarily a direct result of the dependent variable shown on the graph. Since the effect of decreased mixture ratio is decreased energy release efficiency (within the mixture ratio range covered in the testing), the effect of chamber pressure on injector performance is assumed to not be as great as depicted. Figures 53 and 54 would seem to prove valid the conclusions reached from analysis of Phase II gas/gas test data in regard to the effect of chamber pressure and mixture ratio on injector energy release efficiency.

Ideally, in order to proportion the dual influences of mixture ratio and chamber pressure accurately for Phase III injector performance, a mixture ratio survey at each program chamber pressure level was required. In absence of such a survey, Phase II gas/gas test data were used to evaluate the effect of mixture ratio on the energy release efficiency of the Phase III injector at each

X, C, Hot Firing (cont.)

chamber pressure. After subtracting the effect of decreasing mixture ratio, the influence of chamber pressure on energy release efficiency can be noted. Figure 55 shows energy release efficiency as a function of mixture ratio for the Phase II injector using gaseous propellants and for the Phase III injector. These data indicate the decreasing effect of mixture ratio on performance as chamber pressure increases. A corrected energy release efficiency versus chamber pressure plot (Figure 56) was constructed for the Phase III injector at a mixture ratio of 6.45, corresponding to Test 104. Using the Phase II gas/gas data at a chamber pressure of 100 psia, from Figure 55, the change in energy release efficiency attributable to mixture ratio variation from the base value of 6.45:1 (Test 104,  $P_c = 108$  psia) was added to the energy release efficiency calculated for each Phase III test. Thus, a conservative correction was made because the energy release gradient is stronger at 100 psia than at higher pressures. From Figure 56, it appears that increasing chamber pressure is the major influence in reducing Phase III injector energy release efficiency assuming the limited data sample will completely define a variable influence. This is in agreement with Figure 55, which shows a general lower level of performance with increasing pressure.

c. Explanations of the Effect of Chamber Pressure on  
Injector Energy Release Efficiency

Assuming the effect of increased chamber pressure is to decrease the Phase III injector energy release efficiency, several explanations can be discussed in terms of chamber pressure influence on the combustion efficiency of a gaseous oxygen/gaseous hydrogen reaction. The chamber pressure effect will be discussed in terms of an occurrence which could possibly affect injector energy release efficiency. This occurrence will be identified with the proportional increases in the  $\text{GH}_2/\text{GO}_2$  reaction rate with increasing chamber pressure.

In a gas/gas injection process, the propellants are fully prepared for combustion; i.e., no atomization or vaporization processes must take place as with a liquid oxidizer/gaseous fuel system as utilized in Phase II. The Phase III HIPERTHIN injector basically employs a linear showerhead element distribution with alternate rows of fuel and oxidizer orifices. Both of these facts (i.e.,

X, C, Hot Firing (cont.)

a gas/gas injection system and a nonimpinging showerhead injector pattern) would support the theory that the chemical combustion reaction could be interrupting the physical mixing process in the engine combustion chamber. If this phenomenon were occurring, the effect would worsen with increasing chamber pressure since the reaction rates would increase. In this case, more reaction would occur near the injector face forming a zone of reacted gas which would act as a barrier and, hence, inhibit mixing

This type of gas/gas combustion effect on the injection inertia effects has been cited as occurring in the ALRC Hydrogen-Oxygen High  $P_c$  APS Engine Program<sup>(2)</sup>. This gas/gas program has cited differences in mixing efficiency between cold flow and hot fire data for injectors utilizing swirler coaxial elements. Preliminary results from these gas/gas tests have shown that swirler elements do not offer performance advantages over a plain showerhead element, contrary to the cold flow data from which the swirler was synthesized. This would tend to indicate the combustion process is indeed impeding the mixing process and causing this desirable mixing influence to be minimized. This program is operating at chamber pressure levels from 100 psia to 500 psia, with cold flow at 50 psia.

In the parallel Low  $P_c$  APS program<sup>(2)</sup>, opposite results have been obtained in hot fire tests with a swirler coaxial element. The performance gain predicted from cold flow optimization have generally been realized in the hot firings conducted to date. It can be suggested that the lower reaction rates accompanying the low nominal chamber pressure of 15 psia allow the mixing process to be completed without a substantial combustion interface in the critical mixing zone near the injector face.

---

(2) Oxygen-Hydrogen High and Low  $P_c$  APS Thrusters, Contract NAS 3-14354, NASA/Lewis Research Center.

X, C, Hot Firing (cont.)

A recent company-sponsored investigation into hydrogen/oxygen combustion with a unielement showerhead injector has also provided substantiation of this gas/gas mixing interface during hot fire testing. In this program, a coaxial element was cold flow tested using a mass spectrometer to identify the species and the degree of mixing. Next, hot fire tests were conducted and the species again identified. The ensuing result was decreased mixing since the interface water reaction forced the outer hydrogen away from the element and compartmentized the oxygen within the water-cylinder-like shield.

With these two examples of  $\text{GO}_2/\text{GH}_2$  reaction processes tending to inhibit mixing, a relation to the physical Phase III test system must be clarified. These tests were conducted at thrust levels to 2500 lb in a short 2.5-in.-length chamber. It must be assumed at these thrusts and their corresponding high pressure and flow rate that combustion reaction effects are amplified in comparison with longer length chambers currently under evaluation in other  $\text{O}_2/\text{H}_2$  propellant applications. In these gas/gas test programs, higher energy release efficiencies have been noted and with not nearly the influence of chamber pressure. In most cases, the employed chambers were two to three times as long. The end result was less sensitivity to chamber pressure increase as shown in Figure 57. Here, the Phase II and Phase III injector gas/gas data are compared with three other injectors operating with longer combustion chambers. The influence of chamber length on chamber pressure increases is quite apparent. For this reason, a qualification must be made with respect to the trends of the Phase III injector gas/gas data in that increased chamber lengths may tend to minimize this effect and allow high combustion efficiencies to be obtained at high chamber pressures, the slope of which is a function of the particular injector, with gaseous oxygen/gaseous hydrogen injectors.

TABLE I  
GH<sub>2</sub>/CO<sub>2</sub> TEST SUMMARY

Test No.	Chamber Pressure psia	Mixture Ratio O/F	Sea Level Thrust LB <sub>F</sub>	Oxidizer Injection Velocity FT/SEC	Fuel Injection Velocity FT/SEC	Vacuum Spec. Imp. LB <sub>F</sub> SEC/LB <sub>M</sub>	Vacuum Spec. Imp. Efficiency %	Energy Release Efficiency %
101								
102	184	3.91	281	68	577	340	90.5	93.1
103	186	3.93	287	68	581	344	91.8	94.4
104								
105	191	5.13	295	74	485	334	91.8	94.4
106	179	4.19	455	122	987	328	87.4	89.9
107	189	5.24	490	129	832	323	88.8	91.4
108	221	7.50	582	144	656	299	90.0	92.8
109	228	7.59	355	82	368	309	93.8	96.5
110	215	10.15	336	95	316	281	92.7	95.5
111								
112	474	1.50	775	51	1,120	335	89.8	91.9
113	465	3.07	761	60	656	352	92.1	94.2
114	458	4.13	743	68	545	343	91.7	93.7
115	486	4.57	760	68	491	337	91.0	93.0
116	493	5.43	819	75	461	330	91.4	93.5
117	563	6.80	916	79	388	315	92.0	94.0
118	622	9.07	1,024	88	325	293	92.5	94.7
119	100	1.57	133	51	1,067	356	95.1	98.5
120	93	3.20	122	64	656	353	92.8	96.0
121	92	4.12	124	70	560	348	93.2	96.6
122	97	5.14	130	74	477	338	93.1	96.6
123	106	6.16	146	79	423	328	94.7	97.7
124	117	8.00	166	85	354	309	95.9	98.8
125	114	9.36	155	90	323	293	94.9	98.0
126	97	1.51	128	100	526	341	91.5	94.8
127	103	3.01	143	120	319	362	94.6	98.0
128	99	4.48	134	135	241	350	94.5	97.9
129	92	5.87	126	151	206	334	94.7	98.3
130	87	7.19	117	162	180	317	95.6	99.1

TABLE I (cont.)

Test No.	Chamber Pressure psia	Mixture Ratio O/F	Sea Level Thrust LB <sub>F</sub>	Oxidizer Injection Velocity FT/SEC	Fuel Injection Velocity FT/SEC	Vacuum Spec. Imp. LB <sub>F</sub> SEC/LB <sub>M</sub>	Vacuum Spec. Imp. Efficiency %	Energy Release Efficiency %
131	204	4.44	309	128	236	349	94.1	96.8
132	187	5.90	284	142	198	329	93.5	96.1
133	176	7.20	266	154	176	313	93.6	96.4
134	199	1.49	304	98	524	346	93.0	95.6
135	198	3.10	305	121	315	351	92.1	94.7
136	48	4.37	Nozzle Separation					
137	50	2.86						
138	47	1.49						
139	30	4.08						
140	30	2.63						
141	30	1.48						
142	50	4.30						
143	51	2.87						
144	48	1.51						
145	30	4.12						
146	30	2.93						
147	28	1.50						

TABLE II  
 PHASE III NICKEL INJECTOR TEST SUMMARY - LO<sub>2</sub>/GH<sub>2</sub>

Test No.	Date	P <sub>c</sub> , psia	Thrust (Vacuum) lb	MR ( $\dot{w}_o/\dot{w}_f$ )	% Thrust (Approx)	Duration, sec	ERE, %	
101	9-18-70							
102	9-23-70	100						
103	9-24-70	223	351	6.52	7	7	98.3	
104	9-24-70	108	147	6.45	3	32	98.6	
105	9-24-70	510	883	5.73	18	6	97.0	
106	9-28-70	Error in tank pressure setting resulting in MR of 25:1 Minor face damage - repaired						
107	9-28-70	892	1607	5.28	33	7	95.4	
108	9-29-70	1014	1853	5.51	37	7	94.7	
109	10-1-70	1281	2311	4.38	47	5	94.4	
110	10-1-70	Sequencing failure - Ox valve opened early. Resultant hard start failed injector/chamber interface gasket.						

- (1) All tests were conducted with: (a) nickel single canted baffle injector SN 1;  
 (b) water-cooled two-dimensional combustion chamber with 2.5 in. L' and L\* = 7.3 in.
- (2) Tests 107, 108, and 109 were conducted with a nozzle extension which increased the exit area ratio from 2.07:1 to 3.70:1.
- (3) Injector and chamber damaged on Test 110. Both items are repairable.

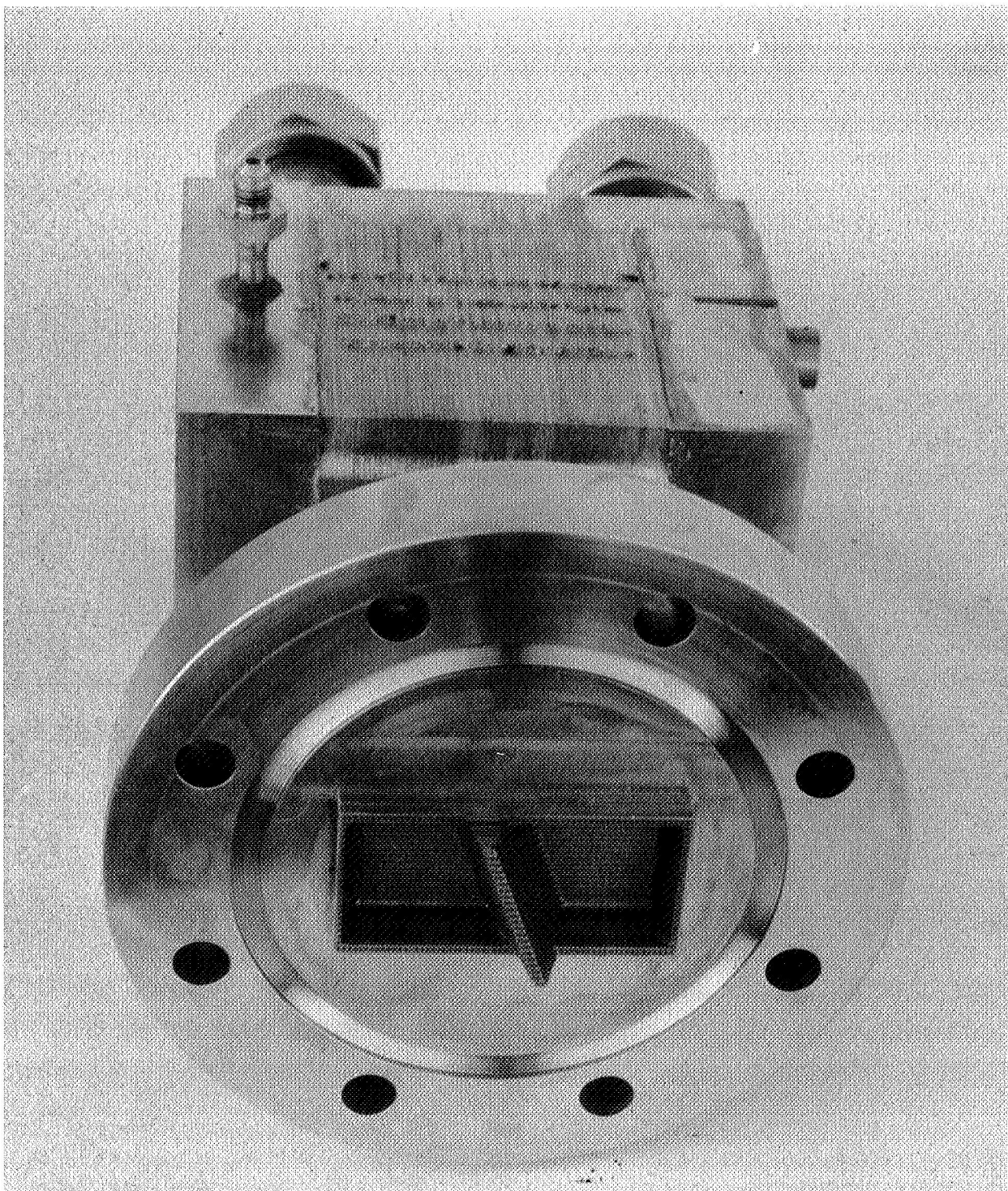


Figure 1. Annular Segment Injector

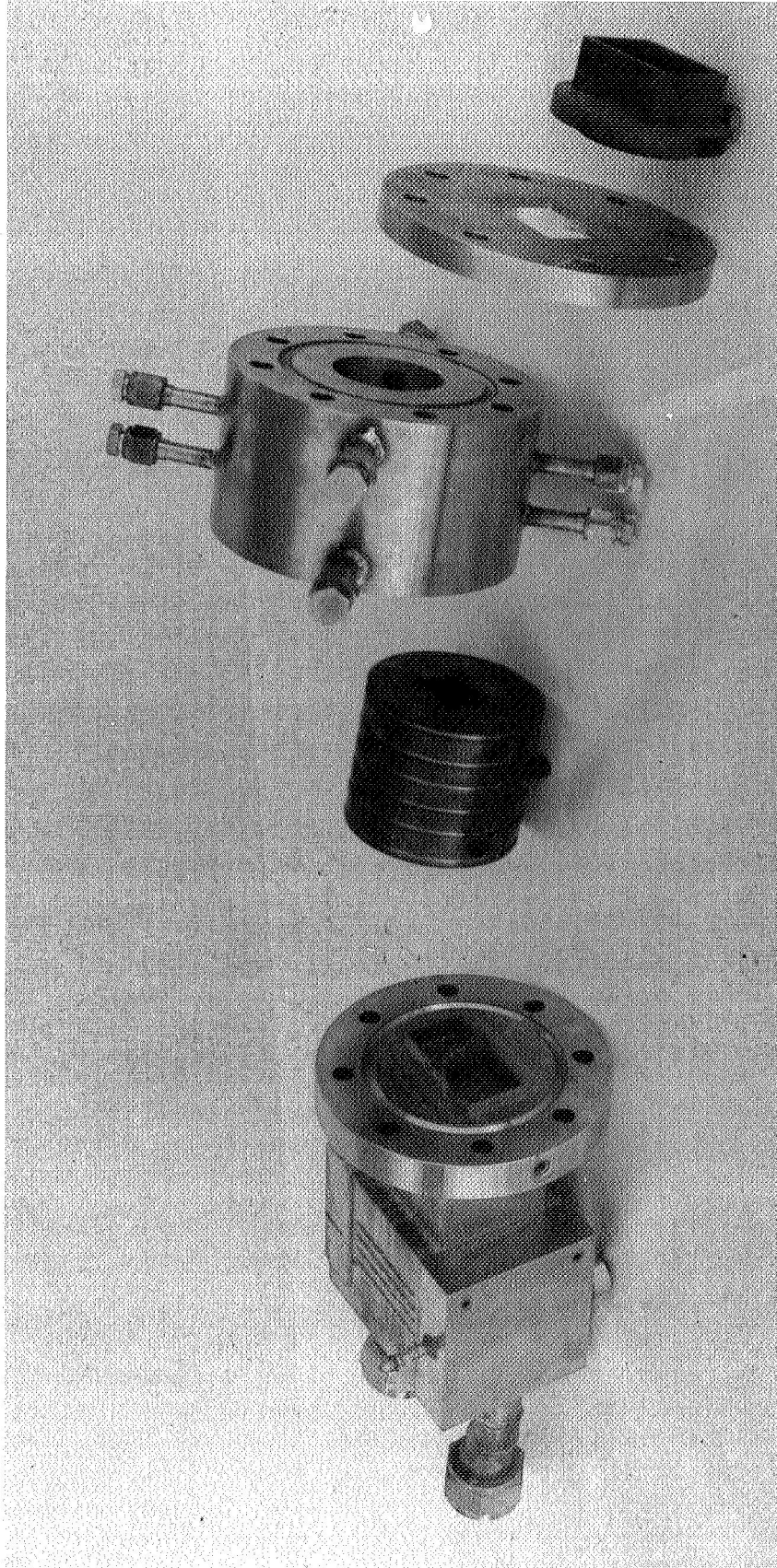


Figure 2. Annular Combustor Assembly Components

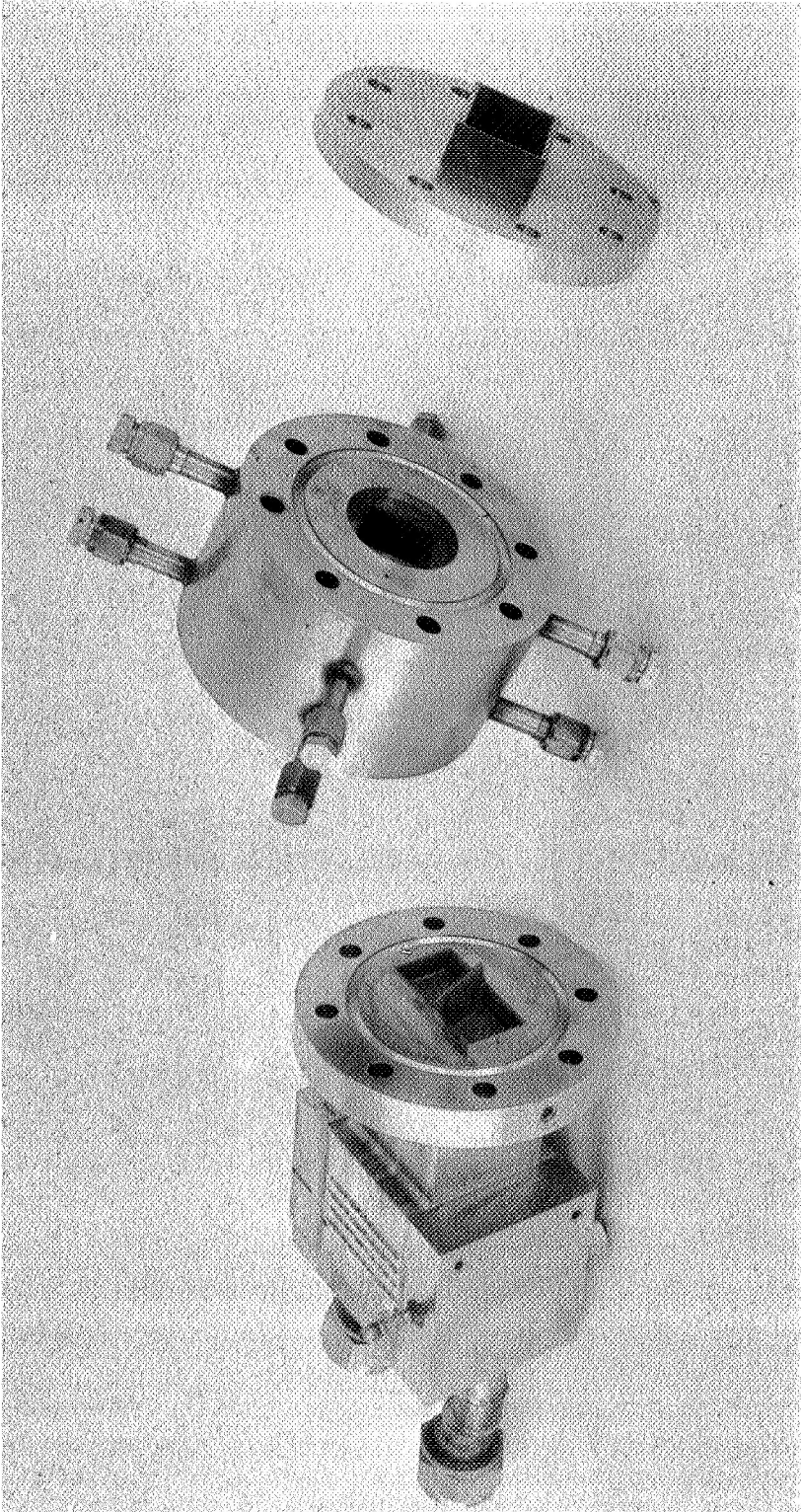


Figure 3. Annular Combustor Assembly





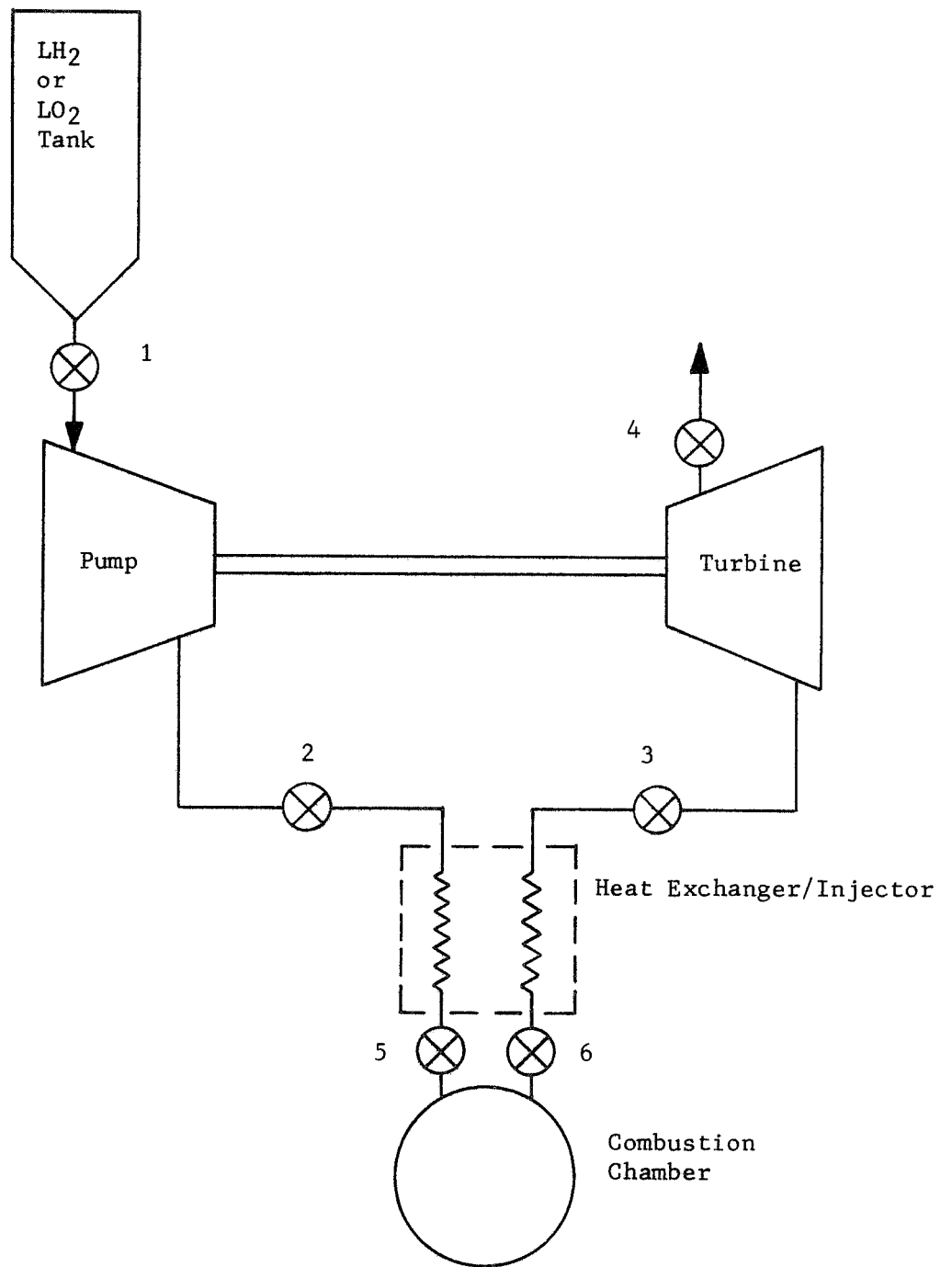


Figure 6. Turbopump Operating System

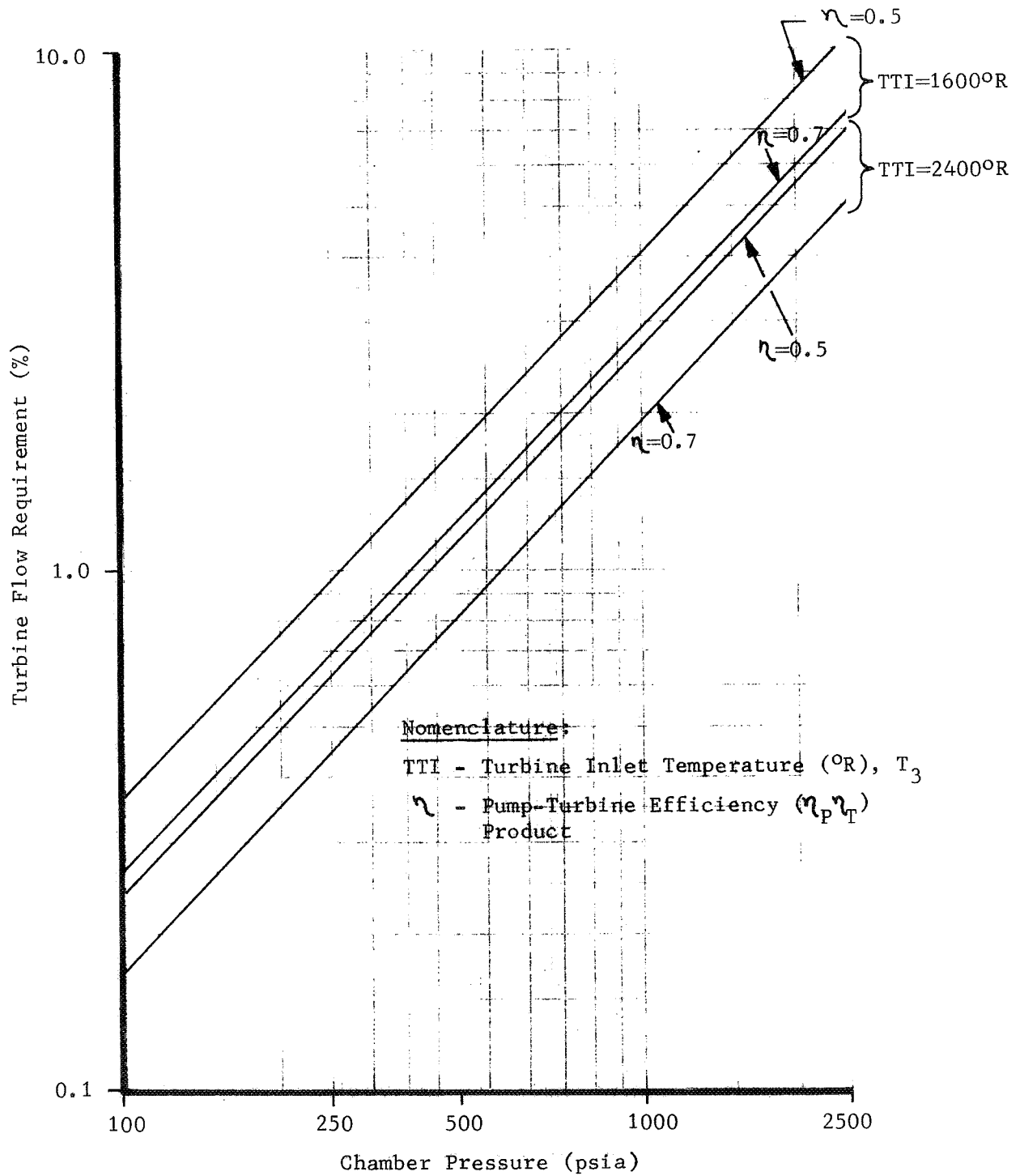


Figure 7. Turbine Flow Requirements for LO<sub>2</sub>/LH<sub>2</sub> at MR = 5.0 for [100 < P<sub>c</sub> (psia) < 2500] Throttling Conditions

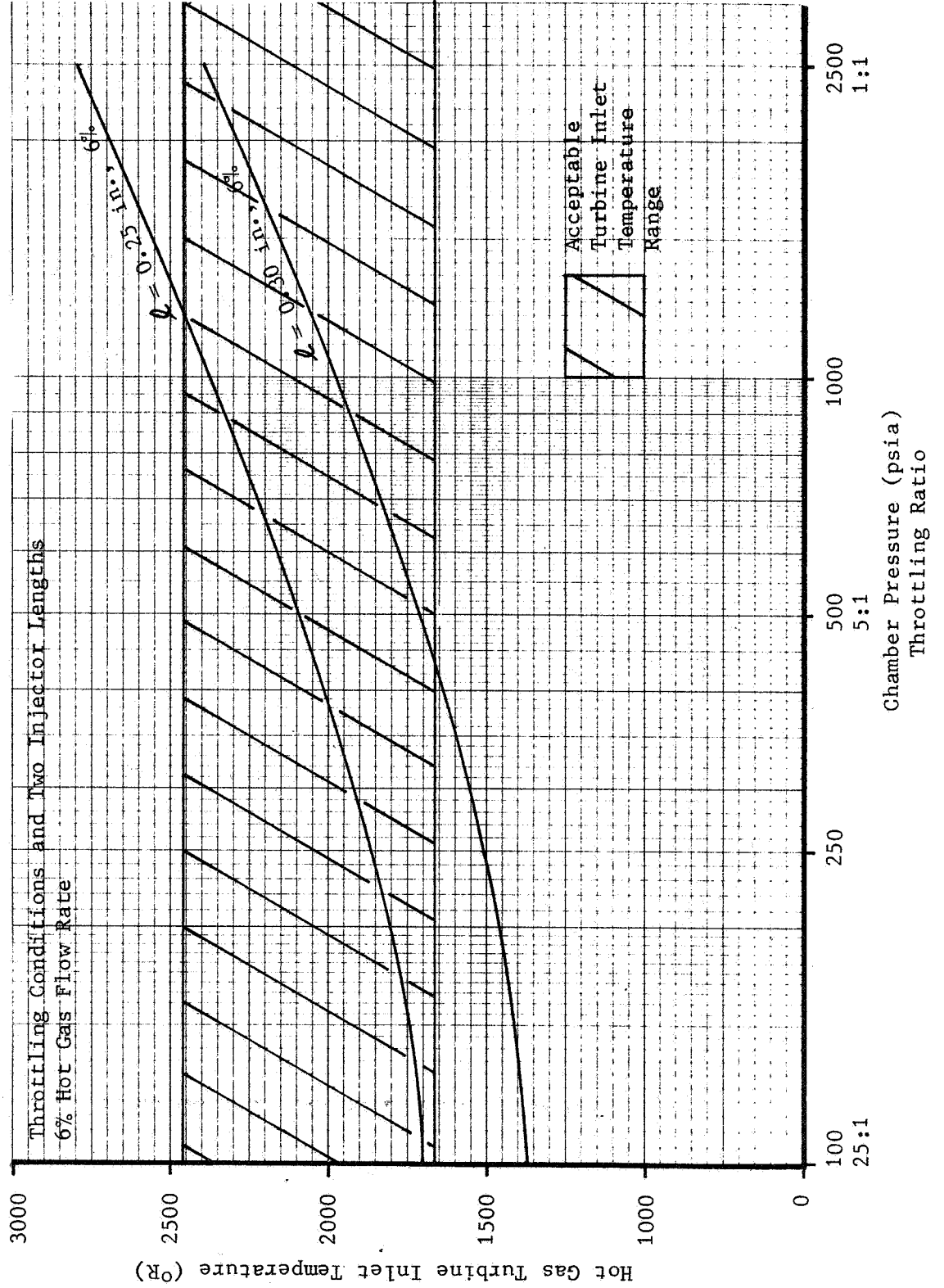


Figure 8. Hot Gas Outlet Temperature

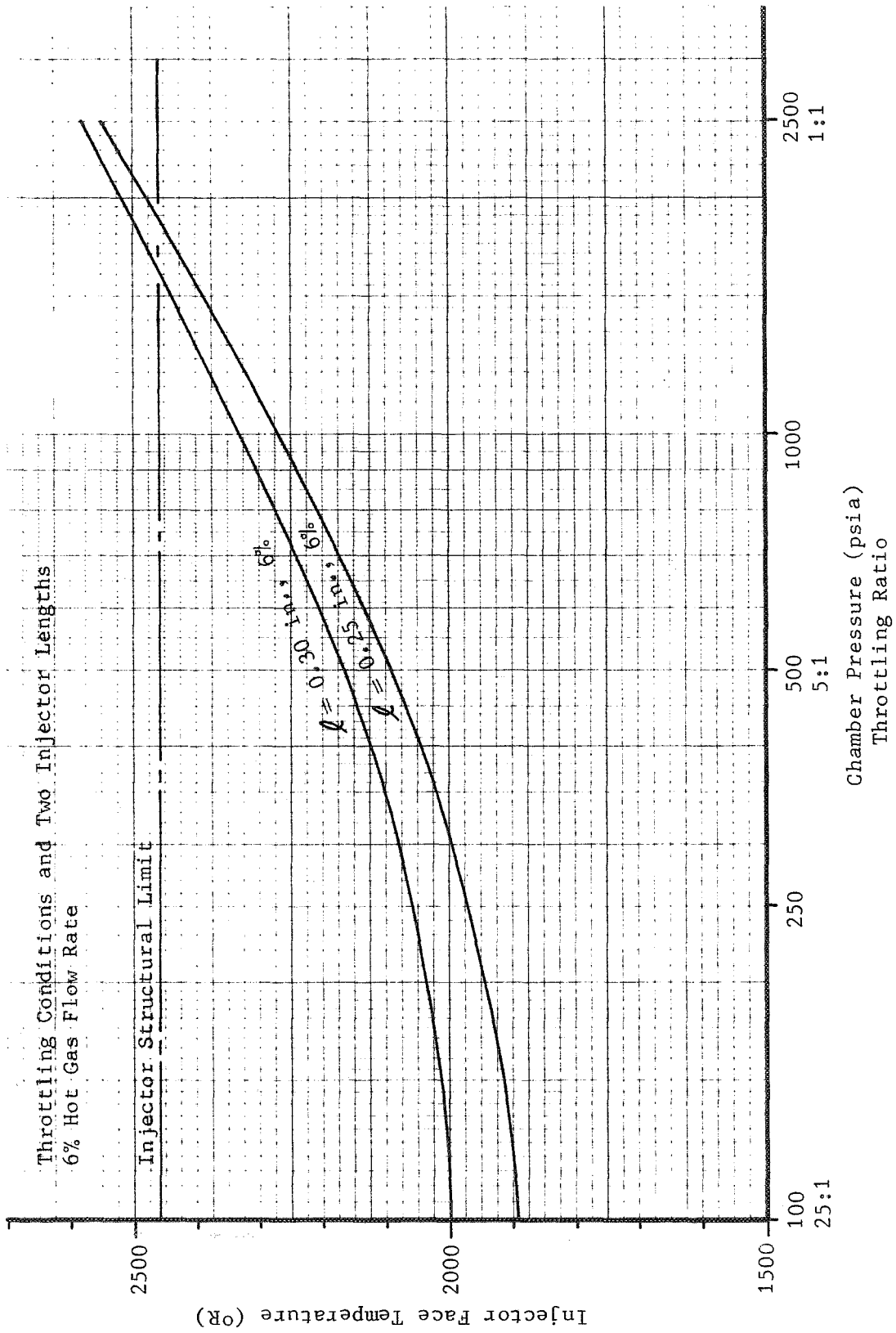


Figure 9. Injector Face Structure Temperature

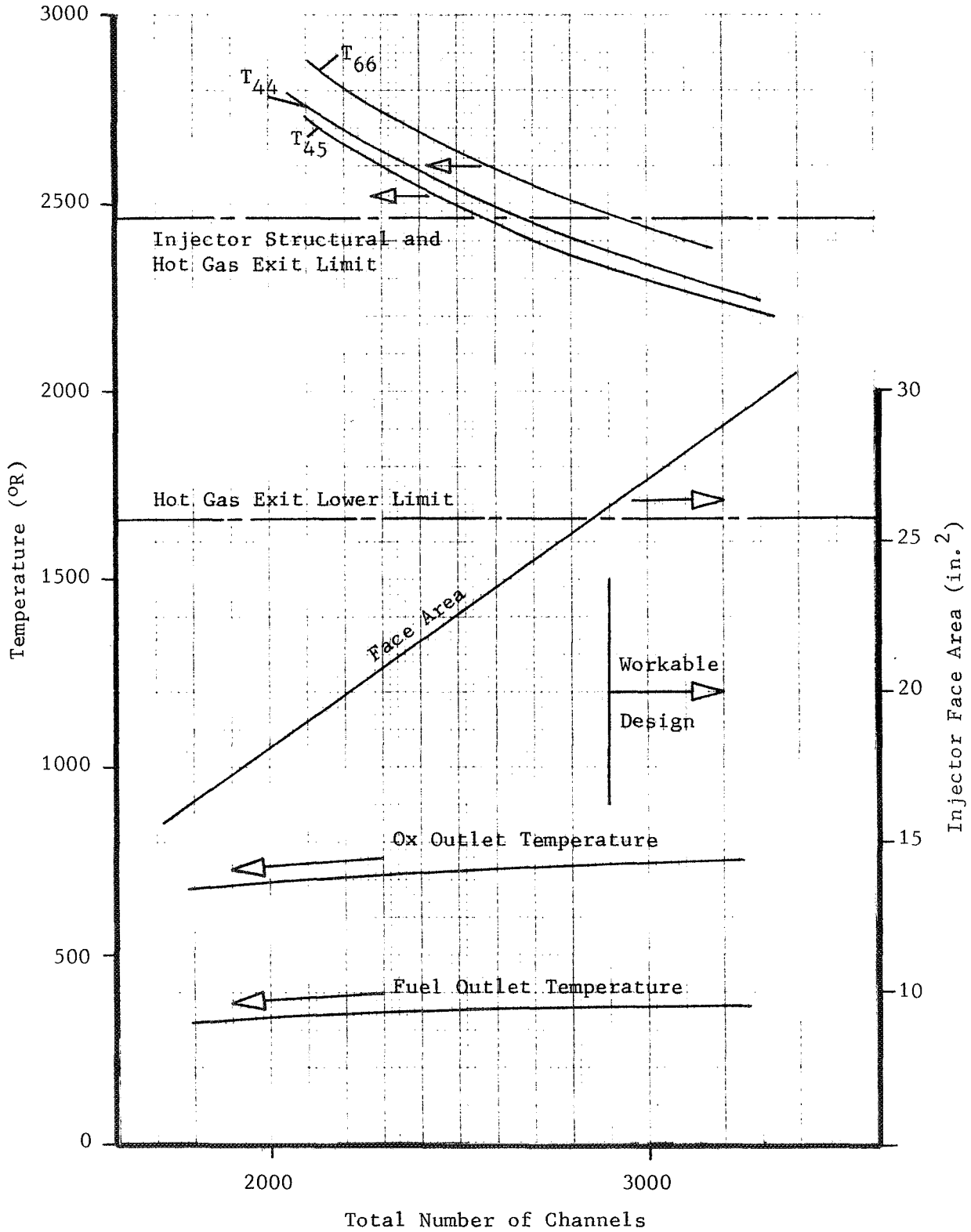


Figure 10. Temperatures of Key Locations

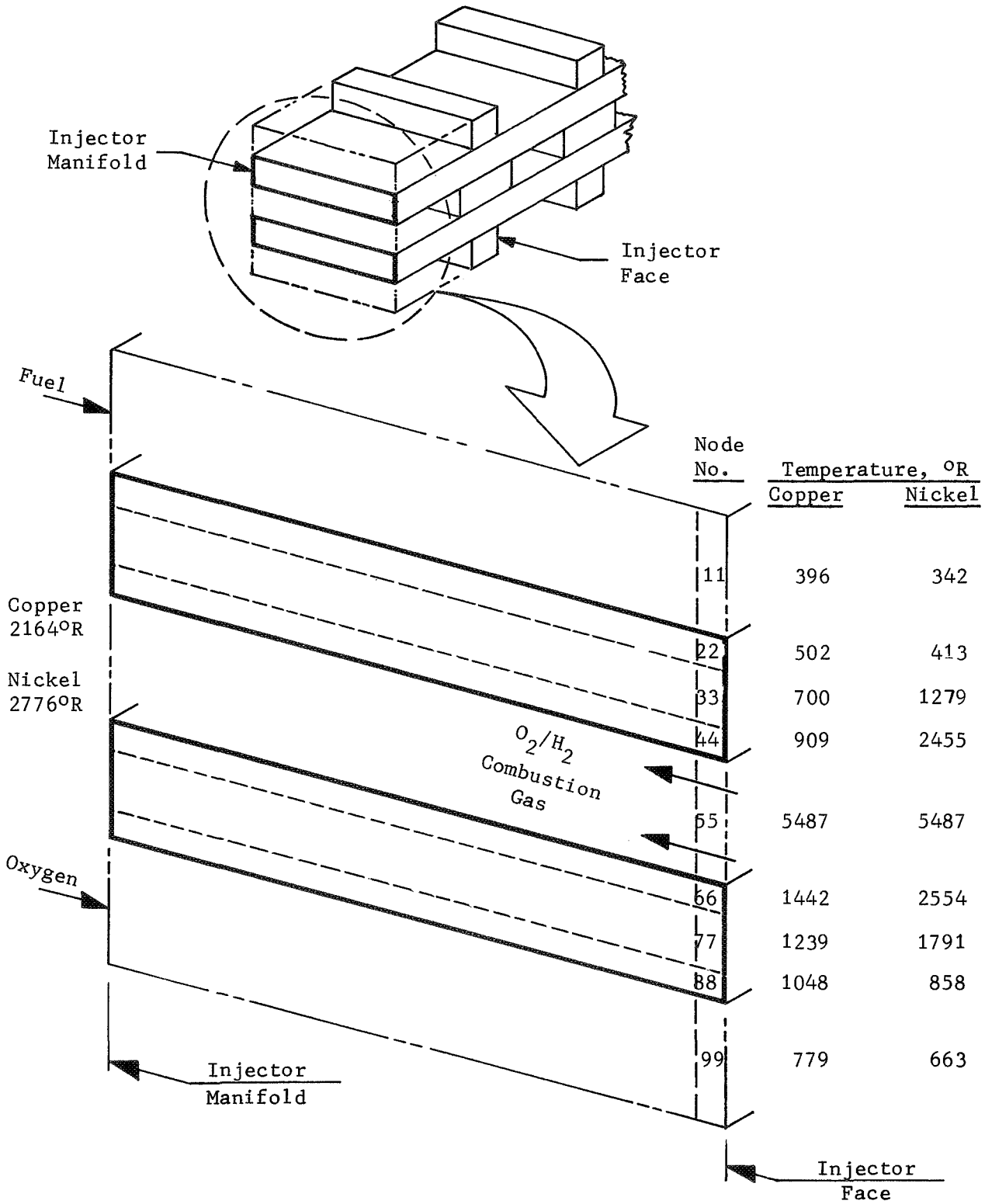


Figure 11. Temperature Comparison Between Copper and Nickel at Injector Face Nodes and Hot Gas Outlet

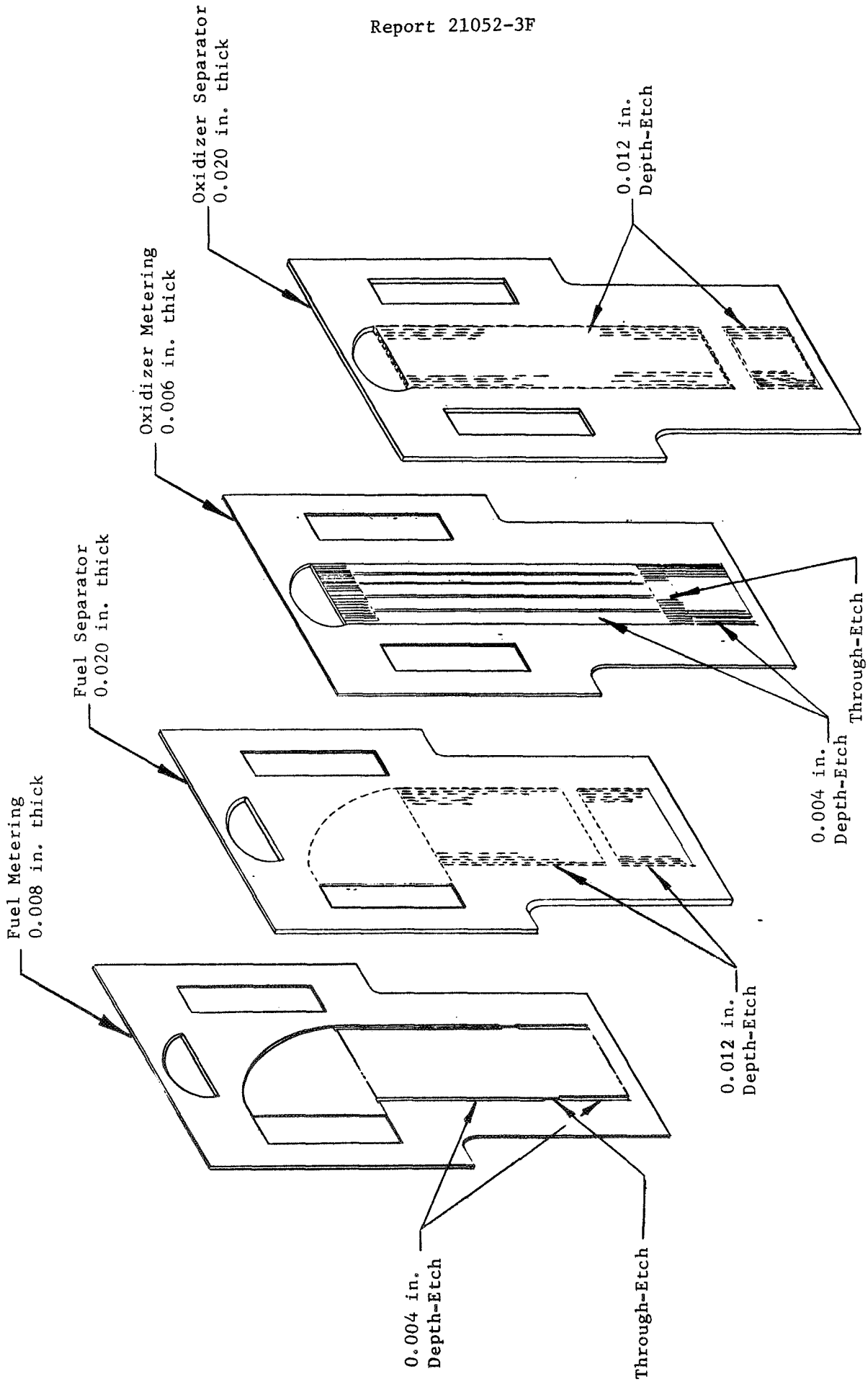


Figure 12. Injector Platelet Assembly Sequence

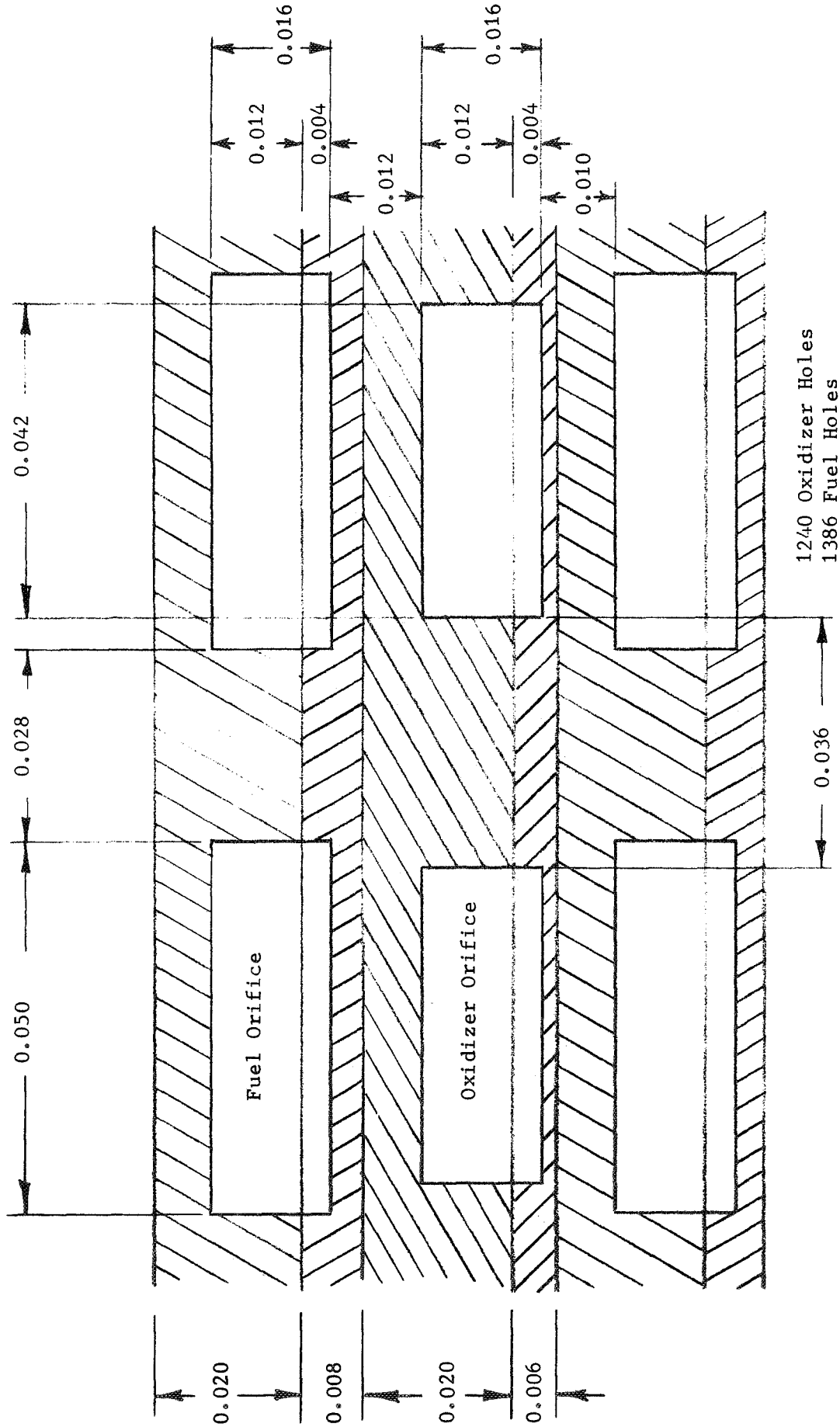


Figure 13. Nickel Injector Orifice Details

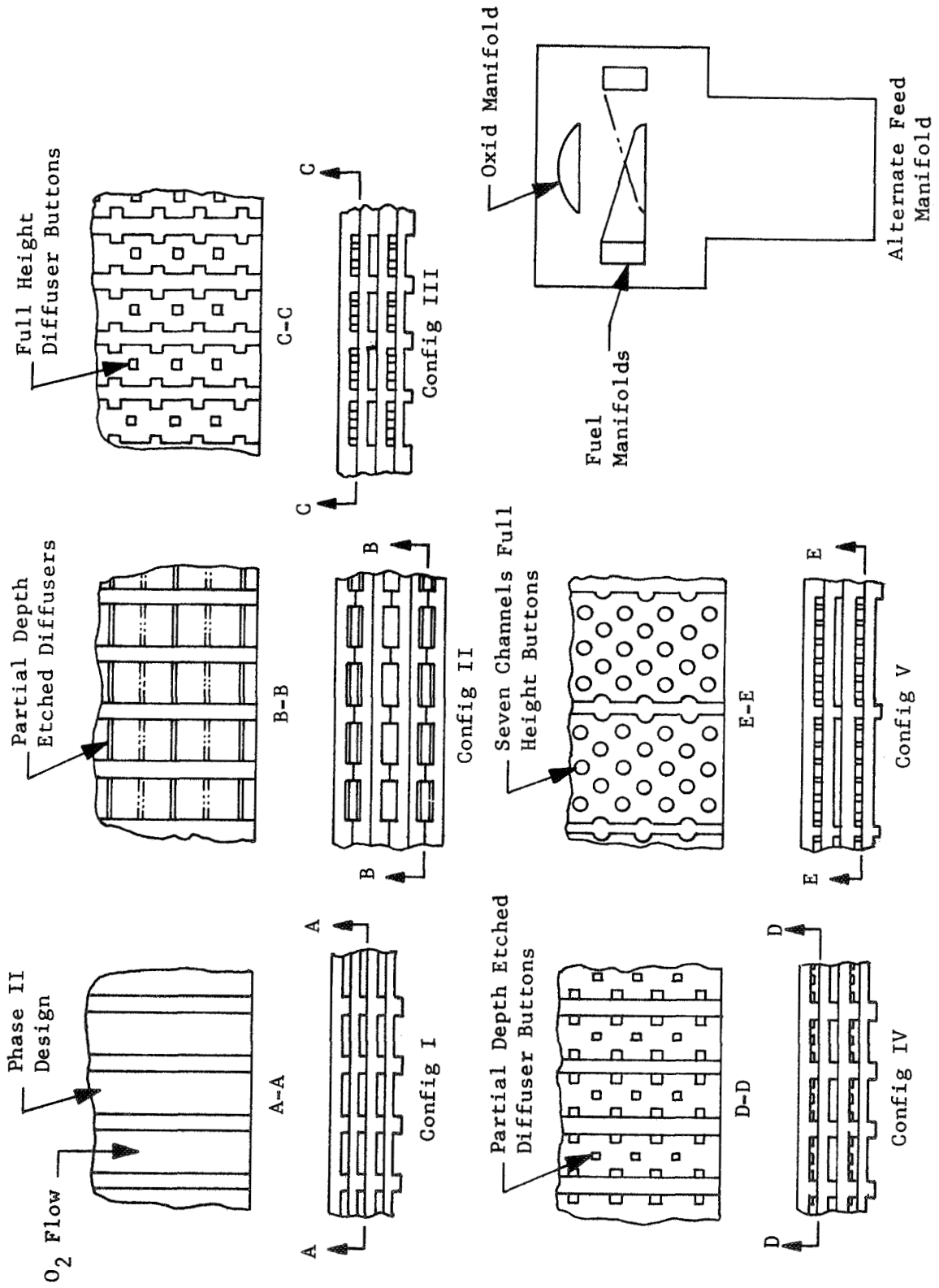


Figure 14. Design Configurations for Sample Heat Exchanger Evaluation

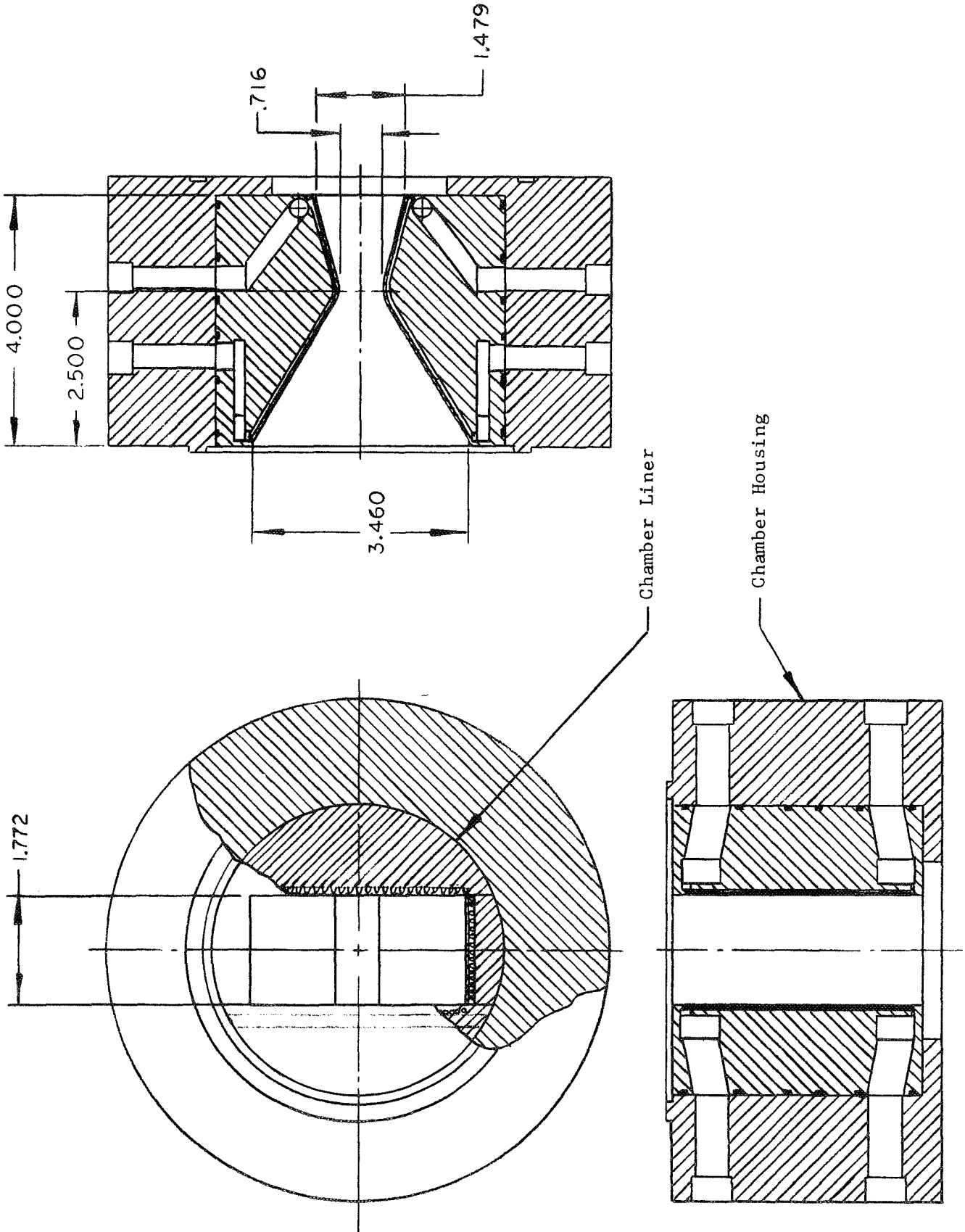


Figure 15. Water-Cooled Combustion Chamber Details

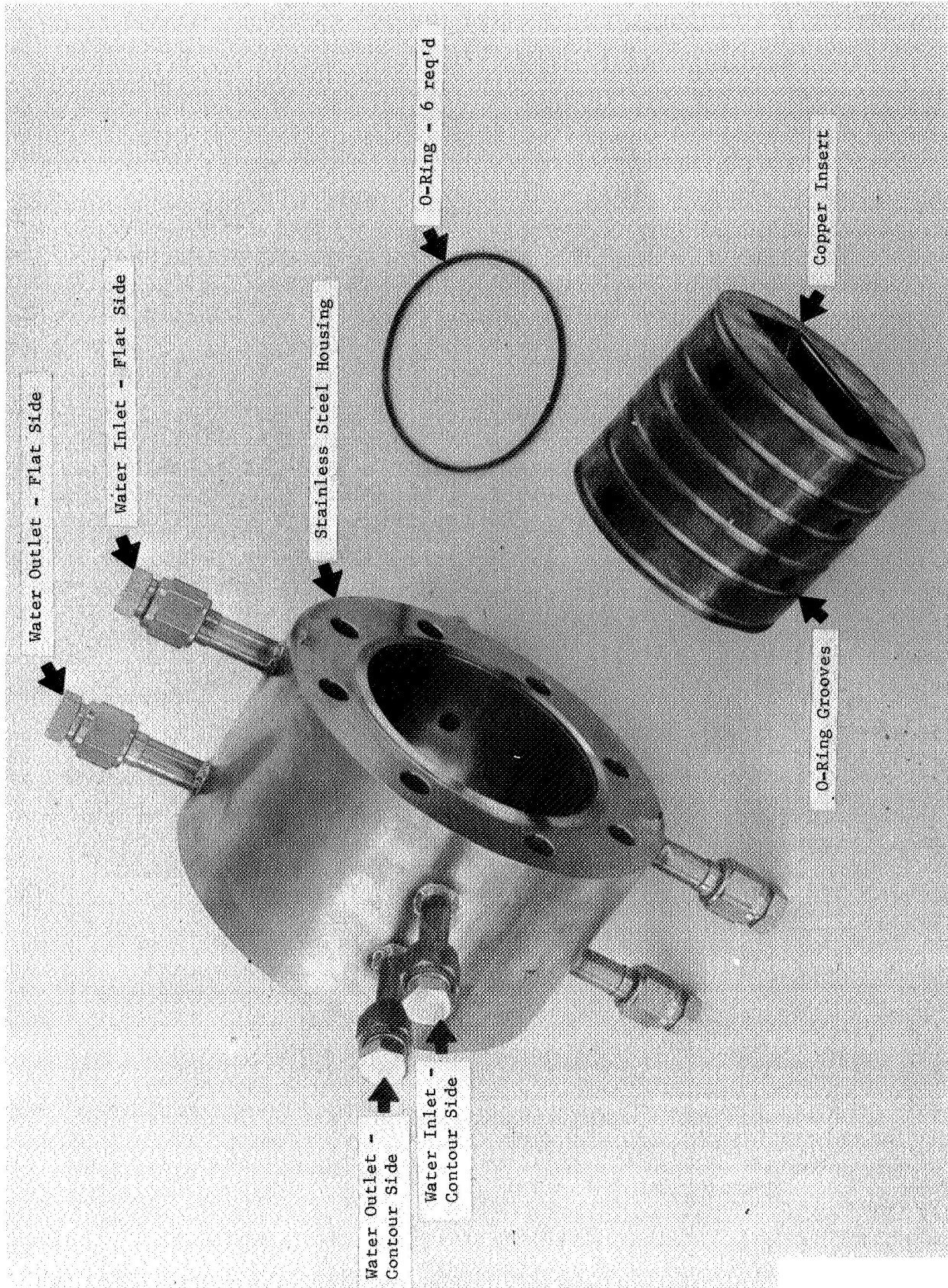


Figure 16. Assembly Details - Water-Cooled Chamber

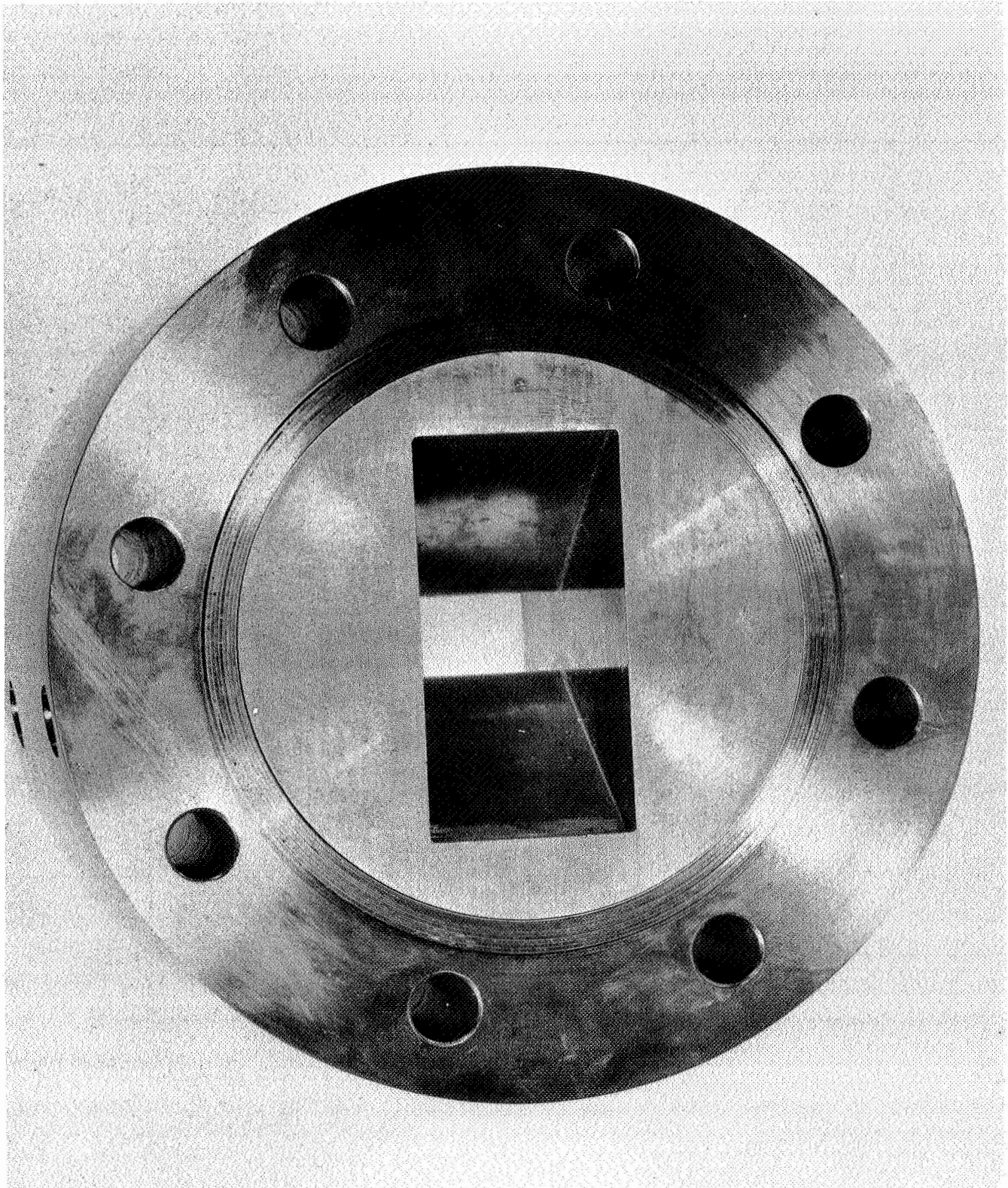


Figure 17. Assembled Water-Cooled Chamber

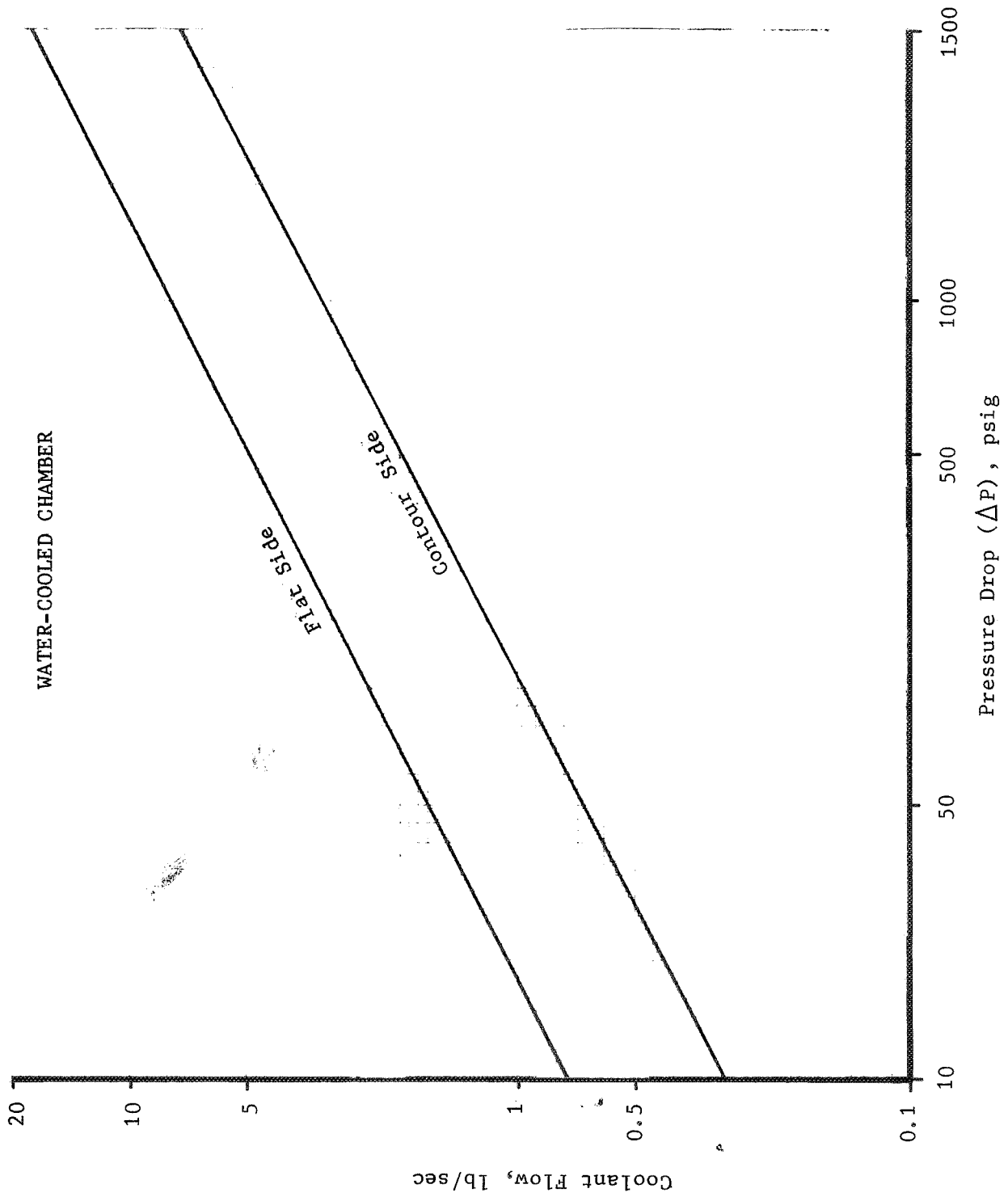


Figure 18. Flow Rate vs Overall Pressure Drop

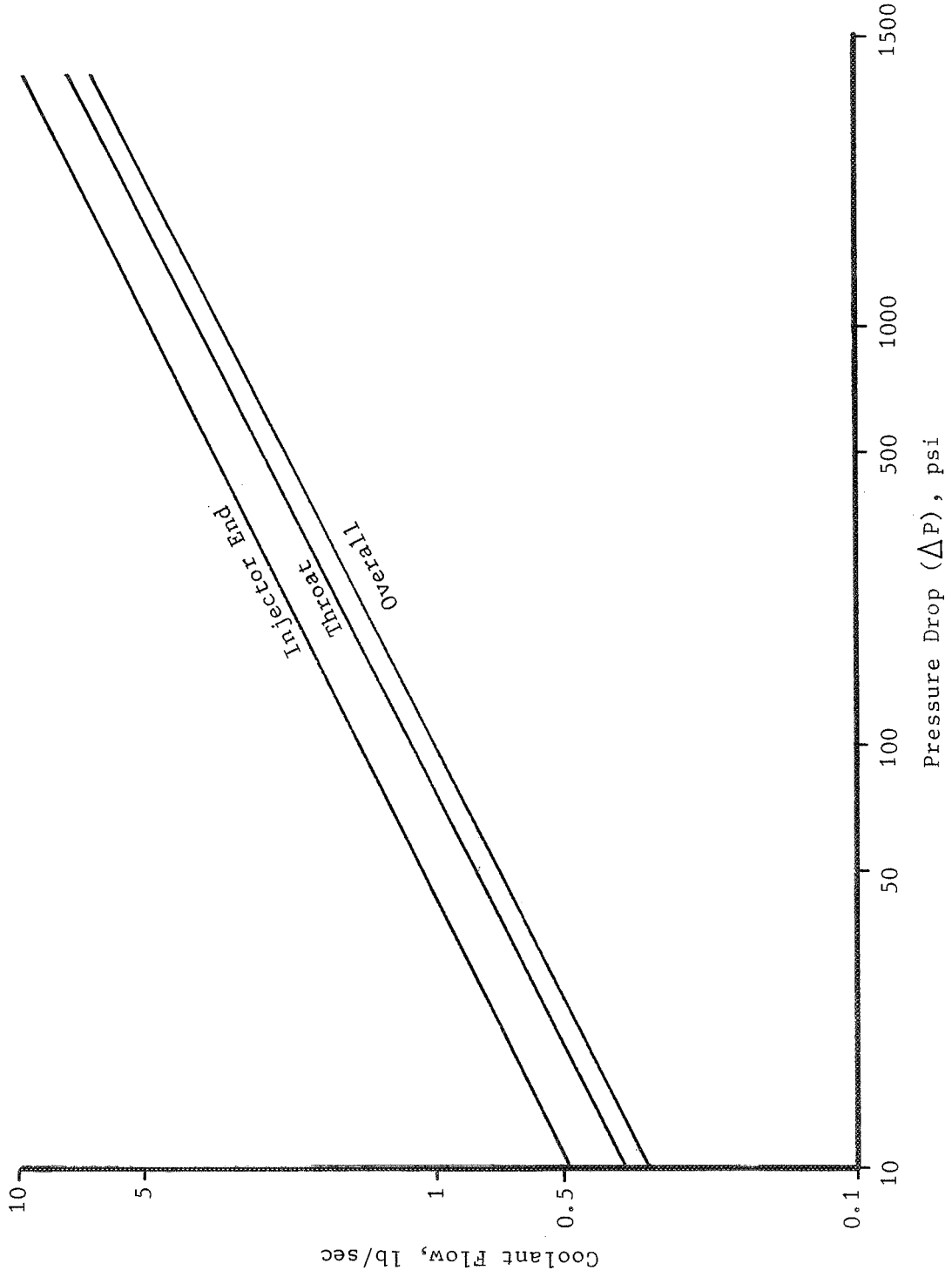


Figure 19. Coolant Flow vs Pressure Drop - Contour Side

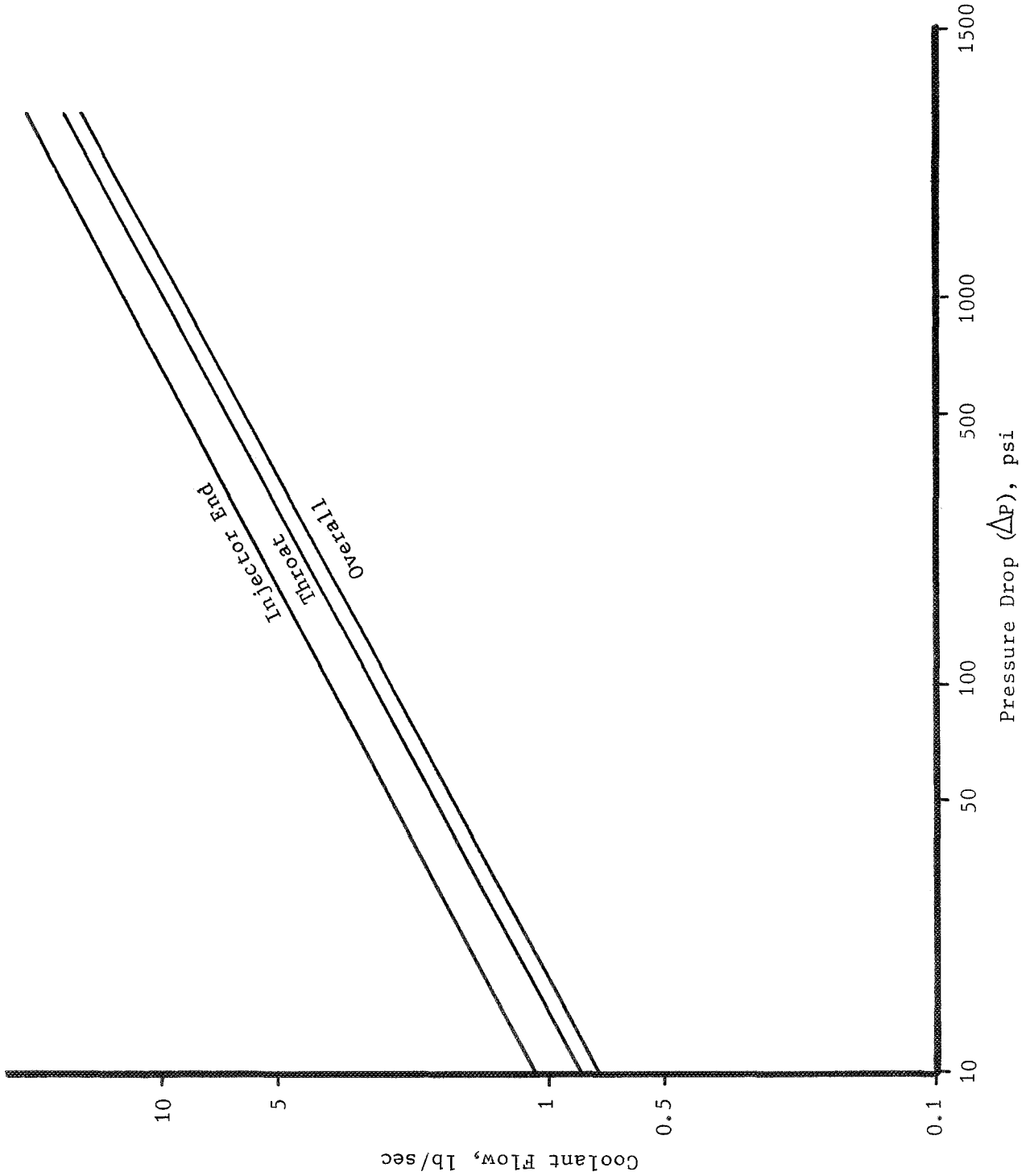


Figure 20. Coolant Flow vs Pressure Drop - Flat Side

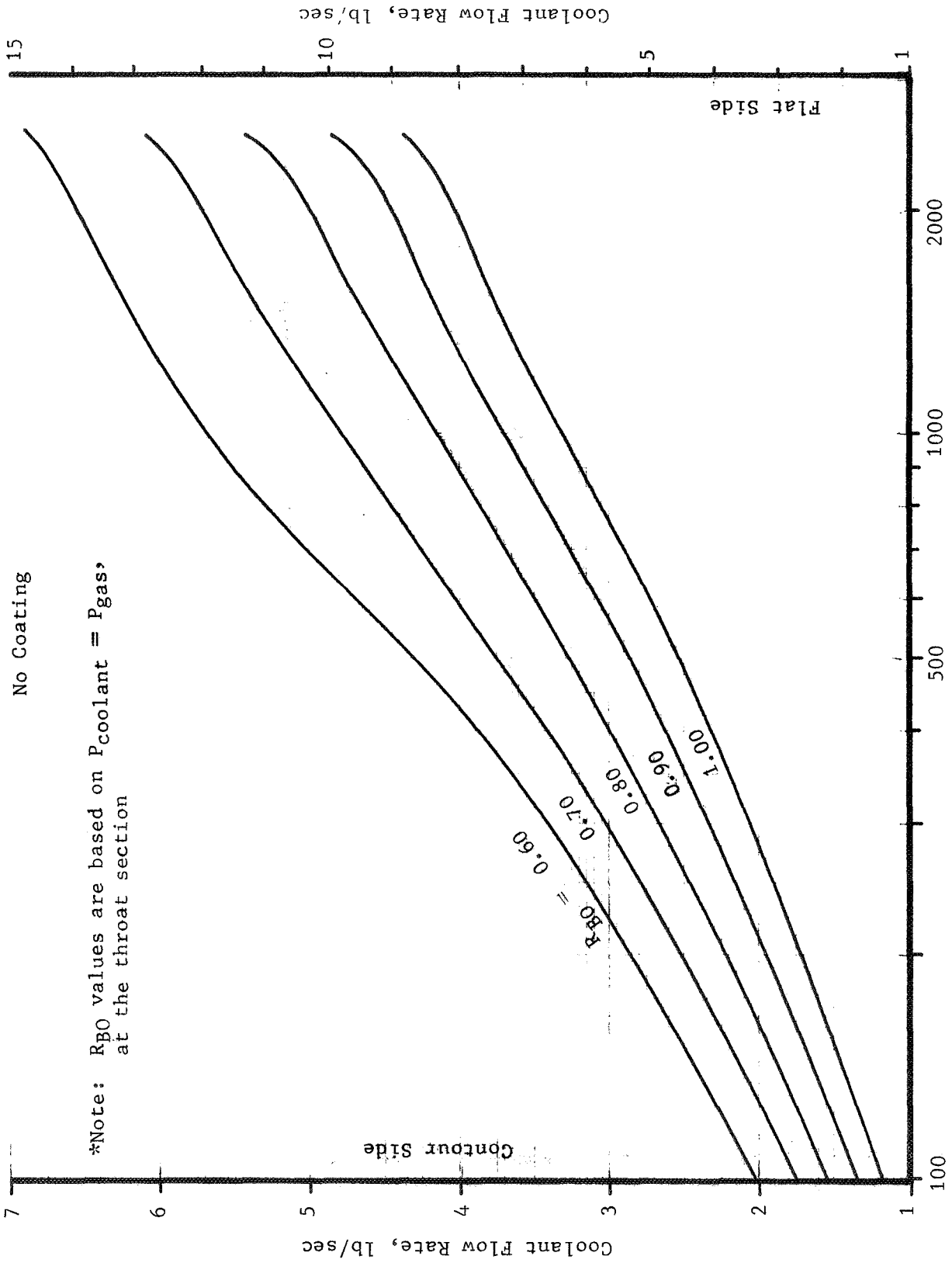


Figure 21. Coolant Flow Rate vs Chamber Pressure - No Coating

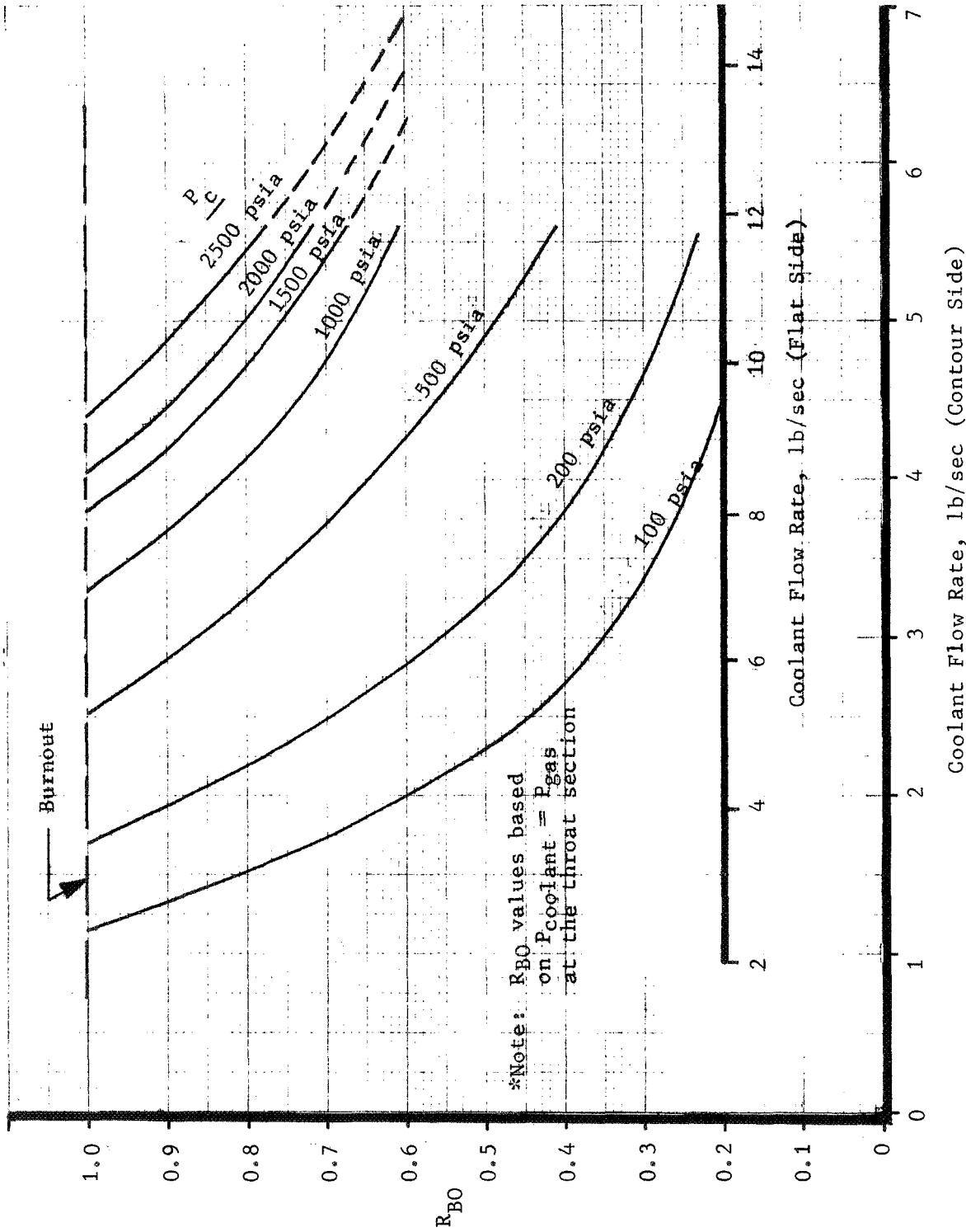


Figure 22.  $R_{BO}$  vs Coolant Flow Rate - Uncoated Copper Chamber Throat Section

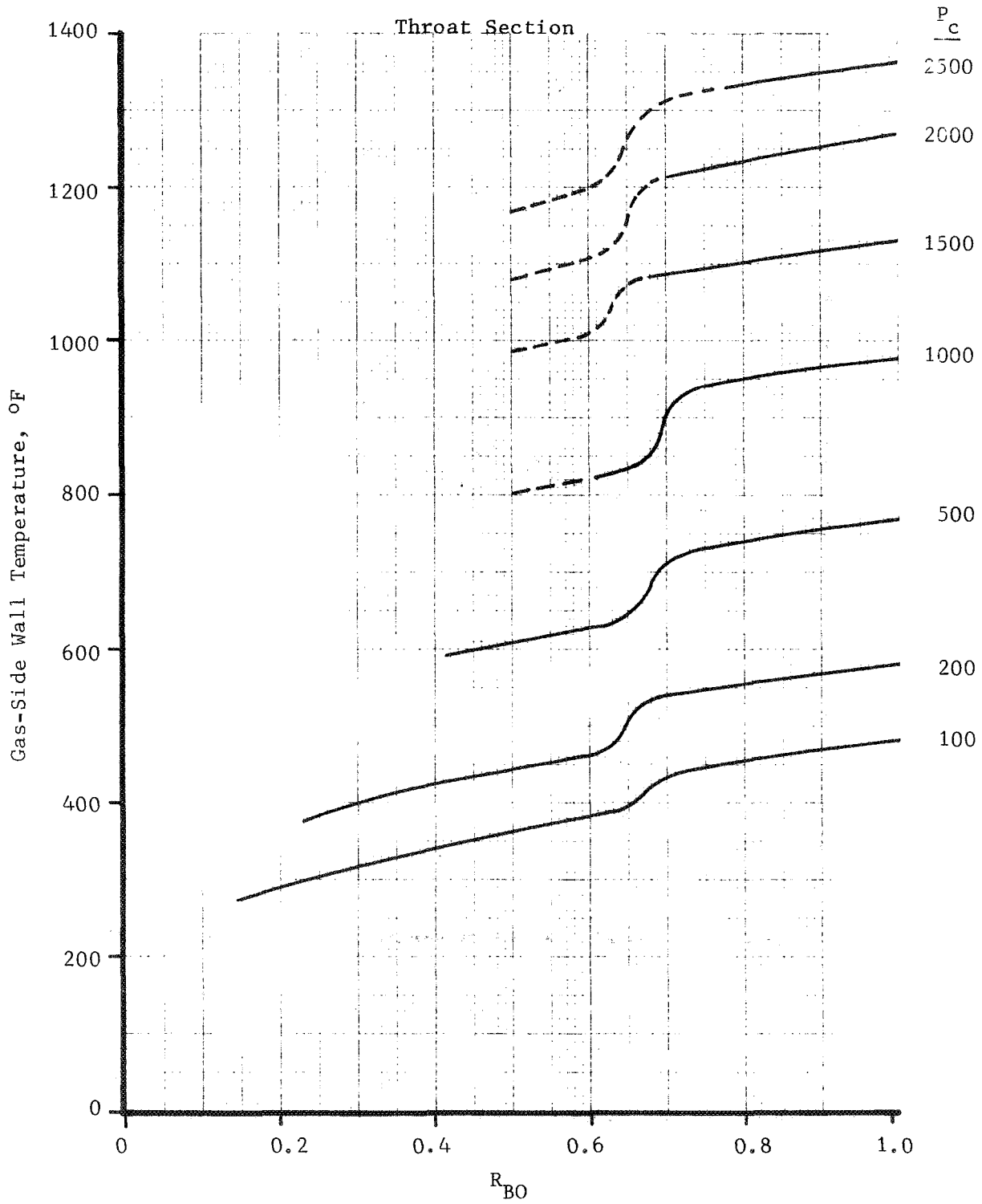


Figure 23. Gas-Side Wall Temperature vs  $R_{BO}$  - Noncoated Wall

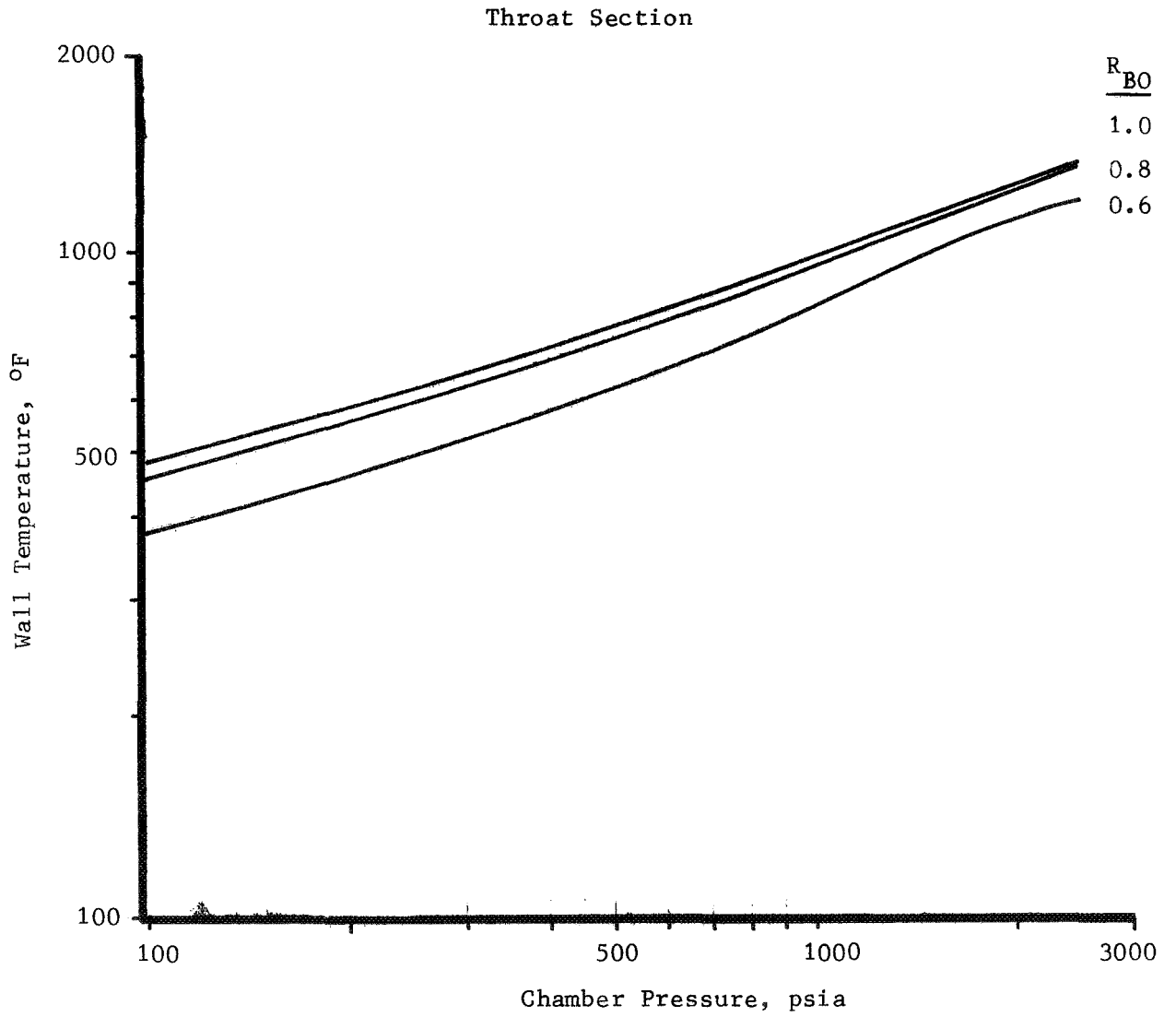


Figure 24. Gas-Side Wall Temperature vs Chamber Pressure - No Coating

\*Note:  $R_{BO}$  values are based on  $P_{coolant} = P_{gas}$  at the throat section.

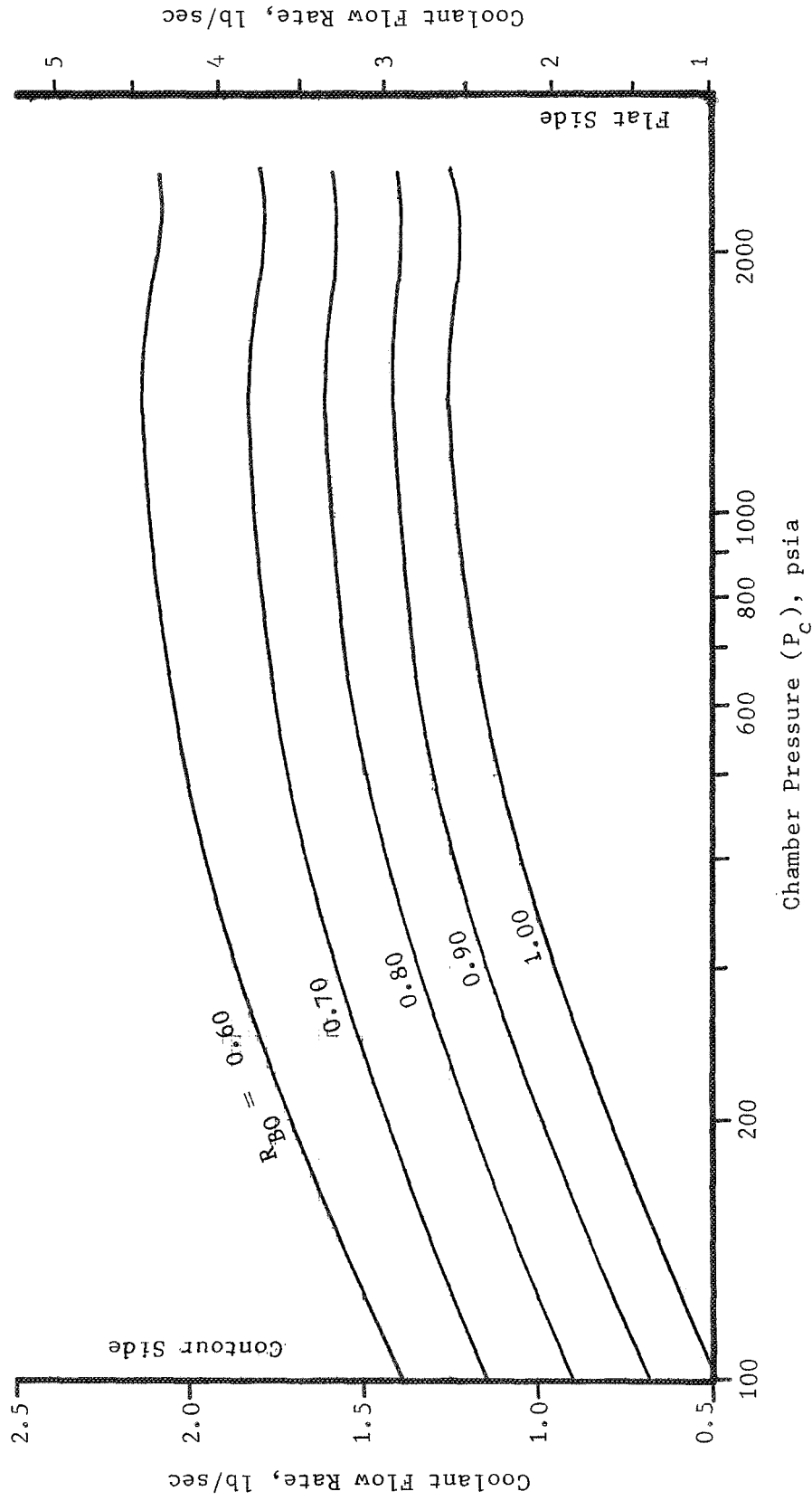


Figure 25. Coolant Flow Rate vs Chamber Pressure - 0.002 in. Hafnia Coating

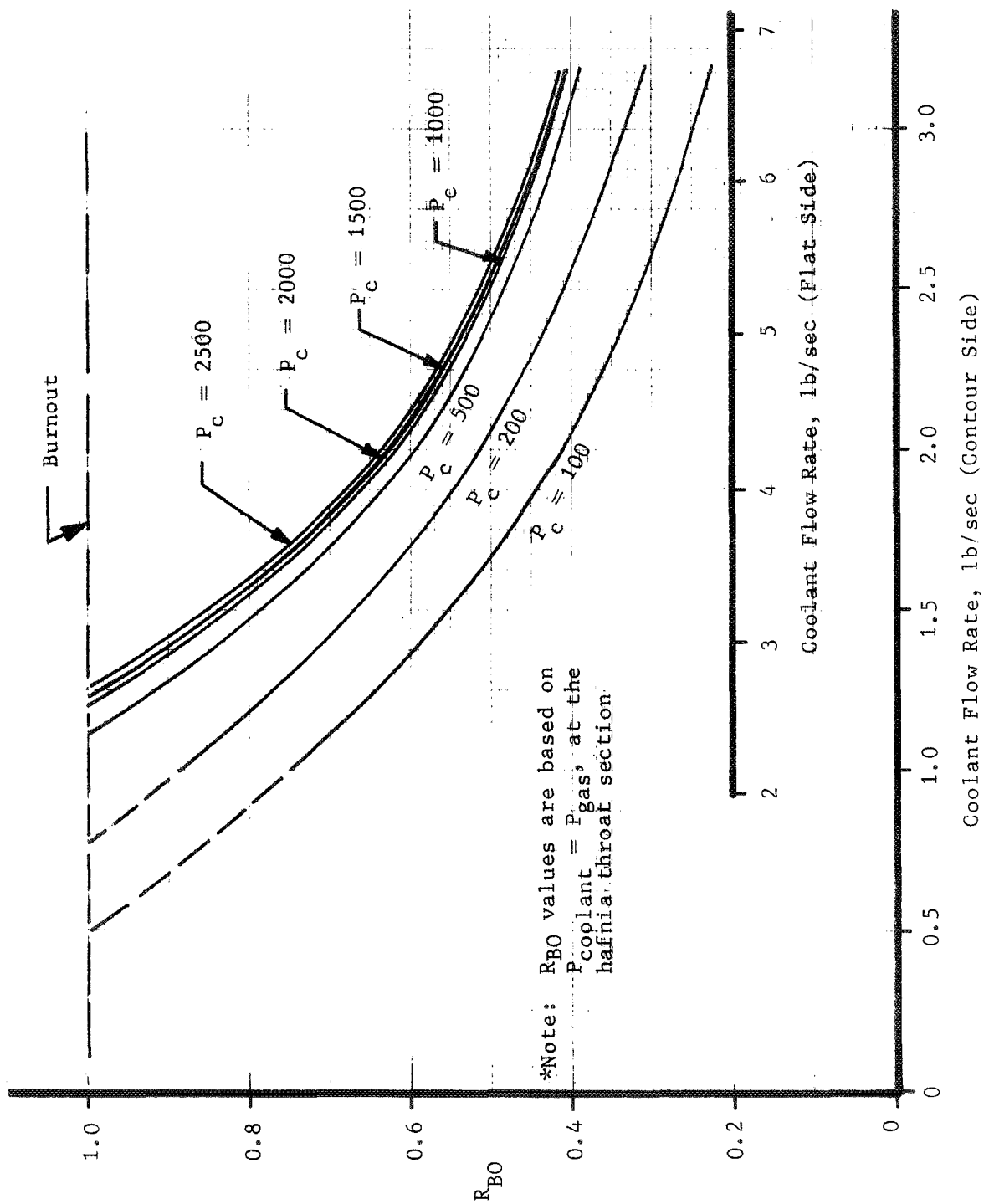


Figure 26. Throat Section  $R_{BO}$  vs Coolant Flow Rate - 0.002 in. Hafnia Coating

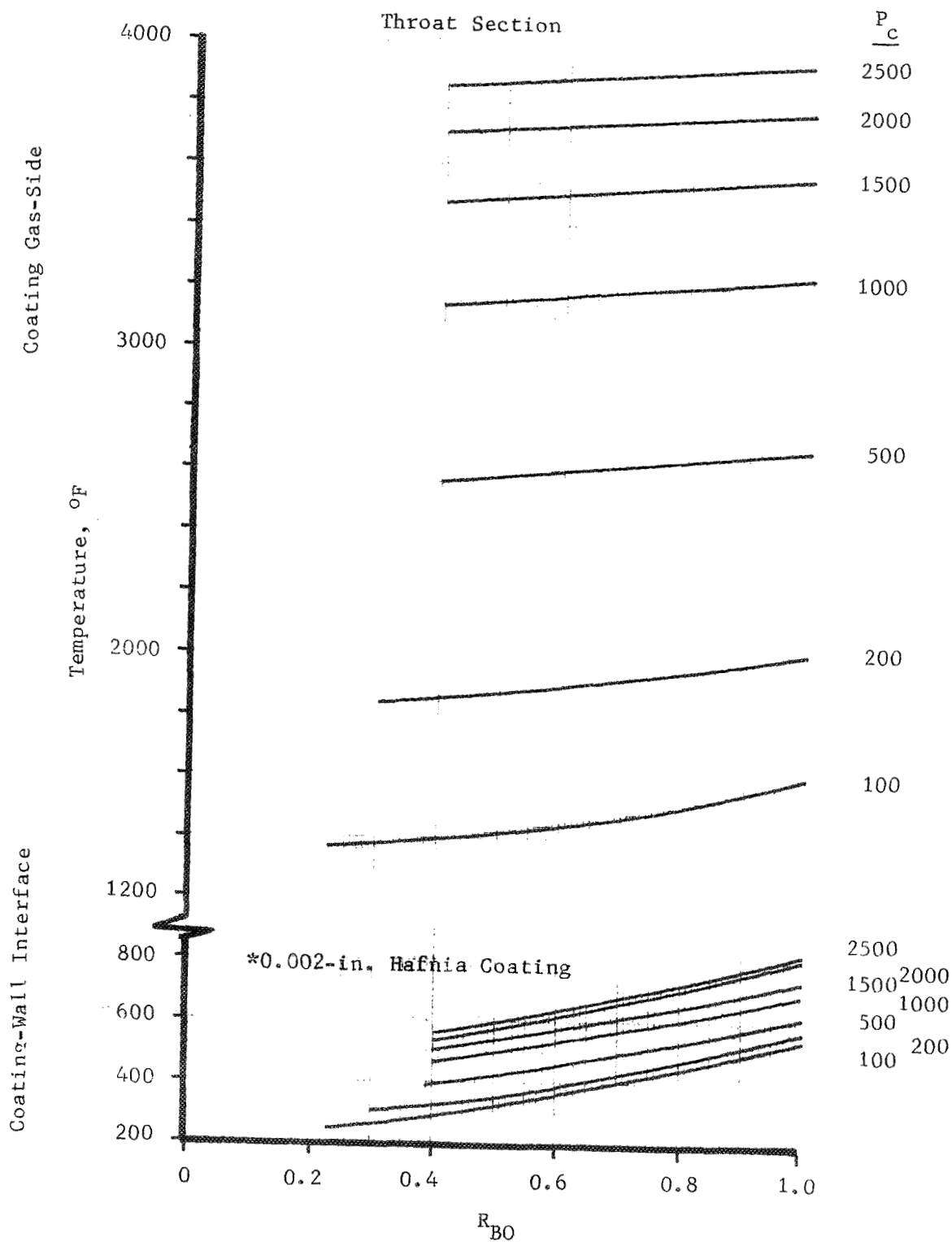


Figure 27. Gas-Side and Wall/Coating Interface Temperature vs  $R_{BO}$  - 0.002 in. Hafnia Coating

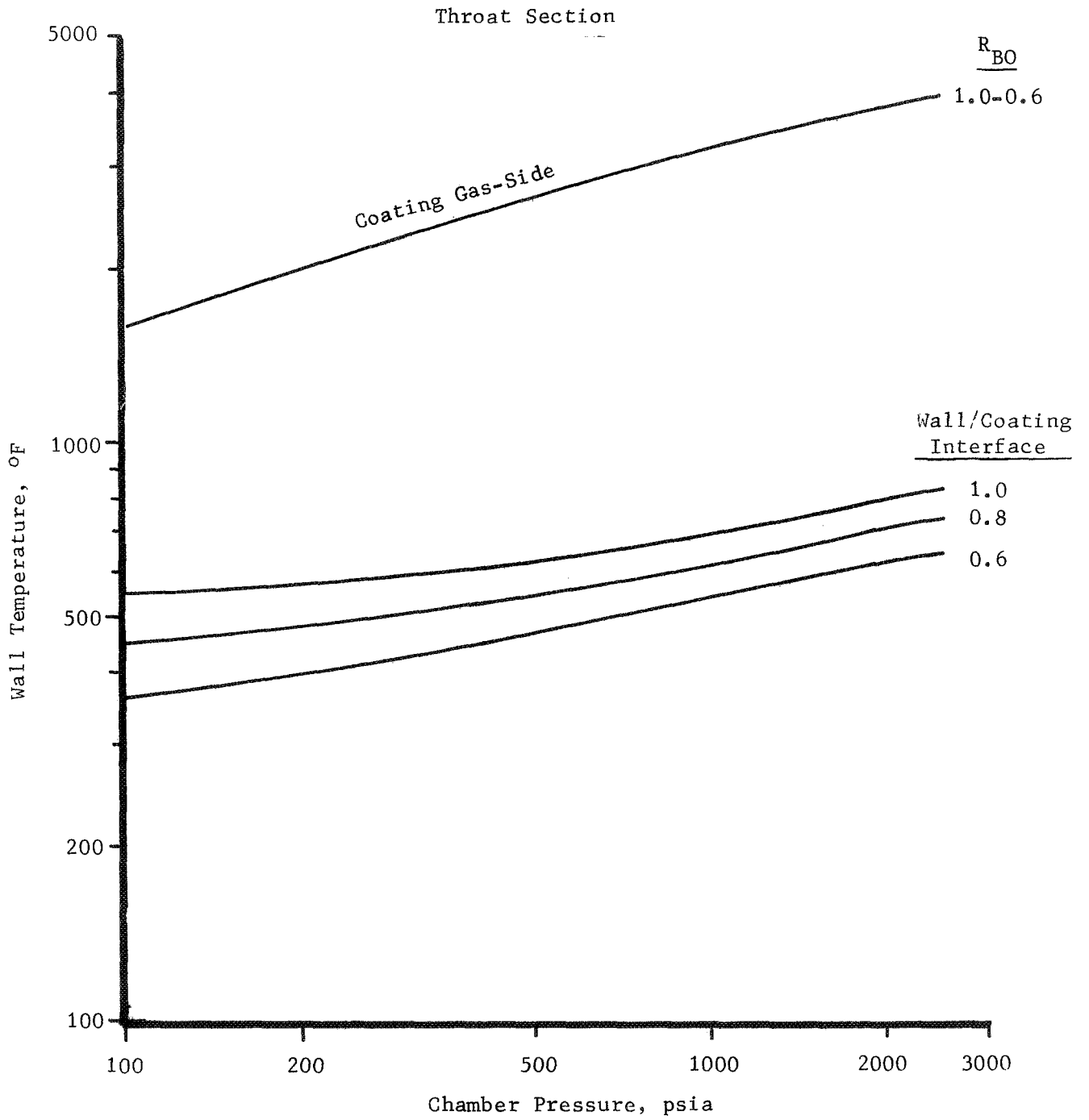


Figure 28. Gas-Side and Wall/Coating Interface Temperature vs Chamber Pressure

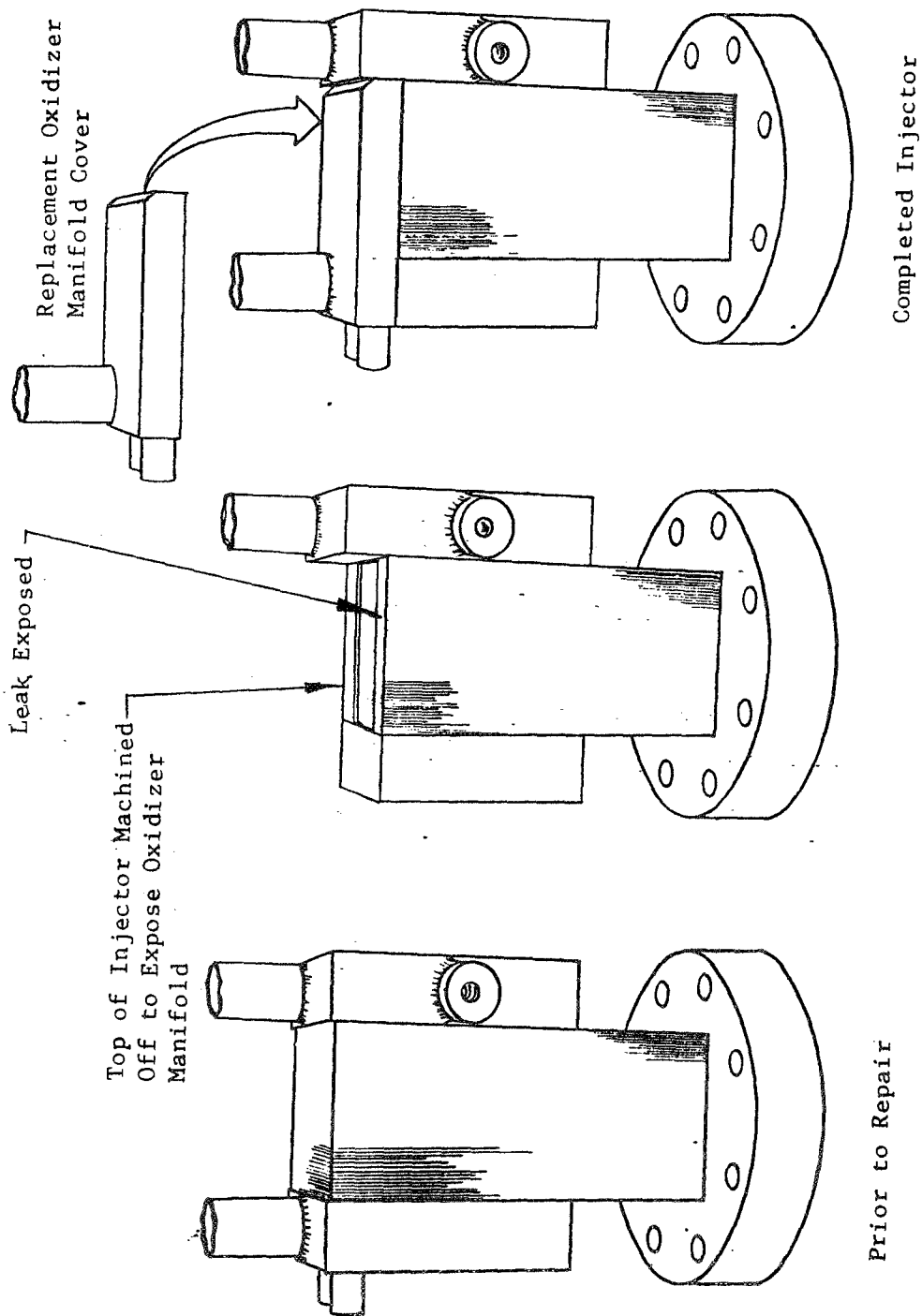


Figure 29. Injector Repair Procedure

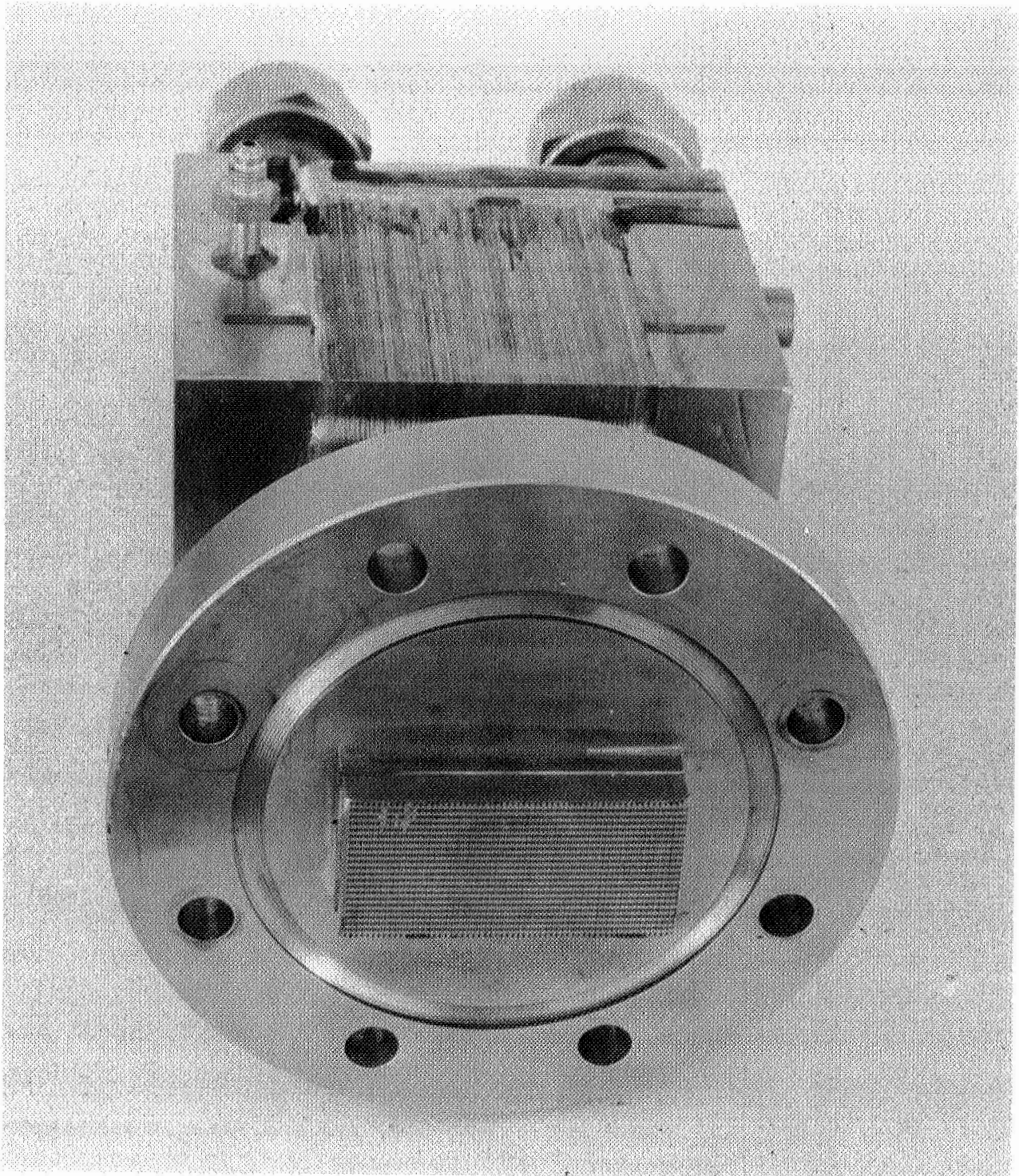


Figure 30. Annular Segment Injector Flat Face Configuration

Copper Flash

Nickel Plating

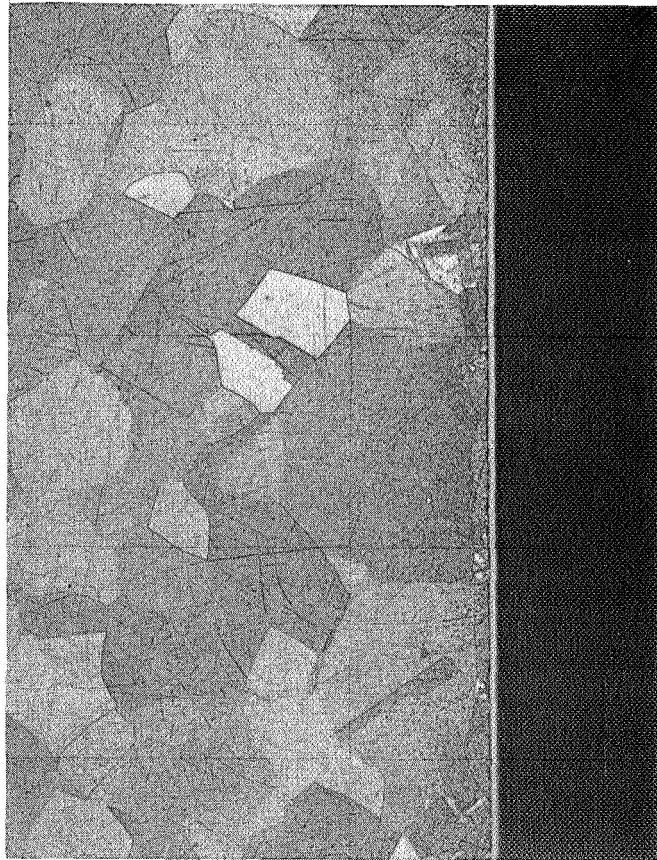


Figure 31. Nickel Platelet with Nickel Plating over Copper Flash

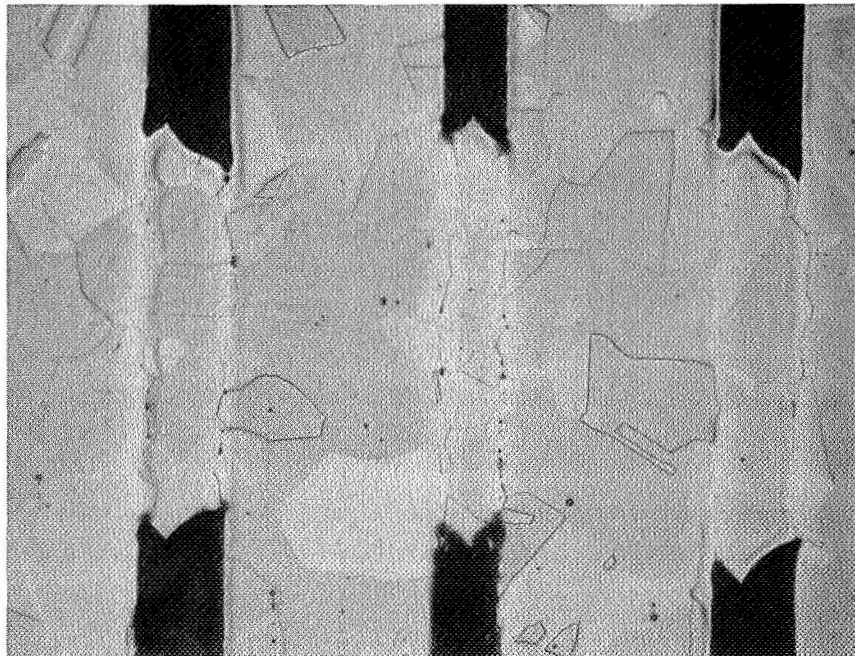
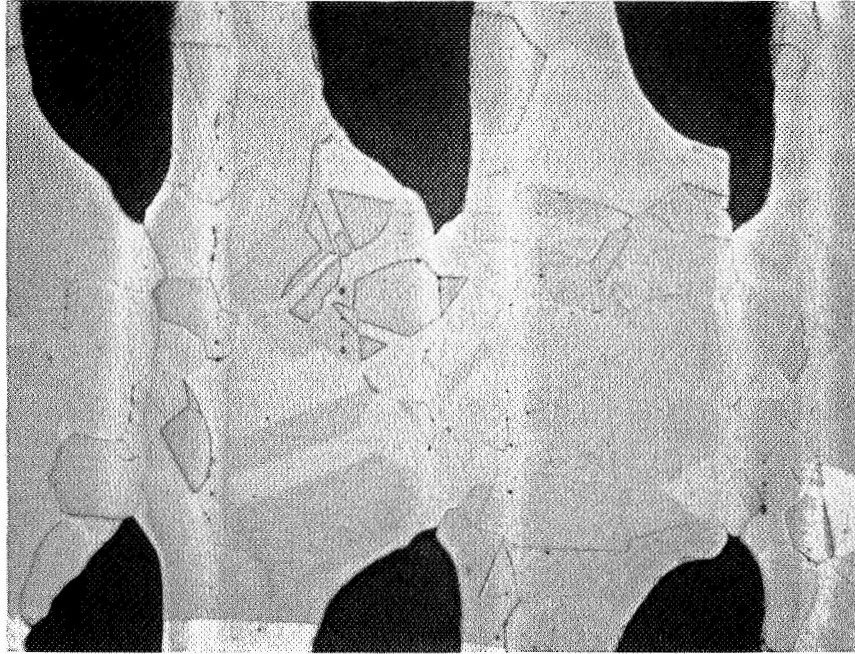


Figure 32. Injector Sample Stack No. 2 Bond Quality

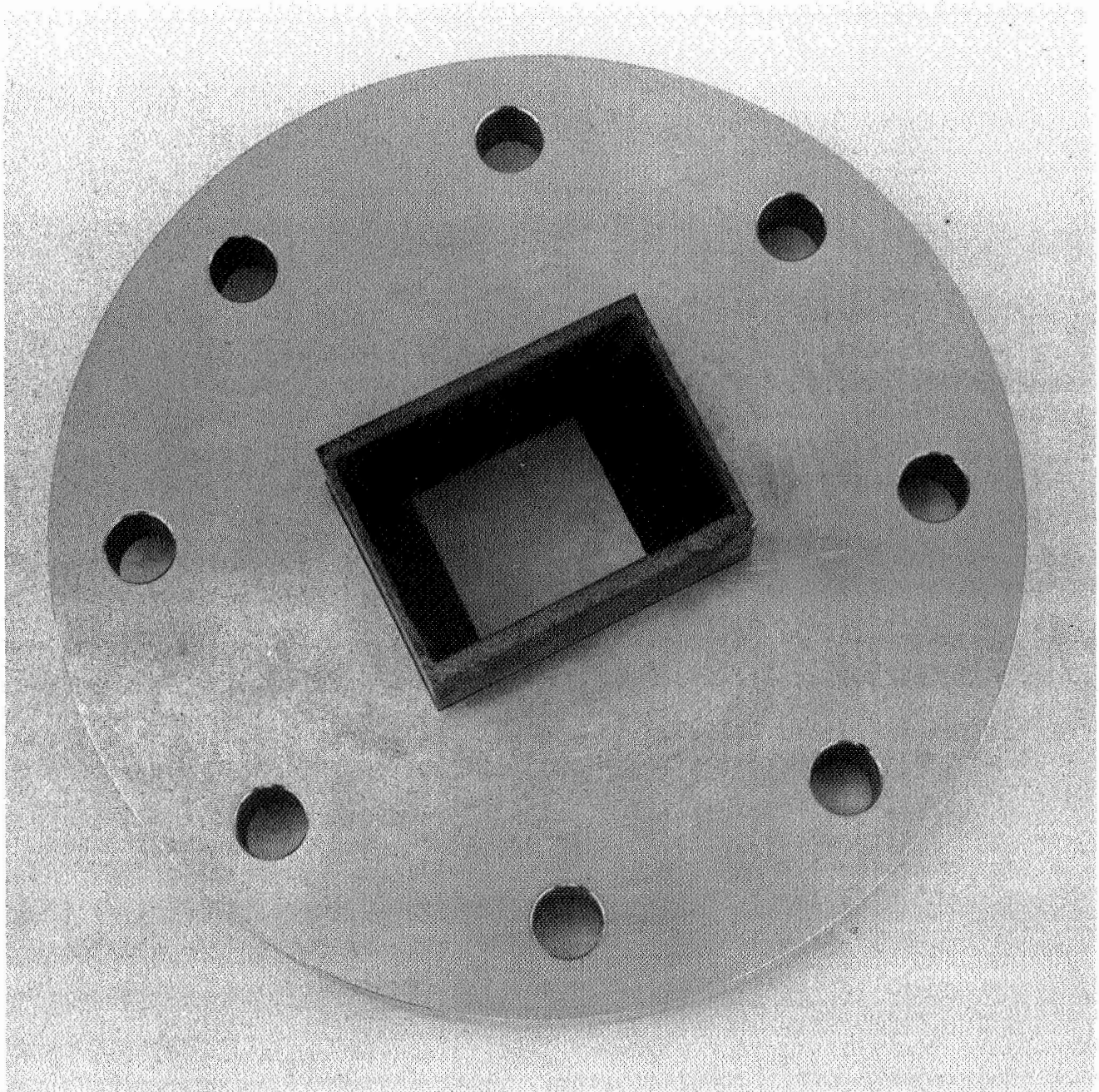


Figure 33. Nozzle Extension

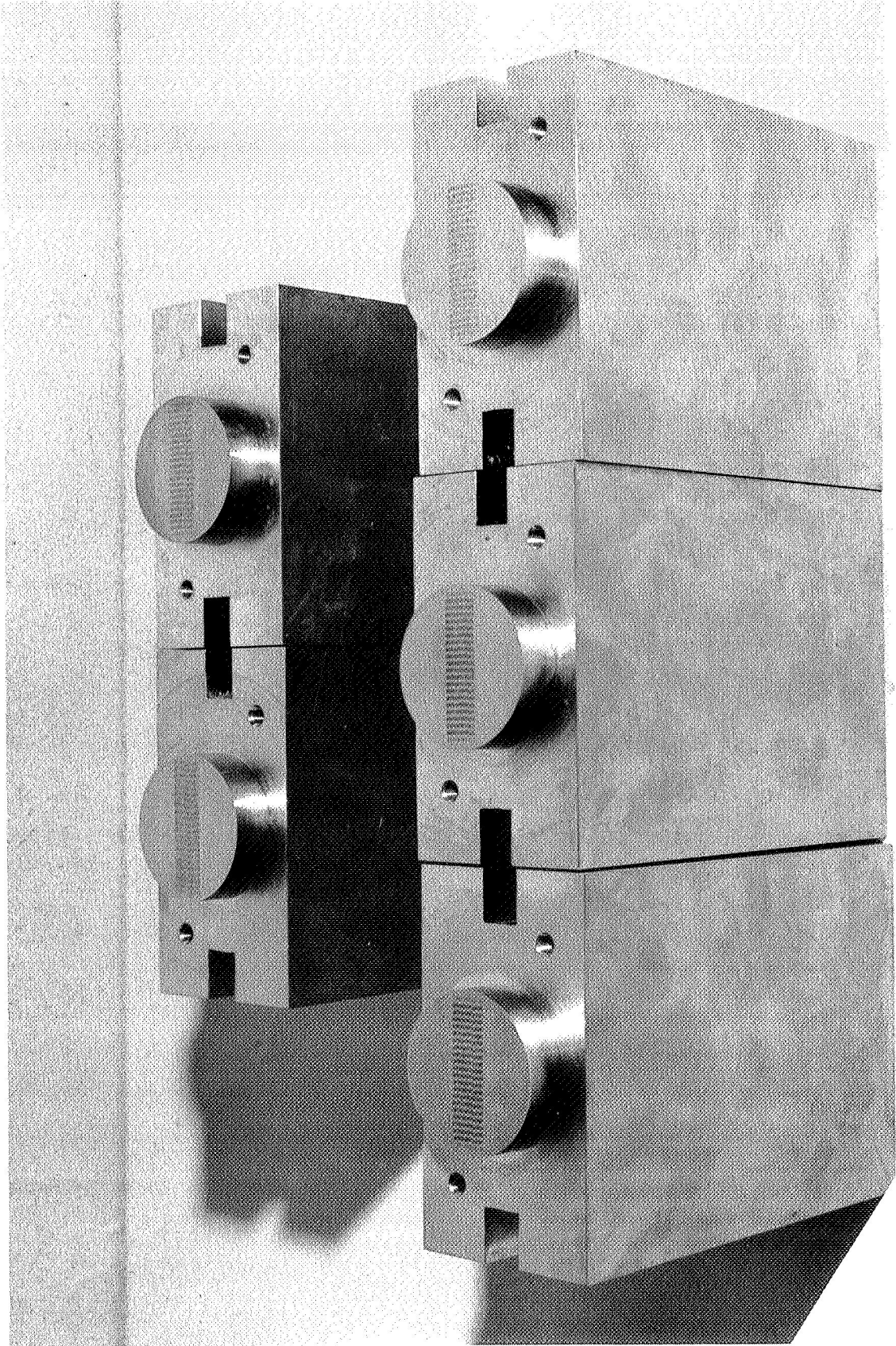


Figure 34. Heat Exchanger Samples

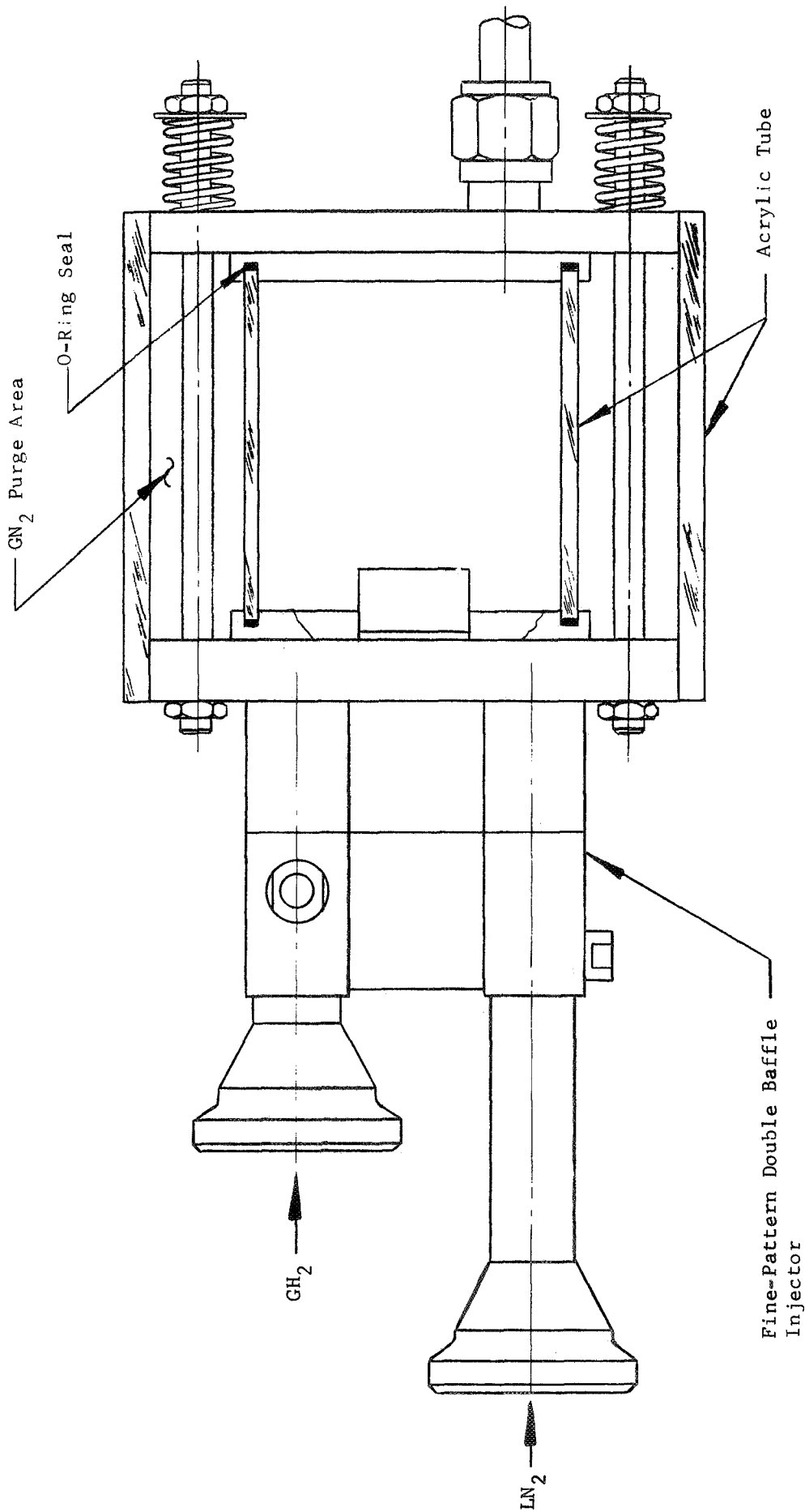


Figure 35. Heat Exchanger Evaluation Test Fixture

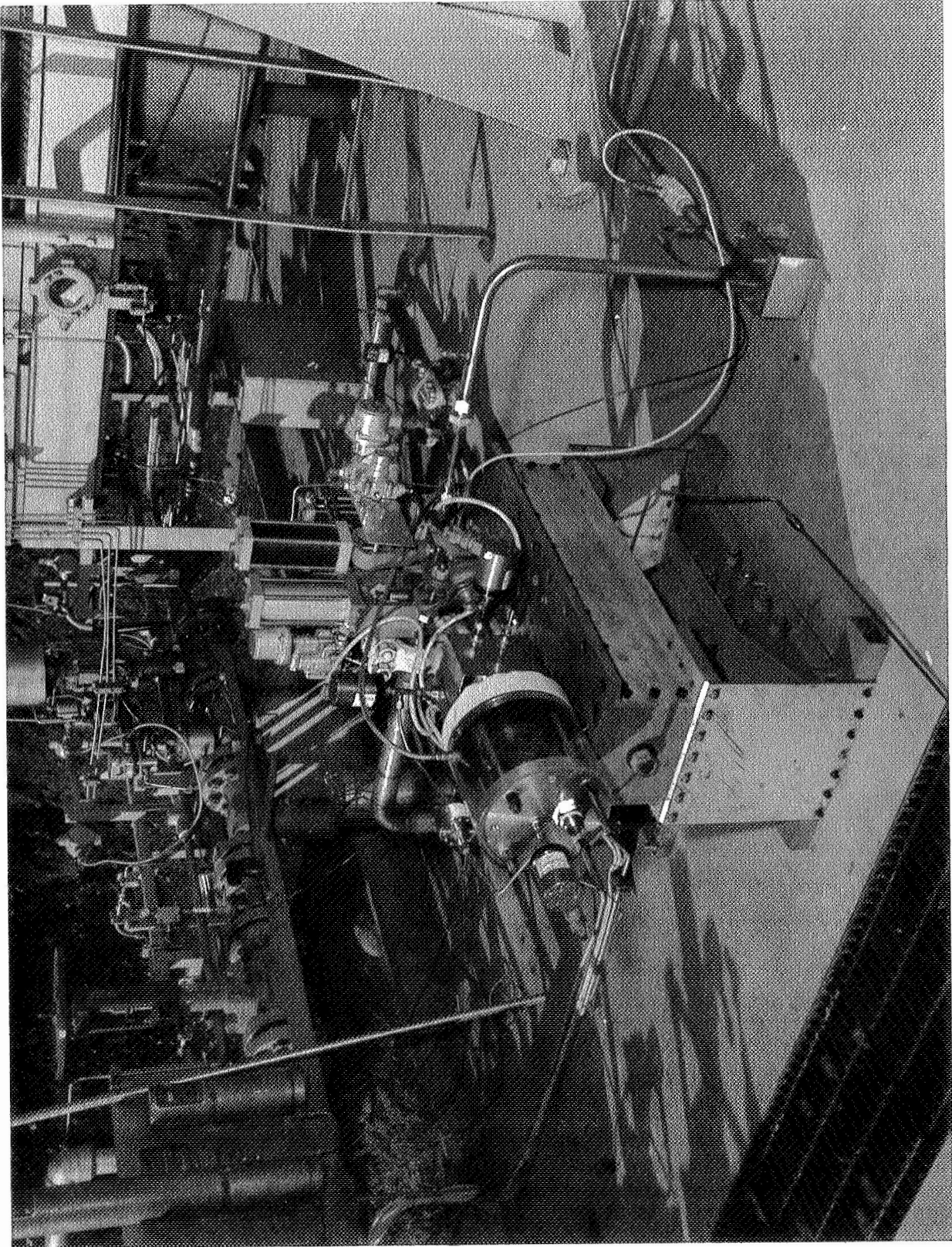
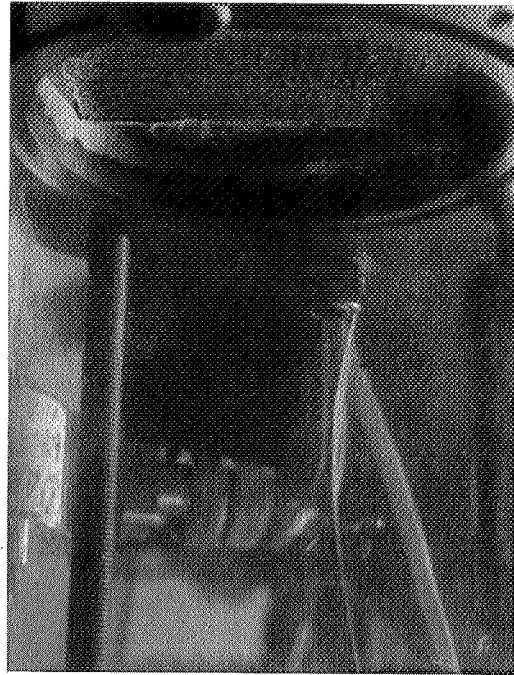


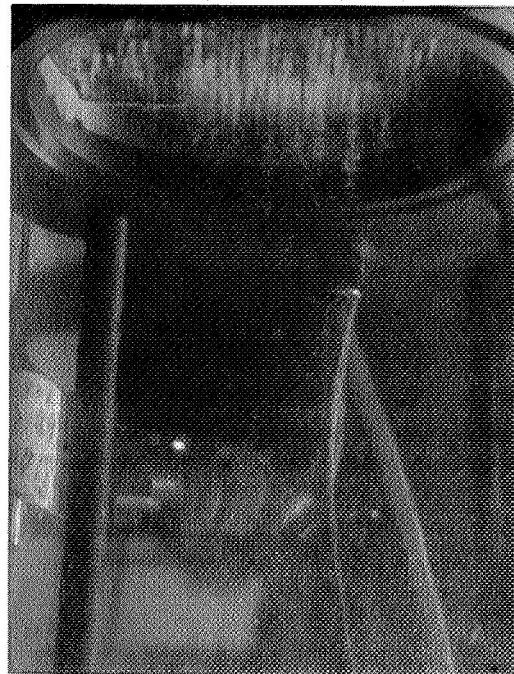
Figure 36. Phase II Injector Heat Exchanger Evaluation Test Setup



A.  
 $LN_2 = 0.734$   
 $GH_2 = 0.0118$



B.  
 $LN_2 = 0.510$   
 $GH_2 = 0.0807$



C.  
 $LN_2 = 0.588$   
 $GH_2 = 0.180$

D.  
 $LN_2 = 0.188$   
 $GH_2 = 0.0806$

Figure 37. Heat Exchanger Evaluation Test Results

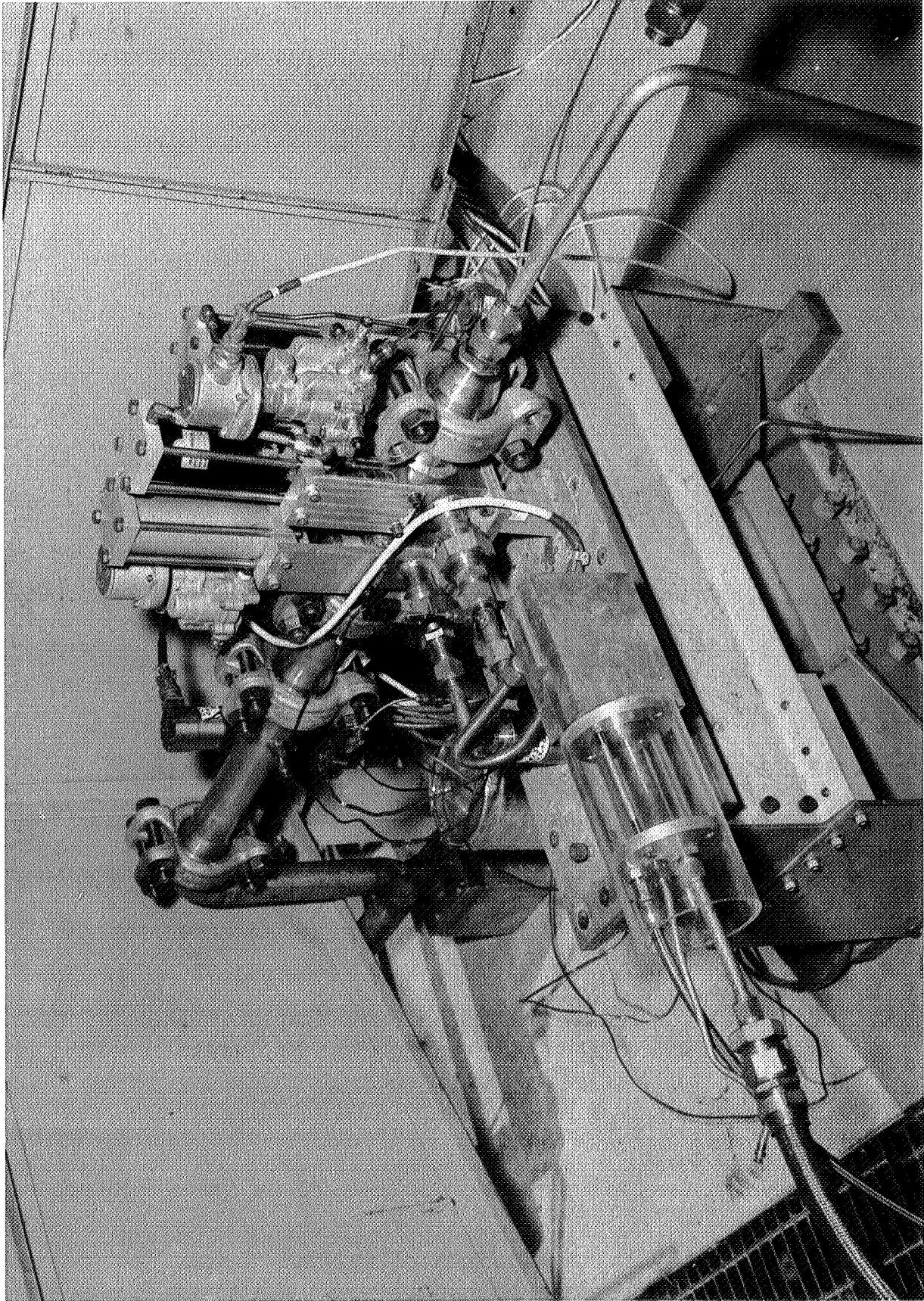
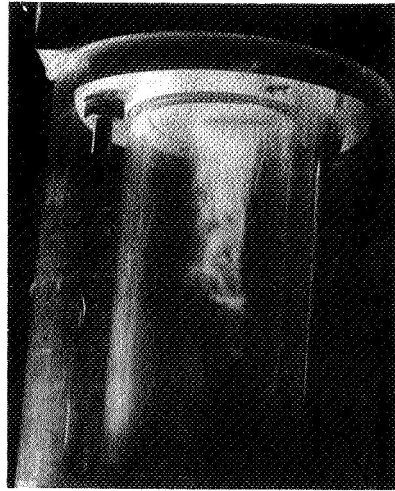
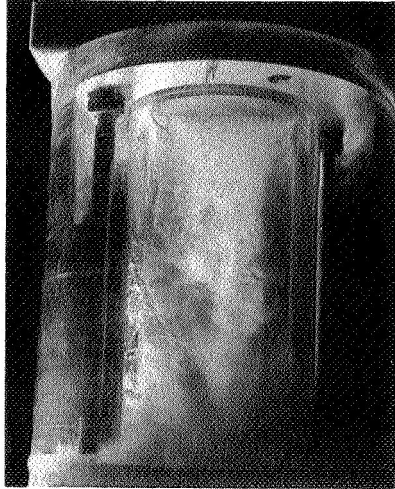


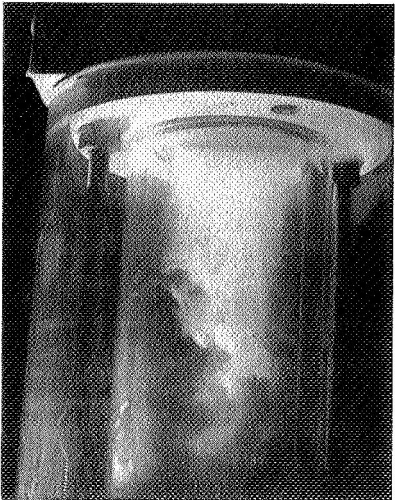
Figure 38. Heat Exchanger Sample Test Setup



III

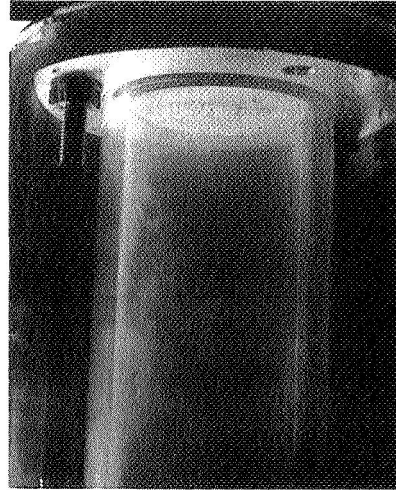


II

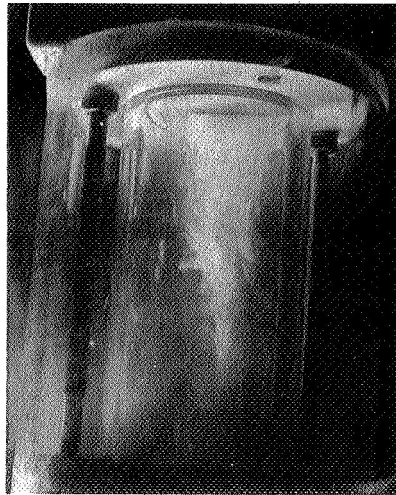


I

$\dot{v}_H = 0.025 \text{ lb/sec}$   
 $\dot{v}_N = 0.330 \text{ lb/sec}$



V



IV

Figure 39. Heat Exchanger Samples - Test Results Comparison

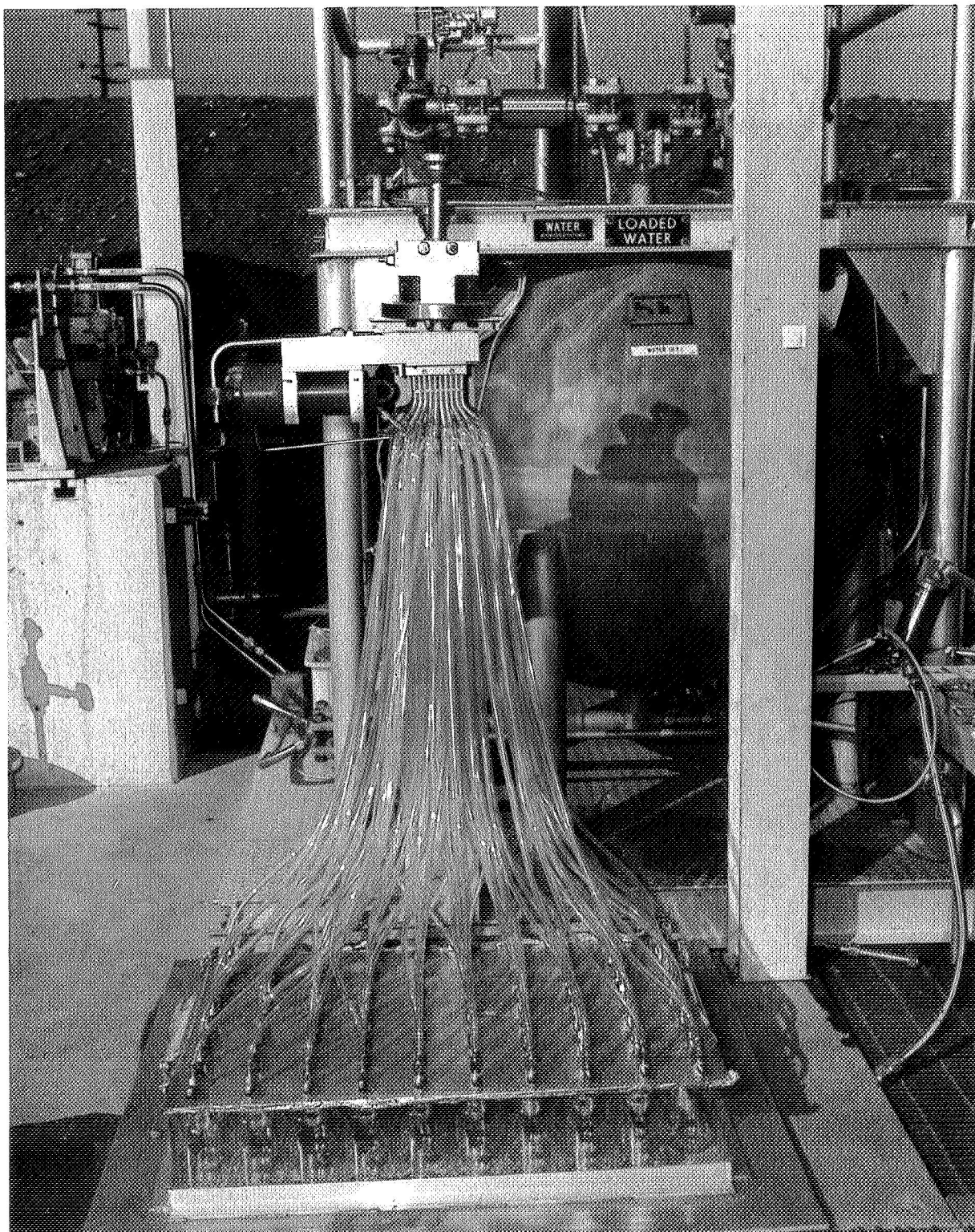


Figure 40. Mass Distribution Test Fixture

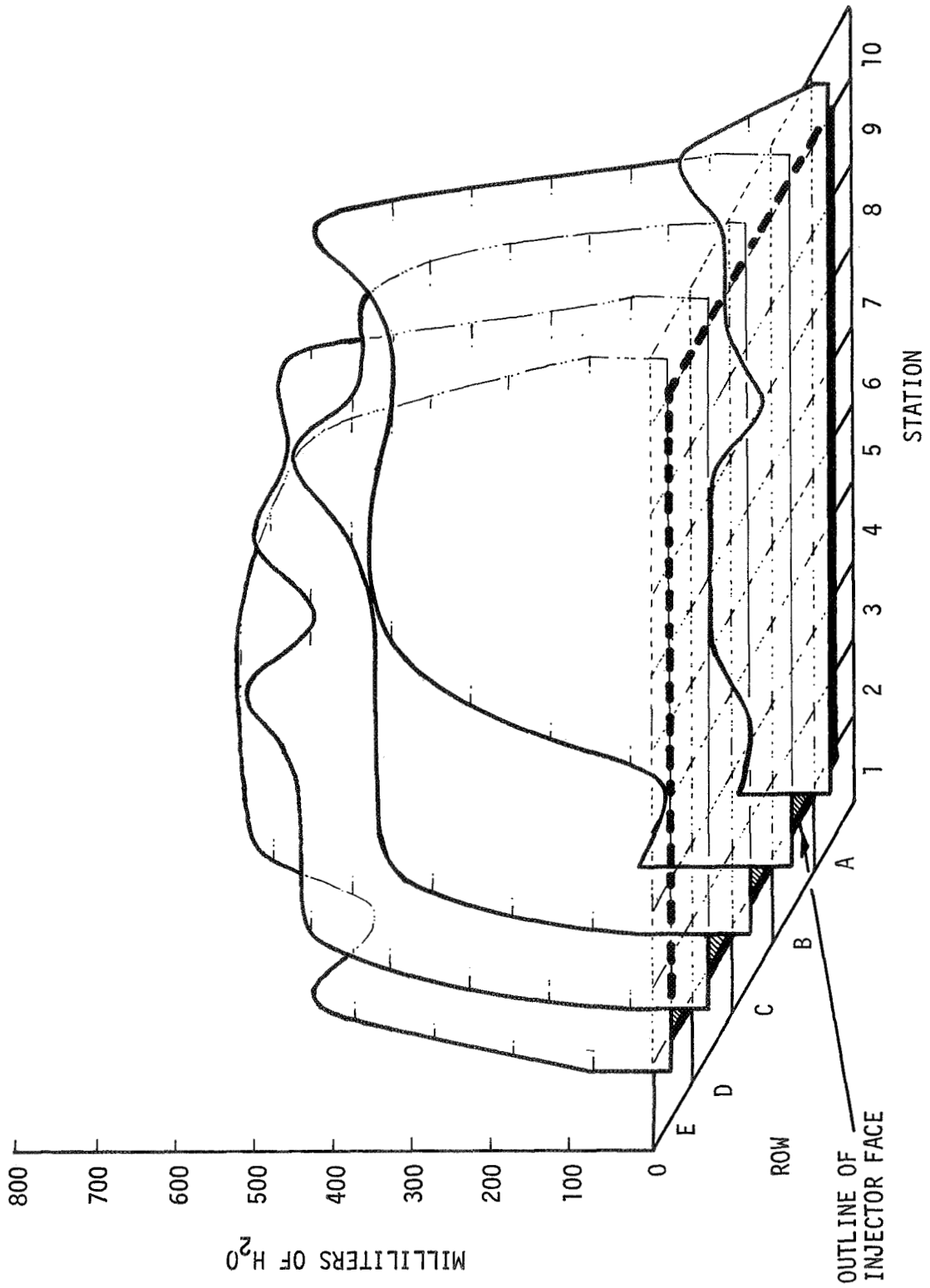


Figure 41. Coarse Pattern Fuel Flow Distribution

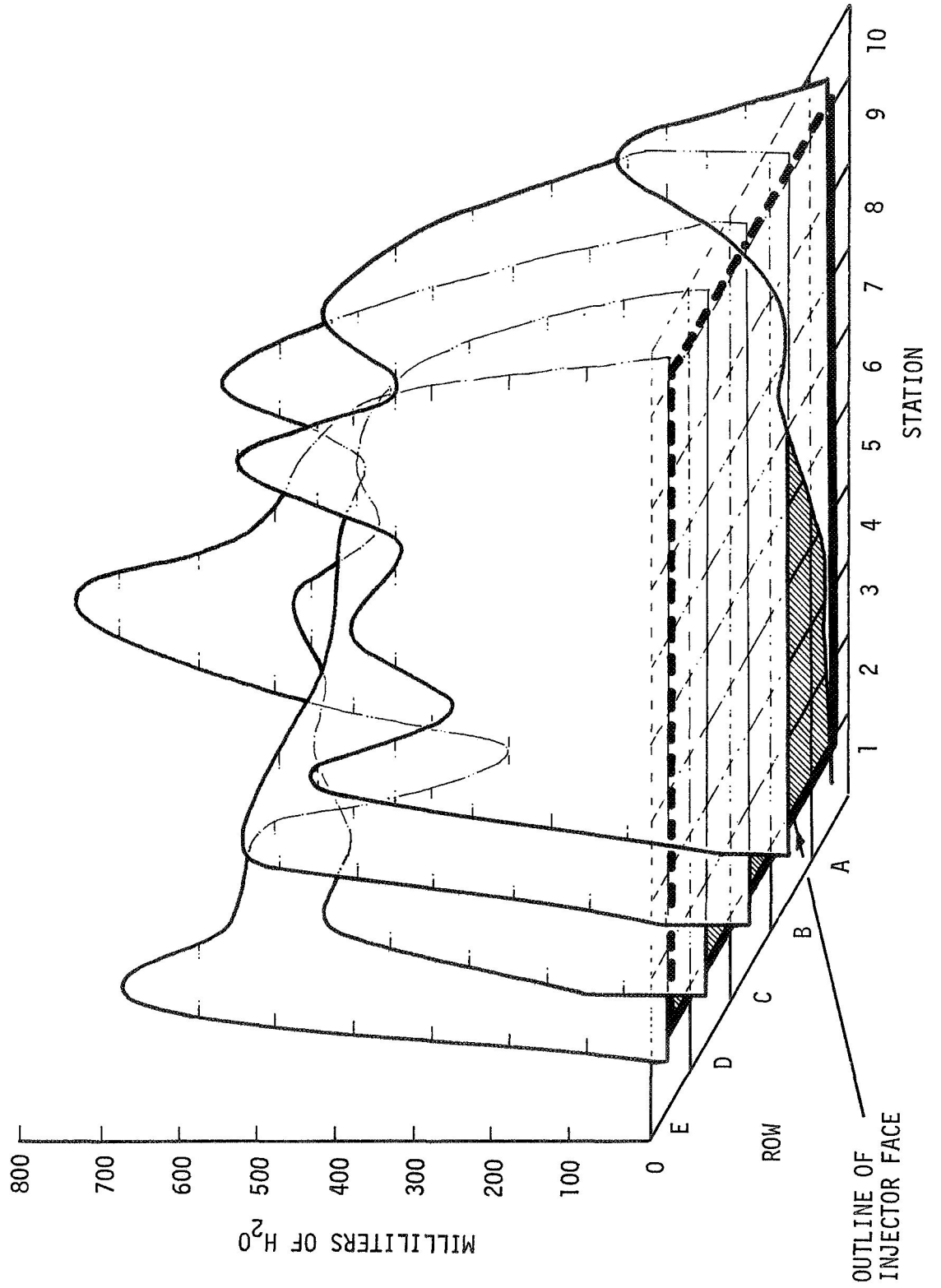


Figure 42. Coarse Pattern Oxidizer Flow Distribution

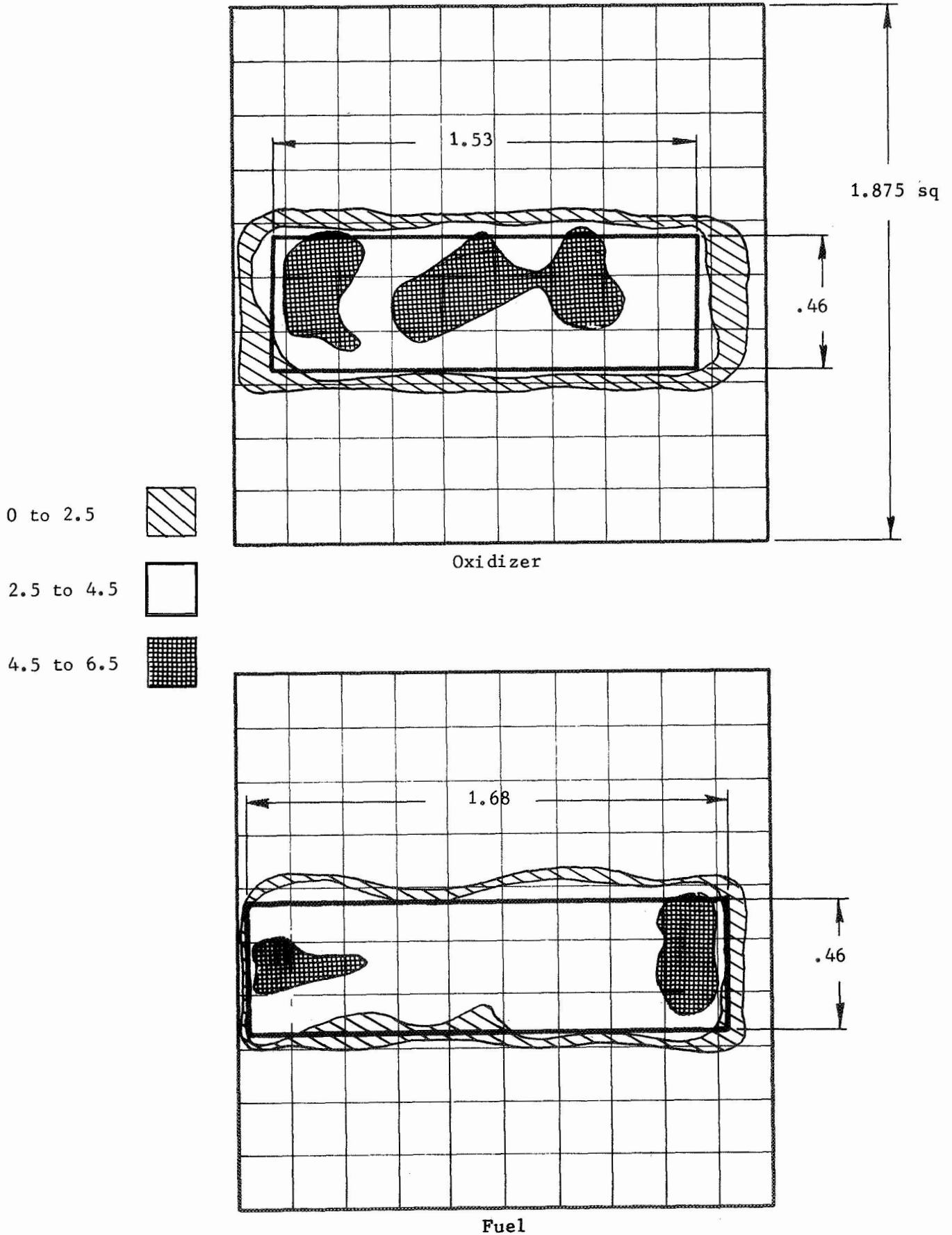


Figure 43. Relative Mass Flux Type I

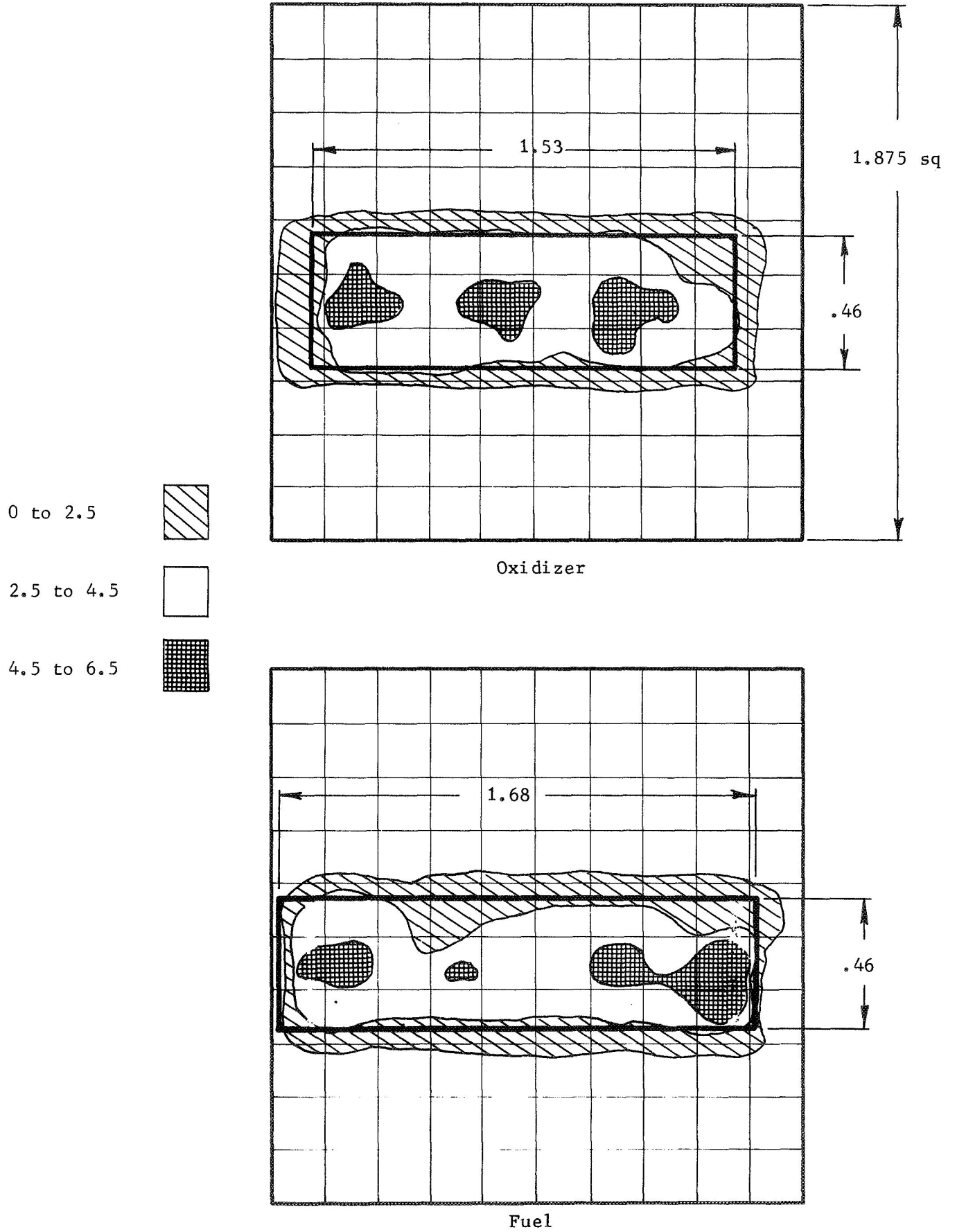


Figure 44. Relative Mass Flux Type II

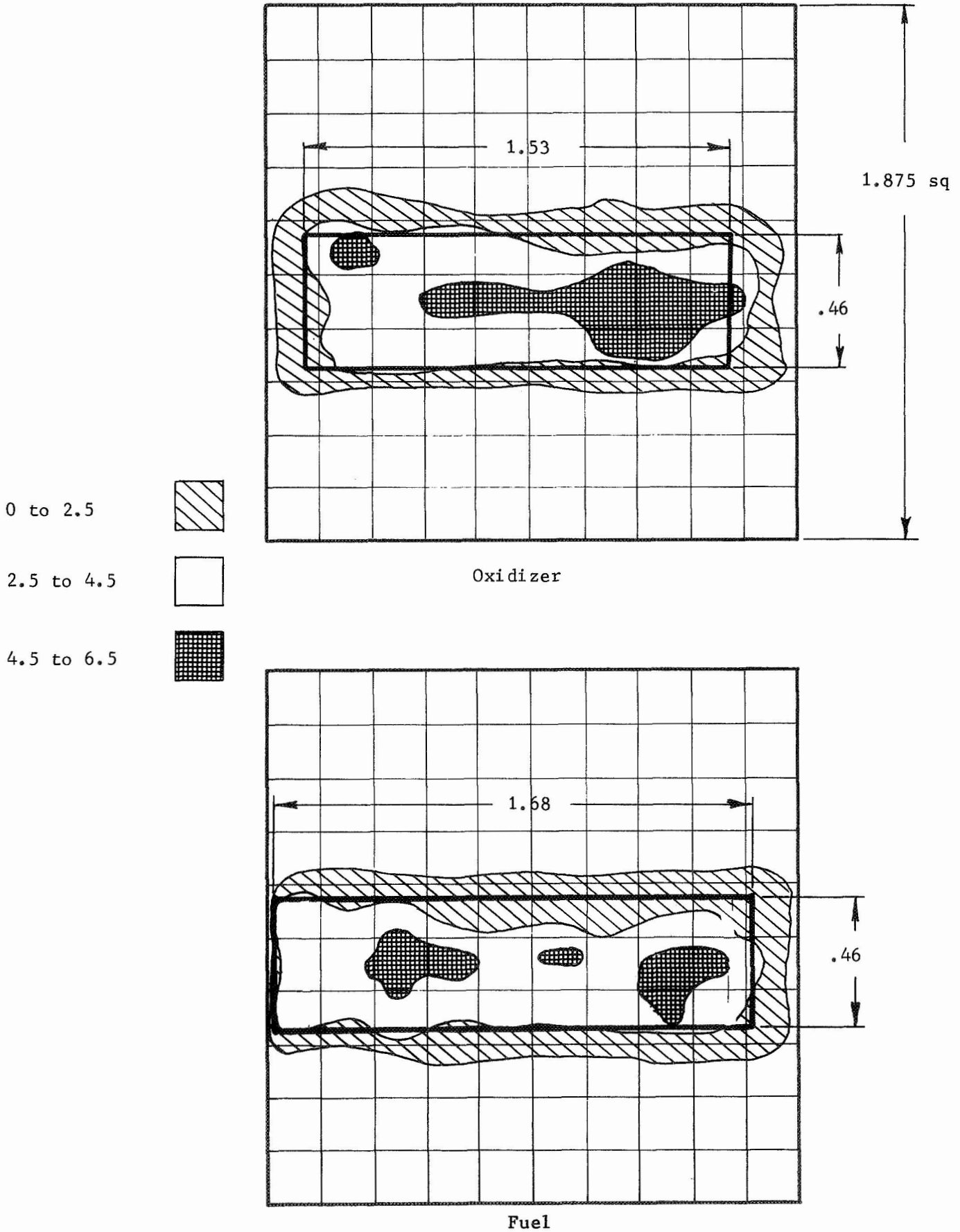


Figure 45. Relative Mass Flux Type III

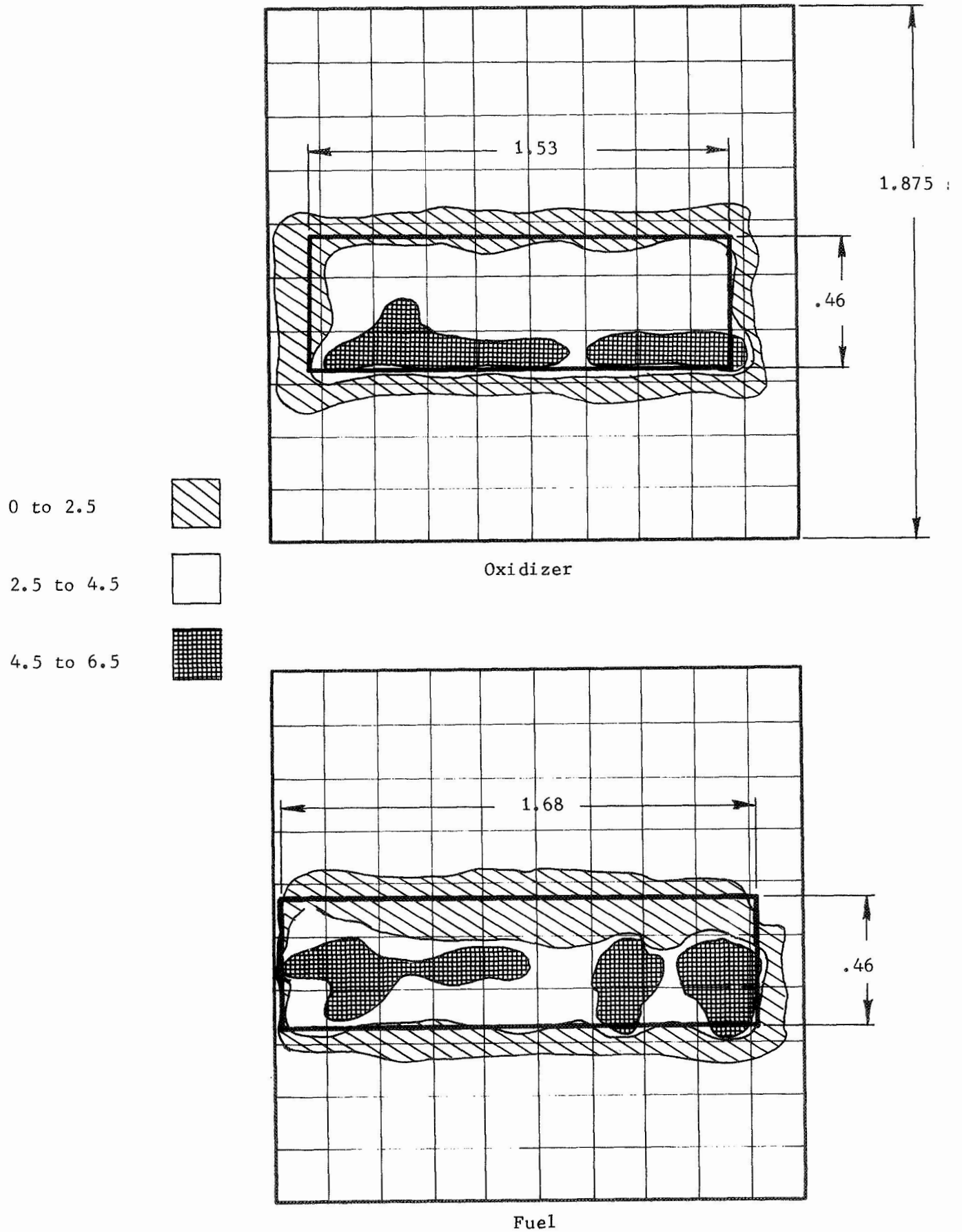


Figure 46. Relative Mass Flux Type IV

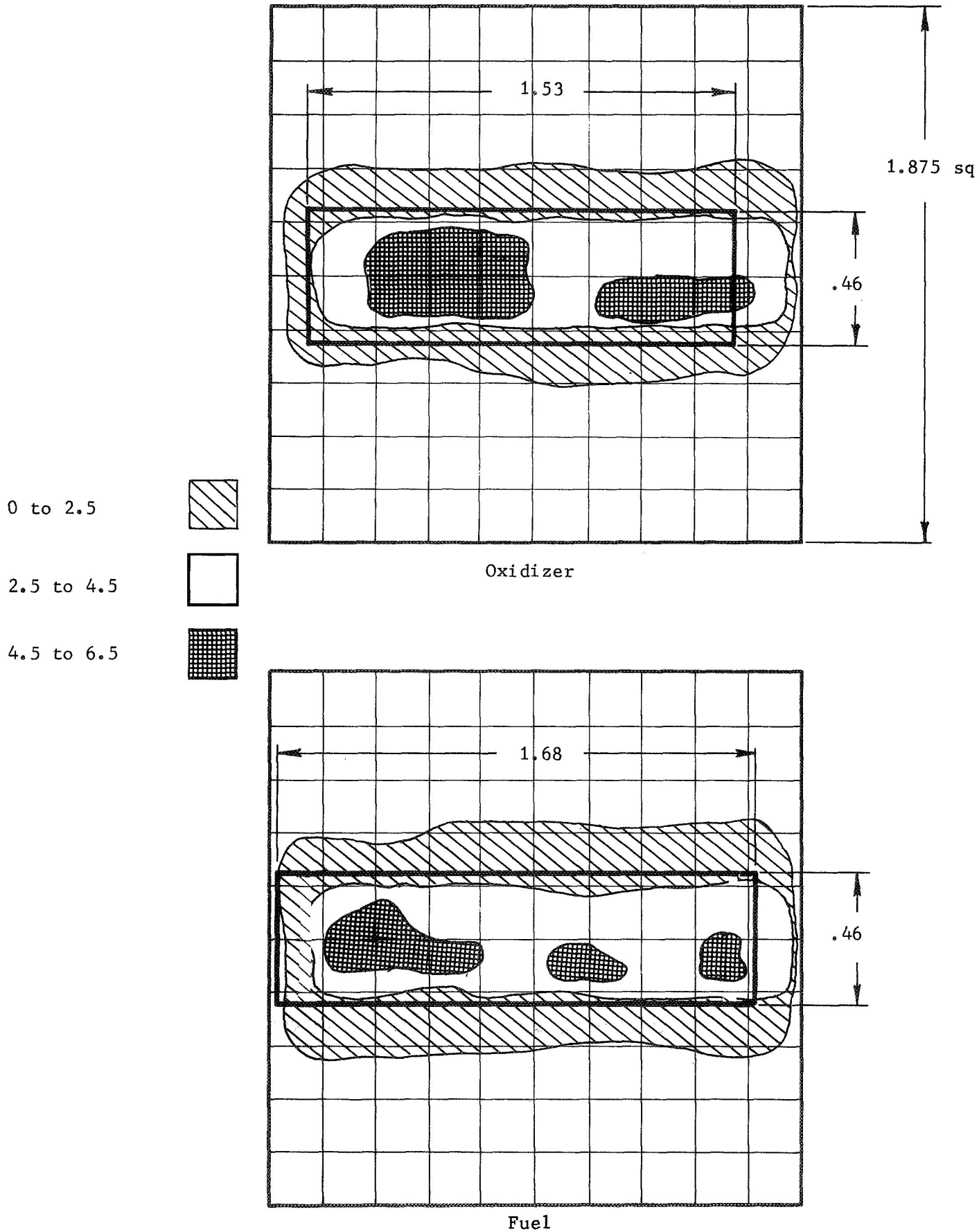


Figure 47. Relative Mass Flux Type V

GO<sub>2</sub>/GH<sub>2</sub> @ 540°R  
 HIPERTHIN Injector  
 2.5-in. Chamber

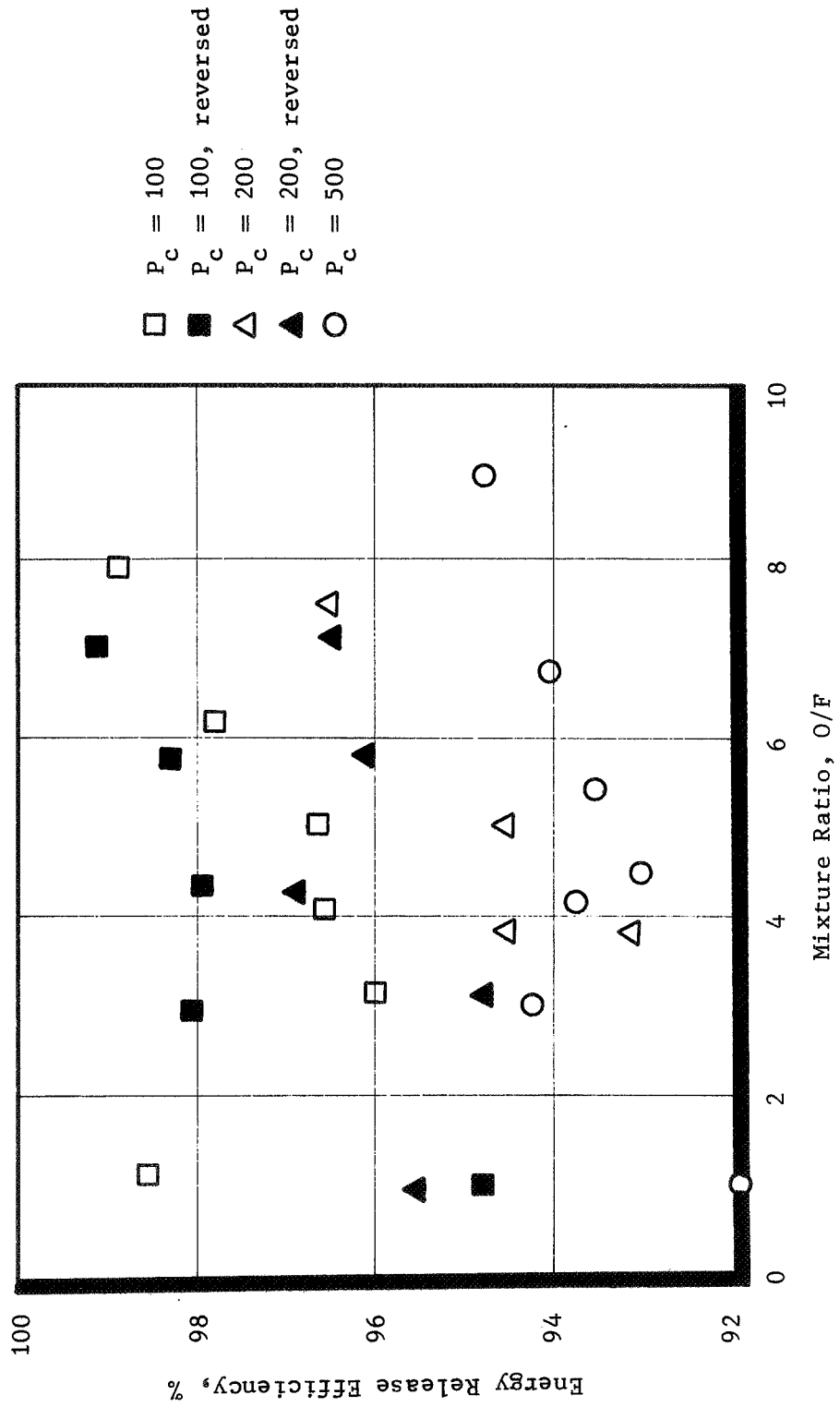


Figure 48. Energy Release Efficiency vs Mixture Ratio

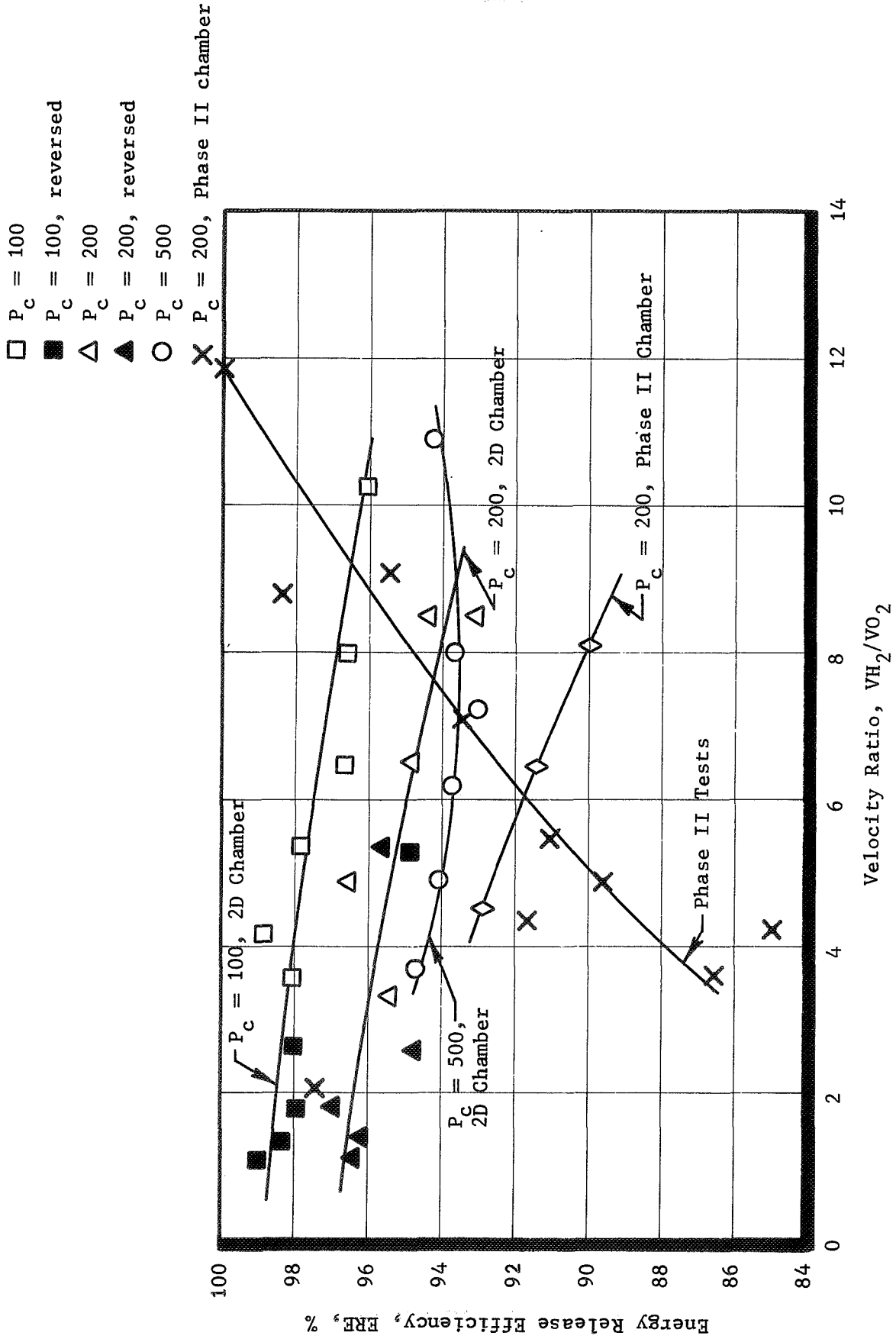
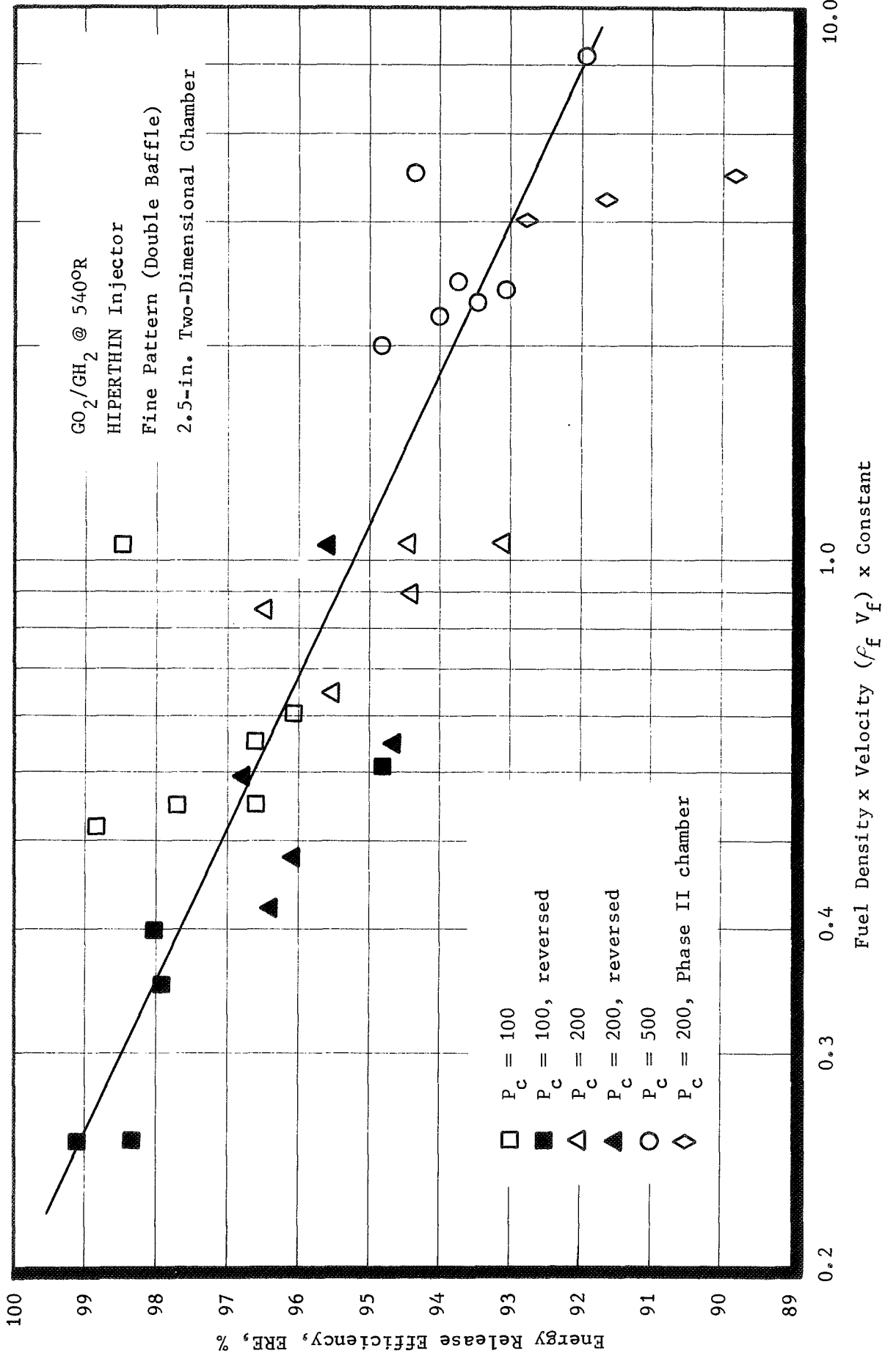


Figure 49. Energy Release Efficiency vs Velocity Ratio



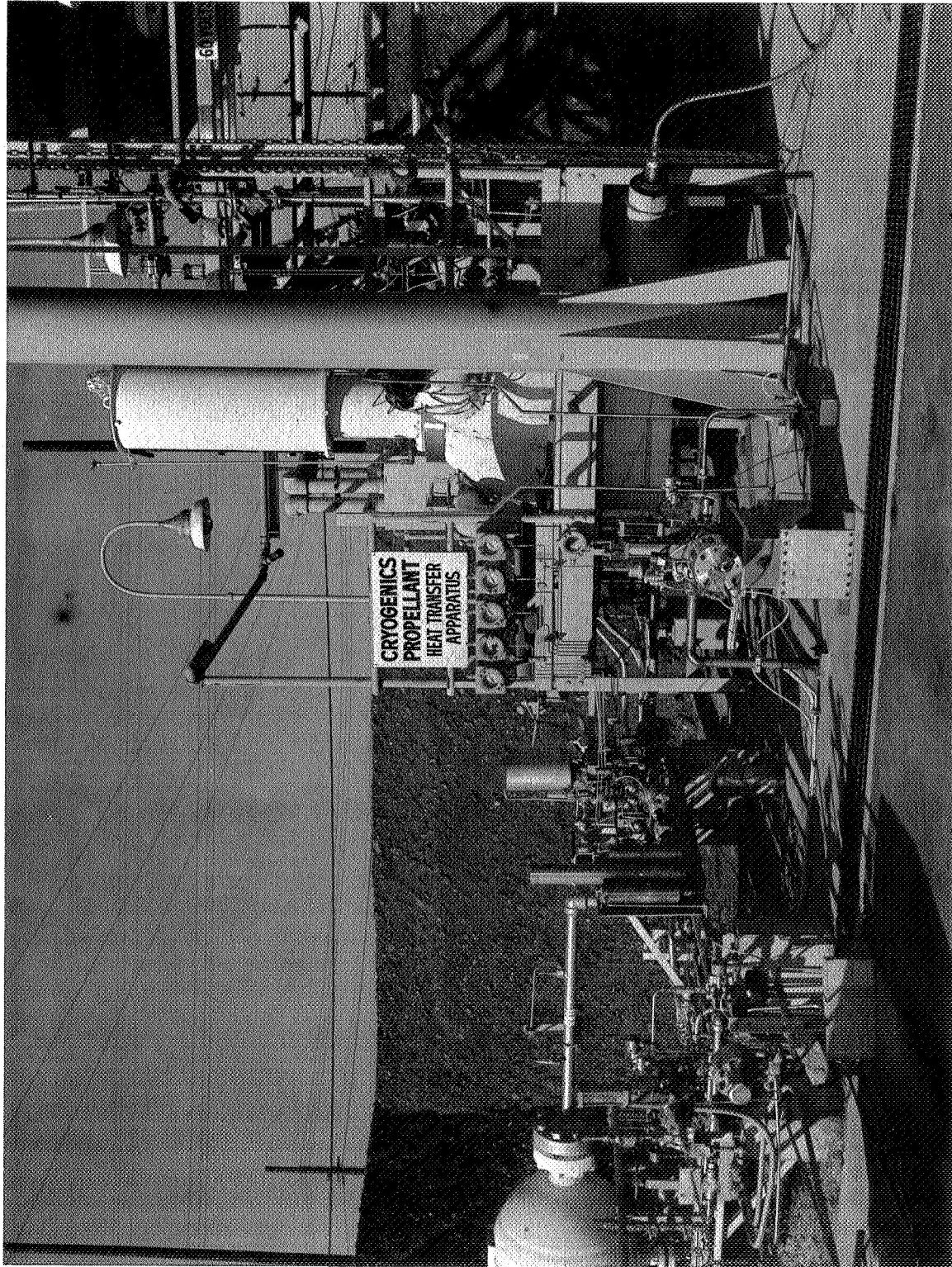


Figure 51. Test Bay Seven - Physics Lab

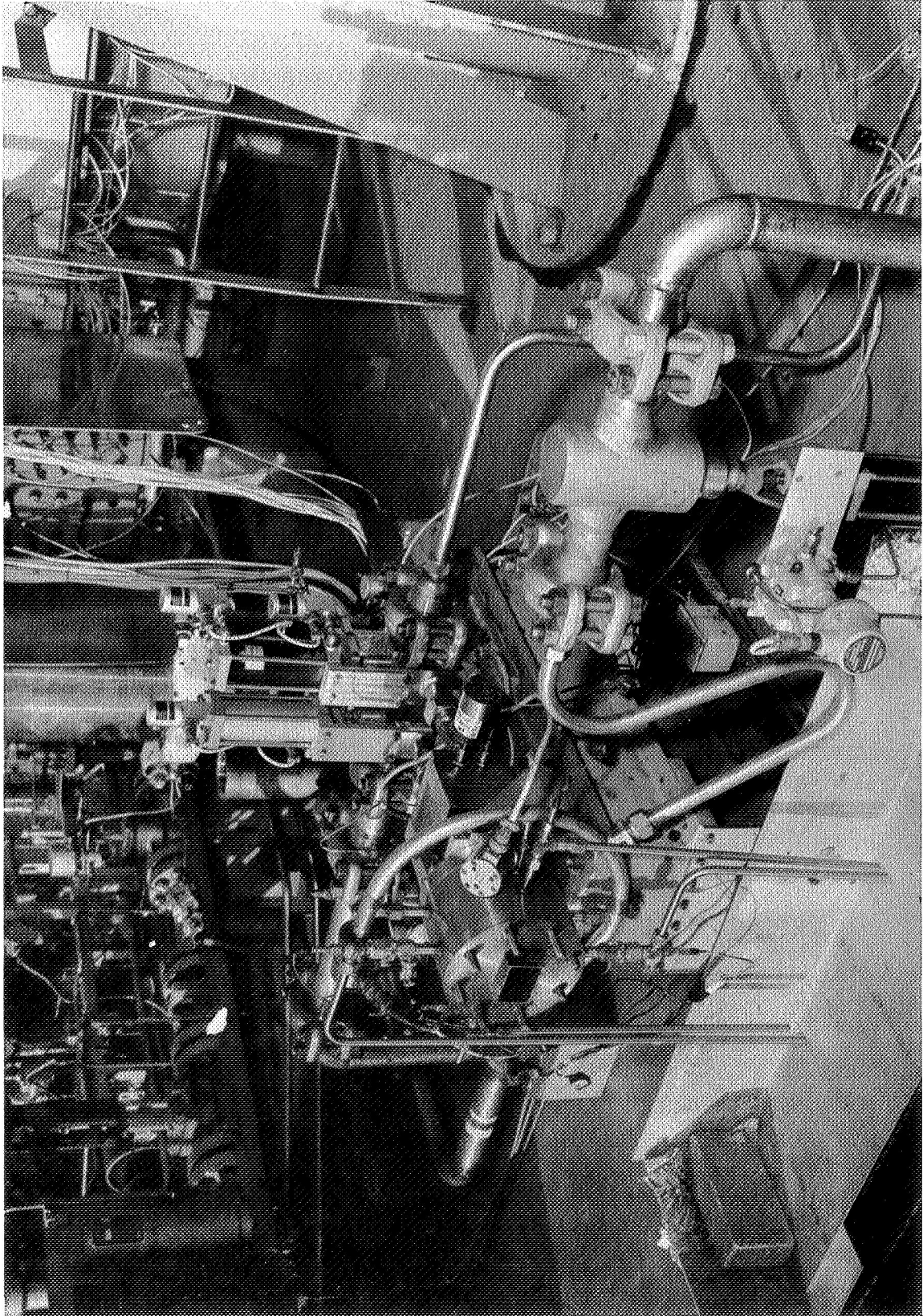


Figure 52. Hardware Setup for Testing

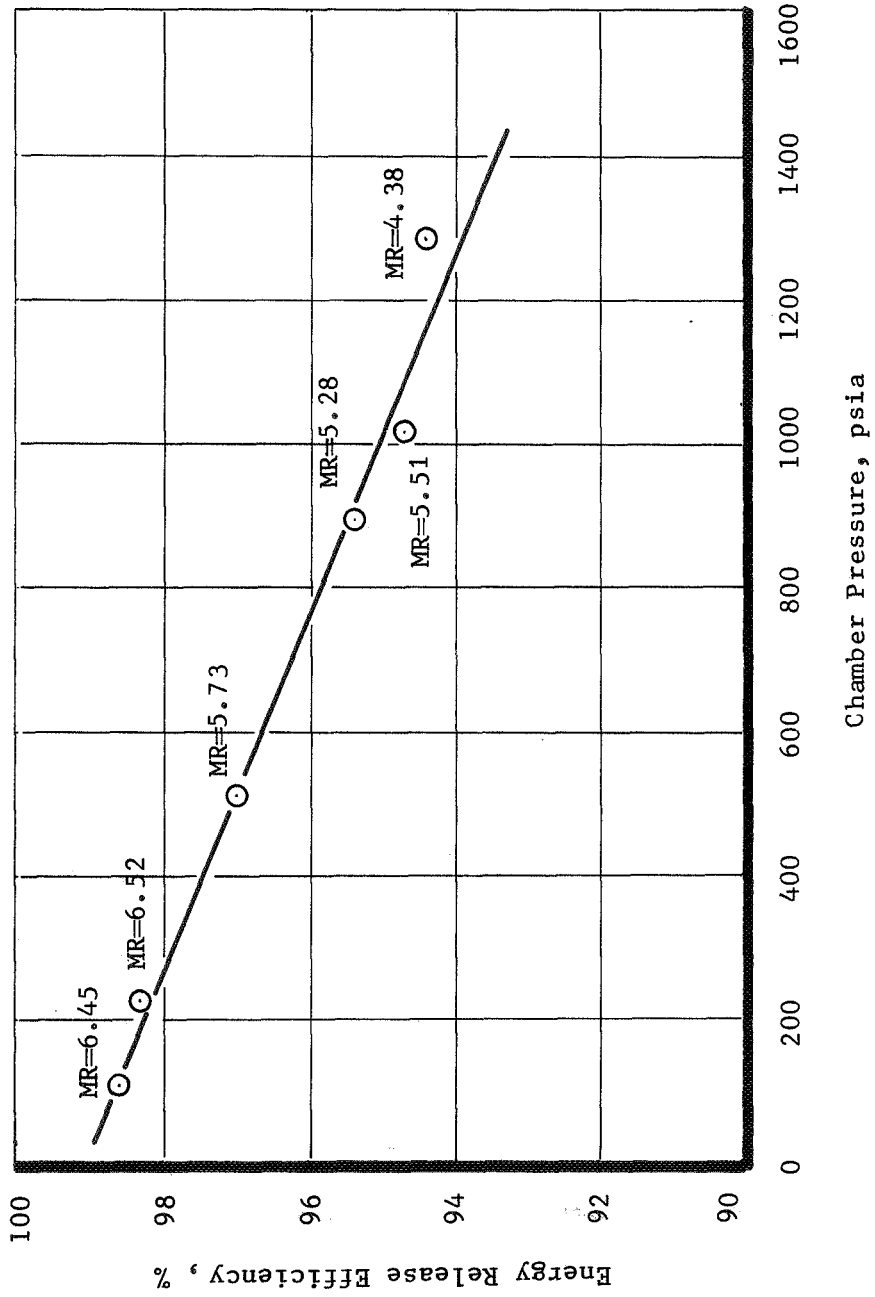


Figure 53. Energy Release Efficiency vs Chamber Pressure

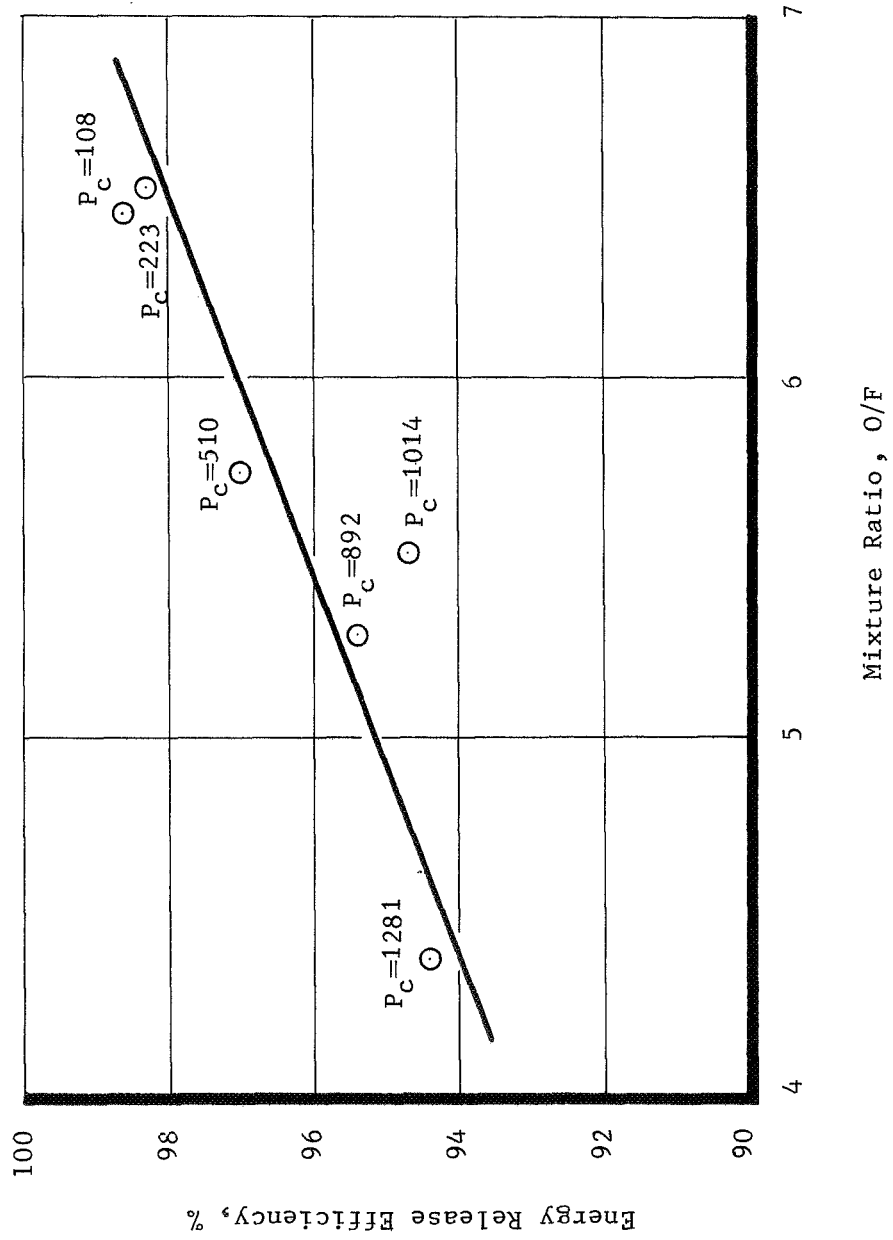


Figure 54. Energy Release Efficiency vs Mixture Ratio

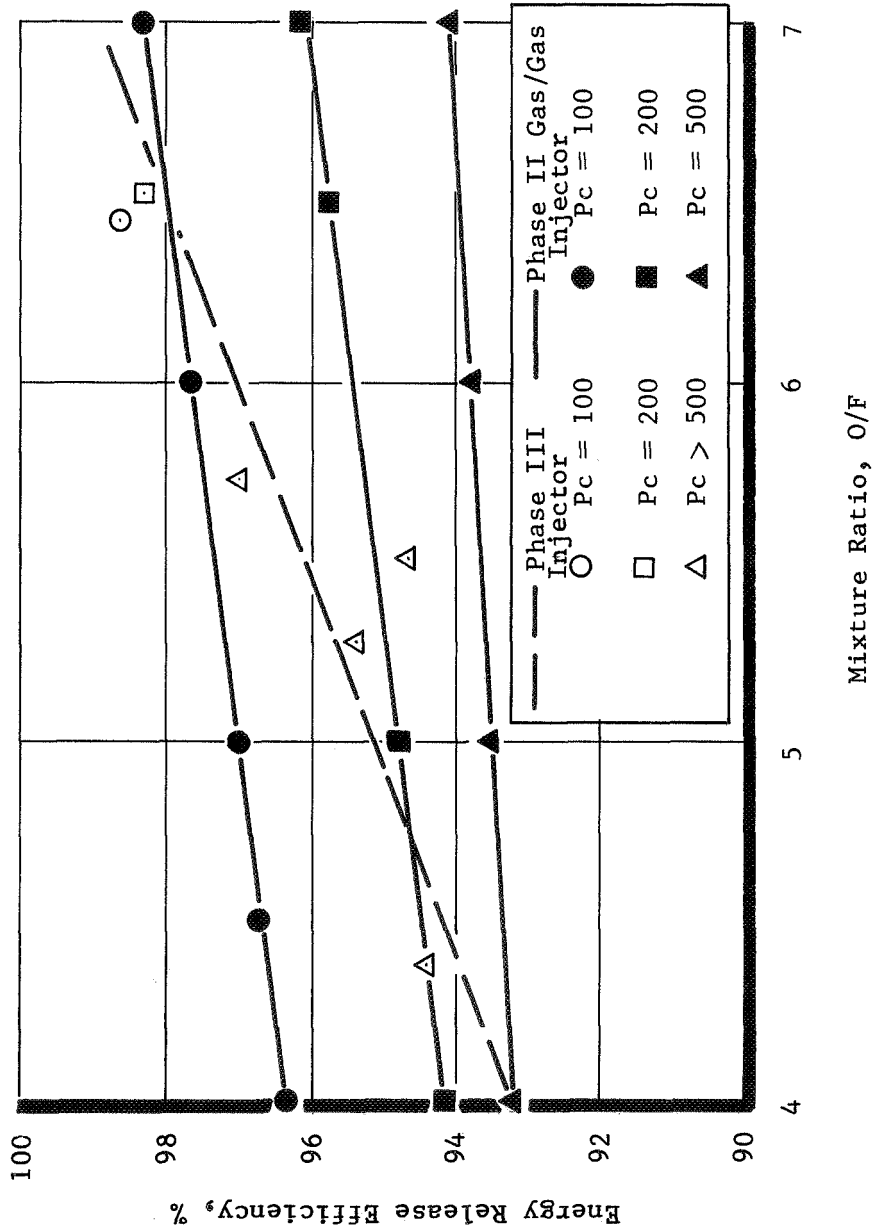


Figure 55. Energy Release Efficiency vs Mixture Ratio for Phase III and Phase II Gas/Gas Injectors.

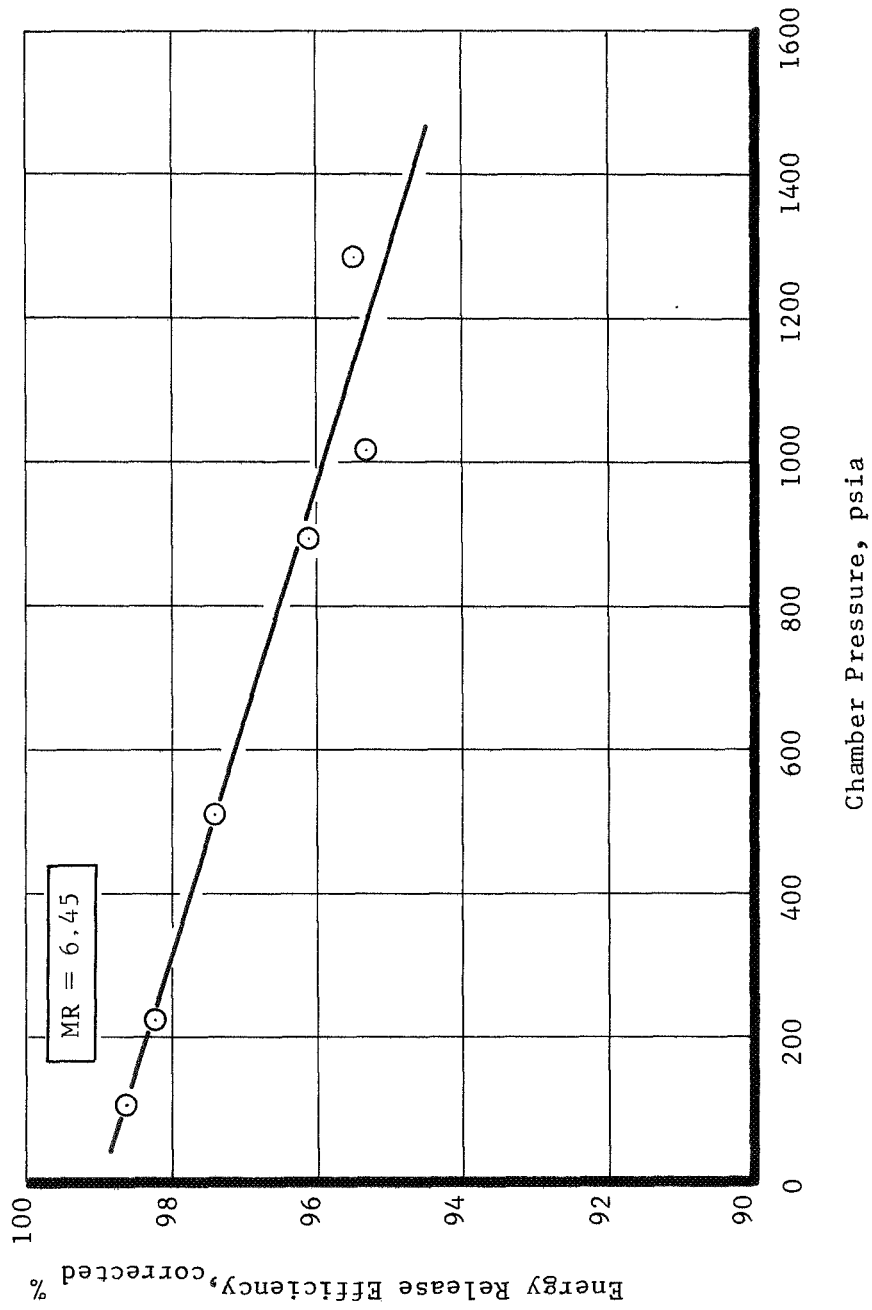


Figure 56. Energy Release Efficiency Corrected for Mixture Ratio Variations vs Chamber Pressure

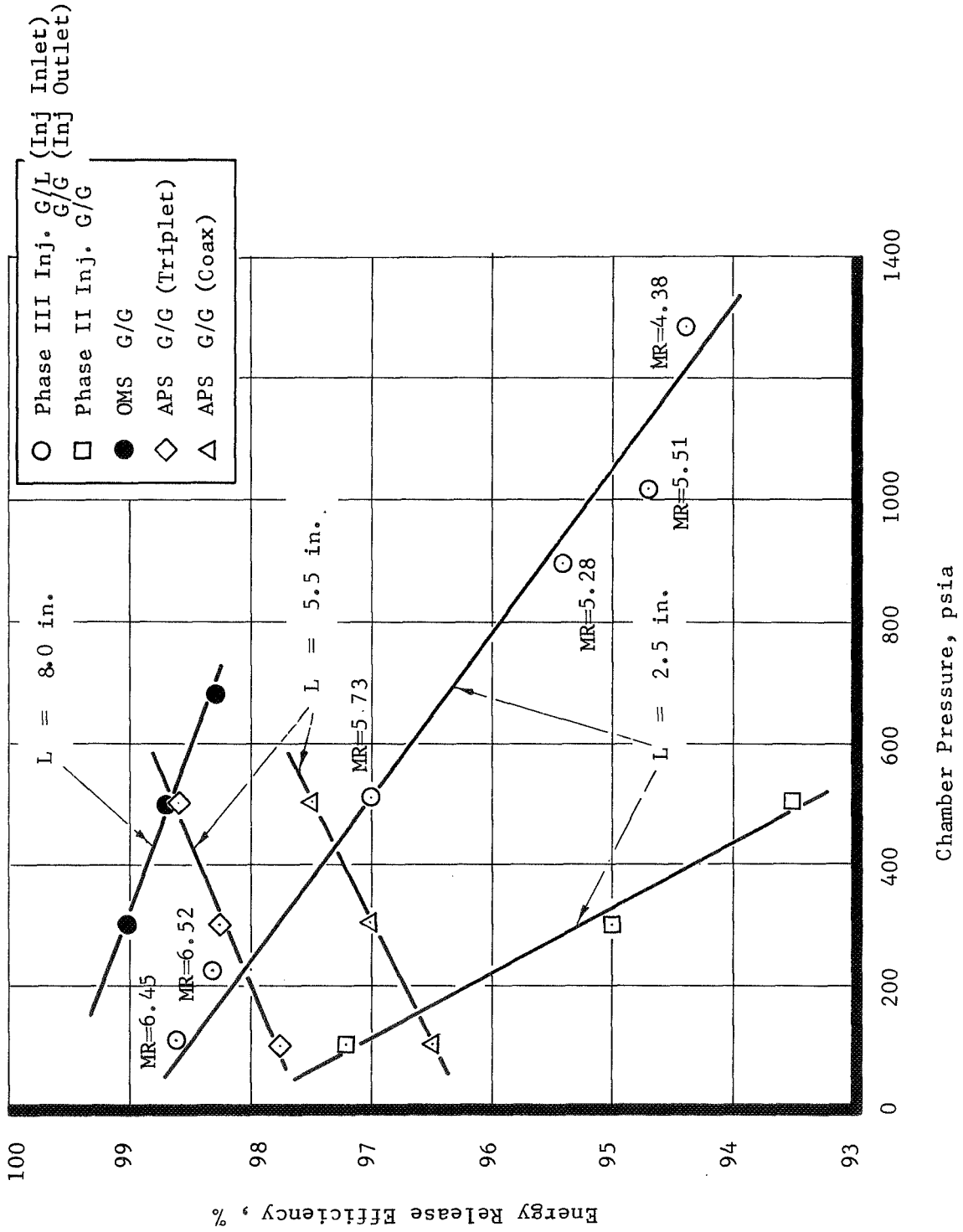


Figure 57. Energy Release Efficiency vs Chamber Pressure for Gas/Gas Engines with Different Chamber Lengths

APPENDIX A

COMPUTER LISTING AND DISCUSSION OF SINDA  
LOGIC AND SUBROUTINES FOR HEAT TRANSFER CALCULATIONS

COMPUTER PROGRAM INPUT AND OPERATION

The unique structural features of the SINDA<sup>(1)</sup> program preclude the use of a set of data cards, in the ordinary sense, supplying necessary "program input". The SINDA program is a master control program which is structured to accept logic as well as numerical data. User logic accepted by the program includes a description of the node network in terms of numeric and alphanumeric descriptors, subroutines to manipulate numerical quantities (a large number of useful subroutines are included in the SINDA library), program execution control constants, and array data. Since the basic SINDA program greatly facilitates nodal definition and network solution, a majority of the time spent on the tapoff cycle design study was used to develop the subroutines required to provide supplementary calculations and data.

Excluding these subroutines, which could be stored on tape or disk with the SINDA program, and the approximate 150 cards containing the user logic described in the first paragraph, the program input will be defined here as the set of three cards which define injector and channel geometry, flow rates, and inlet and outlet temperatures and pressures. These three cards together form array number 30, which contains the following input parameters.

Array 30 Input Parameters

Twenty-two parameters comprise the principal input array. They are input in free format in columns 12 through 72, beginning with the number "30" in columns 12 and 13 of the first card, followed by the numerical value of each array element separated by commas. Array elements are as follows:

---

(1) J. D. Gaski, "Chrysler Improved Numerical Differencing Analyzer for Third Generation Computers," TN-SP-67-287, Chrysler Corp. Space Division, New Orleans, La., October 1967.

Report 21052-3F, Appendix A

<u>Element Number</u>	<u>Program Symbol</u>	<u>Element Definition</u>	<u>Variable Range</u>
1	WF	Total fuel (hydrogen) weight flow, lbm/sec	$0.088 \leq WF \leq 2.2$
2	WØ	Total oxidizer (oxygen) weight flow, lbm/sec	$0.44 \leq WØ \leq 11.0$
3	WG	Ratio of hot gas weight flow to total propellant flow, percent	$0.2 \leq WG \leq 11.0$
4	WTI	Overall injector width, inches	$1.8 \leq WTI \leq 4.0$
5	DTI	Overall injector depth, inches	$3.5 \leq DTI \leq 8.0$
6	D	Channel depth, fuel, inches	$0.002 \leq D \leq 0.005$
7	W	Channel width, oxidizer, fuel, gas, inches	$W = 0.05$
8	WLAND	Channel land width, inches	$0.015 \leq WLAND \leq 0.0$
9	THGAS	Separator platelet thickness, gas, inches	$0.010 \leq THGAS \leq 0.0$
10	THØF	Separator platelet thickness, oxidizer and fuel, inches	$0.010 \leq THØF \leq 0.0$
11	GASD	Channel depth, gas, inches	$0.005 \leq GASD \leq 0.0$
12	L	Channel length, inches	$0.2 \leq L \leq 2.5$
13	PIØ	Inlet manifold pressure, oxidizer, psia	$150 \leq PIØ \leq 3750$
14	PIF	Inlet manifold pressure, fuel, psia	$150 \leq PIF \leq 3750$
15	PIG	Combustion chamber pressure, psia	$100 \leq PIG \leq 2500$
16	KIØ	Inlet pressure loss factor, oxidizer, (-)	$KIØ = 1.0$
17	KIF	Inlet pressure loss factor, fuel, (-)	$KIF = 1.0$
18	KIG	Inlet pressure loss factor, gas, (-)	$KIG = 1.0$
19	KØØ	Outlet pressure loss factor, oxidizer, (-)	$KØØ = 1.0$
20	KØF	Outlet pressure loss factor, fuel, (-)	$KØF = 1.0$
21	KØG	Outlet pressure loss factor, gas, (-)	$KØG = 1.0$
22	DØ	Channel depth, oxidizer, inches	$0.002 \leq DØ \leq 0.005$

The array 30 data are included in the SINDA control program as shown in the listing of Table I. Table II presents a sample output for one of the full thrust cases run.

COMPUTER PROGRAM SUBROUTINES

Subroutines developed for the Tapoff Cycle design study are listed in Table III and discussed individually in the following paragraphs. These represent user developed programs which complemented subroutines available in the SINDA library.

Subroutine WDØT

Subroutine WDØT was used to calculate the total number of flow channels as determined from the channel geometry and overall dimensions input. Flow rates per channel of each of three fluids were then determined from the total flow rates input. Calculational details and symbol definitions are included in the subroutine listing.

Subroutine HGØ

Subroutine HGØ was used to calculate the local oxygen heat transfer coefficient as a function of local temperature at the inlet pressure. Heat transfer coefficient calculations were based on the following standard correlation:

$$Nu = 0.023 Re^{0.8} Pr^{0.4}$$

where the Nusselt, Reynolds and Prandtl numbers are based on free-stream properties.

Subroutine HGF

Subroutine HGF was used to calculate the local hydrogen heat transfer coefficient using the same correlation and transport properties assumption as for oxygen.

Subroutine HGCØMB

Subroutine HGCØMB was used to calculate the heat transfer coefficient for the combustion gas at the injector face. The Dittus-Boelter correlation was used, correcting the "DB" properties factor obtained from the THERMØCAL<sup>(1)</sup> program for the noncircular geometry. The resulting expression used was as follows:

$$hg = DB * \dot{w}_T^{0.8} * D^{1.8} \left(\frac{\pi D}{P}\right)^{0.8}$$

where DB = THERMØCAL properties factor

$\dot{w}_T$  = total propellant weight flow, lb/sec

D = hydraulic diameter of injector face, in.

P = perimeter at injector face, in.

Subroutine HGGAS

Subroutine HGGAS was used to calculate the local hot gas heat transfer coefficient inside the hot gas channel as a function of temperature. The same Dittus-Boelter correlation was used as in Subroutine HGCØMB, substituting appropriate geometry terms.

Subroutine FRICT

Subroutine FRICT was used to calculate hydraulic parameters within the flow channels. Determinations were made of entrance and exit pressure drops as well as momentum and friction losses within the channels. Local pressure calculations were performed after the temperature gradients were established for the entire network. The purpose was to maintain a check on the overall channel pressure drop to assure that channel sizes were reasonable. Pressure calculations were made at each node, using the local temperature and previous pressure for viscosity evaluation. Turbulent flow was assumed and an appropriate friction factor was used.

(1) J. N. Hester and J. Chan, "THERMØCAL - Phase I, Volumes I and II," Thrust Chamber Engineering Report No. 9600:M014, dated 1 September 1969.

Subroutine HYDP

Subroutine HYDP was used to obtain the thermodynamic and transport properties of hydrogen as a function of temperature and pressure. Properties thus obtained were specific heat ratio (-), sonic velocity (ft/sec), viscosity (lb/in.-sec), and density (lbm/ft<sup>3</sup>). HYDP calls Subroutines TABTP and TABHP which contain the Los Alamos tabular para-hydrogen properties and are further described in an Aerojet manual<sup>(2)</sup>. Thermodynamic and transport properties are available over the following range of temperature and pressure:

$$0 < P \leq 5000 \text{ psia}$$

$$36 \leq T \leq 5000^{\circ}\text{R}$$

Subroutine ØXP

Subroutine ØXP was used to obtain thermodynamic and transport properties of oxygen as a function of temperature and pressure. Properties provided by ØXP were specific heat ratio (-), sonic velocity (ft/sec), viscosity (lb/in.-sec), and density (lbm/ft<sup>3</sup>). ØXP calls Subroutines ØXYGP and PTP which contain Aerojet-developed tabular oxygen properties and are further described in two memorandums<sup>(3,4)</sup>. Thermodynamic and transport properties are available over the following ranges of temperatures and pressures:

PTP:	44 ≤ P ≤ 2939 psia	}	k, μ, V, C <sub>p</sub> , H, ρ, Q
	180 ≤ T ≤ 5000°R		
ØXYGP:	14.7 ≤ P ≤ 4850 psia	}	s, γ, V, C <sub>p</sub> , Q, H
	100 ≤ T ≤ 540°R		

(2) N. R. Cull, "O. A. Farmer Hydrogen Property Subroutines TABHP and TABTP," Dept 2380, Reference Manual 2300-M21, Aerojet-General Corp., 2 February 1968.  
 (3) J. J. Williams, "Computer Code for the Thermodynamic Properties of Oxygen," Memorandum 9615:2948, dated 10 September 1969.  
 (4) P. Block, "Phase II Computer Program - Advanced Injector Program," Memorandum 9648:0539, dated 3 November 1969.

Subroutine OXARRY

Subroutine OXARRY was used to load thermodynamic properties of oxygen, thermal conductivity (Btu/in.-sec-°R), viscosity (lb/in.-sec), and specific heat (Btu/lbm-°R) into arrays as a function of incremental temperatures at the inlet pressure specified. These arrays were stored by the main logic of the SINDA control program. This subroutine also called Subroutines OXYGP and PTP which contained the oxygen properties described in the above OXP subroutine. The arrays created by OXARRY were called by the argument list of Subroutines HGØ and FRICT, described earlier, to provide properties for the evaluation of the oxygen heat transfer coefficient and pressure drop.

Subroutine HYARRY

Subroutine HYARRY was used to load thermodynamic properties of hydrogen, thermal conductivity (Btu/in.-sec-°R), viscosity (lb/in.-sec), and specific heat (Btu/lbm-°R) into arrays as a function of incremental temperatures at the inlet pressure specified. These arrays were stored by the main logic of the SINDA control program. This subroutine also called Subroutine TABTP which contained the hydrogen properties described in the HYDP subroutine. The arrays created by HYARRY were called by the argument list of HGF and FRICT, described earlier, to provide properties for the evaluation of the hydrogen heat transfer coefficient and pressure drop.

Subroutine GSARRY

Subroutine GSARRY was used to load the thermodynamic properties, specific heat (Btu/lbm-°R), THERMOCAL DB factor, of the oxygen/hydrogen combustion gas at MR = 5.0 into arrays as a function of incremental temperatures at the chamber pressure specified. These arrays were stored in the main logic of the SINDA control program. This subroutine called GASP, which referred to the /PGAS/ block data where the combustion gas tabular data were stored. The arrays created by GSARRY were called by the argument list of Subroutines HGGAS, HGCØMB and FRICT to evaluate channel and face heat transfer coefficients and pressure drop.

Subroutine GASP

Subroutine GASP was used to obtain the thermodynamic and transport properties of the combustion gas as a function of temperature and pressure. Properties thus obtained were sonic velocity (ft/sec), viscosity (lb/in.-sec), density (lbm/ft<sup>3</sup>), specific heat (Btu/lbm-°R), and the THERMØCAL DB factor. Tabular entries were provided by the common block /PGAS/ at seven temperatures at each of six pressures for a mixture ratio of 5.0. Pressure and temperature ranges covered were as follows:

$$100 \leq P \leq 2500 \text{ psia}$$
$$500 \leq T \leq 6000^\circ\text{R}$$

Properties loaded into the /PGAS/ block were obtained from the Aerojet THERMØCAL program<sup>(1)</sup>.



```

BCD 3CONSTANTS
NLOOP,.250,DRLXCA,.05,ARLXCA,.05
DAMPD,.8,DAMPA,.8
24,H0,.25,HF,.25,HG,.27,H1
30,CPGAS,.31,DBGAS,.32,CONDOX,.33,VISOX,.34,CPOX,.35,CONHYD
36,VISHYD,.37,CPHYD
38,185.0
39,65.0
      $T89

END
BCD JARRAY DATA
1,SPACE,24,END $CP GAS VS T
2,SPACE,24,END $DB GAS VS T
REM PROPERTIES OF NICKEL
7,50,0.000857,535,0.000857,660,0.000980,860,0.000795
1060,0.000613,1260,0.000620,1460,0.000667,1660,0.000735
1860,0.000783,2060,0.000775,2260,0.000828,2460,0.000873
2260,0.000913,2860,0.000951,END $K VS T
4,SPACE,32,END
11,SPACE,32,END
14,SPACE,11,END
15,SPACE,32,END
16,SPACE,32,END
17,SPACE,88,END
18,SPACE,6,END
19,SPACE,33,END
20,100,5603,400,5831,700,5916,1000,5966,1500,6020.
      2000,6056,3000,6104,END $ PC GAS VS T
21,SPACE,92,END $ CONDO
22,SPACE,92,END $ VISO
23,SPACE,92,END $ CPO
24,SPACE,56,END $ CONH
25,SPACE,56,END $ VISH
26,SPACE,56,END $ CPH
30,2,2,11.0,6.0,2.0,0.0,4.0,0.0,0.05,0.05,0.010,0.010,0.050,0.025
      3750,3750,2500,1,1,1,1,SPACE,3,0050,END
      750,0,750,0,500,0,1,1,1,1,SPACE,3,0050,END
31,SPACE,56,END
40,SPACE,33,END

END
BCD 3EXECUTION
DIMENSION X(500)
NOIM=500
NTH=0
GSARRY(A30+15,A1+1,A2+1)
OXARRY(A30+13,A21+1,A22+1,A23+1)
HYARRY(A30+14,A24+1,A25+1,A26+1)
WDOT(A30+1,A31+1)
HGCOMB(.95,A20,A2,A30+1,A31+1,I100)
DIVIDE(A30+12,10,A14+1)
ADELX (10,1,A14+1,A14+2)
DIVIDE(A14+1,2,A14+1)
DIVIDE(A14+1,2,A14+1)
DIVIDE(A30+9,2,A8+12)
DIVIDE(A8+12,2,A8+1)
ADELX (10,1,A8+1,A8+1)
ADELX (10,1,A8+1,A8+23)
ADELX (10,1,A8+12,A8+12)
DIVIDE(A30+10,2,A11+12)
DIVIDE(A11+12,2,A11+1)

```

F  
F  
F

```

ADELX (10,1,A11+1,A11+1)
ADELX (10,1,A11+1,A11+23)
ADELX (10,1,A11+12,A11+12)
ARYMPY (A8,AB+1,A30+7,AB+1)
ARYMPY (A11,A11+1,A30+7,A11+1)
SHFTV (3,AB+1,A18+1)
STFSEP (AB+12,A18+2)
SHFTV (3,A11+1,A18+4)
STFSEP (A11+12,A18+5)
ARYDIV (AB,AB+1,A14+2,A15+1)
ARYDIV (A11,A11+1,A14+2,A16+1)
ARYDIV (AB,AB+1,A30+7,AB+1)
ARYMPY (A14,A14+1,A30+7,A14+1)
ARYDIV (A14,A14+1,AB+12,A17+12)
SHFTV (11,A17+12,A17+23)
ARYDIV (A11,A11+1,A30+7,A11+1)
ARYDIV (A14,A14+1,A11+12,A17+56)
SHFTV (11,A17+56,A17+67)
ARYMPY (3,A18+1,A31+48,6222)
ARYMPY (3,A18+4,A31+48,6266)
ARYDIV (A14,A14+1,A30+7,A14+1)
ITEST=0
PRINTA (K30,A1+1,A1,1)
PRINTA (K31,A2+1,A2,1)
PRINTA (K32,A21+1,A21,1)
PRINTA (K33,A22+1,A22,1)
PRINTA (K34,A23+1,A23,1)
PRINTA (K35,A24+1,A24,1)
PRINTA (K36,A25+1,A25,1)
PRINTA (K37,A26+1,A26,1)
STFSEP (K38,T89)
STFSEP (K39,T1)
CINDSL

END 3VARIABLES 1
ITEST=ITEST+1
DIDIM (1,T1,A26,A31+2,61)
DIDIM (9,T2,A26,A31+2,62)
DIDIM (32,T12,A7,A15+1,612)
DIDIM (10,T45,A1,A31+3,645)
DIDIM (32,T56,A7,A16+1,656)
DIDIM (1,T89,A23,A31+1,689)
DIDIM (9,T90,A23,A31+1,690)
H60 (1,T89,A21,A22,A23,A14+1,A30+1,A31+1,6178)
H60 (10,T90,A21,A22,A23,A14+2,A30+1,A31+1,6179)
DIDIM (22,T12,A7,A17+12,6112)
HGGAS (11,T45,A2,A30+1,A31+1,A14+1,6134)
HGGAS (11,T45,A2,A30+1,A31+1,A14+1,6145)
DIDIM (22,T56,A7,A17+56,6156)
HGF (1,T1,A24,A25,A26,A14+1,A30+1,A31+1,6101)
HGF (10,T2,A24,A25,A26,A14+2,A30+1,A31+1,6102)

END 3VARIABLES 2
SHFTV (1,T1,A19+1)
SHFTV (10,T2,A19+2)
SHFTV (11,T45,A19+12)
SHFTV (1,T89,A19+23)
SHFTV (10,T90,A19+24)
END

```





```
BCD 3INITIAL PARAMETERS
BCD 9PLATELET TEMPERATURE DISTRIBUTION CASE 60
END
BCU 3NODE DATA
END
BCD 3CONDUCTOR DATA
END
BCD 3CONSTANTS DATA
END
BCD 3ARRAY DATA
30,2,2,1,0,6,0,3,000,5,00,005,0,05,050,010,010,050,0,25
3750,3750,2500,1,1,1,1,1,SPACE,3,0050,END
END
```



```
BCD 3INITIAL_PARAMETERS
BCD 9PLATELET_TEMPERATURE_DISTRIBUTION CASE 62
END
BCD 3NODE_DATA
END
BCD 3CONDUCTOR_DATA
END
BCD 3CONSTANTS_DATA
END
BCD 3ARRAY_DATA
30,2,2,11,0,6,0,4,000,6,00,0,005,0,05,0,010,0,010,0,050,0,0,3
3750,,3750,,2500,,1,1,1,1,,SPACE,3,,0050,END
END
```

Report 21052-3F, Appendix A

GN FOR,K LINKO UNIVAC 1108 FORTRAN V LEVEL 2206 0018 F50180 THIS COMPILATION WAS DONE ON 29 APR 70 AT 11:23:45 END OF UNIVAC 1108 FORTRAN V COMPILATION. 0 *DIAGNOSTIC* MESSAGE(S)	29 APR 70 11:23:45.318
GN FOR,K EXECIN UNIVAC 1108 FORTRAN V LEVEL 2206 0018 F50180 THIS COMPILATION WAS DONE ON 29 APR 70 AT 11:23:47 END OF UNIVAC 1108 FORTRAN V COMPILATION. 0 *DIAGNOSTIC* MESSAGE(S)	29 APR 70 11:23:47.718
GN FOR,K VARBL1 UNIVAC 1108 FORTRAN V LEVEL 2206 0018 F50180 THIS COMPILATION WAS DONE ON 29 APR 70 AT 11:23:49 END OF UNIVAC 1108 FORTRAN V COMPILATION. 0 *DIAGNOSTIC* MESSAGE(S)	29 APR 70 11:23:49.415
GN FOR,K VARBL2 UNIVAC 1108 FORTRAN V LEVEL 2206 0018 F50180 THIS COMPILATION WAS DONE ON 29 APR 70 AT 11:23:51 END OF UNIVAC 1108 FORTRAN V COMPILATION. 0 *DIAGNOSTIC* MESSAGE(S)	29 APR 70 11:23:50.942
GN FOR,K OUTCAL UNIVAC 1108 FORTRAN V LEVEL 2206 0018 F50180 THIS COMPILATION WAS DONE ON 29 APR 70 AT 11:23:52 END OF UNIVAC 1108 FORTRAN V COMPILATION. 0 *DIAGNOSTIC* MESSAGE(S)	29 APR 70 11:23:51.935
GN XGT CUR 1. FSTIN CINDAG/ENGLIB END OF FILE 2. FSTIN SINAIIP/BLOCK END OF FILE 3. FSTIN HYDOXY/BLOCK END OF FILE END CUR	29 APR 70 11:23:53.183 11:23:53 11:24:01 11:24:02
GN XGT LINKO	29 APR 70 11:24:05.250

TABLE II. SAMPLE OUTPUT FROM SINDA PROGRAM

IMPROVED NUMERICAL DIFFERENCING ANALYZER		-- -- SINDA -- --		UNIVAC-1108 FORTRAN-V VERSION		PAGE			
PLATELET TEMPERATURE DISTRIBUTION		CASE 61				1			
CPGAS ( 1)	5.00000+02	CPGAS ( 2)	8.14700-01	CPGAS ( 3)	1.00000+03	CPGAS ( 4)	8.14700-01	CPGAS ( 5)	1.50000+03
CPGAS ( 6)	8.14700-01	CPGAS ( 7)	2.00000+03	CPGAS ( 8)	8.14700-01	CPGAS ( 9)	2.50000+03	CPGAS ( 10)	8.28650-01
CPGAS ( 11)	3.00000+03	CPGAS ( 12)	8.42600-03	CPGAS ( 13)	3.50000+03	CPGAS ( 14)	8.81600-01	CPGAS ( 15)	4.00000+03
CPGAS ( 16)	9.20600-01	CPGAS ( 17)	4.50000+03	CPGAS ( 18)	9.83600-01	CPGAS ( 19)	5.00000+03	CPGAS ( 20)	1.04700+00
CPGAS ( 21)	5.50000+03	CPGAS ( 22)	1.22850+00	CPGAS ( 23)	6.00000+03	CPGAS ( 24)	1.41000+00		
DBGAS ( 1)	5.00000+02	DBGAS ( 2)	1.56300-03	DBGAS ( 3)	1.00000+03	DBGAS ( 4)	1.90700-03	DBGAS ( 5)	1.50000+03
DBGAS ( 6)	2.18650-03	DBGAS ( 7)	2.00000+03	DBGAS ( 8)	2.00000+03	DBGAS ( 9)	2.50000+03	DBGAS ( 10)	2.70000-03
DBGAS ( 11)	3.00000+03	DBGAS ( 12)	2.93400-03	DBGAS ( 13)	3.50000+03	DBGAS ( 14)	3.11700-03	DBGAS ( 15)	4.00000+03
DBGAS ( 16)	3.30000-03	DBGAS ( 17)	4.50000+03	DBGAS ( 18)	3.43300-03	DBGAS ( 19)	5.00000+03	DBGAS ( 20)	3.56600-03
DBGAS ( 21)	5.50000+03	DBGAS ( 22)	3.66300-03	DBGAS ( 23)	6.00000+03	DBGAS ( 24)	3.76000-03		
CONDOX( 1)	1.00000+02	CONDOX( 2)	2.44699-06	CONDOX( 3)	1.10000+02	CONDOX( 4)	2.37814-06	CONDOX( 5)	1.20000+02
CONDOX( 6)	2.30930-06	CONDOX( 7)	1.30000+02	CONDOX( 8)	2.24000-06	CONDOX( 9)	1.40000+02	CONDOX( 10)	2.17160-06
CONDOX( 11)	1.50000+02	CONDOX( 12)	2.10276-06	CONDOX( 13)	1.60000+02	CONDOX( 14)	2.03391-06	CONDOX( 15)	1.70000+02
CONDOX( 16)	1.96507-06	CONDOX( 17)	1.80000+02	CONDOX( 18)	1.80000+02	CONDOX( 19)	1.90000+02	CONDOX( 20)	1.82738-06
CONDOX( 21)	2.00000+02	CONDOX( 22)	1.75853-06	CONDOX( 23)	2.10000+02	CONDOX( 24)	1.68933-06	CONDOX( 25)	2.20000+02
CONDOX( 26)	1.62872-06	CONDOX( 27)	2.30000+02	CONDOX( 28)	1.57411-06	CONDOX( 29)	2.40000+02	CONDOX( 30)	1.51949-06
CONDOX( 31)	2.50000+02	CONDOX( 32)	1.46488-06	CONDOX( 33)	2.60000+02	CONDOX( 34)	1.38192-06	CONDOX( 35)	2.70000+02
CONDOX( 36)	1.29439-06	CONDOX( 37)	2.80000+02	CONDOX( 38)	1.20667-06	CONDOX( 39)	2.90000+02	CONDOX( 40)	1.12335-06
CONDOX( 41)	3.00000+02	CONDOX( 42)	1.09096-06	CONDOX( 43)	3.10000+02	CONDOX( 44)	1.08032-06	CONDOX( 45)	3.20000+02
CONDOX( 46)	1.06022-06	CONDOX( 47)	3.30000+02	CONDOX( 48)	1.03629-06	CONDOX( 49)	3.40000+02	CONDOX( 50)	1.00980-06
CONDOX( 51)	4.00000+02	CONDOX( 52)	7.67882-07	CONDOX( 53)	4.50000+02	CONDOX( 54)	7.00590-07	CONDOX( 55)	5.00000+02
CONDOX( 56)	6.68101-07	CONDOX( 57)	5.50000+02	CONDOX( 58)	6.71448-07	CONDOX( 59)	6.00000+02	CONDOX( 60)	6.74820-07
CONDOX( 61)	6.50000+02	CONDOX( 62)	6.78127-07	CONDOX( 63)	7.00000+02	CONDOX( 64)	6.81434-07	CONDOX( 65)	7.50000+02
CONDOX( 66)	6.85741-07	CONDOX( 67)	8.00000+02	CONDOX( 68)	6.80048-07	CONDOX( 69)	6.50000+02	CONDOX( 70)	6.91355-07
CONDOX( 71)	9.00000+02	CONDOX( 72)	6.94662-07	CONDOX( 73)	9.50000+02	CONDOX( 74)	6.97969-07	CONDOX( 75)	1.00000+03
CONDOX( 76)	7.02929-07	CONDOX( 77)	1.50000+03	CONDOX( 78)	8.10141-07	CONDOX( 79)	2.00000+03	CONDOX( 80)	9.95370-07
CONDOX( 81)	2.50000+03	CONDOX( 82)	1.16898-06	CONDOX( 83)	3.00000+03	CONDOX( 84)	1.34259-06	CONDOX( 85)	3.50000+03
CONDOX( 86)	1.48438-06	CONDOX( 87)	4.00000+03	CONDOX( 88)	1.62616-06	CONDOX( 89)	4.50000+03	CONDOX( 90)	1.76794-06
CONDOX( 91)	5.00000+03	CONDOX( 92)	1.96972-06						
VISOX ( 1)	1.00000+02	VISOX ( 2)	2.86455-05	VISOX ( 3)	1.10000+02	VISOX ( 4)	2.71272-05	VISOX ( 5)	1.20000+02
VISOX ( 6)	2.56089-05	VISOX ( 7)	1.30000+02	VISOX ( 8)	2.40906-05	VISOX ( 9)	1.40000+02	VISOX ( 10)	2.25723-05
VISOX ( 11)	1.50000+02	VISOX ( 12)	2.10540-05	VISOX ( 13)	1.60000+02	VISOX ( 14)	1.95357-05	VISOX ( 15)	1.70000+02
VISOX ( 16)	1.80174-05	VISOX ( 17)	1.80000+02	VISOX ( 18)	1.64991-05	VISOX ( 19)	1.90000+02	VISOX ( 20)	1.49808-05
VISOX ( 21)	2.00000+02	VISOX ( 22)	1.34665-05	VISOX ( 23)	2.10000+02	VISOX ( 24)	1.87190-05	VISOX ( 25)	2.20000+02
VISOX ( 26)	1.03874-05	VISOX ( 27)	2.30000+02	VISOX ( 28)	9.25874-06	VISOX ( 29)	2.40000+02	VISOX ( 30)	8.13011-06
VISOX ( 31)	2.50000+02	VISOX ( 32)	7.00148-06	VISOX ( 33)	2.50000+02	VISOX ( 34)	6.31611-06	VISOX ( 35)	2.70000+02
VISOX ( 36)	5.72665-06	VISOX ( 37)	2.80000+02	VISOX ( 38)	5.13719-06	VISOX ( 39)	2.90000+02	VISOX ( 40)	4.57470-06
VISOX ( 41)	3.00000+02	VISOX ( 42)	4.32670-06	VISOX ( 43)	3.10000+02	VISOX ( 44)	4.19261-06	VISOX ( 45)	3.20000+02
VISOX ( 46)	3.98101-06	VISOX ( 47)	3.30000+02	VISOX ( 48)	3.72909-06	VISOX ( 49)	3.40000+02	VISOX ( 50)	3.45030-06
VISOX ( 51)	4.00000+02	VISOX ( 52)	2.17003-06	VISOX ( 53)	4.50000+02	VISOX ( 54)	1.85652-06	VISOX ( 55)	5.00000+02
VISOX ( 56)	1.34811-06	VISOX ( 57)	5.50000+02	VISOX ( 58)	1.25284-06	VISOX ( 59)	6.00000+02	VISOX ( 60)	1.34471-06
VISOX ( 61)	6.50000+02	VISOX ( 62)	1.43536-06	VISOX ( 63)	7.00000+02	VISOX ( 64)	1.52602-06	VISOX ( 65)	7.50000+02
VISOX ( 66)	1.61667-06	VISOX ( 67)	8.00000+02	VISOX ( 68)	1.70733-06	VISOX ( 69)	8.50000+02	VISOX ( 70)	1.79798-06
VISOX ( 71)	9.00000+02	VISOX ( 72)	1.88863-06	VISOX ( 73)	9.50000+02	VISOX ( 74)	1.97929-06	VISOX ( 75)	1.00000+03
VISOX ( 76)	2.06793-06	VISOX ( 77)	1.50000+03	VISOX ( 78)	2.71118-06	VISOX ( 79)	2.00000+03	VISOX ( 80)	3.16891-06
VISOX ( 81)	2.50000+03	VISOX ( 82)	3.67741-06	VISOX ( 83)	3.00000+03	VISOX ( 84)	4.16667-06	VISOX ( 85)	3.50000+03
VISOX ( 86)	4.94167-06	VISOX ( 87)	4.00000+03	VISOX ( 88)	4.91667-06	VISOX ( 89)	4.50000+03	VISOX ( 90)	5.29167-06
VISOX ( 91)	5.00000+03	VISOX ( 92)	5.66667-06						
CPOX ( 1)	1.00000+02	CPOX ( 2)	3.91286-01	CPOX ( 3)	1.10000+02	CPOX ( 4)	3.90168-01	CPOX ( 5)	1.20000+02
CPOX ( 6)	3.89050-01	CPOX ( 7)	1.30000+02	CPOX ( 8)	3.87932-01	CPOX ( 9)	1.40000+02	CPOX ( 10)	3.86814-01

IMPROVED NUMERICAL DIFFERENCING ANALYZER		SINDA		UNIVAC-1108 FORTRAN-V VERSION		PAGE			
PLATELET TEMPERATURE DISTRIBUTION				CASE 61					
CPOX ( 11)	1.50000+02	CPOX ( 12)	3.85878-01	CPOX ( 13)	1.60000+02	CPOX ( 14)	3.85684-01	CPOX ( 15)	1.70000+02
CPOX ( 16)	3.85490-01	CPOX ( 17)	1.80000+02	CPOX ( 18)	3.85236-01	CPOX ( 19)	1.90000+02	CPOX ( 20)	3.85101-01
CPOX ( 21)	2.00000+02	CPOX ( 22)	3.84907-01	CPOX ( 23)	2.10000+02	CPOX ( 24)	3.87131-01	CPOX ( 25)	2.20000+02
CPOX ( 26)	3.89354-01	CPOX ( 27)	2.30000+02	CPOX ( 28)	3.91577-01	CPOX ( 29)	2.40000+02	CPOX ( 30)	3.95711-01
CPOX ( 31)	2.50000+02	CPOX ( 32)	3.99844-01	CPOX ( 33)	2.60000+02	CPOX ( 34)	4.07085-01	CPOX ( 35)	2.70000+02
CPOX ( 36)	4.09722-01	CPOX ( 37)	3.89000+02	CPOX ( 38)	4.10205-01	CPOX ( 39)	2.90000+02	CPOX ( 40)	4.23507-01
CPOX ( 41)	3.00000+02	CPOX ( 42)	4.30385-01	CPOX ( 43)	3.10000+02	CPOX ( 44)	4.35554-01	CPOX ( 45)	3.20000+02
CPOX ( 46)	4.40722-01	CPOX ( 47)	3.30000+02	CPOX ( 48)	4.45890-01	CPOX ( 49)	3.40000+02	CPOX ( 50)	4.50139-01
CPOX ( 51)	4.00000+02	CPOX ( 52)	4.07548-01	CPOX ( 53)	4.50000+02	CPOX ( 54)	3.63454-01	CPOX ( 55)	5.00000+02
CPOX ( 56)	3.22174-01	CPOX ( 57)	5.50000+02	CPOX ( 58)	3.42957-01	CPOX ( 59)	6.00000+02	CPOX ( 60)	3.34043-01
CPOX ( 61)	6.50000+02	CPOX ( 62)	3.20050-01	CPOX ( 63)	7.00000+02	CPOX ( 64)	3.16057-01	CPOX ( 65)	7.50000+02
CPOX ( 66)	3.07063-01	CPOX ( 67)	8.00000+02	CPOX ( 68)	2.98070-01	CPOX ( 69)	8.50000+02	CPOX ( 70)	2.89077-01
CPOX ( 71)	9.00000+02	CPOX ( 72)	2.80084-01	CPOX ( 73)	9.50000+02	CPOX ( 74)	2.71091-01	CPOX ( 75)	1.00000+03
CPOX ( 76)	2.62718-01	CPOX ( 77)	1.50000+03	CPOX ( 78)	2.64556-01	CPOX ( 79)	2.00000+03	CPOX ( 80)	2.75000-01
CPOX ( 81)	2.50000+03	CPOX ( 82)	2.87500-01	CPOX ( 83)	3.00000+03	CPOX ( 84)	3.00000-01	CPOX ( 85)	3.50000+03
CPOX ( 86)	3.10500-01	CPOX ( 87)	4.00000+03	CPOX ( 88)	3.21000-01	CPOX ( 89)	4.50000+03	CPOX ( 90)	3.31500-01
CPOX ( 91)	5.00000+03	CPOX ( 92)	3.42000-01						
CONHYD( 1)	5.00000+01	CONHYD( 2)	2.43209-06	CONHYD( 3)	1.00000+02	CONHYD( 4)	1.82605-06	CONHYD( 5)	1.50000+02
CONHYD( 6)	1.94021-06	CONHYD( 7)	2.00000+02	CONHYD( 8)	2.19125-06	CONHYD( 9)	2.50000+02	CONHYD( 10)	2.39966-06
CONHYD( 11)	3.00000+02	CONHYD( 12)	2.60807-06	CONHYD( 13)	3.50000+02	CONHYD( 14)	2.68535-06	CONHYD( 15)	4.00000+02
CONHYD( 16)	2.78840-06	CONHYD( 17)	4.50000+02	CONHYD( 18)	2.90674-06	CONHYD( 19)	5.00000+02	CONHYD( 20)	3.02509-06
CONHYD( 21)	5.50000+02	CONHYD( 22)	3.14393-06	CONHYD( 23)	6.00000+02	CONHYD( 24)	3.26178-06	CONHYD( 25)	6.50000+02
CONHYD( 26)	3.38012-06	CONHYD( 27)	7.00000+02	CONHYD( 28)	3.51704-06	CONHYD( 29)	7.50000+02	CONHYD( 30)	3.65396-06
CONHYD( 31)	8.00000+02	CONHYD( 32)	3.79088-06	CONHYD( 33)	8.50000+02	CONHYD( 34)	3.92780-06	CONHYD( 35)	9.00000+02
CONHYD( 36)	4.06472-06	CONHYD( 37)	9.50000+02	CONHYD( 38)	4.23167-06	CONHYD( 39)	1.00000+03	CONHYD( 40)	4.39861-06
CONHYD( 41)	1.50000+03	CONHYD( 42)	5.51632-06	CONHYD( 43)	2.00000+03	CONHYD( 44)	6.74190-06	CONHYD( 45)	2.50000+03
CONHYD( 46)	8.25754-06	CONHYD( 47)	3.00000+03	CONHYD( 48)	9.80664-06	CONHYD( 49)	3.50000+03	CONHYD( 50)	1.14344-05
CONHYD( 51)	4.00000+03	CONHYD( 52)	1.32208-05	CONHYD( 53)	4.50000+03	CONHYD( 54)	1.54227-05	CONHYD( 55)	5.00000+03
CONHYD( 56)	3.85321-05								
VISHYD( 1)	5.00000+01	VISHYD( 2)	1.33121-06	VISHYD( 3)	1.00000+02	VISHYD( 4)	5.97353-07	VISHYD( 5)	1.50000+02
VISHYD( 6)	4.39083-07	VISHYD( 7)	2.00000+02	VISHYD( 8)	3.97085-07	VISHYD( 9)	2.50000+02	VISHYD( 10)	4.03201-07
VISHYD( 11)	3.00000+02	VISHYD( 12)	4.09317-07	VISHYD( 13)	3.50000+02	VISHYD( 14)	4.33659-07	VISHYD( 15)	4.00000+02
VISHYD( 16)	4.58417-07	VISHYD( 17)	4.50000+02	VISHYD( 18)	4.84473-07	VISHYD( 19)	5.00000+02	VISHYD( 20)	5.10528-07
VISHYD( 21)	5.50000+02	VISHYD( 22)	5.36584-07	VISHYD( 23)	6.00000+02	VISHYD( 24)	5.62639-07	VISHYD( 25)	6.50000+02
VISHYD( 26)	5.88695-07	VISHYD( 27)	7.00000+02	VISHYD( 28)	6.14419-07	VISHYD( 29)	7.50000+02	VISHYD( 30)	6.40143-07
VISHYD( 31)	8.00000+02	VISHYD( 32)	6.65867-07	VISHYD( 33)	8.50000+02	VISHYD( 34)	6.91591-07	VISHYD( 35)	9.00000+02
VISHYD( 36)	7.17315-07	VISHYD( 37)	9.50000+02	VISHYD( 38)	7.42773-07	VISHYD( 39)	1.00000+03	VISHYD( 40)	7.68231-07
VISHYD( 41)	1.50000+03	VISHYD( 42)	1.02569-06	VISHYD( 43)	2.00000+03	VISHYD( 44)	1.26450-06	VISHYD( 45)	2.50000+03
VISHYD( 46)	1.48658-06	VISHYD( 47)	3.00000+03	VISHYD( 48)	1.70053-06	VISHYD( 49)	3.50000+03	VISHYD( 50)	1.90770-06
VISHYD( 51)	4.00000+03	VISHYD( 52)	2.10965-06	VISHYD( 53)	4.50000+03	VISHYD( 54)	2.30700-06	VISHYD( 55)	5.00000+03
VISHYD( 56)	2.50092-06								
CPHYD( 1)	5.00000+01	CPHYD( 2)	2.02249+00	CPHYD( 3)	1.00000+02	CPHYD( 4)	2.97185+00	CPHYD( 5)	1.50000+02
CPHYD( 6)	3.51442-00	CPHYD( 7)	2.00000+02	CPHYD( 8)	4.04157+00	CPHYD( 9)	2.50000+02	CPHYD( 10)	4.15000+00
CPHYD( 11)	3.00000+02	CPHYD( 12)	4.25850+00	CPHYD( 13)	3.50000+02	CPHYD( 14)	4.09771+00	CPHYD( 15)	4.00000+02
CPHYD( 16)	3.91120+00	CPHYD( 17)	4.50000+02	CPHYD( 18)	3.83655+00	CPHYD( 19)	5.00000+02	CPHYD( 20)	3.76191+00
CPHYD( 21)	5.50000+02	CPHYD( 22)	3.68726+00	CPHYD( 23)	6.00000+02	CPHYD( 24)	3.61262+00	CPHYD( 25)	6.50000+02
CPHYD( 26)	3.53797+00	CPHYD( 27)	7.00000+02	CPHYD( 28)	3.53221+00	CPHYD( 29)	7.50000+02	CPHYD( 30)	3.52645+00
CPHYD( 31)	8.00000+02	CPHYD( 32)	3.52069+00	CPHYD( 33)	8.50000+02	CPHYD( 34)	3.51493+00	CPHYD( 35)	9.00000+02
CPHYD( 36)	3.50917+00	CPHYD( 37)	9.50000+02	CPHYD( 38)	3.50588+00	CPHYD( 39)	1.00000+03	CPHYD( 40)	3.50259+00
CPHYD( 41)	1.50000+03	CPHYD( 42)	3.53312+00	CPHYD( 43)	2.00000+03	CPHYD( 44)	3.62875+00	CPHYD( 45)	2.50000+03
CPHYD( 46)	3.77179+00	CPHYD( 47)	3.00000+03	CPHYD( 48)	3.91115+00	CPHYD( 49)	3.50000+03	CPHYD( 50)	4.05351+00

IMPROVED NUMERICAL DIFFERENCING ANALYZER - - - SINDA - - - UNIVAC-1108 FORTRAN-V VERSION PAGE 3

PLATELET TEMPERATURE DISTRIBUTION CASE 61

CPHYD ( 51) 4.00000+03 CPHYD ( 52) 4.21102+00 CPHYD ( 53) 4.50000+03 CPHYD ( 54) 4.43207+00 CPHYD ( 55) 5.00000+03  
 CPHYD ( 56) 4.77987+00

ITERATION COUNT= 1

```

*****
TIME 0.00000 DTIMEU 0.00000 C5GMIN( 0) 0.00000 DTMPC( 0) 0.00000 ARLXCC( 0) 0.00000
T 2= 5.30000+02 T 3= 5.30000+02 T 4= 5.30000+02 T 5= 5.30000+02 T 6= 5.30000+02 T 7= 5.30000+02
T 8= 5.30000+02 T 9= 5.30000+02 T 10= 5.30000+02 T 11= 5.30000+02 T 12= 5.30000+02 T 13= 5.30000+02
T 14= 5.30000+02 T 15= 5.30000+02 T 16= 5.30000+02 T 17= 5.30000+02 T 18= 5.30000+02 T 19= 5.30000+02
T 20= 5.30000+02 T 21= 5.30000+02 T 22= 5.30000+02 T 23= 5.30000+02 T 24= 5.30000+02 T 25= 5.30000+02
T 26= 5.30000+02 T 27= 5.30000+02 T 28= 5.30000+02 T 29= 5.30000+02 T 30= 5.30000+02 T 31= 5.30000+02
T 32= 5.30000+02 T 33= 5.30000+02 T 34= 5.30000+02 T 41= 5.30000+02 T 42= 5.30000+02 T 43= 5.30000+02
T 38= 5.30000+02 T 39= 5.30000+02 T 40= 5.30000+02 T 46= 5.30000+02 T 47= 5.30000+02 T 48= 5.30000+02
T 49= 5.30000+02 T 50= 5.30000+02 T 51= 5.30000+02 T 52= 5.30000+02 T 53= 5.30000+02 T 54= 5.30000+02
T 55= 5.30000+02 T 56= 5.30000+02 T 57= 5.30000+02 T 58= 5.30000+02 T 60= 5.30000+02 T 61= 5.30000+02
T 62= 5.30000+02 T 63= 5.30000+02 T 64= 5.30000+02 T 65= 5.30000+02 T 66= 5.30000+02 T 67= 5.30000+02
T 68= 5.30000+02 T 69= 5.30000+02 T 70= 5.30000+02 T 71= 5.30000+02 T 72= 5.30000+02 T 73= 5.30000+02
T 74= 5.30000+02 T 75= 5.30000+02 T 76= 5.30000+02 T 77= 5.30000+02 T 78= 5.30000+02 T 79= 5.30000+02
T 80= 5.30000+02 T 81= 5.30000+02 T 82= 5.30000+02 T 83= 5.30000+02 T 84= 5.30000+02 T 85= 5.30000+02
T 86= 5.30000+02 T 87= 5.30000+02 T 88= 5.30000+02 T 90= 5.30000+02 T 91= 5.30000+02 T 92= 5.30000+02
T 93= 5.30000+02 T 94= 5.30000+02 T 95= 5.30000+02 T 96= 5.30000+02 T 97= 5.30000+02 T 98= 5.30000+02
T 99= 5.30000+02 T 1= 6.50000+01 T 89= 1.85000+02 T 100= 5.48720+03
ITERATION COUNT= 66
*****
TIME 0.00000 DTIMEU 0.00000 C5GMIN( 0) 0.00000 DTMPC( 0) 0.00000 ARLXCC( 45) 4.94080-n2
T 2= 9.65997+01 T 3= 1.24359+02 T 4= 1.51531+02 T 5= 1.78558+02 T 6= 2.05603+02 T 7= 2.32936+02
T 8= 2.61660+02 T 9= 2.91866+02 T 10= 3.24161+02 T 11= 3.41901+02 T 12= 3.33305+02 T 13= 1.55221+02
T 14= 1.81061+02 T 15= 2.06093+02 T 16= 2.32504+02 T 17= 2.59570+02 T 18= 2.89023+02 T 19= 3.19422+02
T 20= 3.51672+02 T 21= 3.88776+02 T 22= 4.13471+02 T 23= 5.39590+02 T 24= 5.80505+02 T 25= 6.51912+02
T 26= 7.19258+02 T 27= 7.89217+02 T 28= 8.61553+02 T 29= 9.35378+02 T 30= 1.00869+03 T 31= 1.08733+03
T 32= 1.18446+03 T 33= 1.27869+03 T 34= 1.40453+02 T 35= 9.83358+02 T 36= 1.00669+03 T 37= 1.19462+03
T 38= 1.34380+03 T 39= 1.51182+03 T 40= 1.69823+03 T 41= 1.90404+03 T 42= 2.11369+03 T 43= 2.28912+03
T 44= 2.45475+03 T 45= 2.77580+03 T 46= 2.88422+03 T 47= 3.11150+03 T 48= 3.35836+03 T 49= 3.62033+03
T 50= 3.89693+03 T 51= 4.19131+03 T 52= 4.49943+03 T 53= 4.81887+03 T 54= 5.15132+03 T 55= 5.48711+03
T 56= 1.13040+03 T 57= 1.18693+03 T 58= 1.31845+03 T 59= 1.48033+03 T 60= 1.66154+03 T 61= 1.80886+03
T 62= 1.96516+03 T 63= 2.12209+03 T 64= 2.26645+03 T 65= 2.42294+03 T 66= 2.55386+03 T 67= 2.66895+02
T 68= 6.60801+02 T 69= 7.59991+02 T 70= 9.13693+02 T 71= 1.10392+03 T 72= 1.22283+03 T 73= 1.33035+03
T 74= 1.43095+03 T 75= 1.54869+03 T 76= 1.67148+03 T 77= 1.79050+03 T 78= 1.97094+02 T 79= 3.26408+02
T 80= 3.59450+02 T 81= 4.01642+02 T 82= 4.41147+02 T 83= 4.93217+02 T 84= 5.53504+02 T 85= 6.22067+02
T 86= 6.93766+02 T 87= 7.90651+02 T 88= 8.58089+02 T 90= 2.19011+02 T 91= 2.55568+02 T 92= 2.93404+02
T 93= 3.31683+02 T 94= 3.72126+02 T 95= 4.18427+02 T 96= 4.73728+02 T 97= 5.43099+02 T 98= 6.19455+02
T 99= 6.62946+02 T 1= 6.50000+01 T 89= 1.85000+02 T 100= 5.48720+03
ITERATION COUNT= 66
*****

```

NUMBER OF CHANNELS ACROSS WIDTH = 40.  
 NUMBER OF CHANNELS ACROSS DEPTH = 66.  
 TOTAL NUMBER OF CHANNELS = 2640.

WF	WO	WG	WTI	DTI	FD	W	WLAND	THGAS	THOF	GASD	LENGTH
.2200+01	.1100+02	.6000+01	.4000+01	.6000+01	.5000-02	.5000-01	.5000-01	.1000-01	.1000-01	.5000-01	.2500+00
PIO	PIF	PIG	KIO	KIF	KIG	KOO	KOF	KOG	OD		
.3750+04	.3750+04	.2500+04	.1000+01	.1000+01	.1000+01	.0000	.0000	.0000	.5000-02		
WOC	WFC	WGC	DHF	DHI	MR	TR	DHG	RELO	REHO	RELF	REHF
.6250-02	.1250-02	.9000-03	.9091-02	.4800+01	.0000	.5487+04	.5000-01	.4315+05	.3590+06	.1405+06	.2285+06
RELG	REHG	DHO									
.3796+04	.6342+04	.9091-02									
HF ( 1)	6.21863-02 HF	( 2)	7.11643-02 HF	( 3)	8.06050-02 HF	( 4)	8.84406-02 HF	( 5)	9.56035-02 HF	( 6)	1.04480-01 HF
HF ( 6)	9.87677-02 HF	( 7)	1.02042-01 HF	( 8)	1.05431-01 HF	( 9)	1.05266-01 HF	( 10)	1.04480-01 HF	( 11)	0.00000
HG ( 45)	1.87485-03 HG	( 46)	1.90845-03 HG	( 47)	1.97142-03 HG	( 48)	2.03130-03 HG	( 49)	2.09484-03 HG	( 50)	2.16193-03 HG
HG ( 50)	2.16193-03 HG	( 51)	2.22065-03 HG	( 52)	2.27497-03 HG	( 53)	2.33128-03 HG	( 54)	2.38266-03 HG	( 55)	2.42583-03 HG
H0 ( 89)	3.04964-02 H0	( 90)	3.42353-02 H0	( 91)	3.52951-02 H0	( 92)	3.72284-02 H0	( 93)	3.72900-02 H0		



PRESSURE DROP CALCULATIONS IN FUEL CHANNEL

ENTRANCE HEAD LOSS=	45.026	INITIAL PRES=	3750.000	ENTRANCE VELOCITY =	291.7						
INITIAL VELOCITY=	290.0	ENTRANCE PRESS =	3704.974								
NODE	LENGTH	P(EXIT)	DP(FRICT)	DP(VELOC)	RE(FILM)	F	V(EXIT)	MACH(EXIT)	TW(R)	TG(R)	TF(R)
1	.012	3704.974	1.245	.000	.152+06	.0200	291.7	.054	133.3	65.0	99.2
2	.037	3703.729	2.847	12.115	.185+06	.0200	333.3	.068	155.2	96.6	125.9
3	.062	3688.767	3.269	14.345	.211+06	.0200	362.7	.085	181.1	124.4	152.7
4	.087	3671.153	3.760	16.715	.235+06	.0200	440.3	.105	206.1	151.5	178.8
5	.112	3650.678	4.281	17.785	.231+06	.0200	501.3	.125	232.5	178.6	205.5
6	.137	3628.612	4.832	18.886	.229+06	.0200	565.8	.145	259.6	205.6	232.6
7	.162	3604.894	5.401	19.618	.227+06	.0200	632.5	.160	289.0	232.9	261.0
8	.187	3579.875	6.016	21.198	.225+06	.0200	704.4	.176	319.5	261.7	290.6
9	.212	3552.661	6.653	22.069	.219+06	.0200	779.0	.193	351.7	291.9	321.8
10	.237	3523.939	7.342	23.875	.210+06	.0200	859.7	.207	388.8	324.0	356.4
11	.250	3492.722	8.079	14.745	.205+06	.0200	908.5	.215	413.5	341.9	377.7

FINAL PRES= 3474.098 EXIT HEAD LOSS= .000 TOTAL DELTA P = 275.902

PRESSURE DROP CALCULATIONS IN OXIDIZER CHANNEL

ENTRANCE HEAD LOSS=	78.726	INITIAL PRES=	3749.983	ENTRANCE VELOCITY =	101.5						
INITIAL VELOCITY=	101.4	ENTRANCE PRESS =	3671.257								
NODE	LENGTH	P(EXIT)	DP(FRICT)	DP(VELOC)	RE(FILM)	F	V(EXIT)	MACH(EXIT)	TW(R)	TG(R)	TF(R)
1	.012	3671.256	2.110	.000	.572+05	.0195	101.5	.033	297.1	185.0	241.0
2	.037	3669.145	4.226	11.792	.827+05	.0181	109.4	.041	326.4	219.0	272.7
3	.062	3653.125	5.125	15.784	.110+06	.0200	120.0	.052	359.4	255.6	307.5
4	.087	3632.216	5.781	22.494	.147+06	.0200	135.4	.072	401.6	293.4	347.5
5	.112	3603.941	6.760	33.047	.195+06	.0200	158.3	.101	441.1	331.7	386.4
6	.137	3564.133	8.175	46.983	.246+06	.0200	191.4	.140	493.2	372.1	432.7
7	.162	3508.974	10.050	61.627	.311+06	.0200	235.4	.185	553.5	418.4	486.0
8	.187	3437.097	12.812	89.599	.364+06	.0200	300.0	.242	622.1	473.7	547.9
9	.212	3334.686	16.316	113.740	.331+06	.0200	382.1	.300	694.0	543.1	618.5
10	.237	3204.630	22.475	193.297	.300+06	.0200	526.3	.397	790.6	619.5	705.0
11	.250	2988.857	14.958	236.929	.284+06	.0200	700.6	.519	858.1	662.9	760.5

FINAL PRES= 2736.970 EXIT HEAD LOSS= .000 TOTAL DELTA P = 1013.013

PRESSURE DROP CALCULATIONS IN GAS CHANNEL

ENTRANCE HEAD LOSS=	.565	INITIAL PRESS=	2500.000	ENTRANCE VELOCITY =	101.0						
INITIAL VELOCITY=	101.0	ENTRANCE PRESS =	2499.435								
NODE	LENGTH	P(EXIT)	DP(FRICT)	DP(VELOC)	RE(FILM)	F	V(EXIT)	MACH(EXIT)	TW(R)	TG(R)	TF(R)
1	.012	2499.435	.005	.000	.476+04	.0327	101.0	.019	2454.8	5487.1	3995.7
2	.037	2499.430	.009	-.072	.500+04	.0324	94.8	.019	2289.1	5151.3	3753.7
3	.062	2499.493	.003	-.077	.527+04	.0320	68.2	.018	2113.7	4818.9	3504.5
4	.087	2499.562	.007	-.073	.558+04	.0316	31.9	.017	1904.0	4499.4	3256.2
5	.112	2499.627	.007	-.061	.592+04	.0312	76.6	.017	1698.2	4191.3	3011.5
6	.137	2499.682	.005	-.063	.634+04	.0308	71.2	.016	1511.8	3896.9	2778.6
7	.162	2499.738	.005	-.068	.679+04	.0303	5.3	.015	1343.8	3620.3	2561.5
8	.187	2499.801	.005	-.055	.730+04	.0298	60.6	.015	1194.6	3358.4	2347.9
9	.212	2499.850	.005	-.045	.784+04	.0294	56.8	.014	1067.0	3111.5	2152.1
10	.237	2499.890	.004	-.054	.838+04	.0290	52.2	.014	983.4	2884.2	1984.7
11	.250	2499.939	.002	-.029	.871+04	.0287	49.6	.013	940.5	2775.8	1905.6

FINAL PRES= 2499.966    EXIT HEAD LOSS= .000    TOTAL DELTA P = .034

TABLE III. COMPUTER LISTING OF TAPOFF CYCLE SUBROUTINES

```

      R ELT,FRICT,1+700+24, 58447

000001 SUBROUTINE FRIC(NOD,WID,DEP,PI,KI,KO,TW1,TW2,TG,XL,WDOT,IPROP)
000002 DIMENSION TW1(50),TW2(50),TG(150),XL(150)
000003 REAL KI,KO
000004 500 FORMAT(14,F10.4,T,E10.3,F10.4,F10.1,F10.3,F10.1)
000005 510 FORMAT(/,FINAL PRES=,F10.3,FRIT HEAD LOSS=,F10.3
000006 1, TOTAL DELTA P =,F10.3//)
000007 520 FORMAT(/,FNTVANCE HEAD LOSS=,F10.3,INITIAL PRES=,F10.3,
000008 1, INITIAL VELOCITY=,F10.1,ENTRANCE PRESS =,F10.3,
000009 2, ENTRANCE VELOCITY =,F10.1//)
000010 530 FORMAT(,NODE LENGTH PIEXIT) DP(FRICT) DP(VELOC) RF(FILM)
000011 1 F V(EXIT) MACH(EXIT) TW(0) TGR) IF(R)?)
000012 540 FORMAT(1M1,3IX,PRESSURE DROP CALCULATIONS IN FUEL CHANNEL,/)
000013 550 FORMAT(1M1,3IX,PRESSURE DROP CALCULATIONS IN OXIDIZER CHANNEL,/)
000014 560 FORMAT(1M1,3IX,PRESSURE DROP CALCULATIONS IN GAS CHANNEL,/)
000015 IF(IPROP .EQ. 1) WRITE(6,550)
000016 IF(IPROP .EQ. 2) WRITE(6,550)
000017 IF(IPROP .EQ. 3) WRITE(6,560)
000018 WDOT=WDOT*2.
000019 IF(IPROP .EQ. 3) WDOT=WDOT/2.
000020 A=WDOT*DEP
000021 P=2.*(WID*DEP)
000022 DH=8.*A/P
000023 G=32.2
000024 C INLET VELOCITY HEAD LOSS AND VELOCITY
000025 C IPROP=1 THEN CALL HYD(FUEL) PROPS
000026 C IPROP=2 THEN CALL OXG(OXIDIZER) PROPS
000027 IF(IPROP .EQ. 1) CALL HYDP(ITG(1),PI,0.0,0.0,0.0)
000028 IF(IPROP .EQ. 2) CALL OXP(ITG(1),PI,0.0,0.0,0.0)
000029 IF(IPROP .EQ. 3) CALL GASP(ITG(1),PI,0.0,0.0,0.0,0.0)
000030 VIK=144.*WDOT/(R*A)
000031 DPKI=KI*VIK*2.*2./((2.*G*144.)) DPKI=DPKI*PI/(PI-DPKI)
000032 IF(IPROP .EQ. 3)
000033 P=PI-DPKI
000034 IF(IPROP .EQ. 1) CALL HYDP(ITG(1),P,0.0,0.0,0.0)
000035 IF(IPROP .EQ. 2) CALL OXP(ITG(1),P,0.0,0.0,0.0)
000036 IF(IPROP .EQ. 3) CALL GASP(ITG(1),P,0.0,0.0,0.0,0.0)
000037 VI=144.*WDOT/(R*A)
000038 WRITE(6,520)DPKI,PI,VIK,P,VI
000039 WRITE(6,530)
000040 TL=D.
000041 C
000042 DO 200 I=1,NOD
000043 TL=TL+XL(I)
000044 TF=(TW1(I)+TW2(I))/2.*TG(I)/2.
000045 IF(IPROP .EQ. 1) CALL HYDP(TF,P,0.0,0.0,VELC,0.0)
000046 IF(IPROP .EQ. 1) CALL HYDP(TF,P,0.0,0.0,VIS,0.0)
000047 IF(IPROP .EQ. 2) CALL OXP(TF,P,0.0,0.0,VLC,0.0)
000048 IF(IPROP .EQ. 2) CALL OXP(TF,P,0.0,0.0,VIS,0.0)
000049 IF(IPROP .EQ. 3) CALL GASP(TF,P,VFLC,0.0,0.0,0.0)
000050 IF(IPROP .EQ. 3) CALL GASP(TF,P,0.0,VIS,0.0,0.0,0.0)
000051 V=144.*WDOT/(R*A)
000052 MACH=V/VELC
000053 RE=WDOT*DH/(A*VIS)
000054 F=.02
000055 IF(RE .GT. 2.F+Y .AND. RE .LT. 1.F+5) F=.003+0.221*RE*(-.237)

```

```

000056
000057
000058
000059
000060
000061
000062
000063
000064
000065
000066
000067
000068

```

```

DPF=144.*F*(I)*W/DI*(2.*G+D)*A**2)
DPV=D*(V**2-VI**2)/(2.*144.*G)
VI=V
WRITE(6,500)I,TL,P,DPF,DPV,RF,F,V,XMACH,TW(I),TG(I),TF
P=DPF-DPV
200 CONTINUE
C
DPK0=K0*V**2*R/(2.*G*144.)
P=P-DPK0
DPTOT = PI - P
WRITE(6,510)P,DPK0,DPTOT
RETURN
END

```

ELT GASP,1,700424, 5R455

```
000001 SUBROUTINE CASP(T,P,VFLC,VIS,PHO,CO,DBT)
000002 COMMON /PGAS/ENH(7,6),TEMP(7,6),VELL(7,6),GAMA(7,6),PHOI(7,6),
000003 VISI(7,6),CONDI(7,6),SPHT(7,6),PRANI(7,6),DR(7,6),PRES(6)
000004 CALL DINTP(TEMP,PRES,AVFL,7,6,T,P,VIS)
000005 CALL DINTP(TEMP,PRES,VISI,7,6,T,P,VIS)
000006 CALL DINTP(TEMP,PRES,PHOI,7,6,T,P,PHO)
000007 CALL DINTP(TEMP,PRES,SPHT,7,6,T,P,CO)
000008 CALL DINTP(TEMP,PRES,DB,7,6,T,P,DBT)
000009 RETURN
000010 END
```

3 ELT GSARRY,1,700424, 56455

```
000001 SUBROUTINE GSAPPY(P,ACP,ADR)  
000002 DIMENSION ACP(1),ADR(1)  
000003 IU=23  
000004 IL=1  
000005 YINCR=500.  
000006 T=500.  
000007 DO 17 I=IL,IU,2  
000008 CALL GASP (T,P,VELC,VIS,PHO,ACP(I),ADR(I+1))  
000009 ACP(I)=T  
000010 ADR(I)=T  
000011 10 T=T+YINCR  
000012 RETURN  
000013 END
```



```

000055      3.0147.0426.0706.1.047.1.4107
000057 DATA PRAN/3.5658.5656.5440.4564.4280.
000058      3.5659.5692.5590.5021.4485.
000059      3.5659.5693.5640.5189.4632.
000060      3.5659.5694.5656.5778.4730.
000061      3.5660.5694.5669.5327.4802.
000062      3.5660.5695.5677.5366.4858/
000063 DATA DB/
000064      1 1.563E-3.1.9.7E-3.2.466E-3.2.9.34E-3.3.301E-3.3.574E-3.3.842E-3.
000065      2 1.563E-3.1.9.7E-3.2.466E-3.2.9.34E-3.3.301E-3.3.569E-3.3.783E-3.
000066      3 1.563E-3.1.9.7E-3.2.466E-3.2.9.34E-3.3.301E-3.3.57E-3.3.770E-3.
000067      4 1.563E-3.1.9.7E-3.2.466E-3.2.9.34E-3.3.301E-3.3.565E-3.3.765E-3.
000068      5 1.563E-3.1.9.7E-3.2.466E-3.2.9.34E-3.3.300E-3.3.565E-3.3.762E-3.
000069      6 1.563E-3.1.9.7E-3.2.466E-3.2.9.34E-3.3.300E-3.3.566E-3.3.760E-3/
000070 DATA PRES/100.4500.1070.2000.7500./
000071 END

```

Report 21052-3F, Appendix A

2. ELT. HGCORR. 1.700424. 58442

```

000001 SUBROUTINE HGCORR(ETA,ATO,ADR,A,B,TR)
000002 DIMENSION A(1),B(1)
000003 XI=A(4)
000004 DTI=A(5)
000005 W0=A(2)
000006 WF=A(1)
000007 DX2=WTI-DTI/(WTI+DTI)
000008 P=2*(WTI+DTI)
000009 PC=A(15)
000010 CALL SDEG1(PC,ATO,XATO)
000011 TR=ETA**2*XATO
000012 CALL UDEG1(XATO,ADR,DBPI)
000013 HG=DBPI*(W0+WF)*.8/DTI**1.8*(3.1416*DX/P)**.8
000014 R(5)=DX
000015 R(6)=XMR
000016 B(7)=R
000017 R(48)=HG
000018 RETURN
000019 END
    
```

0 ELT HGF.1.700424. 59441

```

000001 SUBROUTINE HGF(N,T,AK,AV,AC,APFA,A,B,G)
000002 DIMENSION T(11),APEA(11),G(11),A(11),B(11),HG(11)
000003 REL=1.E+10
000004 PEH=0.
000005 Q=A(6)
000006 W=A(7)
000007 DH=B(4)
000008 WOOT=FEB(2)
000009 DO 10 I=1,N
000100 CALL DDEGI(T(I),AV,VISI)
000101 CALL DDEGI(T(I),AK,CON)
000102 CALL DDEGI(T(I),AC,CP)
000103 PE2=WOOTOF*Q/(VIS*Q*W)
000104 IF(Q.LT. REL) REL=PE
000105 IF(Q.GT. REL) PEH=PE
000106 PR=CP*VIS/CON
000107 HG(I)=Q.Q23*PE**8*PR**4*CON/DH
000108 G(I)=HG(I)*APEA(I)
000109 B(I)=G(I)
000200 10 CONTINUE
000201 A(11)=REL
000202 B(11)=PEH
000203 RETURN
000204 END

```

Report 21052-3F, Appendix A

3 ELT HGGAS,1,700424, 58443

```

000001 SUBROUTINE HGGAS(N,T,ADR,A,B,AREA,G)
000002 DIMENSION T(1),G(1),AREA(1),A(1),B(1),HG(11)
000003 REL=1.E+10
000004 REH=0.
000005 WGR=3)
000006 GASD=A(11)
000007 W=A(7)
000008 DHG=2.*(GASD*W)/(GASD*W)
000009 PG=2.*(GASD*W)
000010 DO 10 I=1,N
000011 CALL G10EG1(T(I),ADR,XADR)
000012 HG(I)=XADR*WG**3/DHG**1.8*(3.1416*DHG/PG)**.8
000013 G(I)=HG(I)*APEA(I)
000014 R(I)=T(I)*HG(I)
000015 CALL GASPT(I),A(15),D,VIS,D,D,D.)
000016 REW=DHG/(VIC*GASD*W)
000017 IF (RE .LE. PFL) REL=RE
000018 IF (RE .GE. PEH) REH=RE
000019 10 CONTINUE
000020 R(8)=DHG
000021 R(13)=REL
000022 R(14)=PEH
000023 RETURN
000024 END

```

3 ELT HGO.1.700424. 58439

```

000001 SUBROUTINE HGO(IN,T,AK,AV,AC,AREA,A,B,G)
000002 DIMENSION T(1),AREA(1),G(1),A(1),B(1),HG(11)
000003 REL=1.E+10
000004 REH=0.
000005 D=4172)
000006 W=4(7)
000007 DHEL(43)
000008 WOOTOF=9(1)
000009 DO 10 I=1,N
00010 CALL DIDSGI(Y(I),AV,VIS)
00011 CALL DIDSGI(Y(I),AK,CON)
00012 CALL DIDSGI(Y(I),AC,CP)
00013 RE=2.*WOOTOF+DH/(VIS*D*W)
00014 IF (RE .LE. REL) RE=RE
00015 IF (RE .GE. REH) REH=RE
00016 PR=CON/VIS/CON
00017 HG(I)=D-.023*RE**-.8*PR**-.4*CON/DH
00018 G(I)=HG(I)*AREA(I)
00019 BI(I)=HG(I)
00020 10 CONTINUE
00021 R(9)=REL
00022 B(10)=REH
00023 RETURN
00024 END

```

8 ELT HYARRY,1,700\*24, SR452

```

000001 SUBROUTINE HYARRYIP,ACON,AVIS,ACPI
000002 DIMENSION ACON(1),AVIS(1),ACPI(1)
000003 IU=39
000004 IL=1
000005 TINC=50.
000006 T=50.
000007 DO 10 I=IL,IU,2
000008 CALL TABP(T,P,H*0.,GAMA,ACPI(I+1),VELC,S,ACON(I+1),AVIS(I+1),0)
000009 ACPI(I)=T
000010 AVIS(I)=T
000011 T=T+TINC
000012 IF (.GE.4000.) RETURN
000013 TINC=500.
000014 T=1500.
000015 IL=41
000016 IU=55
000017 GO TO 20
000018 END
000019

```



0 ELT OXARRY,1,700424, 58451

```

000001 SUBROUTINE OXARRY(P,ACON,AVIS,ACP)
000002 DIMENSION :CON(I),AVIS(I),ACPI(I)
000003 IJ=49
000004 IL=1
000005 TIMCR=10.
000006 T=100.
000007
000008 40 DO 10 I=IL,TU+2
000009 IF (T-LE-542.160 TO 3C
000010 CALL PTP(P,T,0.,H,P,GAMA,VELC,ACP(I+1),AVIS(I+1),ACON(I+1),0.)
000011 60 TO 20
000012 30 CALL OXYGP(P,H,S,R,T,VELC,GAMA,ACP(I+1),0,41
000013 CALL PTP(P,T,0.,F,TH,0.,0.,0.,0.,AVIS(I+1),ACON(I+1),0.)
000014 20 ACON(I)=T
000015 ACPI(I)=T
000016 AVIS(I)=T
000017 ACON(I+1)=ACON(I+1)/4.,32E+4
000018 AVIS(I+1)=AVIS(I+1)/4.,32E+4
000019 T=T+TIMCR
000020 TIMCP=50.
000021 T=400.
000022 IL=51
000023 IU=75
000024 GO TO 40
000025
000026 50 IF (T-GE-4000.)RETURN
000027 TIMCR=500.
000028 T=1500.
000029 IL=77
000030 IU=91
000031 GO TO 40
000032 END

```

ELT EXP, 1,700424, 54450

```
000001 SUBROUTINE EXP(T,P,GAMA,VELC,VIS,AR)
000002 WARNING-
000003 IF(P.GT.730.) GO TO 10
000004 CALL FINDI(TSAT,P,HLG,HVP)
000005 10 CALL OXG(P,H,S,R,T,VELC,GAMA,CP,G,4.
000006 QED.
000007 IF(T.GT.TSAT) Q=1.
000008 CALL PTP(P,T,Q,ENTH,RHO,GAM,AVE,SPH,VIS,CON,TS)
000009 CON=CON/4.32E+4
000010 VIS=VIS/4.32E+4
000011 RETURN
000012 END
```

3 ELT PUTOUT,1,700424, 58445

```

000001 SURROUTINE PUTOUT(A,8)
000002 DIMENSION A(1),P(1)
000003 1 FORMAT(1H0,*,WF LENGTH*/)
000004 1FD W WLAND WO THGAS WG THOF WTI G4SD
000005 2 FORMAT(1ZE10,0,/)
000006 3 FORMAT(1H0,*,WOC WFC WGC DHF DHF QPHF*/)
000007 1MR TP DHG RELO WFC REHO DHF RELF
000008 5 FORMAT(1H1,*,NUMBER OF CHANNELS ACROSS WIDTH =,F6,0)
000009 6 FORMAT(1H1,*,NUMBER OF CHANNELS ACROSS DEPTH =,F6,0)
000010 7 FORMAT(1H1,*,TOTAL NUMBER OF CHANNELS =,F6,0)
000011 8 FORMAT(1H0,*,PIO PIF KIO KIF K K
000012 1IG KOO KOF KOG O0*/)
000013 9 FORMAT(1H0,*,RELG REHG DH0*/)
000014 WRITE(6,5) B(54)
000015 WRITE(6,6) B(55)
000016 WRITE(6,7) B(56)
000017 WRITE(6,1)
000018 WRITE(6,2) (A(I),I=1,12)
000019 WRITE(6,8)
000020 WRITE(6,2) (A(I),I=13,22)
000021 WRITE(6,3)
000022 WRITE(6,2) (B(I),I=1,12)
000023 WRITE(6,9)
000024 WRITE(6,2) B(13),B(14),B(49)
000025 RETURN
000026 END

```

8 ELT REVERS,1,700424, 58436

```
000001 SUBROUTINE REVERP(N,T,A)
000002 DIMENSION A(1),T(1)
000003 DO 10 I=1,N
000004 10 A(I)=T(N+1-I)
000005 RETURN
000006 END
```

3 ELT WDOT,1,700424, 5843E

```

000001 SUBROUTINE XDOT(A,R)
000002 DIMENSION A(11),P(11)
000003 W=PERCENT OF GAS WT FLOW
000004 WF=TOTAL FUEL WT FLOW, LB/SEC
000005 W0=TOTAL OX WT FLOW, LB/SEC
000006 WT=TOTAL INJECTOR FACE WIDTH
000007 DTI=TOTAL INJECTOR FACE DEPTH
000008 D=CHANNEL DEPTH (OX AND FUEL)
000009 W=CHANNEL WIDTH (OX AND FUEL)
000010 WLAND=SEPARATING DISTANCE BETWEEN CHANNELS ACROSS WIDTH
000011 THGAS=GAS SEPARATOR PLATLET THICKNESS
000012 THOF=OX AND FUEL SEPARATOR PLATLET THICKNESS
000013 GASD=CHANNEL DEPTH (GAS)
000014 INPUT ARRAY
000015 #F=A(1)
000016 WGA=A(2)
000017 WGA=A(3)
000018 WT=A(4)
000019 DTI=A(5)
000020 DFA=A(6)
000021 DO=A(22)
000022 W=A(7)
000023 WLAND=A(8)
000024 THGAS=A(9)
000025 THOF=A(10)
000026 GAST=A(11)
000027 DHF=2.*DF*W/(DF+W)
000028 DHO=2.*DO*W/(DO+W)
000029 ICHAN=W*TI/(W+WLAND)
000030 ICHAND=TI/(THOF+DF+THGAS+GASD+THOF*DO)
000031 F=WT0 WEIGHT FLOWS ARE DIVIDED BY THREE TO ACCOUNT FOR APPROX NO OF CHAN
000032 WDOT=W/(FLOAT(ICHAN)*2.*3.)
000033 W0DOT=W0/(FLOAT(ICHAN)*2.*3.)
000034 WGWG=W/(FLOAT(ICHAN)*3.)
000035 W0GWG=W0/(FLOAT(ICHAN)*3.)
000036 OUTPUT ARRAY
000037 R(1)=WDOTO
000038 R(2)=WDOTF
000039 R(3)=WG
000040 R(4)=DHF
000041 R(5)=DHO
000042 R(54)=ICHAN
000043 R(55)=ICHAND
000044 R(56)=ICHAN
000045 RETURN
000046 END
000047 FILE SINAP/BLOCK CLOSED, USING 1 BLOCKS OUT OF 1
END CLR

```

APPENDIX B

COMPUTER LISTING AND SAMPLE OUTPUT  
FOR TURBOPUMP FLOW REQUIREMENTS

04 MAY 70 13:30:00.306

BI FOR WTURB,WTURB  
 UNIVAC 1108 FORTRAN V LEVEL 2206 0018 F5018Q  
 THIS COMPILATION WAS DONE ON 04 MAY 70 AT 13:30:00

MAIN PROGRAM

STORAGE USED (BLOCK, NAME, LENGTH)

0001 \*CODE 000316  
 0000 \*DATA 003272  
 0002 \*BLANK 000000

EXTERNAL REFERENCES (BLOCK, NAME)

0003 HYDP  
 0004 OXP  
 0005 TURBIN  
 0006 NWDJ\$  
 0007 NI02\$  
 0010 NI01\$  
 0011 NSTOPS

STORAGE ASSIGNMENT FOR VARIABLES (BLOCK, TYPE, RELATIVE LOCATION, NAME)

0001	000034	1376	0001	000055	1426	0001	000057	1456	0001	000003	20L	0001	000254	2276
0001	000276	2406	0001	000112	30L	0001	000135	40L	0000	003145	50F	0000	003172	51F
0000	003177	60F	0000	003205	61F	0000	003215	70F	0000	003241	71F	0000	R 003122	CPGAS
0000	R 000012	ETAP	0000	R 000640	ETAPU	0000	R 000007	ETAT	0000	R 002300	ETATOT	0000	R 001770	ETATU
0000	R 003134	GAMA	0000	R 003121	GAMAG	0000	I 003125	I	0000	I 003123	IFLAG	0000	I 003120	I\$
0000	I 003126	J	0000	I 003127	K	0000	I 003124	L	0000	R 000000	PC	0000	R 000020	PCC
0000	R 001150	PERC	0000	R 003142	PERCW	0000	R 003131	P1	0000	R 003130	P2	0000	R 003137	RH01
0000	R 003141	SHP	0000	R 003133	T1	0000	R 000015	T3	0000	R 002610	T33	0000	R 003143	T4
0000	R 003135	VELC	0000	R 003136	VIS	0000	R 000330	WP	0000	R 003132	WPUMP	0000	R 003140	WTOT
0000	R 001460	WTOT1	0000	R 003144	WTURB									

00101	1*	DIMENSION	FC(7),ETAT(3),ETAP(3),T3(3),PCC(2,100),WP(2,100),ETAPU
00101	2*	1(2,100),PERC(2,100),WTOT(2,100),ETATU(2,100),ETATOT(2,100),	
00101	3*	2T33(2,100)	
00103	4*	DATA T3/1600.,2000.,2400./	
00105	5*	DATA PC/100.,200.,500.,1000.,1500.,2000.,2500./	
00107	6*	DATA ETAP/.790,.740,.680/	
00111	7*	DATA ETAT/.688,.611,.735/	
00113	8*	DATA GAMAG,CPGAS/1.3,0.615/	
00116	9*	50 FORMAT(1H0,' PC WPUMP ETAPUMP ETATURB PERCW	
00116	10*	1 P2 T1 T3 T4 SHP WTURB RH01')	
00117	11*	51 FORMAT(F9.0,F9.3,F9.4,F9.0,F9.3)	
00120	12*	60 FORMAT(1H1,' FUEL CIRCUIT-----')	
00121	13*	61 FORMAT(1H1,' OXIDIZER CIRCUIT-----')	
00122	14*	70 FORMAT(1H1,' SUMMARY-----')	
00122	15*	1 WTOT ETAPUMP ETATURB ETATOT PERCW-TOT T3')	
00123	16*	71 FORMAT(F9.0,F9.3,F9.0)	

```

00124 17*
00125 18*
00126 19* IF(IFLAG.EQ.1)WRITE(6,60)
00131 20* IF(IFLAG.NE.1)WRITE(6,61)
00134 21* WRITE(6,50)
00136 22* DO 10 I=1,7
00141 23* DO 10 J=1,3
00144 24* DO 10 K=1,3
00147 25* P2=1.5*PC(I)
00150 26* P1=P2/20.
00151 27* IF(IFLAG.NE.1)GO TO 30
00153 28* WPUMP=2.2*PC(I)/2500.
00154 29* T1=40.
00155 30* IF(P1.LE.50.)T1=30.
00157 31* CALL HYDP(T1,P1,GAMA,VELC,VIS,RHO1)
00160 32* GO TO 40
00161 33* WPUMP=11.0*PC(I)/2500.
00162 34* T1=176.
00163 35* IF(P1.LE.50.)T1=140.
00165 36* CALL OXP(T1,P1,GAMA,VELC,VIS,RHO1)
00166 37* WTOT=13.2*PC(I)/2500.
00167 38* CALL TURBIN(T3(K),GAMAG,P1,P2,RHO1,WPUMP,ETAP(J),SPGAS,ETAT(J),
00167 39* ISHP,PERCW,T4,WTURB,WTOT)
00170 40* PCC(IFLAG,L)=PC(I)
00171 41* WP(IFLAG,L)=WPUMP
00172 42* ETAPU(IFLAG,L)=ETAP(J)
00173 43* ETATU(IFLAG,L)=ETAT(J)
00174 44* PERC(IFLAG,L)=PERCW
00175 45* WTOTT(IFLAG,L)=WTOT
00176 46* T3(IFLAG,L)=T3(K)
00177 47* L=L+1
00200 48* WRITE(6,51)PC(I),WPUMP,ETAP(J),ETAT(J),PERCW,P1,P2,T1,T3(K),T4,
00200 49* ISHP,WTURB,RHO1
00222 50* L=1
00223 51* IFLAG=IFLAG+1
00224 52* IF(IFLAG.LE.2)GO TO 20
00226 53* DO 80 L=1,63
00231 54* PERC(L,L)=PERC(1,L)+PERC(2,L)
00232 55* ETATOT(1,L)=ETAPU(1,L)*ETATU(2,L)
00234 56* WRITE(6,70)
00236 57* WRITE(6,71)(PCC(1,L),WP(1,L),WTOTT(1,L),WTOTT(2,L),ETAPU(2,L),ETATU(2
00236 58* 1,L),ETATOT(1,L),PERC(1,L),T3(1,L),L=1,63)
00254 59* STOP
00255 60* END

```

END OF UNIVAC 1108 FORTRAN V COMPILATION. 0 \*DIAGNOSTIC\* MESSAGE(S)

04 MAY 70 13:30:03.667  
 QIX FOR TURBIN,TURBIN  
 UNIVAC 1108 FORTRAN V LEVEL 2206 0018 F50160  
 THIS COMPILATION WAS DONE ON 04 MAY 70 AT 13:30:03

SUBROUTINE TURBIN ENTRY POINT 000055

STORAGE USED (BLOCK, NAME, LENGTH)

0001 \*CODE 000113  
 0000 \*DATA 000032  
 0002 \*BLANK 000000

EXTERNAL REFERENCES (BLOCK, NAME)

0003 ALOG  
 0004 EXP  
 0005 NERR3\$

STORAGE ASSIGNMENT FOR VARIABLES (BLOCK, TYPE, RELATIVE LOCATION, NAME)

0003 R 000000 ALOG 0000 R 000002 DELH 0000 R 000001 DELP 0000 R 000000 P2P1

00101 1\* SUBROUTINE TURBIN(T3,GAMAG,P1,P2,RHO1,WPUMP,ETAP,CPGAS,ETAT,  
 00101 2\* 1\$HP,PERCW,Tu,WTURB,WTOT)  
 00103 3\* P2P1=P2/P1  
 00104 4\* T4=T3\*EXP((1.-GAMAG)\*ALOG(P2P1)/GAMAG)  
 00105 5\* DELP=P2-P1  
 00106 6\* DELH=DELP\*14./RHO1  
 00107 7\* SHP=DELH\*WPUMP/(550.\*ETAP)  
 00110 8\* WTURB=SHP\*550./(CPGAS\*(T3-T4)\*779.\*ETAT)\*1.05  
 00111 9\* PERCW=WTURB/WTOT\*100.  
 00112 10\* RETURN  
 00113 11\* END

END OF UNIVAC 1108 FORTRAN V COMPILATION. 0 \*DIAGNOSTIC\* MESSAGE(S)

```
@ XGT CUR          04 MAY 70  13:30:04.868
1.  FSTIN HYDOXY/BLOCK  13:30:05
    END OF FILE
2.  FSTIN SINAIP/BLOCK  13:30:07
    END OF FILE
    END CUR
```

Report 21052-3F, Appendix B

FUEL CIRCUIT

PC	WPUMP	ETAPUMP	ETATURB	PERCWF	P1	P2	T1	T3	T4	SHP	WTURB	RHO1
100.	.088	.7900	.8880	.1935	8.	150.	30.	1600.	801.	.795	.001	5.225
100.	.088	.7900	.8880	.1548	8.	150.	30.	2000.	1002.	.795	.001	5.225
100.	.088	.7900	.8880	.1290	8.	150.	30.	2400.	1202.	.795	.001	5.225
100.	.088	.7400	.8110	.2262	8.	150.	30.	1600.	801.	.849	.001	5.225
100.	.088	.7400	.8110	.1809	8.	150.	30.	2000.	1002.	.849	.001	5.225
100.	.088	.7400	.8110	.1508	8.	150.	30.	2400.	1202.	.849	.001	5.225
100.	.088	.6800	.7350	.2716	8.	150.	30.	1600.	801.	.924	.001	5.225
100.	.088	.6800	.7350	.2173	8.	150.	30.	2000.	1002.	.924	.001	5.225
200.	.176	.7900	.8880	.3952	15.	300.	30.	2400.	1202.	.924	.001	5.225
200.	.176	.7900	.8880	.3162	15.	300.	30.	1600.	801.	3.250	.004	5.116
200.	.176	.7900	.8880	.2535	15.	300.	30.	2000.	1002.	3.250	.003	5.116
200.	.176	.7400	.8110	.4620	15.	300.	30.	1600.	801.	3.469	.005	5.116
200.	.176	.7400	.8110	.3696	15.	300.	30.	2000.	1002.	3.469	.004	5.116
200.	.176	.7400	.8110	.3080	15.	300.	30.	2400.	1202.	3.469	.003	5.116
200.	.176	.6800	.7350	.5548	15.	300.	30.	1600.	801.	3.775	.006	5.116
200.	.176	.6800	.7350	.4438	15.	300.	30.	2000.	1002.	3.775	.005	5.116
500.	.440	.7900	.8880	1.0357	38.	750.	30.	2400.	1202.	21.287	.027	4.881
500.	.440	.7900	.8880	.8285	38.	750.	30.	1600.	801.	21.287	.022	4.881
500.	.440	.7400	.8110	.6905	38.	750.	30.	2000.	1002.	21.287	.018	4.881
500.	.440	.7400	.8110	1.2106	38.	750.	30.	1600.	801.	22.726	.032	4.881
500.	.440	.7400	.8110	.9685	38.	750.	30.	2000.	1002.	22.726	.026	4.881
500.	.440	.6800	.7350	.8071	38.	750.	30.	2400.	1202.	22.726	.021	4.881
500.	.440	.6800	.7350	1.4537	38.	750.	30.	1600.	801.	24.731	.038	4.881
500.	.440	.6800	.7350	1.1629	38.	750.	30.	2000.	1002.	24.731	.031	4.881
1000.	.880	.7900	.8880	2.3637	75.	1500.	40.	1600.	801.	97.169	.125	4.277
1000.	.880	.7900	.8880	1.8910	75.	1500.	40.	2000.	1002.	97.169	.100	4.277
1000.	.880	.7900	.8880	1.5758	75.	1500.	40.	2400.	1202.	97.169	.083	4.277
1000.	.880	.7400	.8110	2.7630	75.	1500.	40.	1600.	801.	103.734	.146	4.277
1000.	.880	.7400	.8110	2.2104	75.	1500.	40.	2000.	1002.	103.734	.117	4.277
1000.	.880	.7400	.8110	1.8420	75.	1500.	40.	2400.	1202.	103.734	.097	4.277
1000.	.880	.6800	.7350	3.3177	75.	1500.	40.	1600.	801.	112.887	.175	4.277
1000.	.880	.6800	.7350	2.6542	75.	1500.	40.	2000.	1002.	112.887	.140	4.277
1000.	.880	.6800	.7350	2.2118	75.	1500.	40.	2400.	1202.	112.887	.117	4.277
1500.	1.320	.7900	.8880	3.5155	112.	2250.	40.	1600.	801.	216.771	.278	4.314
1500.	1.320	.7900	.8880	2.8124	112.	2250.	40.	2000.	1002.	216.771	.223	4.314
1500.	1.320	.7900	.8880	2.3436	112.	2250.	40.	2400.	1202.	216.771	.186	4.314
1500.	1.320	.7400	.8110	4.1093	112.	2250.	40.	1600.	801.	231.418	.325	4.314
1500.	1.320	.7400	.8110	3.2875	112.	2250.	40.	2000.	1002.	231.418	.260	4.314
1500.	1.320	.7400	.8110	2.7395	112.	2250.	40.	2400.	1202.	231.418	.217	4.314
1500.	1.320	.6800	.7350	4.9343	112.	2250.	40.	1600.	801.	251.837	.391	4.314
1500.	1.320	.6800	.7350	3.9474	112.	2250.	40.	2000.	1002.	251.837	.313	4.314
1500.	1.320	.6800	.7350	3.2895	112.	2250.	40.	2400.	1202.	251.837	.261	4.314
2000.	1.760	.7900	.8880	4.6495	150.	3000.	40.	1600.	801.	382.264	.491	4.349
2000.	1.760	.7900	.8880	3.7196	150.	3000.	40.	2000.	1002.	382.264	.393	4.349
2000.	1.760	.7900	.8880	3.0997	150.	3000.	40.	2400.	1202.	382.264	.327	4.349
2000.	1.760	.7400	.8110	5.4349	150.	3000.	40.	1600.	801.	408.093	.574	4.349
2000.	1.760	.7400	.8110	4.3479	150.	3000.	40.	2000.	1002.	408.093	.459	4.349
2000.	1.760	.7400	.8110	3.6233	150.	3000.	40.	2400.	1202.	408.093	.383	4.349
2000.	1.760	.6800	.7350	6.5260	150.	3000.	40.	1600.	801.	444.101	.689	4.349
2000.	1.760	.6800	.7350	5.2208	150.	3000.	40.	2000.	1002.	444.101	.551	4.349
2000.	1.760	.6800	.7350	4.3507	150.	3000.	40.	2400.	1202.	444.101	.459	4.349
2500.	2.200	.7900	.8880	5.7638	188.	3750.	40.	1600.	801.	592.345	.761	4.385

Report 21052-3F, Appendix B

2500.	2.200	.7900	.6680	4.6110	188.	3750.	40.	2000.	1002.	592.345	.609	4.385
2500.	2.200	.7900	.6680	3.5425	188.	3750.	40.	2400.	1202.	592.345	.507	4.385
2500.	2.200	.7400	.6110	6.7374	188.	3750.	40.	1600.	801.	632.369	.889	4.385
2500.	2.200	.7400	.6110	5.3899	188.	3750.	40.	2000.	1002.	632.369	.711	4.385
2500.	2.200	.7400	.6110	4.4916	188.	3750.	40.	2400.	1202.	632.369	.593	4.385
2500.	2.200	.6800	.7350	8.0900	188.	3750.	40.	1600.	801.	688.166	1.068	4.385
2500.	2.200	.6800	.7350	6.4720	188.	3750.	40.	2000.	1002.	688.166	.854	4.385
2500.	2.200	.6800	.7350	5.3934	188.	3750.	40.	2400.	1202.	688.166	.712	4.385

Report 21052-3F, Appendix B

OXIDIZER CIRCUIT

PC	MPUMP	ETAPUMP	ETATURB	PERCW	P1	P2	T1	T3	T4	SHIP	WTURB	RHO1
100.	.440	.7900	.8880	.0674	8.	150.	140.	1600.	801.	.277	.000	74.960
100.	.440	.7900	.8880	.0539	8.	150.	140.	2000.	1002.	.277	.000	74.960
100.	.440	.7900	.8880	.0450	8.	150.	140.	2400.	1202.	.277	.000	74.960
100.	.440	.7400	.8110	.0788	8.	150.	140.	1600.	801.	.296	.003	74.960
100.	.440	.7400	.8110	.0631	8.	150.	140.	2000.	1002.	.296	.000	74.960
100.	.440	.7400	.8110	.0526	8.	150.	140.	2400.	1202.	.296	.000	74.960
100.	.440	.6800	.7350	.0947	8.	150.	140.	1600.	801.	.322	.000	74.960
100.	.440	.6800	.7350	.0757	8.	150.	140.	2000.	1002.	.322	.000	74.960
100.	.440	.6800	.7350	.0631	8.	150.	140.	2400.	1202.	.322	.000	74.960
200.	.680	.7900	.8880	.1349	15.	300.	140.	1600.	801.	1.109	.001	74.963
200.	.680	.7900	.8880	.1079	15.	300.	140.	2000.	1002.	1.109	.001	74.963
200.	.680	.7900	.8880	.0899	15.	300.	140.	2400.	1202.	1.109	.001	74.963
200.	.680	.7400	.8110	.1576	15.	300.	140.	1600.	801.	1.184	.002	74.963
200.	.680	.7400	.8110	.1261	15.	300.	140.	2000.	1002.	1.184	.001	74.963
200.	.680	.7400	.8110	.1051	15.	300.	140.	2400.	1202.	1.184	.001	74.963
200.	.680	.6800	.7350	.1893	15.	300.	140.	1600.	801.	1.288	.002	74.963
200.	.680	.6800	.7350	.1514	15.	300.	140.	2000.	1002.	1.288	.001	74.963
200.	.680	.6800	.7350	.1262	15.	300.	140.	2400.	1202.	1.288	.001	74.963
500.	2.200	.7900	.8880	.3371	38.	750.	140.	1600.	801.	6.930	.009	74.967
500.	2.200	.7900	.8880	.2697	38.	750.	140.	2000.	1002.	6.930	.007	74.967
500.	2.200	.7900	.8880	.2248	38.	750.	140.	2400.	1202.	6.930	.006	74.967
500.	2.200	.7400	.8110	.3941	38.	750.	140.	1600.	801.	7.398	.010	74.967
500.	2.200	.7400	.8110	.3153	38.	750.	140.	2000.	1002.	7.398	.008	74.967
500.	2.200	.7400	.8110	.2627	38.	750.	140.	2400.	1202.	7.398	.007	74.967
500.	2.200	.6800	.7350	.4732	38.	750.	140.	1600.	801.	8.051	.012	74.967
500.	2.200	.6800	.7350	.3786	38.	750.	140.	2000.	1002.	8.051	.010	74.967
500.	2.200	.6800	.7350	.3155	38.	750.	140.	2400.	1202.	8.051	.008	74.967
1000.	4.400	.7900	.8880	.7358	75.	1500.	176.	1600.	801.	30.249	.039	68.695
1000.	4.400	.7900	.8880	.5887	75.	1500.	176.	2000.	1002.	30.249	.031	68.695
1000.	4.400	.7900	.8880	.4906	75.	1500.	176.	2400.	1202.	30.249	.026	68.695
1000.	4.400	.7400	.8110	.8602	75.	1500.	176.	1600.	801.	32.293	.045	68.695
1000.	4.400	.7400	.8110	.6881	75.	1500.	176.	2000.	1002.	32.293	.036	68.695
1000.	4.400	.7400	.8110	.5734	75.	1500.	176.	2400.	1202.	32.293	.030	68.695
1000.	4.400	.6800	.7350	1.0328	75.	1500.	176.	1600.	801.	35.143	.055	68.695
1000.	4.400	.6800	.7350	.8263	75.	1500.	176.	2000.	1002.	35.143	.044	68.695
1000.	4.400	.6800	.7350	.6886	75.	1500.	176.	2400.	1202.	35.143	.036	68.695
1500.	6.600	.7900	.8880	1.1049	112.	2250.	176.	1600.	801.	68.132	.088	68.623
1500.	6.600	.7900	.8880	.6839	112.	2250.	176.	2000.	1002.	68.132	.070	68.623
1500.	6.600	.7900	.8880	.7366	112.	2250.	176.	2400.	1202.	68.132	.058	68.623
1500.	6.600	.7400	.8110	1.2916	112.	2250.	176.	1600.	801.	72.736	.102	68.623
1500.	6.600	.7400	.8110	1.0333	112.	2250.	176.	2000.	1002.	72.736	.082	68.623
1500.	6.600	.7400	.8110	.8611	112.	2250.	176.	2400.	1202.	72.736	.068	68.623
1500.	6.600	.6800	.7350	1.5509	112.	2250.	176.	1600.	801.	79.154	.123	68.623
1500.	6.600	.6800	.7350	1.2407	112.	2250.	176.	2000.	1002.	79.154	.098	68.623
1500.	6.600	.6800	.7350	1.0339	112.	2250.	176.	2400.	1202.	79.154	.082	68.623
2000.	8.800	.7900	.8880	1.4761	150.	3000.	176.	1600.	801.	121.363	.156	68.488
2000.	8.800	.7900	.8880	1.1809	150.	3000.	176.	2000.	1002.	121.363	.125	68.488
2000.	8.800	.7900	.8880	.9841	150.	3000.	176.	2400.	1202.	121.363	.104	68.488
2000.	8.800	.7400	.8110	1.7255	150.	3000.	176.	1600.	801.	129.563	.182	68.488
2000.	8.800	.7400	.8110	1.3804	150.	3000.	176.	2000.	1002.	129.563	.146	68.488
2000.	8.800	.7400	.8110	1.1503	150.	3000.	176.	2400.	1202.	129.563	.121	68.488
2000.	8.800	.6800	.7350	2.0719	150.	3000.	176.	1600.	801.	140.995	.219	68.488
2000.	8.800	.6800	.7350	1.6575	150.	3000.	176.	2000.	1002.	140.995	.175	68.488
2000.	8.800	.6800	.7350	1.3813	150.	3000.	176.	2400.	1202.	140.995	.146	68.488
2500.	11.000	.7900	.8880	1.8465	187.	3750.	176.	1600.	801.	189.765	.244	68.439

Report 21052-3F, Appendix B

2500.	11.000	.7900	.6880	1.4772	187.	3750.	176.	2000.	1002.	189.765	.195	68.439
2500.	11.000	.7900	.6880	1.2310	187.	3750.	176.	2400.	1202.	189.765	.162	68.439
2500.	11.000	.7400	.8110	2.1584	187.	3750.	176.	1600.	801.	202.587	.285	68.439
2500.	11.000	.7400	.8-10	1.7267	187.	3750.	176.	2000.	1002.	202.587	.228	68.439
2500.	11.000	.7400	.8110	1.4389	187.	3750.	176.	2400.	1202.	202.587	.190	68.439
2500.	11.000	.6800	.7350	2.5917	187.	3750.	176.	1600.	801.	220.463	.342	68.439
2500.	11.000	.6800	.7350	2.0734	187.	3750.	176.	2000.	1002.	220.463	.274	68.439
2500.	11.000	.6800	.7350	1.7278	187.	3750.	176.	2400.	1202.	220.463	.228	68.439

Report 21052-3F, Appendix B

SUMMARY

PC	WFPUMP	WOPUMP	WTOT	ETAPUMP	ETATURB	ETATOT	PERC-TOT	T3
100.	.088	.440	.528	.790	.888	.702	.261	1600.
100.	.088	.440	.528	.790	.888	.702	.209	2000.
100.	.088	.440	.528	.790	.888	.702	.174	2400.
100.	.088	.440	.528	.740	.811	.600	.305	1600.
100.	.088	.440	.528	.740	.811	.600	.244	2000.
100.	.088	.440	.528	.740	.811	.600	.203	2400.
100.	.088	.440	.528	.680	.735	.500	.366	1600.
100.	.088	.440	.528	.680	.735	.500	.293	2000.
100.	.088	.440	.528	.680	.735	.500	.244	2400.
200.	.176	.880	1.056	.790	.888	.702	.536	1600.
200.	.176	.880	1.056	.790	.888	.702	.424	2000.
200.	.176	.880	1.056	.790	.888	.702	.353	2400.
200.	.176	.880	1.056	.740	.811	.600	.620	1600.
200.	.176	.880	1.056	.740	.811	.600	.496	2000.
200.	.176	.880	1.056	.680	.735	.500	.744	1600.
200.	.176	.880	1.056	.680	.735	.500	.595	2000.
200.	.176	.880	1.056	.680	.735	.500	.496	2400.
500.	.440	2.200	2.640	.790	.888	.702	1.373	1600.
500.	.440	2.200	2.640	.790	.888	.702	1.096	2000.
500.	.440	2.200	2.640	.790	.888	.702	.915	2400.
500.	.440	2.200	2.640	.740	.811	.600	1.605	1600.
500.	.440	2.200	2.640	.740	.811	.600	1.284	2000.
500.	.440	2.200	2.640	.680	.735	.500	1.076	2400.
500.	.440	2.200	2.640	.680	.735	.500	1.927	1600.
500.	.440	2.200	2.640	.680	.735	.500	1.542	2000.
500.	.440	2.200	2.640	.680	.735	.500	1.285	2400.
1000.	.880	4.400	5.280	.790	.888	.702	3.100	1600.
1000.	.880	4.400	5.280	.790	.888	.702	2.480	2000.
1000.	.880	4.400	5.280	.790	.888	.702	2.066	2400.
1000.	.880	4.400	5.280	.740	.811	.600	3.623	1600.
1000.	.880	4.400	5.280	.740	.811	.600	2.899	2000.
1000.	.880	4.400	5.280	.680	.735	.500	2.415	2400.
1000.	.880	4.400	5.280	.680	.735	.500	4.351	1600.
1000.	.880	4.400	5.280	.680	.735	.500	3.480	2000.
1500.	1.320	6.600	7.920	.790	.888	.702	4.624	1600.
1500.	1.320	6.600	7.920	.790	.888	.702	3.696	2000.
1500.	1.320	6.600	7.920	.790	.888	.702	3.080	2400.
1500.	1.320	6.600	7.920	.740	.811	.600	5.401	1600.
1500.	1.320	6.600	7.920	.740	.811	.600	4.321	2000.
1500.	1.320	6.600	7.920	.680	.735	.500	3.601	2400.
1500.	1.320	6.600	7.920	.680	.735	.500	6.485	1600.
1500.	1.320	6.600	7.920	.680	.735	.500	5.183	2000.
1500.	1.320	6.600	7.920	.680	.735	.500	4.323	2400.
2000.	1.760	8.800	10.560	.790	.888	.702	6.126	1600.
2000.	1.760	8.800	10.560	.790	.888	.702	4.901	2000.
2000.	1.760	8.800	10.560	.790	.888	.702	4.084	2400.
2000.	1.760	8.800	10.560	.740	.811	.600	7.160	1600.
2000.	1.760	8.800	10.560	.740	.811	.600	5.728	2000.
2000.	1.760	8.800	10.560	.680	.735	.500	4.774	2400.
2000.	1.760	8.800	10.560	.680	.735	.500	8.598	1600.
2000.	1.760	8.800	10.560	.680	.735	.500	6.878	2000.
2000.	1.760	8.800	10.560	.680	.735	.500	5.732	2400.
2500.	2.200	11.000	13.200	.790	.888	.702	7.610	1600.
2500.	2.200	11.000	13.200	.790	.888	.702	6.088	2000.

Report 21052-3F, Appendix B

2500.	2.200	11.000	13.200	.790	.888	.702	5.074	2400.
2500.	2.200	11.000	13.200	.740	.811	.600	8.896	1600.
2500.	2.200	11.000	13.200	.740	.811	.600	7.117	2000.
2500.	2.200	11.000	13.200	.680	.735	.500	5.931	2400.
2500.	2.200	11.000	13.200	.680	.735	.500	10.682	1600.
2500.	2.200	11.000	13.200	.680	.735	.500	8.545	2000.
2500.	2.200	11.000	13.200	.680	.735	.500	7.121	2400.

APPENDIX C

ADVANCED INJECTOR COMPUTER PROGRAM

TABLE OF CONTENTS

	<u>Page</u>
I. Introduction	1
II. Injector Configuration	1
III. Computer Program	2
IV. Main Logic	2
A. Subroutine PRØPH	3
B. Subroutine PMETAL	5
C. Subroutine HGEØM	5
D. Subroutine SINDEK	6
E. Subroutine BINTP	6
F. Subroutine PTP	7
V. Input/Output	8
A. Input for Design Mode	8
B. Input for Data Reduction Mode	9
C. Input for Quality Prediction Mode	9
VI. Phase I Computer Program Logic and Equations	10

FIGURE LIST

	<u>Figure</u>
Oxidizer Platelet Configuration for Phase II Fine-Pattern Injector	1

TABLE LIST

	<u>Table</u>
Phase II Injector Design Data	I
Test Number - Design Data Correlation	II
Nomenclature	III

I. INTRODUCTION

This is the computer program written to estimate heat transfer and pressure drop within the Phase II injector. The computer program considers the parallel-channel interpropellant heat transfer as well as the flow and pressure drop through the injector core. The program treats the injector as a parallel-flow heat exchanger flowing gaseous fuel ( $H_2$ ) at  $550^{\circ}R$  and liquid oxidizer ( $O_2$ ) at  $200^{\circ}R$  at the inlet to the injector. Interpropellant heat transfer and propellant pressure drop are calculated by dividing each channel into a number of small segments and performing energy and momentum balances at each segment.

The program originated during the Phase I work but was entirely rewritten incorporating analytical changes as well as propellant property subroutines and other modifications to facilitate the design and analysis of the Phase II and Phase III injectors.

II. INJECTOR CONFIGURATION

Figure 1 is a schematic drawing of the oxidizer metering and separator platelets for the fine-pattern injector. Superimposed on the oxidizer separator platelet is the fuel metering manifold which shows the relationship of the oxidizer to the fuel passages in the fuel manifold section. A cross-flow heat exchange situation exists here but was not considered in this analysis. The effective heat exchanger section was assumed to start at the entrance to the fuel metering grooves from which point the fuel and oxidizer are in a parallel flow situation (Section 1 on Figure 1). An expression is included in the program to account for the pressure drop for the excess length of the oxygen channel (over the fuel manifold).

The injector is designed such that oxidizer passages are of constant width but variable depth (effected by selectively depth etching the oxidizer separator platelet), and fuel passages are variable width (by section) and constant depth.

III. COMPUTER PROGRAM

Three versions of the parallel flow heat transfer program establish the design, data reduction and quality prediction modes of operation. The source versions are written in FORTRAN IV. Separate versions were established in order to minimize program conversion run time. Basic equations and compute sequence are the same in all versions; only the input, output, reference tables, and geometry subroutines were added/omitted/changed as required. Basic equations and logic diagram are discussed subsequently. Options exist as to length and type of output desired with each of the three versions used. The following information applies to all three programs except where noted.

IV. MAIN LOGIC

Input to the program is via paper tape and keyboard from the TWX terminal. The first part of the program contains the logic for accepting the data, printing the input conditions, and propellant properties and injector configuration called for. Depending on the program version, the applicable geometry is either input or recalled from a subroutine flagged by a test number (discussed later). Calculations are then performed for inlet conditions and other items, such as weight flow per channel, which remain constant over an entire section. Calculations are then made at each of a previously specified number of stations or nodes within each section. A looping procedure is used to go from one node to the next and another loop is used to proceed from one section to the next until the last section has been completed.

No internal iterations are required to obtain a solution. The principal input to the program is fuel and oxidizer manifold pressures, temperatures, and weight flows with output being final fuel and oxidizer pressures (corresponding to chamber pressure), temperatures and velocities.

IV, Main Logic (cont.)

Limitations on program operation include:

- (1) Oxidizer channels cannot be shorter than fuel channels except in the design version.
- (2) Properties of 347 stainless steel are assumed for the platelet material except an option in the design version provides for a nickel injector.
- (3) Physical and thermodynamic properties:

<u>Propellant</u>	<u>Pressure (psia)</u>	<u>Temperature (°R)</u>	<u>Interpolation Between Tables</u>
Oxygen	44 - 2939	180 - 450	Yes - 10 tables
Nitrogen	50 - 577	139.6 - 500	No except on density - 3 tables
Hydrogen	50 - 1700	200 - 570	No except on density - 4 tables

- (4) Subsonic flow in oxidizer and fuel passages.

Subroutines used within the program will be discussed following:

A. SUBROUTINE PRØPH

Purpose: To store gaseous hydrogen properties.

Source Reference: "Properties of Principal Cryogenics," AGC, October 1966.

Properties and Units Stored: The following properties are stored at pressures of 50, 215, 577 and 1700 psia.

Temperature, TH	200 to 570°R
Enthalpy, ENTHH	Btu/lbm

IV, A, Subroutine PRØPH (cont.)

Thermal conductivity, CØNH	
Input	Btu/ft-hr-°R
Output	Btu/in.-sec-°R
Viscosity, XMH	lb/ft-sec
Specific heat, CPHH	Btu/lbm-°R
Density, HRHØ	lbm/cu ft
Specific heat ratio, GAMH	(-)

Calling Sequence and Options: Two parameters are specified in the argument list. They are KPRES and KGALC.

- KPRES = 1    Indicates the 50 psia table value will be used.  
           2    Indicates the 215 psia table value will be used.  
           3    Indicates the 577 psia table value will be used.  
           4    Indicates the 1700 psia table value will be used.
- KGALC = 1    Store table values only; no interpolations made (used for printing reference table).  
           2    Determine enthalpy HHY from temperature TFJ; get density, RHØH from enthalpy; correct density by multiplying RHØH by actual pressure/ table reference pressure.  
           3\*    Determine as a function of enthalpy, HHY, the following: thermal conductivity, XKKH; viscosity, XMUH; specific heat, CPH; bulk hydrogen temperature, TBH; density, RHØH; specific heat ratio, GAMH. Apply same density correction as above.

\*NOTE: All properties are explicitly for the reference pressure and are not interpolated for actual pressure except where a pressure correction factor is applied to the density.

IV, Main Logic (cont.)

B. SUBROUTINE PMETAL

Purpose: To store platelet material properties.

Properties and Units Stored:

Temperature, TM	At 160, 410, and 660°R
Thermal conductivity of 347 stainless steel, CØNM	Btu/in.-sec-°R
Thermal conductivity of nickel, CØNMN	Btu/in.-sec-°R

Calling Sequence and Options: KPAT is the only argument required to obtain thermal conductivity as a function of wall temperature, TW.

KPAT = 1 or 2    347 stainless steel properties are used.  
          3        Nickel properties are used.

(Optional input in the design version only.)

C. SUBROUTINE HGEØM

Purpose: To store platelet geometry information for the coarse- and fine-pattern configurations. KPAT is the only parameter in the argument list required to specify channel geometry within each of the five possible sections of each of the coarse and fine patterns.

KPAT = 1    Used for fine-pattern/steel injector.  
          2    Used for coarse-pattern/steel injector.  
          3    Used for fine-pattern/nickel injector.

The geometry is built into this subroutine and is given in Table I as well as the entrance loss factors applied to the beginning of each section.

IV, Main Logic (cont.)

D. SUBROUTINE SINDEK

Purpose: To associate injector pattern, baffle configuration, the hydrogen properties reference pressure, and percent thrust achieved with test number for the Phase II hot firing test program.

The main program logic is set up such that the last significant digits of the test number is input along with the test conditions. Subroutine SINDEK establishes other pertinent data previously mentioned. The purpose of this subroutine was to facilitate input for the numerous runs required to analyze the data and debug the computer program. Table II gives the data stored within the subroutine.

Calling Parameters:

KPRES      Hydrogen properties reference pressure (see Subroutine PRØPH).  
KPAT      Injector pattern (see Subroutine PMETAL).  
NTEST      Last significant digit(s) of hot fire test number (see Table II).

E. SUBROUTINE BINTP

Purpose: To provide linear interpolation between successive data points.

Calling Parameters:

U            Independent variable.  
V1          Array of independent variable data.  
V2          Array of dependent variable data.  
NV          Number of stations in each array.  
VINTP      Dependent variable returned.

IV, E, Subroutine BINTP (cont.)

Note that no extrapolation is done outside the range of V1; rather a constant value is returned, which is the first or last element in the V2 array, to whichever end of the table U is nearer.

F. SUBROUTINE PTP

Purpose: To provide oxygen properties as a function of pressure, temperature and quality.

Calling Parameters:

P	Independent variable, pressure (lbf/in. <sup>2</sup> )
T	Independent variable, temperature (°R)
Q	Independent variable, quality (-)
ENT	Dependent variable, enthalpy (Btu/lbm)
RHØ	Dependent variable, density (lbm/ft <sup>3</sup> )
GAM	Dependent variable, gamma (-)
AVE	Dependent variable, velocity of sound (ft/sec)
SPH	Dependent variable, specific heat (Btu/lbm-°R)
VIS	Dependent variable, dynamic viscosity (lbf/ft-sec)
CØN	Dependent variable, thermal conductivity (Btu/in.-sec-°R)
TS	Dependent variable, saturation temperature (°R)

Discussion:

The subroutine calls Subroutine PRØPØ which finds oxygen properties as a function of enthalpy and pressure. Complete tables are input at ten pressure levels (44, 73, 147, 294, 441, 588, 735, 882, 1470, 2939 psia) as a function of temperature ranging from 180 to 450°R in ten increments. Data were obtained from the following references:

IV, F, Subroutine PTP (cont.)

- (1) "The Thermodynamic Properties of Oxygen," Richard B. Stewart, The University of Iowa, June 1966 (Density, Temperature and Enthalpy).
- (2) "Properties of Principal Cryogenics," Aerojet-General Corporation, October 1966 (Thermal Conductivity and Viscosity).
- (3) "Thermodynamic and Related Properties of Oxygen--," L. A. Weber, NBS Report 9710, National Bureau of Standards, 20 June 1968 (Ratio of Specific Heats, Specific Heat at Constant Pressure, Velocity of Sound).

Subroutines required with PTP are:

SATPØ        which finds saturation temperature as a function of pressure  
SATTØ        which finds saturation pressure as a function of temperature  
DINTP        a double interpolation routine  
SINTP        a single interpolation routine  
BLOCK DATA    which stores the oxygen properties

V.    INPUT/OUTPUT

Program input and output is via TWX terminal; the majority of parameters are input via paper tape and the rest from the terminal keyboard as the program calls for them. Sample input for each of the three versions is given. The four output options are the same for all three versions.

A.    INPUT FOR DESIGN MODE

From Paper Tape:

$P_c$ ,  $T_{fj}$ ,  $T_{oj}$ ,  $P_{fj}$ ,  $P_{oj}$ ,  $\dot{w}_f$ ,  $\dot{w}_o$ , XNH, XNG, XN, KPRES, KØP, KPAT,  
SECT, HL, ØL, SH1, SH2, SG1, SG2, A, XF, YKH, YKG  
(Repeat for as many sections as desired--last section is input as a negative section number.)

V, A, Input for Design Mode (cont.)

From Keyboard:

Data file name

B. INPUT FOR DATA REDUCTION MODE

From Paper Tape:

Test number,  $P_{c1}$ ,  $P_{c2}$ ,  $T_{fj}$ ,  $T_{oj}$ ,  $P_{fj}$ ,  $P_{oj}$ ,  $\dot{w}_f$ ,  $\dot{w}_o$

From Keyboard:

Data file name

Gg (for gas-side heat transfer correlation, usually 0.027)

Conductance factors, UMG, UMH

Output option flag, IFLAG

-2 = Injector pressure drop ratios are calculated

C. INPUT FOR QUALITY PREDICTION MODE

From Paper Tape:

Test number,  $P_{c1}$ ,  $P_{c2}$ ,  $T_{fj}$ ,  $T_{oj}$ ,  $P_{fj}$ ,  $P_{oj}$ ,  $\dot{w}_f$ ,  $\dot{w}_o$

From Keyboard:

Data file name

Output option flag, IFLAG

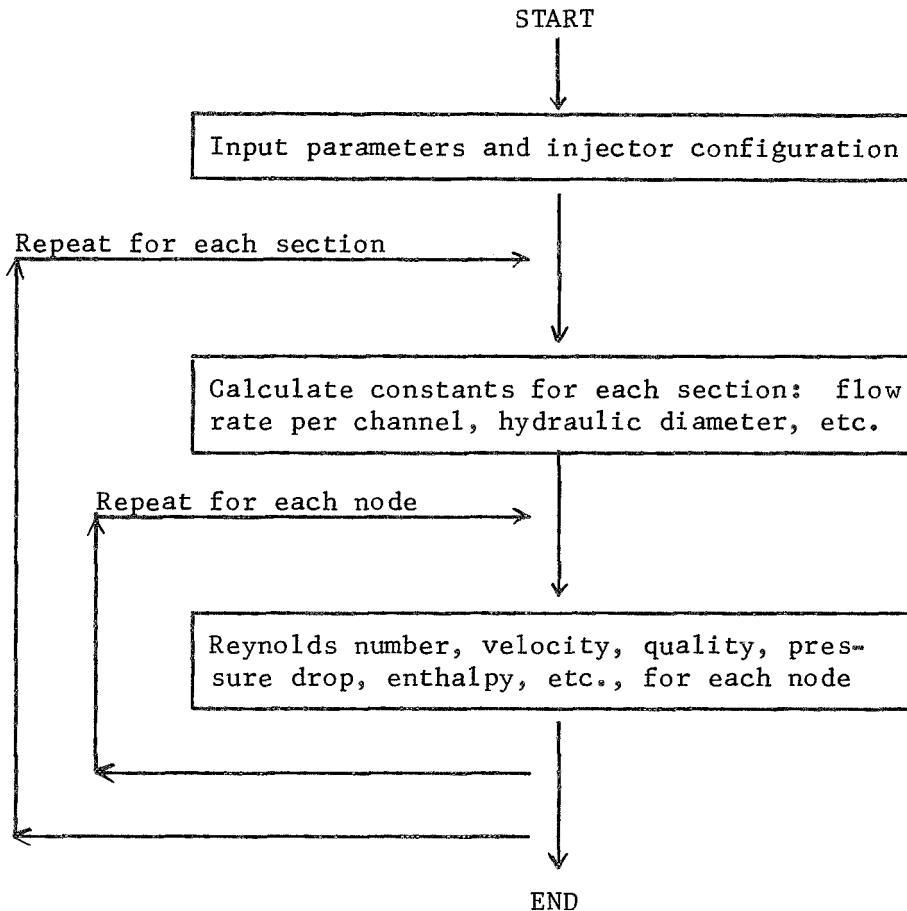
Nitrogen reference pressure flag, KPRES

Baffle configuration, KBAF

Injector pattern, KPAT

VI. PHASE I COMPUTER PROGRAM LOGIC AND EQUATIONS

There are principally three sections to the computer program which are depicted in the following simplified logic diagram:



Fluid properties are evaluated at each nodal calculation, thus approximating the variable property momentum and energy expressions. Hydrogen is assumed to enter the injector as a gas. However, since the oxygen enters as a liquid (200°R) and is, in turn, vaporized by the warm (540°R) hydrogen in the heat exchanger section of the injector (see Figure 1), it is necessary to calculate oxygen vapor quality

VI, Phase I Computer Program Logic and Equations (cont.)

and provide for a specific volume averaged oxygen heat transfer coefficient. No attempt has been made to account for any type of film boiling which might exist in this region and result in lower heat transfer coefficients than the correlations provide.

A check is made at each node for sonic flow. The program assumes that both propellants enter the injector from the same end in a parallel flow relationship. The equations used by the program are presented more or less in the order used. Nomenclature is presented in Table III.

SECTIONAL CALCULATIONS

$$A_t = 2 A w l_n \quad (1)$$

$$D = 2 w d / (w + d) \quad (2)$$

$$A_x = w d \quad (3)$$

$$l_n = l_h / n \quad \text{for } l_o > l_h \text{ in first section} \quad (4a)$$

$$= l_o / n \quad \text{for } l_o < l_h \text{ in first section} \quad (4b)$$

NOTE: Equation (4b) is programmed for the Design Program only. In the other two programs, it is assumed that the oxygen channel is longer than the hydrogen channel in the first section. In all other sections, both channels are of equal length.

$$A_{tn} = 2w l/n \quad (5)$$

$$\dot{w}_n = \dot{w}/n \quad (6)$$

VI, Phase I Computer Program Logic and Equations (cont.)

$$c = 144 K / (2g A_x^2) \quad (7)$$

NOTE: K is input in the Design Program only. In the other two versions, it is stored in Subroutine HGEØM as c directly.

$$\Delta p_k = c \dot{w}_n^2 / \rho \quad \text{applied at entrance to each section} \quad (8)$$

$$\Delta p_{ne} = \Delta p_k p / (p - \Delta p_k) + \Delta p_f \quad (9)$$

$$Re = \frac{12 \dot{w}_n D}{A_x \mu} \quad (10)$$

$$f = 0.003 + 0.0221 Re^{-0.237} \quad \text{for } Re \leq 1 \times 10^5 \quad (11a)$$

$$= 0.02 \quad \text{for } Re > 1 \times 10^5 \quad (11b)$$

$$\Delta P_f = 144 f \dot{w}_n^2 / (2 g \rho D A_x^2) \quad (12)$$

$$\Delta P_{oe} = \Delta P_k + \Delta P_f \quad (13)$$

NODAL CALCULATIONS

$$Q = (h - h_g) / (h_v - h_g) \quad (14)$$

$$T_w = (T_h + T_o) / 2 \quad (15)$$

$$h_h = Cg \frac{k}{D} Re^{0.8} Pr^{0.4} \left( \frac{T_h}{T_w} \right)^{0.4} \quad (16)$$

$$R_w = t/k \quad (17)$$

$$V = 144 \dot{w}_n / (\rho A_x) \quad (18)$$

VI, Phase I Computer Program Logic and Equations (cont.)

$$\Delta P_d = \rho(v^2 - v_i^2)/2 \quad g \quad (19)$$

$$\Delta P_n = \Delta P_f + \Delta P_d \quad (20)$$

$$h_o = Cg \frac{k}{D} Re^{0.8} Pr^{0.4} \left(\frac{\mu}{\mu_w}\right)^{0.46} \left(\frac{\rho}{\rho_w}\right)^{0.3} \quad \text{for } Q=1.0 \text{ and } Q=0 \quad (21)$$

$$h_o = \frac{h_{ov} (1 - Q)}{Q \left(1 - \frac{\rho_v}{\rho_l}\right) + 1} + \frac{h_o Q}{Q \left(1 - \frac{\rho_v}{\rho_l}\right) + \frac{\rho_v}{\rho_l}} \quad 0 \leftarrow Q \leftarrow 1 \quad (22)$$

$$U = \frac{1}{\frac{1}{h_o} + R_w + \frac{1}{h_h}} \quad (23)$$

$$\dot{w}_n \Delta H = u U A_{tn} \Delta T_{oh} \quad (24)$$

TABLE I

PHASE II INJECTOR DESIGN DATA

GEOMETRY DATA

	<u>Oxygen Circuit</u>			<u>Fuel Circuit</u>			<u>Separator Thickness (in.)</u>
	<u>Length (in.)</u>	<u>Width (in.)</u>	<u>Depth (in.)</u>	<u>Length (in.)</u>	<u>Width (in.)</u>	<u>Depth (in.)</u>	
<u>Fine-Pattern Injector (347 Stainless Steel)</u>							
1. Heat Exchanger	3.54	0.05	0.0013	2.39	0.05	0.007	0.008
2. First $\Delta P$	1.0	0.05	0.005	1.0	0.045	0.007	0.012
3. First Injector	0.35	0.05	0.0013	0.35	0.05	0.007	0.008
4. Second $\Delta P$	0.5	0.05	0.005	0.5	0.045	0.007	0.012
5. Second Injector	0.35	0.05	0.0013	0.35	0.05	0.007	0.008
Number of Channels	2346			2397			

Coarse-Pattern Injector (347 Stainless Steel)

1. Heat Exchanger	5.75	0.085	0.026	4.65	0.085	0.016	0.015
2. First $\Delta P$	1.3	0.035	0.016	1.3	0.035	0.016	0.020
3. First Injector	0.25	0.085	0.026	0.25	0.085	0.016	0.015
4. Second $\Delta P$	0.5	0.035	0.016	0.5	0.035	0.016	0.020
5. Second Injector	0.25	0.085	0.026	0.25	0.085	0.016	0.015
Number of Channels	759			792			

ENTRANCE AND EXIT LOSSES (Applied at entrance to each section)

$$\Delta P_k = c \dot{w}_n^2 / \rho \quad \text{where } \dot{w}_n \text{ is based on flow/channel}$$

	<u>Fine-Pattern Injector</u>		<u>Coarse-Pattern Injector</u>	
	<u>Oxygen "c"</u>	<u>Hydrogen "c"</u>	<u>Oxygen "c"</u>	<u>Hydrogen "c"</u>
1. Heat Exchanger	$0.42 \times 10^8$	$0.19 \times 10^9$	$0.35 \times 10^7$	$0.23 \times 10^8$
2. First $\Delta P$	0	$0.43 \times 10^7$	$0.43 \times 10^7$	0
3. First Injector	$0.20 \times 10^8$	$0.43 \times 10^7$	$0.11 \times 10^7$	$0.38 \times 10^7$
4. Second $\Delta P$	0	$0.43 \times 10^7$	$0.06 \times 10^7$	0
5. Second Injector	$0.20 \times 10^8$	$0.43 \times 10^7$	$0.11 \times 10^7$	$0.38 \times 10^7$

Report 21052-3F, Appendix C

TABLE II

TEST NUMBER - DESIGN DATA CORRELATION

<u>Test No.</u>	<u>KBAFS</u>	<u>KPRESS</u>	<u>KPATS</u>	<u>Interpretation</u>
1	0	2	1	Fine Pattern, No Baffle, 215 psia*
2	↓	3	1	Fine Pattern, No Baffle, 577 psia
3	↓	2	2	Coarse Pattern, No Baffle, 215 psia
4	↓	3	2	Coarse Pattern, No Baffle, 577 psia
5	↓	3	2	Coarse Pattern, No Baffle, 577 psia
6	0	4	2	Coarse Pattern, No Baffle, 1700 psia
7	-1	3	1	Fine Pattern, Baffled, 577 psia
8	↓	4	↓	Fine Pattern, Baffled, 1700 psia
9	↓	3	↓	Fine Pattern, Baffled, 577 psia
10	↓	2	↓	Fine Pattern, Baffled, 215 psia
11	↓	1	↓	Fine Pattern, Baffled, 50 psia
12	↓	4	1	Fine Pattern, Baffled, 1700 psia
13	↓	3	2	Coarse Pattern, Baffled, 577 psia
14	↓	2	2	Coarse Pattern, Baffled, 215 psia
15	↓	1	2	Coarse Pattern, Baffled, 50 psia
16	↓	4	2	Coarse Pattern, Baffled, 1700 psia
17	↓	2	1	Fine Pattern, Baffled, 215 psia
18	↓	1	↓	Fine Pattern, Baffled, 50 psia
19	↓	3	↓	Fine Pattern, Baffled, 577 psia
20	↓	3	↓	Fine Pattern, Baffled, 577 psia
21	↓	4	↓	Fine Pattern, Baffled, 1700 psia
22	-1	4	1	Fine Pattern, Baffled, 1700 psia

\* Hydrogen reference pressure

TABLE III

## NOMENCLATURE

## 1. English Letters and Program Symbols

<u>Text</u>	<u>Program Symbol(s)</u>	
A	AG, AH, AHT	Area (in. <sup>2</sup> )
c	XKG, XKH	Entrance loss factor, Eq (7) (lbf/in. <sup>2</sup> -lbm/ft <sup>3</sup> -sec <sup>2</sup> /lbm <sup>2</sup> )
d	SG2, SH2	Channel depth (in.)
D	DG, DH	Hydraulic diameter (in.)
f	XFG, XFH	Friction factor (-)
g		Gravitational constant (lbm-ft/lbf-sec <sup>2</sup> )
h	HG, HH, HØG, HØF, HGG, HGF	Heat transfer coefficient (Btu/lbm-in.-sec <sup>2</sup> )
H	HØX, HHY, HGG, HGF, ENTHG, ENTHH	Enthalpy (Btu/lbm)
k	XKKG, XKKH, XKGG, XKGF	Thermal conductivity (Btu/in.-sec-°R)
K	YKG, YKH	Entrance loss factor, Design Mode only (-)
ℓ	ØL, HL	Channel length, each section (in.)
n	XN	Number of nodes in each section (in.)
P	PG, PH	Local pressure (lbf/in. <sup>2</sup> )
ΔP	DELPG, DELPH, DPGXK	Pressure drop (lbf/in. <sup>2</sup> )
Pr		Prandtl number (-)
Q	QUALG	Quality; vapor mass/total mass (-)
Re	REYG, REYH	Reynolds number (-)
T	TBG, TBH, TW, TSAT	Temperature (°R)
u	UMG, UMH	Conductance multiplier (-)
U	U	Overall conductance (Btu/in.-sec-°R)
V	VG, VGT, VH, VHT	Velocity (ft/sec)
w	SG1, SH1	Channel width (in.)
ẅ	WØ, WF, WGI, WHI	Total weight flow of each propellant (lbm/sec)

TABLE III (cont.)

2. Greek Letters

<u>Text</u>	<u>Program Symbol(s)</u>	
$\mu$	XMUG, XMUGW, XMUH, XMUGG, XMUGF	Dynamic viscosity (lbm/ft-sec)
$\rho$	RHØG, RHØGW, RHØH, GRHØG, GRHØF	Density (lbm/ft <sup>3</sup> )

3. Subscripts

d	Velocity head
e	Entrance
f	Friction loss
h	Hydrogen
i	Initial
k	Head loss
$l$	Saturated liquid
n	Node
o	Oxygen
t	Heat transfer
v	Saturated vapor
w	Wall
x	Cross Section

4. Internal Program Symbols

A	Area enhancement factor for heat transfer, Eq (1) (-)
IFLAG	Output option flag
	1 = Long form
	0 = Short form
	-1 = Final velocity ratios
	-2 = Pressure drop and ratios
	= Quality predictions and Reynolds number in the first $\Delta P$ section

TABLE III (cont.)

4, Internal Program Symbols (cont.)

KBAF	Injector baffle configuration 0 = Unbaffled injector -1 = Baffled injector
KØP	Oxygen properties table print flag
KPAT	Injector pattern flag 1 = Fine pattern, 347 SS 2 = Coarse pattern, 347 SS 3 = Input pattern, nickel
KPRES	Propellant properties table reference flag 1 = 50 psia 2 = 215 psia 3 = 577 psia 4 = 1700 psia
SECT	Injector section number (see Figure 1). Preface the last section with a minus sign
WG, WH	Weight flow per channel (lb/sec)
XLH, XLN	Nodal length, Eq (4a) and (4b) (in.)

Oxidizer Platelet Configuration for Phase II Fine-Pattern Injector

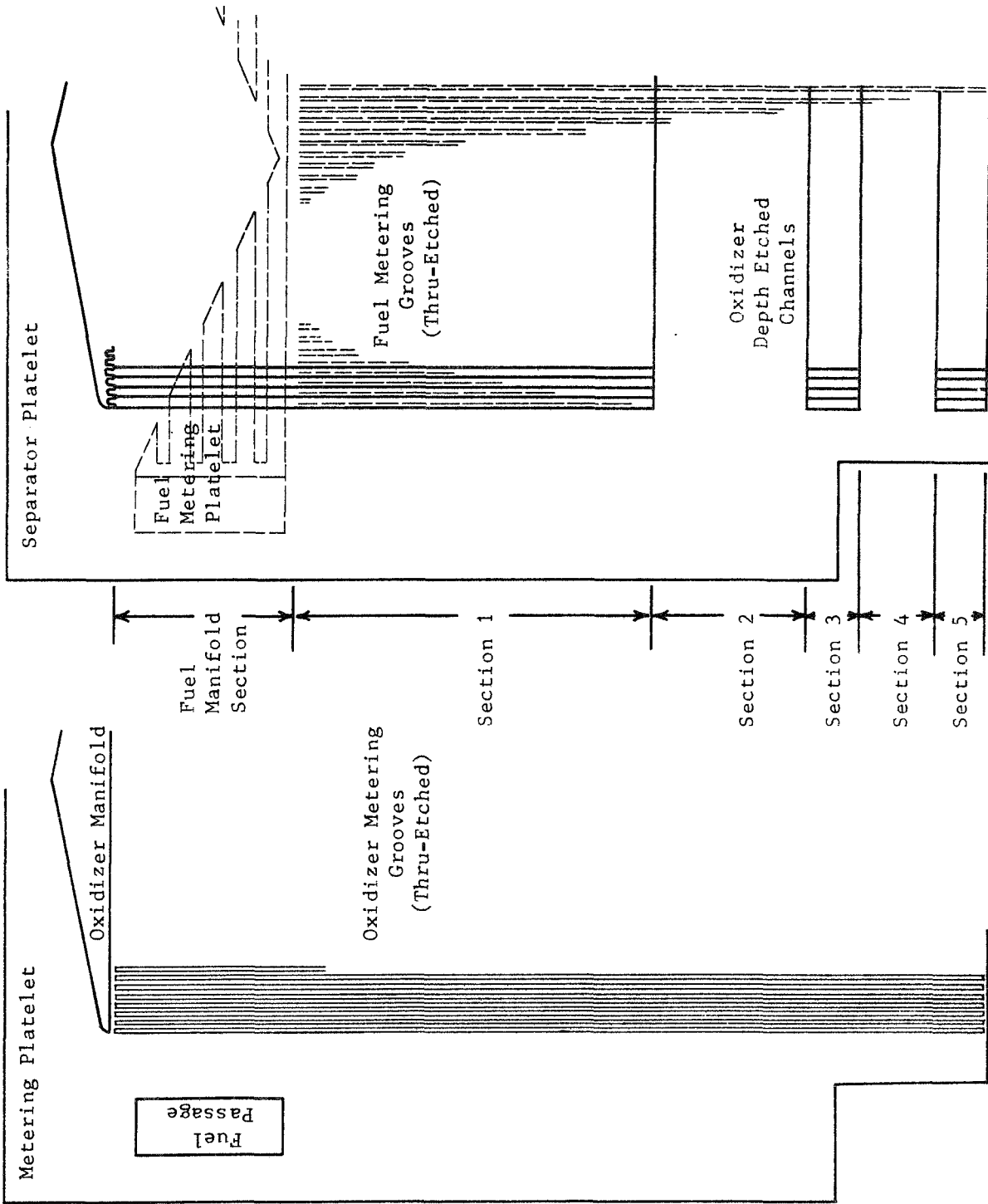


Figure 1. Oxidizer Platelet Configuration for Phase II Fine-Pattern Injector (Scale: Approximately 1:1)

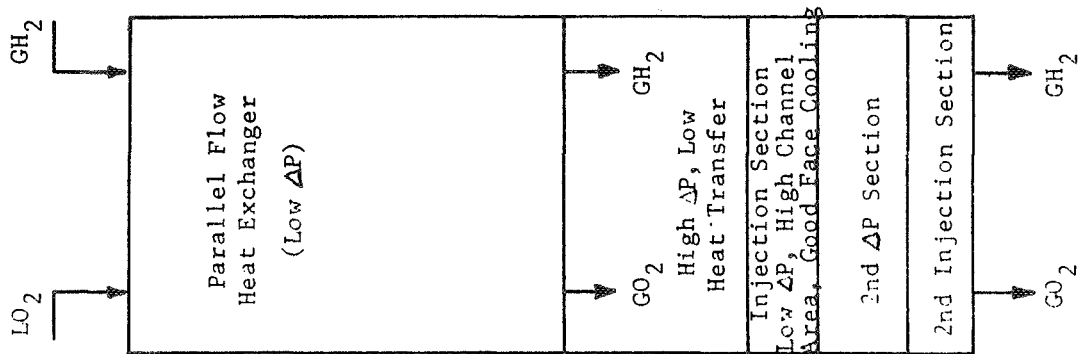


Figure 1

Report 21052-3F

APPENDIX D

DISTRIBUTION LIST

Report 21052-3F, Appendix D

DISTRIBUTION LIST

	<u>Copies</u>
NASA Headquarters Washington D.C. 20546 Attn: Chief, Liquid Propulsion Technology, RPL Office of Advanced Research and Technology	2
NASA Headquarters Washington D.C. 20546 Attn: A. O. Tischler, RP	1
NASA Headquarters Washington D.C. 20546 Attn: R. S. Levine, RP	1
NASA Headquarters Washington D.C. 20546 Attn: Director, Launch Vehicles and Propulsion, SV Office of Space Sciences and Applications	1
NASA Headquarters Washington D.C. 20546 Attn: Director, Technology Utilization	1
NASA Headquarters Washington D.C. 20546 Attn: Director, Advanced Manned Missions, MT Office of the Manned Space Flight	1
NASA Marshall Space Flight Center Huntsville, Alabama 35812 Attn: Purchasing Office, A&TS-PR-MB	1
NASA Marshall Space Flight Center Huntsville, Alabama 35812 Attn: Office of Scientific and Technical Information, A&TS-MS-IP	1
NASA Marshall Space Flight Center Huntsville, Alabama 35812 Attn: Technical Library, A&TS-MS-IL	1
NASA Marshall Space Flight Center Huntsville, Alabama 35812 Attn: Patent Office, A&TS-M-PAT	1

DISTRIBUTION LIST (cont.)

	<u>Copies</u>
NASA Marshall Space Flight Center Huntsville, Alabama 35812 Attn: Technology Utilization Office, A&TS-MS-T	1
NASA Marshall Space Flight Center Huntsville, Alabama 35812 Attn: Robert Richmond, S&E-ASTN-PP	2
NASA Marshall Space Flight Center Huntsville, Alabama 35812 Attn: Rex Bailey, S&E-ASTN-P	1
NASA Marshall Space Flight Center Huntsville, Alabama 35812 Attn: Dale Burrows, S&E-ASTN-P	1
NASA Ames Research Center Moffett Field, California 94035 Attn: Mission Analysis Division	1
NASA Ames Research Center Moffett Field, California 94035 Attn: Hans M. Mark	1
NASA Goddard Space Flight Center Greenbelt, Maryland 20771 Attn: Technical Librarian for Merland L. Moseson, Code 620	1
NASA Lewis Research Center 21000 Brookpark Road Cleveland, Ohio 44135 Attn: Richard Priem	1
NASA Lewis Research Center 21000 Brookpark Road Cleveland, Ohio 44135 Attn: E. W. Conrad, Ms500-204	1
NASA Lewis Research Center 21000 Brookpark Road Cleveland, Ohio 44135 Attn: Technical Librarian for Abe Silverstein, Director	1

Report 21052-3F, Appendix D

DISTRIBUTION LIST (cont.)

	<u>Copies</u>
NASA Jet Propulsion Laboratory California Institute of Technology 4800 Oak Grove Drive Pasadena, California 91103 Attn: Technical Librarian for Robert F. Rose, Propulsion Division, 38	1
NASA Jet Propulsion Laboratory California Institute of Technology 4800 Oak Grove Drive Pasadena, California 91103 Attn: Henry Burlage, Jr.	1
NASA Jet Propulsion Laboratory California Institute of Technology 4800 Oak Grove Drive Pasadena, California 91103 Attn: Jack H. Rupe	1
NASA Langley Research Center Langley Station Hampton, Virginia 23365 Attn: Technical Librarian for Edward Cortwright, Director	1
NASA Manned Spacecraft Center Houston, Texas 77058 Attn: Technical Librarian for Robert R. Gilruth, Director	1
NASA Manned Spacecraft Center Houston Texas 77058 Attn: J. G. Thibodaux, Propulsion & Power Division	1
NASA John F. Kennedy Space Center Cocoa Beach, Florida 32391 Attn: Technical Librarian for Kurt H. Debus, Director	1
Scientific and Technical Information Facility P.O. Box 33 College Park, Maryland 20740	10
Air Force Missile Development Center Holloman Air Force Base, New Mexico 88330 Attn: Major R. E. Bracken	1

DISTRIBUTION LIST (cont.)

	<u>Copies</u>
Air Force Missile Test Center Patrick Air Force Base, Florida Attn: L. H. Ullian	1
Headquarters, U. S. Air Force Washington, D. C. 20546 Attn: Col. C. K. Stambaug, AFRST	1
Advanced Research Projects Agency Washington 25, D. C. Attn: Technical Librarian for D. E. Mock	1
Defense Documentation Center Headquarters Cameron Station, Bldg. 5 5010 Duke Street Alexandria, Virginia 22314 Attn: Technical Librarian for TISIA	1
Picatinny Arsenal Dover, New Jersey 07801 Attn: Technical Librarian for I. Forsten, Chief, Liquid Propulsion Laboratory, SMUPA-DL	1
Air Force Rocket Propulsion Laboratory Air Force Systems Command Edwards, California 93523 Attn: Technical Librarian for Commander	1
Air Force Rocket Propulsion Laboratory Air Force Systems Command Edwards, California 93523 Attn: Tom Chew	1
Air Force Rocket Propulsion Laboratory Air Force Systems Command Edwards, California 93523 Attn: H. Main	1
U. S. Army Missile Command Redstone Arsenal, Alabama 35808 Attn: Technical Librarian for Commander	1
U. S. Army Missile Command Redstone Arsenal, Alabama 35808 Attn: Walter W. Wharton, AMSMI-RKL	1

DISTRIBUTION LIST (cont.)

	<u>Copies</u>
U. S. Naval Ordnance Test Station China Lake, California 93557 Attn: Technical Librarian for Chief, Mission Propulsion Division, Code 4562	1
U. S. Naval Ordnance Test Station China Lake, California 93557 Attn: T. Inouye, Code 4581	1
Chemical Propulsion Information Agency Johns Hopkins University Applied Physics Laboratory 8621 Georgia Avenue Silver Spring, Maryland 20910 Attn: Tech. Librarian for Tom Reedy	1
Chemical Propulsion Information Agency Johns Hopkins University Applied Physics Laboratory 8621 Georgia Avenue Silver Spring, Maryland 20910 Attn: T. W. Christian	1
Air Force Systems Command Wright-Patterson AFB Dayton, Ohio 45433 Attn: K. Scheller	1
Air Force Systems Command Wright-Patterson AFB Dayton, Ohio 45433 Attn: D. L. Schmidt, ASRCNC-2	1
Space and Missile Systems Organization Air Force Unit Post Office Los Angeles, California 90045 Attn: Col. Clark, Technical Data Center	1
Arnold Engineering Development Center Arnold Air Force Station Tullahoma, Tennessee 37388 Attn: H. K. Doetsch	1
Bureau of Naval Weapons Department of the Navy Washington, D. C. Attn: J. Kay, RTMS-41	1

DISTRIBUTION LIST (cont.)

	<u>Copies</u>
Headquarters Air Force Office of Scientific Research Propulsion Division 1400 Wilson Blvd. Arlington, Virginia 22209 Attn: R. Haffner	1
Department of the Navy Office of Naval Research Washington, D. C. 20360 Attn: R. O. Jackel, 429	1
Aerojet-General Corporation P. O. Box 15847 Sacramento, California 95809 Attn: Technical Librarian for R. Stiff	1
Aerojet-General Corporation P. O. Box 15847 Sacramento, California 95809 Attn: J. M. McBride	1
Sacramento State College School of Engineering 6000 J. Street Sacramento, California 95819 Attn: Fred H. Reardon	1
Bellcomm 955 L'Enfant Plaza, S.W. Washington, D. C. Attn: H. S. London	1
Research Center Fairchild Hiller Corporation Germantown, Maryland Attn: R. Hall	1
Republic Aviation Corporation Farmingdale, Long Island, New York Attn: Technical Librarian	1
Avco Systems Division Wilmington, Massachusetts Attn: H. B. Winkler	1

DISTRIBUTION LIST (cont.)

	<u>Copies</u>
Beech Aircraft Corporation Boulder Division P.O. Box 631 Boulder, Colorado Attn: J. H. Rodgers	1
General Dynamics, Convair Division Library & Information Services (128-00) P.O. Box 1128 San Diego, California 92112 Attn: Frank Dore	1
Grumman Aircraft Engineering Corp. Bethpage, Long Island, New York Attn: Joseph Gavin	1
Hughes Aircraft Company Aerospace Group Centinela and Teale Streets <b>Culver City, California</b> <b>Attn: E. H. Meier</b> Walter Kidde and Company, Inc. Aerospace Operations 567 Main Street Belleville, New Jersey Attn: R. J. Hanville	1
Ling-Temco-Vought Corporation P. O. Box 5907 Dallas, Texas 75222 Attn: Warren G. Trent	1
Aerospace Corporation P.O. Box 95085 Los Angeles, California 90045 Attn: Technical Librarian for J. C. Wilder	1
Aerospace Corporation P.O. Box 95085 Los Angeles, California 90045 Attn: O. W. Dykema	1
Astropower Laboratory Douglas Aircraft Company 2121 Paularino Newport Beach, California 92663 Attn: Technical Librarian for George Moc	1

DISTRIBUTION LIST (cont.)

	<u>Copies</u>
Astrosystems International, Inc. 1275 Bloomfield Avenue Fairfield, New Jersey 07007 Attn: Technical Librarian for A. Mendenhall	1
Atlantic Research Corporation Edsall Road and Shirley Highway Alexandria, Virginia 22314 Attn: Technical Librarian for R. Friedman	1
Arther D. Little, Inc. Acorn Park Cambridge, Massachusetts 02140 Attn: Technical Librarian	1
Bell Aerosystems Company P.O. Box 1 Buffalo, New York 14240 Attn: Technical Librarian for W. M. Smith	1
Bell Aerosystems Company P.O. Box 1 Buffalo, New York 14240 Attn: K. Berman	1
Bell Aerosystems Company P.O. Box 1 Buffalo, New York 14240 Attn: L. M. Wood	1
Boeing Company P. O. Box 3707 Seattle, Washington 98124 Attn: Technical Librarian for J. D. Alexander	1
Missile Division Chrysler Corporation P. O. Box 2628 Detroit, Michigan 48231 Attn: J. Gates	1
Curtiss-Wright Corporation Wright Aeronautical Division Wood-ridge, New Jersey 07075 Attn: Technical Librarian for G. Kelly	1

DISTRIBUTION LIST (cont.)

	<u>Copies</u>
General Electric Company Cincinnati, Ohio 45125 Attn: Technical Librarian for D. Suichu	1
Lockheed Missiles and Space Company Technical Information Center P. O. Box 504 Sunnyvale, California 94008 Attn: Technical Librarian for J. Guill	1
The Marquardt Corporation 16555 Saticoy Street Van Nuys, California 91409 Attn: Technical Librarian for H. McForland	1
North American Rockwell, Inc. Space and Information systems Division 12214 Lakewood Boulevard Downey, California 90241 Attn: Technical Librarian	1
TRW Incorporated One Space Park Redondo Beach, California 90278 Attn: G. W. Elverum	1
Stanford Research Institute 333 Ravenswood Avenue Menlo Park, California 94025 Attn: Technical Librarian for G. Marksman	1
McDonnell Douglas Aircraft Corporation P. O. Box 516 Municipal Airport St. Louis, Missouri 63166 Attn: R. A. Herzmark	1
TAPCO Division TRW, Incorporated 23555 Euclid Avenue Cleveland, Ohio 44117 Attn: Technical Librarian for P. T. Angell	1

DISTRIBUTION LIST (cont.)

	<u>Copies</u>
Thiokol Chemical Corporation Redstone Division Huntsville, Alabama Attn: Technical Librarian for John Doodloe	1
United Aircraft Corporation Research Laboratories 400 Main Street East Hartford, Connecticut 06108 Attn: Technical Librarian for Erle Martin	1
United Technology Center 587 Mathilda Avenue P. O. Box 358 Sunnyvale, California 94088 Attn: Technical Librarian for D. Altman	1
Rocketdyne Division of North American Rockwell, Inc. 6633 Canoga Avenue Canoga Park, California 91304 Attn: Technical Librarian for S. Hoffman	1
Rocketdyne Division of North American Rockwell, Inc. 6633 Canoga Avenue Canoga Park, California 91304 Attn: J. Nestlerode	1
Rocketdyne Division of North American Rockwell, Inc. 6633 Canoga Avenue Canoga Park, California 91304 Attn: R. Lawhead	1
Rocketdyne Division of North American Rockwell, Inc. 6633 Canoga Avenue Canoga Park, California 91304 Attn: S. F. Iacobellis	1
Martin Marietta Corporation Baltimore Division Baltimore, Maryland 21203 Attn: J. Calathes	1
Northrop Space Laboratories 3401 West Broadway Hawthorne, California Attn: W. Howard	1

DISTRIBUTION LIST (cont.)

	<u>Copies</u>
Pratt and Whitney Aircraft P.O. Box 2691 West Palm Beach, Florida 33402 Attn: Technical Librarian for R. J. Coar	1
Pratt and Whitney Aircraft P. O. Box 2691 West Palm Beach, Florida 33402 Attn: Gary Garrison	1
Rocket Research Corporation 520 South Portland Street Seattle, Washington 98108 Attn: Technical Librarian for Foy McCullough, Jr.	1
Polytechnic Institute of Brooklyn Graduate Center Route 110 Farmingdale, New York 11735 Attn: V. D. Agosta	1
Ohio State University Department of Aeronautical & Astronautical Engineering Columbus, Ohio 43210 Attn: R. Edse	1
Dynamics Science Corporation 1900 Walker Avenue Monrovia, California 91016 Attn: B. P. Breen	1
Tulane University 6823 St. Charles Avenue New Orleans, Louisiana Attn: J. C. O'Hare	1
Colorado State University Mechanical Engineering Department Fort Collins, Colorado 80521 Attn: C. E. Mitchell	1
University of California Mechanical Engineering Department Berkeley, California Attn: R. Sawyer	1

DISTRIBUTION LIST (cont.)

	<u>Copies</u>
University of California Aerospace Engineering Department P. O. Box 109 La Jolla, California 92037 Attn: F. A. Williams	1
University of Illinois Aeronautic and Astronautic Engineering Dept. Transportation Bldg., Room 101 Urbana, Illinois 61801 Attn: R. A. Strehlow	1
The Pennsylvania State University Mechanical Engineering Department 207 Mechanical Engineering Bldg. University Park, Pennsylvania 16802 Attn: G. M. Faeth	1
Princeton University Forrestal Research Center Princeton, New Jersey Attn: D. T. Harrje 08540	1
Princeton University Forrestal Research Center Princeton, New Jersey Attn: I. Glassman	1
University of Wisconsin Dept. Mechanical Engineering 1513 University Avenue Madison, Wisconsin 53706 Attn: P. S. Myers	1
University of Michigan Dept. of Aerospace Engineering Ann Arbor, Michigan 48104 Attn: J. A. Nicholls	1
University of California Dept. of Chemical Engineering 6161 Etcheverry Hall Berkeley, California 94720 Attn: A. K. Oppenheim	1

DISTRIBUTION LIST (cont.)

	<u>Copies</u>
Purdue University School of Mechanical Engineering Lafayette, Indiana 47407 Attn: J. R. Osborn	1
Purdue University School of Mechanical Engineering Lafayette, Indiana 47407 Attn: B. A. Reese	1
Purdue University School of Mechanical Engineering Lafayette, Indiana 47407 Attn: R. Goulard	1
Massachusetts Institute of Technology Department of Mechanical Engineering 77 Massachusetts Avenue Cambridge, Massachusetts 02139 Attn: T. Y. Toong	1
Illinois Institute of Technology Room 200 M. H. 3300 S. Federal Street Chicago, Illinois 60616 Attn: P. T. Torda	1
Georgia Institute of Technology Aerospace School Atlanta, Georgia 30332 Attn: B. T. Zinn	1
NASA Lewis Research Center 21000 Brookpart Road Cleveland, Ohio 44135 Attn: T. Male	1